

Springer Series in Materials Science 338

Rebeka Rudolf
Peter Majerič
Vojkan Lazić
Karlo T. Raić

Advanced Dental Metallic Materials

 Springer

Springer Series in Materials Science

Volume 338

Series Editors

Robert Hull, Center for Materials, Devices, and Integrated Systems, Rensselaer Polytechnic Institute, Troy, NY, USA

Chennupati Jagadish, Research School of Physics and Engineering, Australian National University, Canberra, ACT, Australia

Yoshiyuki Kawazoe, Center for Computational Materials, Tohoku University, Sendai, Japan

Jamie Kruzic, School of Mechanical and Manufacturing Engineering, UNSW Sydney, Sydney, NSW, Australia

Richard Osgood Jr., Columbia University, Wenham, MA, USA

Jürgen Parisi, Universität Oldenburg, Oldenburg, Germany

Udo W. Pohl, Department of Materials Science and Engineering, Technical University of Berlin, Berlin, Germany

Tae-Yeon Seong, Department of Materials Science and Engineering, Korea University, Seoul, Korea (Republic of)

Shin-ichi Uchida, Electronics and Manufacturing, National Institute of Advanced Industrial Science and Technology, Tsukuba, Ibaraki, Japan

Zhiming M. Wang, Institute of Fundamental and Frontier Sciences, University of Electronic Science and Technology of China, Chengdu, China

The Springer Series in Materials Science covers the complete spectrum of materials research and technology, including fundamental principles, physical properties, materials theory and design. Recognizing the increasing importance of materials science in future device technologies, the book titles in this series reflect the state-of-the-art in understanding and controlling the structure and properties of all important classes of materials.

Rebeka Rudolf · Peter Majerič · Vojkan Lazić ·
Karlo T. Raić

Advanced Dental Metallic Materials

 Springer

Rebeka Rudolf 
Faculty of Mechanical Engineering
University of Maribor
Maribor, Slovenia

Pomurje Science and Innovation Centre
Murska Sobota, Slovenia

Vojkan Lazić
School of Dental Medicine
University of Belgrade
Belgrade, Serbia

Peter Majerič
Faculty of Mechanical Engineering
University of Maribor
Maribor, Slovenia

Karlo T. Raić
Professor Emeritus, Faculty of Technology
and Metallurgy
University of Belgrade
Belgrade, Serbia

ISSN 0933-033X ISSN 2196-2812 (electronic)
Springer Series in Materials Science
ISBN 978-3-031-47350-0 ISBN 978-3-031-47351-7 (eBook)
<https://doi.org/10.1007/978-3-031-47351-7>

© The Editor(s) (if applicable) and The Author(s), under exclusive license to Springer Nature Switzerland AG 2024

This work is subject to copyright. All rights are solely and exclusively licensed by the Publisher, whether the whole or part of the material is concerned, specifically the rights of translation, reprinting, reuse of illustrations, recitation, broadcasting, reproduction on microfilms or in any other physical way, and transmission or information storage and retrieval, electronic adaptation, computer software, or by similar or dissimilar methodology now known or hereafter developed.

The use of general descriptive names, registered names, trademarks, service marks, etc. in this publication does not imply, even in the absence of a specific statement, that such names are exempt from the relevant protective laws and regulations and therefore free for general use.

The publisher, the authors, and the editors are safe to assume that the advice and information in this book are believed to be true and accurate at the date of publication. Neither the publisher nor the authors or the editors give a warranty, expressed or implied, with respect to the material contained herein or for any errors or omissions that may have been made. The publisher remains neutral with regard to jurisdictional claims in published maps and institutional affiliations.

This Springer imprint is published by the registered company Springer Nature Switzerland AG
The registered company address is: Gewerbestrasse 11, 6330 Cham, Switzerland

Paper in this product is recyclable.

Preface

Due to their excellent mechanical and biological properties, the use of metallic materials in Dentistry has continued since time immemorial. This trend is particularly pronounced in modern life. As alternative materials such as ceramics become increasingly popular, metallic materials are likely to continue to play an important role, due to their functional properties and proven excellent clinical responses in dental applications. In that sense, this monograph aims to cover the most recent topics regarding the development and application of advanced dental metallic materials.

With examples that are the result of the authors' long-term research, an attempt is made to bring the readers closer to the specific purpose of dental metallic materials, which must meet criteria and properties such as biocompatibility, non-toxicity, resistance to corrosion, durability (long-term), appropriate strength and toughness, as well as corresponding values of modulus of elasticity.

Within the monograph, after the comprehensive introduction, the following are discussed: Frontiers in the stability of Titanium Implants, processing of Cobalt-Chrome Dental Alloys, prosperous Shape Memory Alloys, emerging Gold Dental Alloys and Nano Foils in Dental Joining Practice. The illustrative experimental outcomes contribute to a better understanding of the emerging requirements.

Maribor, Slovenia
Belgrade, Serbia
Maribor, Slovenia
Belgrade, Serbia

Rebeka Rudolf
Vojkan Lazić
Peter Majerič
Karlo T. Raić

Contents

1	Introduction	1
1.1	Classification of Dental Alloys	3
1.1.1	Classification of Dental Casting Alloys	5
1.2	Surface Oxide Film on Metallic Biomaterials in the Human Environment	7
1.3	Requirements that Must Be Met by Metal Implants	9
1.3.1	Interaction Human Organism↔Metallic Implant	9
	References	11
2	Frontiers in the Stability of Titanium Implants	13
2.1	Structure and Properties of Titanium and Titanium-Based Alloys	14
2.2	Applications of Titanium and Titanium Alloys in Dentistry	19
2.2.1	Mechanical Properties	21
2.2.2	Elements of Choice of Alloying Elements of Titanium	22
2.2.3	Formation of a Surface Oxide Layer on Titanium	24
2.2.4	Elements of Production	27
2.3	Implant Osseointegration	28
2.4	Surface Modification of Dental Implants	31
2.4.1	Micro Level Surfaces	33
2.4.2	Surfaces with Nanostructures	34
2.4.3	Example of Etching	36
2.4.4	Example of Surface Sol-Gel Processing (SSP)	37
2.4.5	Example Using a Variety of Methods and Materials	38
2.5	Examples of Expertise	41
2.5.1	Plasma Spraying Hydroxide Apatite Coatings on Cp-Titanium Grade 2 Surfaces	41

2.5.2	Corrosion on the Surface of a Titanium Substrate Generated by a Combination of Alkaline and Heat Treatment	48
2.6	Dental Implant Antimicrobial Surface Engineering	49
	References	50
3	Processing of Cobalt-Chrome Dental Alloys	53
3.1	Introduction to Cobalt-Chrome Dental Alloys	53
3.2	Development of Co–Cr Alloys	54
3.3	Production of Co–Cr Alloys	54
3.4	Physico-Chemical Properties	55
3.5	Corrosion-Resistant Properties	56
3.6	Possible Indications	58
3.7	Fabrication Techniques of Dental Prostheses	58
3.7.1	Precision Casting of Co–Cr Dental Alloys	60
3.7.2	Milling of Co–Cr Dental Alloys	63
3.7.3	Additive Manufacturing of Co–Cr Dental Alloys	65
3.7.4	Veneering of Co–Cr Dental Alloys	68
	References	71
4	Prosperous Shape Memory Alloys (SMAs)	75
4.1	Introduction	76
4.2	Shape Memory Mechanism	77
4.3	Nickel–Titanium Alloys	78
4.3.1	Manufacture of Ni–Ti Alloys	80
4.4	Copper-Based Alloys	82
4.5	Orthodontic Appliance by SMA NiTi Orthodontic Wire	83
4.6	Examples of Expertise	84
4.6.1	Comparison of Commercially Available NiTi Orthodontic Wires	84
4.6.2	Experimental Continuous Casting of Nitinol	89
4.6.3	Microstructure, Mechanical Properties and Corrosion Behaviour of NiTi and CuAlNi Alloys Prepared by Continuous Casting	93
4.6.4	Stress Dependent Electrical Resistivity of Orthodontic NiTi Wire	107
4.6.5	Biocompatibility of Ni–Ti Wires	116
4.6.6	Biocompatibility of Rapidly Solidified Cu–Al–Ni SMA Thin Ribbon	122
4.6.7	Deposition of an Atomic Layer of a TiO ₂ on Ni–Ti SMAs/Corrosion Protection in a Simulated Body Fluid	122
	References	124

5 Emerging Gold Dental Alloys	129
5.1 Introduction	129
5.1.1 Historical Background of Gold Alloys in Dentistry	131
5.2 Dental Gold Alloys	131
5.2.1 Biocompatibility of Dental Alloys	134
5.2.2 Corrosion Resistance	135
5.2.3 Resistance to Wear and Damage	137
5.2.4 Substance Release and Allergies	139
5.2.5 Recasting Gold Dental Alloys	140
5.2.6 Life Expectancy	141
5.2.7 Comparison of Gold Dental Alloys to Ceramic Alternatives	142
5.2.8 Outlook for Gold Dental Alloys	143
5.3 Examples of Expertise	144
5.3.1 Use of Dental Alloys with a High Proportion of Gold (High-Gold Dental Alloys)	144
5.3.2 Development of a New Au–La Alloy	148
5.3.3 Development of an AuCuZnGe Alloy	152
References	159
6 Nanofolds in Dental Joining Practice	165
6.1 Introduction	165
6.2 Dental Applications of Al-Au Nano-Multilayered Foil	166
6.3 Example of Expertise	167
6.3.1 Results with Discussion	169
6.4 CFD Analysis of Exothermic Reactions in Al-Au Nanofolds	171
6.4.1 Numerical Modelling	172
6.4.2 Numerical Procedure	175
6.4.3 Results and Discussion	175
References	177

About the Authors

Prof. Dr. Rebeka Rudolf after graduation from the Faculty of Mechanical Engineering in the University of Maribor, Slovenia, continued with postgraduate studies (Master's degree in 1997) up to a Doctorate in 2002. She has been employed permanently at the University since 1993. In 2006, she was additionally employed by Zlatarna Celje d.o.o. (ZC) as Research Manager and as Leader of the Research Group. In 2017, she achieved the level of Research Counsellor, and in 2023 full position of Professor at the University of Maribor within the habilitation field: Materials. Rebeka Rudolf has been appointed as a Research Councillor since 31/12/2023 at Pomurje Science and Innovation Centre, Murska Sobota, Slovenia. She has focused intensively on the development of new gold dental alloys, studying their biocompatibility and corrosion resistance, which are the applicable values for the field of dentistry. Under her leadership, ZC has put six new dental alloys on the EU market, for which they conducted preclinical investigations complying with the Standards EN ISO 10993-1: 2009 and 10993-5: 2009. The dental alloys are also protected by patents. In the last 10 years, she has been involved actively in the field of nanotechnology—the synthesis of gold and other different metal nanoparticles based on the ultrasonic spray pyrolysis (USP) process. The USP pilot device has been currently installed and is in operation. She has published in co-authorship many top references in the last five years in the fields of dental alloys and nanotechnology. e-mail: rebeka.rudolf@um.si

Dr. Peter Majerič completed his university education in 2012 at the Faculty of Mechanical Engineering, University of Maribor. He then continued with doctoral studies at the Institute of Materials Technology at the same faculty. He worked on a production process for the production of gold nanoparticles in collaboration with IME, the Institut für Metallurgische Prozesstechnik und Metallrecycling, RWTH Aachen University in Germany. In 2016, he finished his Ph.D. dissertation entitled “Synthesis of Gold Nanoparticles with a Modified Ultrasonic Spray Pyrolysis”. In the same year, he continued his employment at the Institute of Materials Technology as Assistant with a Ph.D. He works primarily on research and development projects and programs in the field of materials, nanotechnology and nanomaterials production.

He also operates and maintains instruments for scanning electron microscopy (SEM) and has experience in metallography and testing of mechanical properties from cooperation on various projects focused on the functional properties of materials. e-mail: peter.majeric@um.si

Prof. Dr. Vojkan Lazić is Full Professor and Vice Dean at the School of Dental Medicine at the University of Belgrade. After graduation from the School of Dental Medicine in Belgrade in 1991, he continued with a Master of Science degree in 1998 to a Doctorate in 2003. He has been employed at the University permanently since 1994. Since then, he has been involved in teaching and research, especially in dental materials. The main research is in the field of new dental alloys for ceramic fused to metal restorations, acrylic resin with nanoparticles for complete or partial dentures and silicones for epitheses. He was a Participant and Main Researcher in six scientific projects, mainly in dental materials. In July 2008, he was visiting professor at the Advanced Prosthodontic Division at UCLA, CA—USA. Until now, he has published 52 papers, of which 45 were scientific papers, then 110 reports at international and domestic conferences and six books, of which he co-authored in three textbooks. So far, he has been Mentor in six completed doctoral dissertations. e-mail: vojkan.lazic@stom.bg.ac.rs

Dr. Karlo T. Raić is a Professor Emeritus at the Department of Metallurgical Engineering (DME), Faculty of Technology and Metallurgy, University of Belgrade, Serbia (FTM-UB-Ser). His teachings span a broad range of courses, including Transport Phenomena in Materials Engineering, Surface Engineering, Metallic Materials in Medicine, and Iron and Steel-selected Topics.

Throughout his illustrious career, Prof. Raić has held numerous key positions, demonstrating his leadership and commitment to metallurgical education and research. His extensive experience includes terms as President of the Metallurgical Division at FTM-UB-Ser, Head of the DME, Member of the Faculty Council, Editor-in-Chief of FTM-UB-Ser editions and Vice President of the Association of Metallurgical Engineers of Serbia (AMES). His editorial roles have encompassed several esteemed publications within his field.

His scholarship encompasses several prestigious programs worldwide, including DAAD Braunschweig, Max-Planck-Institute for Metals Research, Washington State University, OeAD Leoben and Erasmus+ initiatives in Slovakia and Austria.

Professor Raić's primary expertise lies in Transport Phenomena in Materials Engineering, with a particular emphasis on surface modification and characterization of metallic materials for a diverse array of applications. He has made substantial contributions to the scientific community, with over 170 publications including peer-reviewed journals, national journals and conference books, as well as more than 10 textbooks.

Actively involved in academic and research communities, Prof. Raić has participated in and coordinated numerous national and international projects. Additionally, he has provided invaluable mentorship as a thesis advisor and served on various organizing committees. As a reviewer for international and national journals, monographs, conference papers and grant applications, his expertise has guided the advancement of new materials and technologies. His influence extends further as a dedicated member and leader of international and national conference committees. e-mail: karlo@tmf.bg.ac.rs

Chapter 1

Introduction



Abstract The classification of metallic biomaterials is illustrated in detail, with special reference to dental casting alloys. The behavior of surface oxide films on metallic biomaterials in the human environment is taken into account. The requirements that metal implants must meet during the interaction between the human organism and the metal implant are discussed.

Biomaterials are materials used for the production of components and assemblies that are incorporated in a physiologically acceptable way into the human body, with the aim of replacing a certain part and/or function of the human body. Biomaterials are natural or synthetic materials that come into touch with cells, tissues, or biofluids without harming the human body. The Clemson University Biomaterials Association (Clemson University, USA) has, for example, defined biomaterials as “systemically and pharmacologically inert substances intended for incorporation into a living system”. The National Institute of Health (NIH, USA) has defined a biomaterial as “any substance or combination of substances, natural or synthetic, that can be used for a period of time, as a part, or as a system as a whole, and that treats or replaces a tissue or organ, or improves a function of the human organism” [1–6].

Biomaterials in Dentistry can be metal, ceramic and glass biomaterials, non-degradable synthetic polymers, composite biomaterials, biodegradable polymers, etc. Metallic materials are used extensively in Dentistry for different devices [7] due to their excellent mechanical properties, Table 1.1.

Metallic materials used in Dentistry are biocompatible materials that come into contact with human cells, tissues, or body fluids on a temporary or permanent basis. They are used most commonly to replace or upgrade structural components of teeth as a component of the human body, to compensate for harm caused by ageing, illness, or accidents.

Due to their specific purpose, these metallic materials must meet certain criteria and properties, such as: biocompatibility, non-toxicity, resistance to corrosion, durability (long life), appropriate strength and toughness, as well as appropriate values of the modulus of elasticity.

Table 1.1 Typical metallic materials used for dental devices

Dental device	Examples of metallic material
Inlay, crown, bridge, clasp, denture base	Au-Cu-Ag, Au-Cu-Ag-Pt-Pd, Ag-Pd-Cu-Au, Ti, Co-Cr
Porcelain fused to metal	Au-Pt-Pd
Dental implant	Ti, Ti-6Al-4 V
Orthodontic wire	316L, Co-Cr, Ni-Ti, Ti-6Al-4 V
Magnetic attachment	Sm-Co, Nd-Fe-B, Pt-Fe-B, Pt-Fe-Nb, 316L, 444

316L and 444 are stainless steels

When it comes to complex structures and restorations which are exposed to an aggressive corrosive environment and heavy loads in the human body, there are no other building materials that could replace metals. Metals' superior mechanical qualities, such as high strength, toughness, and wear resistance, distinguish them from other materials, and make them indispensable in dental applications.

Metallic materials also have significant disadvantages. The main disadvantages are the mismatch of the modulus of elasticity of metals and solid human tissues (bones and teeth) [8, 9], Fig. 1.1, their susceptibility to corrosion in contact with biofluids and the release of metal ions with a potential cytotoxic effect, which may affect the occurrence of neurological disorders and/or other serious health problems. In addition, for the application in Dentistry, the undesirable characteristics of the metals are a high coefficient of thermal conductivity, high density (replacements are too heavy), low aesthetic value and difficult workability. The main goal of developing biocompatible metallic materials is to ensure the functioning of implants in the human organism without causing harm, as well as to increase patients' lifespans and quality of life [10–14].

The most commonly used metallic materials for replacing a specific part or function of the human organism, physiologically acceptable and economical, are titanium and titanium alloys, that show good resistance to corrosion, appropriate biocompatibility and low stiffness, that enable the best transmission of the mechanical stresses of the implants to the bone. An additional advantage is the formation of titanium dioxide (TiO_2) on the surface of Ti, which has bioactive properties of inducing new bone growth. Cobalt-based alloys (e.g. Co-Cr-Mo) also have good mechanical and biocompatible properties, while the use of stainless steels has recently been abandoned due to insufficient resistance to corrosion and the effects of the body's hypersensitivity to nickel (Ni), which is released during exploitation from steel. Namely, implant corrosion occurs when the passive film formed on the surface of the metallic material is damaged by friction and/or micromovements, during which the metallic implant comes into direct contact with biofluids, which results in the degradation of the implant material and the release of metal ions. For this reason, knowing the type and concentration of released elements from the surface of implant materials is very important for predicting and evaluating their local and systemic effect on the human body. The released metal ions can be toxic in certain concentrations, and can lead to

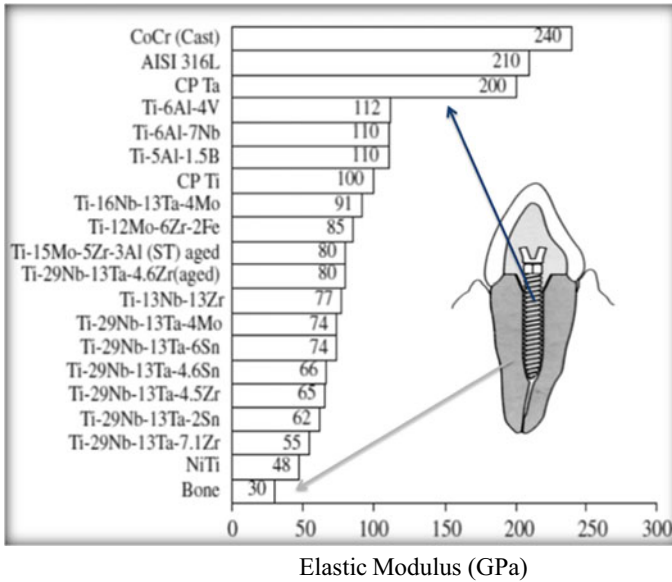


Fig. 1.1 Modulus of elasticity of biomedical alloys, adapted from [8]

various health problems due to ion diffusion throughout the body. Therefore, in order to improve the properties and durability of implants, it is necessary to develop a material with a low modulus of elasticity, high strength and good corrosion resistance. Since metal biomaterials are most often used to replace damaged solid tissues in the human body, extreme care is needed when examining the properties of this group of materials, especially in light of their biocompatibility. Consequently, the main goal of developing metallic biomaterials is, in addition to improving their mechanical characteristics, reducing the degree of their corrosion damage and improving their biocompatibility, which is why there is a need to modify the chemical composition, microstructure and surface condition of metallic materials [14–16].

1.1 Classification of Dental Alloys

The world market is flooded with hundreds of different dental alloys, which can be classified based on the primary metal and alloying elements, Table 1.2, as well as, according to use in Dentistry, Table 1.3. A more detailed classification of casting alloys for metal ceramic prostheses and partial dentures is given in Table 1.4. Certainly, a different field of application, as well as a different price, can be the basis for a different division of dental alloys [10–15].

Dental alloys are classified not only by function, but also by composition in fixed prosthodontics. When identifying an alloy by the elements it contains,

Table 1.2 Classification of dental alloys based on the primary metal and alloying elements [10–15]

Primary metal	Alloying elements
Au	Ag, Au, Cu, In, Pd, Pt, Zn
Pd	Ag, Pd, Ga, Cu
Ag	Ag, Pd
Co	Co, Cr, Mo, Fe, C, Si, Mn
Ni	Ni, Co, Cr, Mo, Fe, C, Be, Mn
Ti	Ti, O, N, C, Fe, H
Stainless steel	Fe, Cr, Ni

Table 1.3 Typical components of dental alloys [10–15]

Dental use	Alloy/metal	Typical component elements
Inlays, onlays	Mercury-based (amalgam)	Ag, Sn, Cu, Zn, Pd
Crowns, bridges, inlays, onlays	Gold-based	Au, Ag, Cu, In, Pd, Pt, Zn
	Palladium-based	Pd, Ag, Cu, Ga
	Silver-based	Ag, Pd, Cu, Zn
	Cobalt-based	Co, Cr, Mo, Fe, C, Si, Mn
	Nickel-based	Ni, Co, Cr, Mo, Fe, C, Be, Mn
Orthodontics (wires, brackets, retainers)/endodontics (drills)	Titanium–vanadium alloys	Ti, V, Cr, Al, Sn
	Stainless steel (iron-based)	Fe, Ni, Cr, C
	Nickel–titanium (Nitinol [®])	Ni, Ti
	Cobalt–chromium–nickel (Elgallloy [®])	Co, Cr, Ni, Mo, Mn, Be, C, Fe
	Beta titanium	Ti, Mo, Zr, Sn
Implants (posts, screws, abutments)	“Pure” titanium (cp titanium)	Ti, O, N, C, Fe, H
	Titanium alloy (Ti6Al4V)	Ti, Al, V, O, N, C, Fe, H
	316 stainless steel	Fe, Ni, Cr, C, Si, Mn, P, Co, Mo
	Cobalt–chromium (Vitallium [®])	Co, Cr, Mo, Fe, C, Si, Mn

the constituents are given in decreasing order of composition, with the greatest constituent listed first, followed by the second largest constituent, for example, Au–Ag–Pt (Au 78 wt.%, Ag 12 wt.%, Pt 10 wt.%). An exception to this rule is the identification of certain alloys by constituents that influence physical qualities significantly, or indicate potential biocompatibility concerns, or both, such as Au–Cu–Ag–Pd (Au 40 wt.%, Cu 7.5 wt.%, Ag 47%, Pd 4 wt.%).

Table 1.4 Classification of casting alloys for metal ceramic prostheses and partial dentures [10–15]

Alloy type ^a	All-metal prostheses	Metal ceramic prostheses	Partial denture frameworks
High noble (HN)	Au–Ag–Pd	Pure Au (99.7 wt.%)	Au–Ag–Cu–Pd
	Au–Pd–Cu–Ag	Au–Pt–Pd	
	HN metal ceramic Alloys	Au–Pd–Ag (5–12 wt.% Ag) Au–Pd–Ag (>12 wt.% Ag) Au–Pd	
Noble (N)	Ag–Pd–Au–Cu	Pd–Au	
	Ag–Pd	Pd–Au–Ag	
	Noble metal ceramic alloys	Pd–Ag Pd–Cu–Ga Pd–Ga–Ag	
Predominantly base metal (PB)	CP Ti, Ti–Al–V	CP Ti Ti–Al–V	CP Ti Ti–Al–V
	Ni–Cr–Mo–Be	Ni–Cr–Mo–Be	Ni–Cr–Mo–Be
	Ni–Cr–Mo	Ni–Cr–Mo	Ni–Cr–Mo
	Co–Cr–Mo	Co–Cr–Mo	Co–Cr–Mo
	Co–Cr–W	Co–Cr–W	Co–Cr–W
	Cu–Al		
Alloy type	Total Noble metal		
High noble metal (HN)	≥ 40 wt.% Au and ≥ 60 wt.% of the noble metal elements (Au + Ir + Os + Pt + Rh + Ru + Pt)		
Noble metal (N)	≥ 25 wt.% of the noble metal elements		
Predominantly base metal (PB)	<25 wt.% of the noble metal elements		

^a Alloy classification of the American Dental Association (ADA)

1.1.1 Classification of Dental Casting Alloys

Cast metals are used to make inlays, onlays, crowns, classic all-metal bridges, metal-ceramic bridges, resin-bonded bridges, endodontic posts, and removable partial denture frameworks [10, 11]. Casting alloys have desirable properties, such as biocompatibility, ease of melting, casting, soldering and polishing, little solidification shrinkage, minimal reactivity with the mold material, good wear resistance, high strength and sag resistance (metal-ceramic alloys), and excellent tarnish and corrosion resistance. In general, typical types 2 and 3 of gold alloys serve as the benchmarks against which the performance of other castings is measured (see Tables 1.5 and 1.6).

On the other hand, all the casting alloys used in the oral cavity must be biocompatible. The potential biologic hazards of base metal alloys, especially nickel and

Table 1.5 Four types of gold alloys (1927)


	Type	wt.% Au and Pt	VHN	Restoration
	I (soft)	83	50–90	Inlay
	II (medium)	78	90–120	Inlay and Onlay
	III (hard)	78	120–150	Onlay, crown and bridge
	IV (extra hard)	75	150–250	Crown and bridge/RPD

Table 1.6 Types of metal alloys and their main indications, adapted from [17]

Type I/Soft Alloy/weak and soft, being useful in areas not subject to occlusal stresses, not used widely

Type II/Medium Alloy/used for inlays and onlays, in which there is a possibility to burnish the edges to increase the strength of the restorations

Type III/Hard Alloy/used in inlays, onlays, three-quarter crowns, retainers and pontics of fixed prosthodontics, where burnishing is less important than resistance

Type IV/Extra Hard Alloy/hard and not ductile, being indicated in regions of high tension as a removable partial denture, not used extensively due to cost

Type V/Alloy for metal-ceramic restorations (copings)/used for metal-ceramic restorations (copings)

beryllium, are debatable. These risks may impact not only the patient, but also the dentist and technician [12, 14].

In 1927, four types of gold alloys were recognised, according to dental function, with hardness (VHN) increasing from Type I to Type IV [16–19], Table 1.5. Analogously, in 1989, the Specification No. 5 of the ADA classified the four alloy types, in addition with the fifth type, by their properties and not by their compositions, Table 1.6 [17].

So, since 1989, any composition can be used in ADA authorised casting alloys, as long as it passes the tests for toxicity, tarnish, yield strength, and percentage of elongation. The evaluations produce strength, and the percentage of elongation varies, depending on the stresses applied to the restorations.

It is clear that there is no ideal dental alloy which is the best and irreplaceable, and this is the reason why there is a large selection of metallic materials with the possibility of various applications in Dentistry.

Pure metals are used rarely in dental prosthetics. For example, gold has low hardness, silver oxidises, etc. Therefore, pure metals cannot meet the high demands placed on dental metal materials. Therefore, careful alloying is used to achieve the necessary combination of positive properties. For example, by alloying we change the mechanical properties, corrosion resistance, workability, colour and many other necessary properties.

When making castings from dental alloys, the aim is to achieve a fine grained microstructure with the lowest possible degree of chemical segregation. Depending on the chemical composition and formatted microstructure, dental alloys can be

homogeneous or heterogeneous. Homogeneous dental alloys have the same physical and chemical properties in the entire volume, i.e. they are composed of grains belonging to only one phase. Heterogeneous dental alloys are composed of areas with different physical and chemical properties, i.e. they contain grains of different phases. These changes are achieved by regular alloying and appropriate heat treatment.

High strength, low modulus of elasticity, good corrosion resistance and biocompatibility are desired characteristics of implant materials that are very difficult to achieve at the same time, and for this reason the development of materials for dental implants is very complex and represents a real challenge. In order to obtain a material with optimal characteristics, various technological procedures are used (thermo-mechanical, chemical, electrochemical, surface modification, etc.), by which the desired properties of the material can be improved, while harmful properties can be reduced to a minimum or removed completely. Lately, modern procedures of intensive plastic deformation have been used to obtain fine-grained metal materials that show improved mechanical characteristics compared to materials obtained by conventional manufacturing methods, while the question of their corrosion resistance and biocompatibility remains open. Given that metallic biomaterials are in long-term intimate contact with living tissues, it can be concluded that knowledge and understanding of the interactions between the surface of the implant material and human tissues is extremely important for the development of new materials for use in medicine [20], so the material's non-toxicity and biocompatibility become critical factors of the further development of implant metallic materials [16–19].

1.2 Surface Oxide Film on Metallic Biomaterials in the Human Environment

In this regard it should be noted that the surface oxide film formed on metallic materials serves as an inhibitor for the release of metallic ions, and the behaviour of the surface oxide varies with ion release. Furthermore, the composition of the surface oxide layer varies as a result of reactions between the metallic material surfaces and living tissues. Metal ion release can be accelerated by even modest concentrations of dissolved oxygen, inorganic ions, proteins and cells. The oxide film that inhibits metal ion dissolution is not always stable in the human body, so a comprehensive knowledge of the behaviour of the oxide film *in vivo* is required to gain a better understanding of the corrosion phenomenon [21]. Table 1.7 provides an overview of the surface oxide film on different metallic biomaterials.

When the surface oxide coating of a metallic substance is broken, corrosion develops and metal ions are discharged constantly unless the film is regenerated. The interactions between the physiological medium and the metal influence how long it takes for the oxide layer to regenerate. The amount of time necessary for re-passivation, also known as regeneration time, varies according to the alloy employed. The corrosion rate after the disruption and the amount of metal ions released are

Table 1.7 Review of the surface oxide films which can arise on selected metallic biomaterials [21]

Metallic biomaterial	Surface oxides
Titanium (Ti)	Ti ⁰⁺ , Ti ²⁺ , Ti ³⁺ , Ti ⁴⁺
<i>Titanium alloys</i>	
Ti-6Al-4 V	TiO ₂
Ni-Ti Ti-56Ni	TiO ₂ -based oxide
Ti-Zr	TiO ₂
<i>Stainless steel</i>	
Austenitic stainless	Iron and chromium
Steel 316L	Oxides of iron, chromium, nickel, molybdenum and manganese (thickness about 3.6 nm)
<i>Co-Cr-Mo alloy</i>	
Co-36.7Cr-4.6Mo	Oxides of cobalt and chromium without molybdenum (thickness 2.5 nm)

both affected by the regeneration period mentioned above [22]. Table 1.8 shows the regeneration time required to form surface oxide films for different alloys. Based on these findings, it was discovered that the regeneration time is longer in stainless steel and shorter in Ti-6Al-4 V, an alloy well known and used widely for orthopaedic applications, indicating that stainless steel releases a greater number of metal ions than the latter, highlighting one of the superior qualities possessed by this alloy in addition to its other advantageous properties.

The reactivity of metallic ions that drain away from the implant owing to corrosion in the human body affects several biological variables. Metal dissolution causes erosion as a substance corrodes, leading eventually to brittleness and breakage of the implant. Corrosion increases when a metal splits due to an increase in the exposed surface area and the loss of the protective oxide covering. If the metal pieces are not extracted surgically, they may dissolve and fragment further, causing inflammation of the surrounding tissues [22]. Table 1.9 depicts the potential hazards connected with the corroded implant material. Corrosion products will undoubtedly create undesirable biological reactions in the host, and various authors have found increased concentrations of corroded particles in tissue near implants and other regions of the human body, such as the kidney and liver. Meanwhile, no histological evidence exists to support the slow release of metallic ions caused by corrosion. The darkening of

Table 1.8 Regeneration time of surface oxide films for selected alloys, adapted from [21]

Alloy	Regeneration time (min)
SS316L	35.3
Zr-2.5Nb	13.8
Co-28Cr-6Mo	12.7
Ti-6Al-4 V	8.2

Table 1.9 Corrosion effects in the human body caused by different metals [21]

Biomaterial metals	Effect of corrosion
Nickel	Affects skin—such as dermatitis
Cobalt	Anaemia B, inhibiting iron from being absorbed into the blood stream
Chromium	Ulcers and Central nervous system disturbances
Aluminium	Epileptic effects and Alzheimer’s disease
Vanadium	Toxic in the elementary state

the surrounding tissue, however, and the foreign body reactions clearly suggest that this is due to implant corrosion [21, 22].

1.3 Requirements that Must Be Met by Metal Implants

1.3.1 Interaction Human Organism ↔ Metallic Implant

Body fluids are a 0.9% NaCl solution containing amino acids and proteins under normal circumstances. Body fluids include fluids such as tissue fluids, lymph and blood, as well as solid components such as moving cells (leukocytes and macrophages) and blood particles (lymphocytes, platelets, and erythrocytes). The pH of body fluids is 7 under normal circumstances (although the pH value may drop to 4–5 due to the appearance of inflammatory processes caused by injury or surgery). The temperature and pressure of bodily fluids in the human body are 37 °C and 0.1 MPa, respectively [23–25].

The biological environment outlined for the human organism is highly corrosive to metallic materials. To begin with, the reduced partial pressure of oxygen in the human body compared to air speeds up the corrosion process of biocompatible metal materials by slowing the recovery of the passivating surface oxide layer after it is damaged or removed from the material’s surface.

The appearance of material fatigue during friction is caused by the stress that is added to the fundamental stress of the material during cyclic friction. When frictional fatigue happens, the foreign body (metallic implant) is pressed statically against the cyclically stressed object’s surface. (bone). Friction occurs as a result of small amplitude relative displacements on the contact surfaces of the two components, which reduces the compactness of the oxide layer formed on the surface of the implant, allowing the formation of a free metal surface.

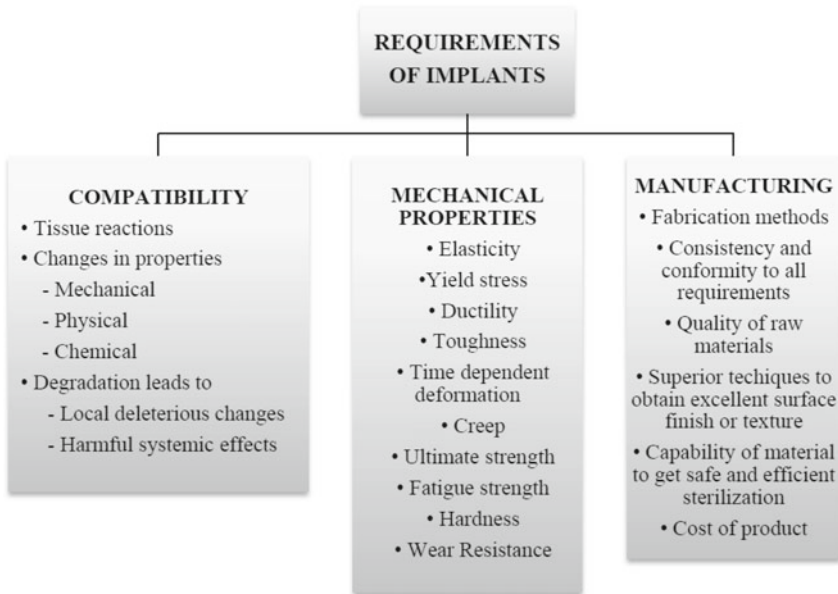
Wear and tear are caused by the friction of metallic components within the human body, which results in the constant release of metal ions, metal compounds, and wear products (metal filings). The release of all metal products mentioned above into the living tissues surrounding the medical implant can cause poisoning of the local problem or diseased organ, with the appearance of black tissue surrounding the

implant indicating the presence of metallosis in clinical orthopaedics being a good example.

This demonstrates that the human body is an extremely aggressive habitat for metallic materials, both chemically and mechanically, which reduces their durability and biocompatibility further.

The materials used to make medical implants must meet certain requirements, where the following properties are of exceptional importance:

- **biocompatibility.** Materials that are implanted in a living organism must be characterised by marked biocompatibility, that is, a marked affinity of cells to the surface of the implant. There are numerous materials that are perfect for making implants from an engineering standpoint. However, if the tissue cannot take the “foreign body,” it is unsuitable for implant fabrication, no matter how superior its engineering qualities are.
- **non-toxicity.** This is a critical feature of biomedical materials, because the discharge of metal ions and other products can influence the occurrence of cancer, deformities, allergies, necrosis, calcification and inflammatory processes.
- **corrosion resistance.** When in touch with living tissues, biocompatible metallic materials should not corrode at all.
- **durability.** Metallic materials implanted in the human body in the form of implants should function without any damage during their entire working life, which implies their high fatigue strength during corrosion and fatigue strength during friction and corrosion, but also minimal release of particles during the occurrence of friction and wear.
- **strength and toughness.** The dimensions of the implant are limited, and must be as small as possible due to the limited space in the human body, and the strength and toughness values must be high enough.
- **low values of the modulus of elasticity.** The Young’s modulus of biocompatible materials, which are used today in Orthopaedic surgery and Dentistry, are five to ten times higher than the Young’s modulus of bone, Fig. 1.1, which is an extremely unfavourable characteristic of these materials, considering that the difference in the modulus of elasticity of the metal material and bone, which are in contact, causes a significant load on the bone and results in a decrease in bone density. Implants have a complex configuration, and are made of alloys suitable for precision vacuum casting, forging and cold forming, as well as the required final mechanical processing, with the goal of increasing the implant’s resistance to fracture due to material fatigue.

Table 1.10 Overview of the total requirements

The overview of the total requirements that must be met by the embedded metallic implant can be divided into three segments [1]:

- (I) Compatibility,
- (II) Mechanical properties, and
- (III) Manufacturing,

as given in Table 1.10.

References

1. N.A. Peppas, A.S. Hoffman, Biomaterials science: an introduction to materials in medicine, in *Biomaterials Science: An Introduction to Materials in Medicine*. (Elsevier, Toronto, ON, Canada), pp. 100
2. J. Park, R.S. Lakes, *Biomaterials: an Introduction*. (Springer Science & Business Media, 2007)
3. P. Parida, A. Behera, S.C. Mishra, Classification of Biomaterials used in Medicine (2012)
4. J. Black, G. Hastings (eds.), *Handbook of Biomaterial Properties*. (Springer Science & Business Media, 2013)
5. J.D. Bronzino, *Biomedical Engineering Handbook*, vol. 2. (CRC Press, 1999)
6. N.R. Patel, P.P. Gohil, A review on biomaterials: scope, applications & human anatomy significance. *Int. J. Emerg. Technol. Adv. Eng* **2**(4), 91–101 (2012)
7. H. Hermawan, D. Ramdan, J.R. Djuansjah, Metals for biomedical applications, in *Biomedical Engineering-from Theory to Applications*, vol. 1, (2011), pp. 411–430

8. M. Geetha, A.K. Singh, R. Asokamani, A.K. Gogia, Ti based biomaterials, the ultimate choice for orthopaedic implants—a review. *Prog. Mater. Sci.* **54**(3), 397–425 (2009)
9. S.H. Teoh, Fatigue of biomaterials: a review. *Int. J. Fatigue* **22**(10), 825–837 (2000)
10. R.M. Pilliar, Metallic biomaterials. *Biomed. Mater.* 41–81 (2009)
11. M. Niinomi, Metallic biomaterials. *J. Artif. Organs* **11**, 105–110 (2008)
12. M. Niinomi, M. Nakai, J. Hieda, Development of new metallic alloys for biomedical applications. *Acta Biomater.* **8**(11), 3888–3903 (2012)
13. ISO Standard 5832-Implants for surgery--Metallic materials--Parts 1-14
14. K. Prasad, O. Bazaka, M. Chua, M. Rochford, L. Fedrick, J. Spoor, R., Symes, M. Tieppo, C. Collins, A. Cao, D. Markwell, K. Ostrikov, K. Bazaka, Metallic biomaterials: current challenges and opportunities. *Materials* **10**(8), 884 (2017)
15. J.C. Wataha, G. Schmalz, Dental alloys, in *Biocompatibility of Dental Materials* (2009)
16. L. Slokar, J. Pranjić, A. Carek, Metallic materials for use in dentistry. *Holistic Approach Environ.* **7**(1), 39–58 (2017)
17. J.D.M. de Matos, A.C.M. dos Santos, L.J.N. Nakano, J.E.L. de Vasconcelos, V.C. Andrade, R.S. Nishioka, M.A. Bottino, G.D. Lopes, Metal alloys in dentistry: An outdated material or required for oral rehabilitation? *Int. J. Odontostomat* **15**(3), 702–711 (2021)
18. K.J. Anusavice, C. Shen, H.R. Rawls, *Phillips' Science of Dental Materials*, 12th edn., vol. 100, no. 7. (St. Louis, Saunders, 2013), pp. 483–90
19. M. Asakura, Y. Kominami, T. Hayashi, S. Tsuruta, T. Kawai, The effect of zinc levels in a gold-based alloy on porcelain–metal bonding. *Dent. Mater.* **28**(5), e35–e41 (2012)
20. Y.D. Hu, X.M. Wu, H.Y. Yu, T.Y. Ma, Comparison of the influences of gold alloy metal crown and ni-cr alloy metal crown on gingival health. *Zhongguo yi xue ke xue Yuan xue bao. Acta Academiae Medicinae Sinicae*, 32(3), 269–271 (2010)
21. G. Manivasagam, D. Dhinasekaran, A. Rajamanickam, Biomedical implants: corrosion and its prevention—a review, in *Recent Patents on Corrosion Science*, vol. 2, no. 1 (2010)
22. T. Hanawa, Reconstruction and regeneration of surface oxide film on metallic materials in biological environments. *Corros. Rev.* **21**(2–3), 161–182 (2003)
23. B. Aksakal, Ö.S. Yildirim, H. Gul, Metallurgical failure analysis of various implant materials used in orthopedic applications. *J. Fail. Anal. Prev.* **4**, 17–23 (2004)
24. C.A. de Souza Costa, J. Hebling, D.L. Scheffel, D.G. Soares, F.G. Basso, A.P.D. Ribeiro, Methods to evaluate and strategies to improve the biocompatibility of dental materials and operative techniques. *Dent. Mater.* **30**(7), 769–784 (2014)
25. M. Sumita, T. Hanawa, I. Ohnishi, T. Yoneyama, *Volume 9: Bioengineering—Comprehensive Structural Integrity*, ed by I. Milne, RO Ritchie, B. Karihaloo, YW Mai, SH Teoh.

Chapter 2

Frontiers in the Stability of Titanium Implants



Abstract In the introduction, the structure and properties of titanium and titanium-based alloys relevant to dental applications are thoroughly examined. The osseointegration of titanium implants is examined from the standpoint of implant surface modification. Micro level surfaces and nanostructured surfaces are accurately considered using etching, surface Sol- Gel Processing (SSP), and a variety of processes and materials. Here are two instances of our expertise: (i) Plasma spraying hydroxide apatite coatings on Cp-Titanium Grade 2 surfaces; and (ii) Corrosion on the surface of a Titanium substrate caused by an alkaline and heat treatment combination. The topic of dental implant antimicrobial surface engineering is briefly discussed at the end of the chapter.

Titanium was discovered by William Gregor in 1791 in England, and was named in 1795 by Martin Heinrich Klaproth, after the Titans from Greek mythology. However, titanium entered industrial use only in the 1960s, in the aviation industry, thanks to its high strength and low density, which allowed aeronautical engineers to solve many of the structural requirements of the time. The main difficulty for the use of titanium was the process of obtaining or separating titanium from oxygen, until Wilhelm Kroll developed a process for the commercial production of titanium. This process was based on the deoxidation of titanium tetrachloride through reduction with magnesium and sodium, whereby spongy titanium was obtained that can be melted and cast, e.g. in the form of long solid rods. In dentistry, precisely because of this invention, Kroll is known as the “father of titanic dentistry” [1, 2].

Titanium is an extremely reactive element that is found in the earth’s crust in the form of a stable oxide, which confirms that metallic titanium and oxygen are difficult to separate. Titanium is also very reactive at high temperatures, and burns easily in the presence of oxygen, thus requiring an inert atmosphere for high temperature processing. In addition, its processing in the liquid state (melting) is possible only in vacuum conditions. As oxygen diffuses into titanium easily, any heat treatment procedure should be performed at a temperature below 925 °C [3].

For medical purposes titanium began to be applied much later. However, its use was soon increased, due to the fact that it possesses exceptional, i.e. suitable mechanical and chemical properties. The most commonly used titanium alloys for implant fabrication are commercially pure titanium (CPTi) and the Ti-6Al-4 V alloy. These alloys have found application in dentistry for the production of dental implants, although they are also used in orthopaedics in the form of wire mesh [4].

Compared to stainless steels and cobalt-chromium alloys titanium has significantly better specific strength, but also worse tribological characteristics. Also, the value of the elasticity modulus of titanium is almost half that of stainless steels and cobalt-chromium alloys, while, at room temperature, thanks to the rapid reaction of titanium with oxygen, a very stable passivating protective oxide film is formed on the surface of the titanium [5–7].

2.1 Structure and Properties of Titanium and Titanium-Based Alloys

Titanium occurs in nature in two crystalline modifications. A hexagonal close-packed structure ($c/a = 1.587$) is characteristic of titanium up to $882.5\text{ }^{\circ}\text{C}$, and this crystalline modification of titanium is called α -titanium. Above $882.5\text{ }^{\circ}\text{C}$, titanium is characterised by a volume-centred cubic structure, which is designated as β -titanium, Fig. 2.2. The density of α -titanium is 4.505 g/cm^3 , while, for β -titanium, the density value is 4.320 g/cm^3 .

Categorisation of titanium alloys is usually done according to the phases present in the microstructure, and, based on that, these alloys are divided into α , α - β and β alloys, Fig. 2.1.

As with any other single-phase alloy, the microstructure of pure titanium depends on whether it is obtained by cold deformation, as well as on the type of annealing. The microstructure that occurs during cooling from the β region (above $882.5\text{ }^{\circ}\text{C}$) depends on the cooling process itself, which affects the $\beta \rightarrow \alpha$ transformation, and, hence, the size and shape of the obtained α phase grains. Since the kinetics of the

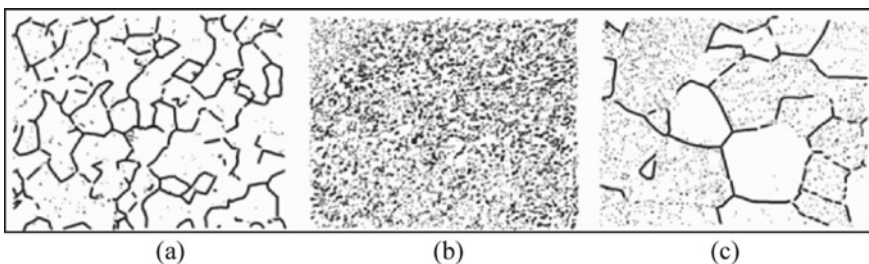


Fig. 2.1 Microstructure of annealed Ti alloys: **a** α -alloy; **b** Ti6Al4V, α - β alloy, **c** β -alloy (all are $500\times$) [8]

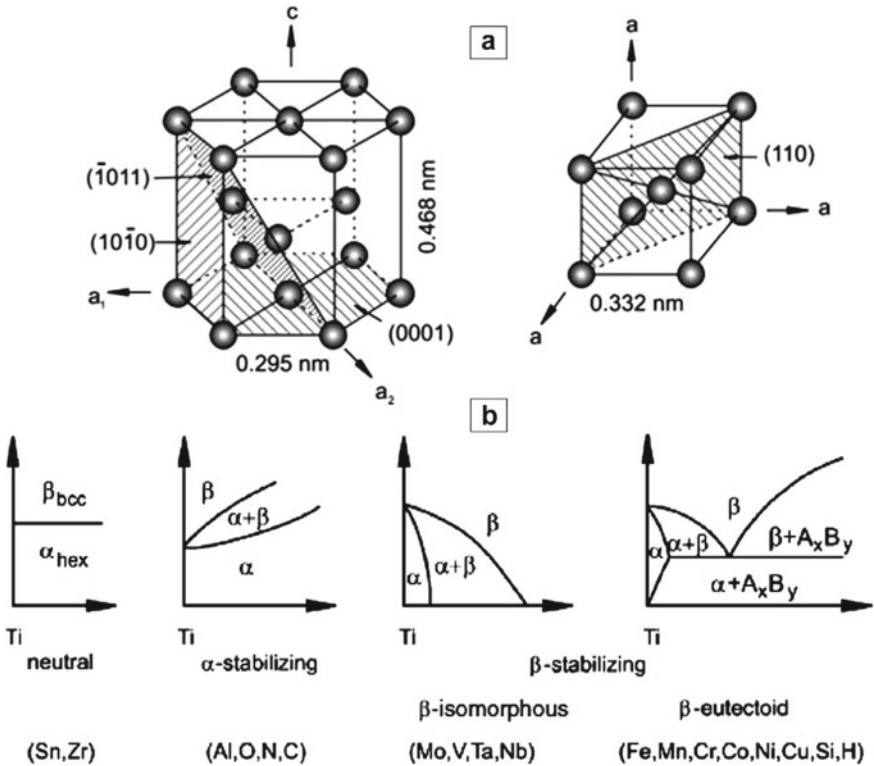


Fig. 2.2 a The titanium hcp (α) and bcc (β) structures. b Titanium phase diagram categories generated with various alloying additions [10]

$\beta \rightarrow \alpha$ phase transformation affects the properties of titanium and its alloys greatly, the effect achieved by adding alloying elements should be taken into account when choosing a heat treatment. The properties of titanium and its alloys are particularly sensitive to the presence of even small amounts of interstitial elements (hydrogen, oxygen, nitrogen and carbon) [1–7].

In the literature, along with the properties of α , α - β and β basic alloys, the properties of technically pure titanium (so-called CP Ti) are often presented, as given in Table 2.1 [9].

An illustration of the influence of alloying elements on the phase diagrams of Ti alloys is displayed in Fig. 2.2 [10].

Thus, alloying elements of titanium are divided into three categories [11]:

- (1) α stabilisers (Al, O, N, C);
- (2) β stabilisers, divided into two groups: isomorphous (Mo, V, Ta Nb,) and eutectoid (Fe, Mn, Cr, Co, Ni, Cu, Si, H);
- (3) neutral (Sn, Zr).

Table 2.1 General properties of commercially pure titanium and titanium alloys of different types [9]

Material characteristics	Commercially Pure (CP) Ti	α alloys	$(\alpha-\beta)$ alloys	β alloys
Yield strength at 20 °C (MPa)	300–700	700–850	850–1050	900–1000
High-temperature strength	Low (up to 300 °C)	Good (up to 600 °C)	Good (up to 500 °C)	Good (up to 500 °C)
Creep resistance	Low (up to 250 °C)	Good (up to 450 °C)	Good (up to 450 °C)	Good (up to 480 °C)
Heat stability	Good	Good (up to 500–600 °C)	Good (300–500 °C)	Good (up to 300 °C)
Strength increase capability	No	no, in most cases	Yes	Yes, in most cases
Deformability at 20 °C	Good or moderate, good at 300 °C	Low, good at 600–700 °C	Low, good at 500–650 °C	Moderate, good at 500 °C
Weldability	Good	Good	From good to poor	Good

By alloying, the properties of the selected material can be modified significantly, Fig. 2.2, which, with appropriate thermomechanical processing, can influence the choice of the desired properties.

α titanium alloys The basic phase of the titanium alloy, α , is present in the microstructure at temperatures below 800 °C. Heat treatment cannot alter the characteristics of these alloys appreciably. Titanium alloys are strengthened through cold deformation, a combination of cold deformation and annealing, which controls grain size, and solution strengthening. Aluminium, silicon, vanadium, zirconium, niobium and tin, elements with high or medium solubility in titanium, have the greatest influence on solvent strengthening. When considering the effects of solid solution strengthening, only three elements are usually taken into account: aluminium, tin and zirconium. The addition of aluminium and tin strengthens titanium significantly, but also increases the brittleness of the material. The addition of zirconium increases the strength only slightly. The presence of carbon, oxygen and nitrogen in interstitial positions lead to a change in the mechanical properties of α alloys, so these elements increase the strength and reduce the ductility of these alloys.

Special consideration must be given to stress corrosion cracking in the use of titanium alloys. Corrosive environments, such as salt water or humid air, can diminish the high level of strength produced by heat treatment, making the material prone to crack formation and propagation. The content of aluminium in the alloy affects the occurrence and development of stress corrosion significantly, especially in thermally treated titanium alloys with less than 7% by mass Al. A good example is annealing at 1200 °C in the β region, and then cooling in water with the formation of α martensite,

when even with rapid cooling it is not possible to avoid the formation of a certain amount of the $\alpha_2\text{-Ti}_3\text{Al}$ phase. The formation of the $\alpha_2\text{-Ti}_3\text{Al}$ phase reduces the possibility of cracking due to stress corrosion in salt water, and to some extent in air, but, with the formation of a two-phase $\alpha + \alpha_2\text{-Ti}_3\text{Al}$ microstructure, the effect of stress corrosion intensifies.

The following important property of high-strength alloys, significant in use, i.e. exploitation, is their sensitivity to notches, i.e. sensitivity to voltage concentration. Stress concentration sensitivity is defined as a measure of a material's ability to deform locally plastically in areas of high stress, instead of cracking or breaking. The sensitivity of the material to notches is determined by tensile testing of a test tube on which a notch has previously been engraved for stress concentration. By comparing the obtained value with the value obtained by testing the tension of the smooth test tube, information is obtained on the sensitivity of the material to the notch. In Ti–Al alloys, even for low Al content in the alloy, notch sensitivity is pronounced, and the deposition of the brittle $\alpha_2\text{-Ti}_3\text{Al}$ phase has been shown to be the main reason for this. Ternary alloys are used in order to increase the strength of the alloy, and, at the same time, maintain a certain level of toughness. The most commonly used α alloy of titanium contains 5% wt. Al and 2.5% wt. Sn [10, 11].

β titanium alloys The basic alloying elements of β alloys are vanadium, molybdenum, tungsten, chromium and niobium (so-called β stabilisers). In addition to these elements, aluminium is often included in the composition of this alloy, which increases strength significantly. Thanks to the cubic lattice, β alloys are more easily subjected to cold deformation. The strength of these alloys can be increased by heat treatment, and their good weldability can be singled out as one of the basic characteristics. β alloys are characterised by an exceptional possibility of plastic deformation, while ageing enables the deposition of the α phase in the β microstructure, which ensures excellent strength.

Although they are characterised by high strength up to 400 °C, the creep resistance of β alloys is lower than that of α titanium alloys.

Due to the great symmetry and the large number of sliding planes enabled by their structure, these alloys are characterised by an exceptional possibility of plastic deformation. Ageing, on the other hand, enables the deposition of the α phase in the β microstructure, which ensures excellent strength [10, 11].

$\alpha\text{-}\beta$ titanium alloys are obtained by alloying titanium with elements that form α and β solid solutions. By thermal treatment of these alloys, it is possible to increase their strength significantly with a relatively small reduction in plasticity. The weldability of $\alpha\text{-}\beta$ alloys is limited.

In addition to aluminium, $\alpha\text{-}\beta$ titanium alloys contain additional alloying elements that stabilise the β phase. These are elements with a volume-centred cubic lattice, such as molybdenum and vanadium, which are also the most important alloying elements of titanium $\alpha\text{-}\beta$ alloys.

When it comes to thermal treatment of titanium alloys, the β transus temperature is of great importance, which represents the temperature of the phase transformation $\beta \rightarrow \alpha\text{-}\beta$, and above which only the β phase is stable. Namely, the formation of

the α phase will occur during the slow cooling of α - β alloys with a low content of alloying elements in the β region. However, when a sufficiently large amount of alloying elements is present in the alloy, a two-phase α - β microstructure will be formed with a titanium-rich α phase and an alloying element-rich β phase. The share of the β phase depends on the degree of alloying, and increases with the increase in the alloying element content.

In all standard titanium alloys, this β transus temperature plays a critical role in the evolution of the microstructure, and is crucial in setting a heat treatment and processing schedule. Figure 2.3 illustrates the various microstructures formed under various thermomechanical processing settings [12].

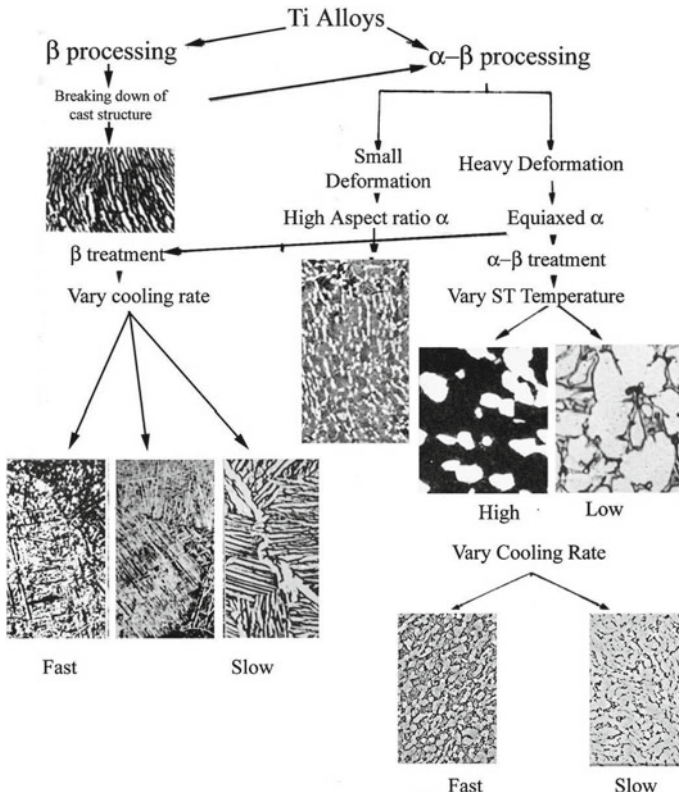


Fig. 2.3 The effect of thermomechanical processing on the formation of different microstructures in α - β titanium alloys [12]

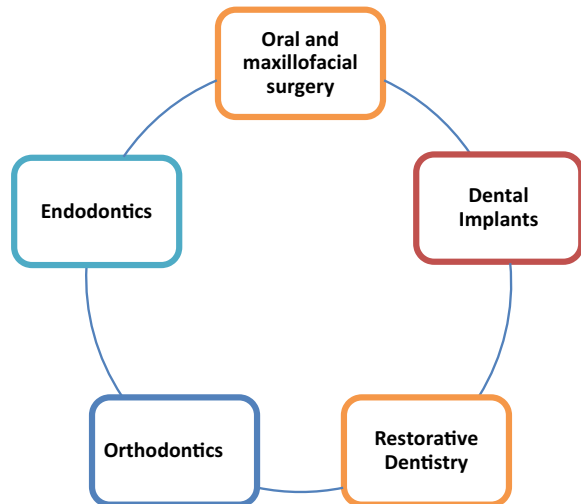
2.2 Applications of Titanium and Titanium Alloys in Dentistry

Titanium and titanium alloys are extremely interesting for applications in dentistry due to their exceptional biocompatibility, specific strength, low Young's moduli and good corrosion resistance. Their exceptional biocompatibility has been confirmed by animal tests, as well as long-term clinical trials with patients. Also, the oxidised surfaces of titanium and titanium alloys behave exceptionally well when in contact with bone, becoming osseointegrated in a very short time, with a slight fibrous layer between the bone itself and the implant [13–15]. A general overview of the application of titanium and its alloys in dentistry is given in Fig. 2.4.

Titanium alloys have relatively low values of the modulus of elasticity, which affects the reduction of the stiffness of the constructed implants. The relatively low hardness of these alloys affects their poor wear resistance.

Titanium's low density compared to other biomaterials and good mechanical as well as chemical properties are the main reasons for its use in biomedicine. However, although the modulus of elasticity of titanium is 110 GPa, which is half the modulus of elasticity of stainless steel and Co-Cr alloys, this value is still significantly higher compared to the modulus of elasticity of human bone, which is 10–40 GPa (see Table 1.6). In addition, the mechanical strength of titanium is often below the required value for replacing certain solid tissues in the human body. Given that a high value of strength and a low value of the modulus of elasticity are important characteristics that a metal material for making implants with long-term use in the body should possess, it is necessary to develop titanium-based materials further. Various thermomechanical processing procedures of this group of materials are applied in order to achieve the improvement of the mentioned combination of mechanical properties,. However, it

Fig. 2.4 Titanium and Ti alloys in dentistry



is important to mention that some of these procedures lead to an increase in both mechanical strength and modulus of elasticity. For this very reason, alloying elements are added to titanium to stabilise the β phase at room temperature, because it has been shown that alloys in which the β phase dominates in the microstructure have lower elastic modulus values, which is extremely important for their application in Implantology [16].

Commercially Pure Titanium (CPTi) is 98–99.6% pure titanium. Due to very small, but strictly defined differences in composition, there are four degrees of CPTi purity, which are marked with numbers from 1 to 4 (Table 2.2). The four grades of purity of unalloyed CPTi, which are used to make implants, actually differ in their impurity content, where oxygen, iron and nitrogen must be controlled carefully, with oxygen in particular having a large effect on flexibility and strength. A higher content of impurities in the composition of CPTi (from grade 1 to grade 4) results in a higher value of tensile strength and reduced flexibility. Thus, for example, CPTi-1 is characterised by the highest plasticity, while CPTi-4 features the highest strength and moderate deformability. CPTi-2 has a higher strength than CPTi-1 with excellent corrosion resistance, and belongs to the biocompatible materials that are often used in cases where direct contact between the implant and the bone is required. The largest number of implants are made of CPTi-2 and CPTi-4. Apart from CPTi, the Ti-6Al-4 V alloy is also used widely in biomedicine. For comparison, the chemical composition of CPTi and Ti-6Al-4 V alloy according to the ASTM F67-89 and ASTM F136-84 Standards is shown in Table 2.2 [6, 7].

CPTi, or commercially pure titanium, has a single-phase microstructure. It has extremely low levels of iron, nitrogen and oxygen, and the total amount of other elements must be less than 0.7%. In comparison to titanium alloys, pure titanium has higher corrosion resistance, whereas titanium alloys have higher resilience to extreme temperatures and greater weldability than alloys, but poorer strength and formability.

Table 2.2 Chemical composition of CPTi and Ti-6Al-4V alloy [in wt.%] [6, 7]

	CPTi-1	CPTi-2	CPTi-3	CPTi-4	Ti-6Al-4 V
	(ASTM F67-89)				(ASTM F136-84)
N	0,03	0,03	0,05	0,05	0,05
C	0,10	0,10	0,10	0,10	0,08
H	0,015	0,015	0,015	0,015	0,0125
Fe	0,20	0,30	0,30	0,50	0,25
O	0,18	0,25	0,35	0,40	0,13
Al	–	–	–	–	5,50–6,50
V	–	–	–	–	3,50–4,50
Ti	Rest	Rest	Rest	Rest	Rest

Commercially pure titanium is largely utilised in dentistry to make dental implants, but it is also employed in orthopaedics in the form of wire meshes that act as porous coatings sintered on the surface of titanium alloy artificial joints.

Alloy Ti-6Al-4 V Long-term research has developed two-phase α - β alloys, with a dispersed β phase in the α phase successfully, with excellent characteristics of both phases. A two-phase α - β alloy that has found wide application in medical engineering is the Ti-6Al-4 V alloy. The microstructure, and therefore the properties of this alloy, depend largely on the thermomechanical treatment to which it is exposed during production, so the tensile strength can range from ~ 930 MPa for the cast state, and up to ~ 1200 MPa for the solvent, annealed and aged states. The alloy, in the composition of which the content of impurities is reduced in order to improve toughness at low temperatures and resistance to crack propagation, is called an alloy with extremely low interstitials (ELI), that is, the ELI Ti-6Al-4 V alloy [7].

2.2.1 Mechanical Properties

The relatively low values of the modulus of elasticity, characteristic of titanium alloys, affect the reduction of the stiffness of the constructed implants without the need to change their shape. A good example of this is the values of the axial, bending and torsional stiffness of bone fixation plates made of titanium alloy, which are half as low as those of bone fixation plates of the same dimensions and shape, but made of stainless steel or cobalt alloy. For this reason, in the case of the application of fixation plates, which are attached rigidly to the human bone, the stress present in the bone would be significantly less when applying titanium alloys. These considerations of the mechanical properties of titanium alloys have confirmed that these alloys are ideal for the production of aids for the fixation of spinal vertebrae and broken bones, including the manufacture of plates, angles and screws, but also as a basis for the manufacture of artificial joints and joint implants.

The relatively low hardness of titanium alloys, however, affects their poor resistance to wear, so these alloys, without previous additional surface treatment such as ion implementation, cannot be used for the production of joint surfaces. Regardless of many years of clinical trials, which have shown the excellent biocompatibility of titanium alloys, there is still a fear of the release of toxic elements such as vanadium, which is why new titanium alloys in which vanadium has been replaced by a more inert material have begun to be introduced into biomedical engineering elements, such as niobium.

The modulus of elasticity of characteristic biomedical titanium alloys were compared in Fig. 2.5. As can be seen, the modulus of elasticity of β -type titanium alloys is 55 to 85 GPa, and these values are significantly lower than the modulus of elasticity of biomedical titanium alloys α and type α - β , so lately β -type titanium alloys have been developed intensively for use in biomedicine [1, 2, 17].

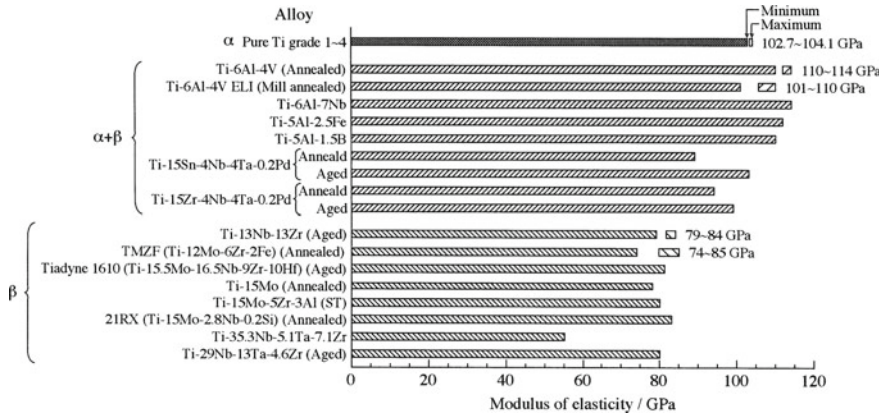


Fig. 2.5 Overview of the modulus of elasticity of biomedical Ti alloy [17]

2.2.2 Elements of Choice of Alloying Elements of Titanium

The disadvantage of titanium-based implant materials is relatively weak mechanical strength, which reduces the possibility of their application in places in the human body that are exposed to high loads. In addition, although titanium has a lower modulus of elasticity compared to stainless steel and Co-Cr alloys, the value is still much higher compared to the modulus of elasticity of bone, so the placement of titanium implants can lead to bone atrophy and slow down the healing process. In order to make titanium implants that will perform a supporting function and be compatible with the human tissues with which they are in contact, alloying elements that should increase the strength and reduce the elasticity modulus of titanium are added to titanium, where it is extremely important that the alloying elements are non-toxic α .

Previous research indicates that titanium is safe for use in the human body because it is biocompatible and does not cause allergic reactions. It was found that Ta, Nb and Zr are the most optimal alloying elements, which are non-toxic and compatible with living tissues, on the one hand, and non-allergenic on the other. Also, alloying titanium with neutral elements (Zr) and β stabilisers (Mo, Ta, Nb) leads to a decrease in the modulus of elasticity, which makes the manufactured implant more mechanically compatible with solid tissues in the human body, which reduces the possibility of bone atrophy and/or rejection of the implant further [17–21].

α - β Ti alloys, such as Ti-6Al-4 V and Ti-6Al-4 V ELI (Extra Low Interstitial, ELI) alloys of higher purity, were developed primarily as structural materials in the aviation industry, while later they found application in biomedicine. The Ti-6Al-4 V ELI alloy is very similar to the Ti-6Al-4 V alloy, with the difference that it contains a lower percentage of O, C, N, and H, which provides greater strength, improved toughness at low temperatures, and greater resistance to crack propagation. Ti-6Al-4 V alloy has more favourable mechanical properties than CPTi, i.e. it is characterised

by higher strength and resistance to wear, so it is used in conditions of greater load on implants, unlike CPTi, which is used in places where wear resistance is not of primary importance. Due to the aforementioned mechanical characteristics, the Ti-6Al-4 V alloy is often used to make implants in dentistry. However, numerous studies have shown that V, β , the stabilising element of the Ti-6Al-4 V alloy, is extremely toxic, both in its elemental state and in the form of the oxide V_2O_5 present on the surface of the Ti-6Al-4 V alloy. Also, Al, an α stabilising element, leads to allergic reactions. By the way, the presence of V and Al is associated with the development of Alzheimer's disease, neuropathy and other neurological disorders, so, in the literature, you can find test results that prove that the application of various techniques of subsequent surface treatment of the Ti-6Al-4 V alloy improves its biocompatible properties. So, for example, Ti-6Al-4 V alloy, sandblasted with aluminium oxide and passivated in the presence of nitric acid, subjected to biocompatibility tests, showed that it exhibits neither cytotoxic nor genotoxic properties and can be used safely in dentistry [21].

Due to the confirmed cytotoxic effect of V and the allergenic effect of Al, there was a need to develop new titanium alloys for use in medicine and dentistry. Thus, the Ti-6Al-7Nb and Ti-5Al-2.5Fe alloys were developed, which were obtained by replacing V with Nb and Fe, and which are much safer, and safer for use in the human body. The mentioned alloys, which belong to α - β type Ti alloys, have recently been used intensively in biomedical engineering, whereby the Ti-6Al-7Nb alloy, was developed in the USA, and the Ti-5Al-2.5Fe alloy in Europe, (Table 4.4). Based on a similar concept, other biomedical alloys of the α - β type, such as Ti-6Al-2Nb-1Ta and Ti-15Al-4Nb-4Ta, were developed, in which the V is replaced by Nb and Ta. Also, α - β type titanium alloys that do not contain either V or Al, and which contain Zr or Sn, such as Ti-15Zr-4Nb-4Ta and Ti-15Sn-4Nb-2Ta-0.2Pd, have also been put into practice [17, 18].

Of the β -type titanium biomedical alloys, the Ti-13Nb-13Zr and Ti-12Mo-6Zr-2Fe alloys are registered according to the ASTM Standard. The Ti-13Nb-13Zr alloy, developed in the USA, is characterised by a low value of the elastic modulus and significantly improved strength compared to the Ti-6Al-4 V alloy, which is why it is interesting for use in Implantology. The presence of Nb and Zr leads to the formation of a passive film on the surface of the alloy, which has exceptional protective properties and reduces the degradation of the material in the corrosive conditions of the human body. In addition, research has shown that the Ti-13Nb-13Zr alloy does not exhibit a cytotoxic effect, that is, it is safe for use in biomedicine. Also, Liu et al. produced Ti-Zr-Nb alloys with different Nb content (Ti-(5,10,15)Nb-9Zr), and, in their studies, showed that the Ti-15Nb-9Zr alloy is characterised by an elastic modulus of 39 GPa and a tensile strength of 850 MPa, which makes it an excellent material for making implants [20].

The strategy in the development of new alloys for use in medicine and dentistry is to replace potentially toxic and allergenic elements with elements that are safer for use in the human body, as well as to achieve lower values of the modulus of elasticity. Therefore, the goal of the further development of metal biomaterials is the production of new alloys that possess outstanding chemical, mechanical and biological compatibility. In this regard, a large number of titanium alloys that have

been developed in recent years contain the biocompatible elements Zr, Nb, Mo and Ta, and exhibit excellent mechanical properties, including low elastic modulus, high strength and improved toughness. Also, the latest biocompatible titanium alloys containing a large percentage of Ta and Nb (e.g, Ti-15Zr-4Nb-4Ta), whose melting point and density are much higher compared to titanium, condition the development of new technologies for making these alloys [17].

2.2.3 Formation of a Surface Oxide Layer on Titanium

Titanium is a very reactive metal and oxidises almost instantly in the presence of oxygen in air, water and/or body fluids. An oxide film consisting of amorphous or low-crystalline and non-stoichiometric TiO_2 forms spontaneously on the surface of titanium. It is important for the application of titanium in biomedicine that the TiO_2 formed in this way is stable, resistant to corrosion, bio inert, and has excellent biochemical characteristics that are important for the integration of the implant with the surrounding bone tissue. It should be emphasised that the mechanically damaged oxidised surface of titanium regenerates very quickly, that is, the oxide layer is formed again. Therefore, one of the main reasons for the corrosion resistance of titanium implants is the spontaneous and rapid formation of a thin solid surface layer of a stable and inert oxide. At the same time, it is a stable product of the in vivo reaction, which results in complete or partial passivation of the material.

Titanium, as a very reactive element, which reacts easily with oxygen, nitrogen, carbon and other elements, reacts with water molecules in the solution and/or with moisture from the air, forming a thin oxide layer on its surface. In fact, an oxide layer with a thickness of about 1 nm is formed spontaneously on the surface of titanium within one millisecond, and, within the first minute, the thickness of the oxide layer is about 10 nm. Many research groups have investigated the surface oxide layer formed on titanium using various methods, and concluded that the surface layer contains TiO_2 , TiO , Ti_2O_3 , Ti_3O_2 and Ti_3O_5 , and that its thickness is in the range of 4.9–12.5 nm [22]. A schematic view of the contaminated oxide film formed at room temperature on pure titanium is shown in Fig. 2.6.

It is known that, even after the formation of a protective oxide film, the surface is still reactive, that is, the titanium continues to react with moisture from the air, whereby hydroxyl groups are formed on the surface in 30 ms. Hydroxyl groups become ionised in solution, and the surface charge increases depending on the pH value of the medium. The positive and negative charges are equalised at a certain pH so that the total charge is zero. This pH value is known as the isoelectric point (IEP; point of zero charge, pzc). The IEP value is unique for each oxide, so for TiO_2 rutile it is 5.3 and for anatase 6.2. In the case of TiO_2 anatase this actually means that, in solutions with a pH lower than 6.2, the positive charge will overpower the negative, while, in solutions with a pH higher than 6.2, the negative charge will overpower the positive [23]. The IEP value for different oxides is shown in Table 2.3.

Fig. 2.6 The illustration of oxide film growth on pure titanium

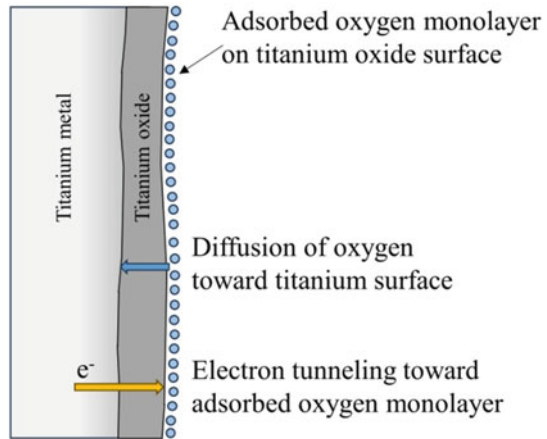


Table 2.3 IEP values for different oxides

Oxide	IEP value
SiO ₂	2,0–3,7
SnO ₂	4,7–5,3
TiO ₂ rutil	5,3
TiO ₂ anatas	6,2
Fe ₂ O ₃	6,6–6,7
Cr ₂ O ₃	7,0
Al ₂ O ₃	9,0

In the event that the surface oxide layer is damaged, a new oxide layer forms quickly which covers the surface, making it inert. One of the reasons for the good corrosion resistance of titanium and its alloys is precisely the tendency of titanium to repassivate the surface, which occurs spontaneously after the appearance of damage to the passivating oxide layer.

At the macroscopic level, the passive oxide film on the titanium surface is undissolved and very stable, while repeated partial processes of dissolution (solubilisation) and re-formation (reprecipitation) can be observed at the microscopic level. When titanium-based materials are incorporated into the human body, ions and molecules are incorporated into the surface oxide film, so it can be said that the structure of the oxide film is changing constantly in accordance with the biological environment.

Surface analysis of surgically installed implants made of titanium-based materials shows that the chemical composition of the oxide film changes by incorporating Ca, P and S, and the extremely rapid formation of calcium phosphate is the reason for the strong compatibility of titanium and its alloys with solid tissues. By simulating biological conditions in vitro, it was shown that by immersing titanium and its alloys in Hank’s solution, calcium phosphate is deposited, while sulfites and sulfides are

formed in conditions where cells are present. This further indicates that the physiological processes occurring in the organism can be simulated very well by *in vitro* experiments. Calcium phosphate is also formed on the surface of stainless steel and Co-Cr alloys, however, the rate of formation and Ca/P ratio is much higher in titanium and the Ti-6Al-4 V alloy [21].

A passive oxide film can form spontaneously on the surface of certain metals, or be obtained by chemical (e.g. immersion in nitric acid), electrochemical (anodisation) and thermal (air oxidation) treatment in the final stage of implant manufacturing [24]. Chemical changes of the titanium surface followed by thermal treatment lead to the formation of a TiO₂ hydrogel on the surface of the TiO₂ oxide layer [25].

The layer of TiO₂ hydrogel formed in this way enables a better union of hydroxylapatite, which further enhances the integration of living bone with the metal implant.

In the final consideration we can state that the formation of a stable oxide film on the surface of titanium and its alloys is the basis of the corrosion resistance and biocompatibility of these materials. Titanium oxidises by building an oxide film that is less reactive than pure titanium because it contains grain boundaries and structural defects, which protects the material from further oxidation. It should be emphasised that the mechanically damaged titanium surface regenerates very quickly, i.e. the re-formation of the oxide layer occurs quickly through the repassivation process. Therefore, one of the main reasons for the outstanding corrosion resistance of implants made of titanium-based materials is precisely the extremely fast formation of a thin solid surface layer of stable and inert oxide. In addition, for the application of titanium in biomedicine, the outstanding biochemical characteristics of TiO₂ are important, such as the ability to hydrate (TiO₂ adsorbs 2–3 water molecules per 1 nm²), adsorption of inorganic ions (Ca²⁺, PO₄³⁻) and organic macromolecules (proteins, lipoproteins, peptides), and interactions of TiO₂ that adsorbed inorganic ions and organic macromolecules with fibrin fibres and osteoblasts.

The mentioned properties of the oxide film are of exceptional importance for the integration of titanium-based implants with the surrounding bone tissue. For example, Pilliar [26] indicates that the formed protective oxide layer with a thickness of 5–10 nm remains on the surface of titanium even after *in vivo* application, which confirms its persistence and stability. Simply put, the oxide film *in vivo* passivates the material and provides an effective barrier for the transport of ions or electrons, thus reducing the possibility of material degradation as a result of corrosion.

Surface structural changes can be very complex. So, Fig. 2.7 indicates roughly how such electrolyte-surface reactions might impact the chemistry in the oxide film and at the oxide film surface. It can be observed that the titanium oxide surface clearly has the benefit of binding both calcium and phosphate [27].

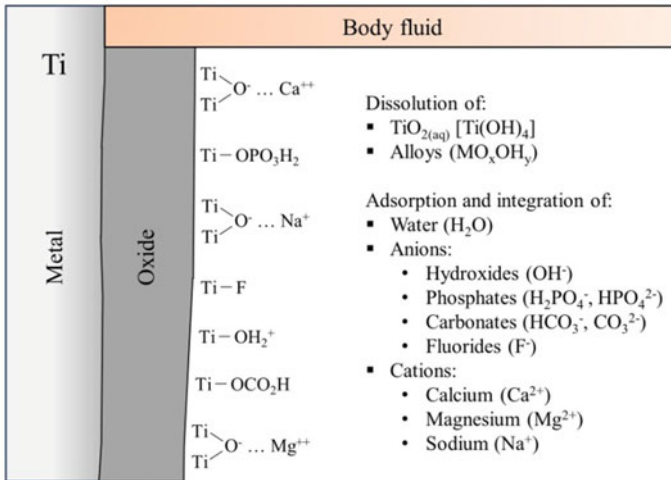


Fig. 2.7 The illustration of adsorption or integration of elements of a simulated or actual body-fluid electrolyte onto or into the oxide layer

2.2.4 Elements of Production

Casting and machining of titanium-based materials are extremely complex and require special conditions and precision [9]. Unlike thermal processing, mechanical processing of titanium (forging, rolling, bending) is a simpler shaping technique when it comes to dental implants. However, when making alloys for dental applications, the casting process is dominant, and cast titanium alloys are characterised by very small elongations and high strength values (see Table 2.4). The main problems that arise in the production of dental implants by the casting process are the pronounced reactivity of titanium alloys and their high melting temperature compared to other dental alloys, such as gold and silver alloys. For this reason, the choice of titanium alloys for dental applications is often based not only on their properties, but also on the value of the melting temperature, and during their production it is necessary to use weakly reactive casting moulds. The most commonly used method for manufacturing dental implants and devices is precision casting.

The complexity of the production of these alloys can be shown as follows. The sequence of microstructure development with processing is illustrated schematically in Fig. 2.8., coupled with a description of the accompanying texture. The capacity to model these microstructural variants and their underlying texture will be required to have a thorough knowledge of the plasticity of these materials and their fracture. Figure 2.8 [10] illustrates the progression of microstructure formation with processing, and aims to describe the already known texture development, so it is appropriate to compare this Fig. 2.8 with Fig. 2.3.

Table 2.4 Selected mechanical properties of titanium and titanium alloys for use in dentistry [9]

Alloy	Process	Tensile strength [MPa]	Yield strength [MPa]	Elongation [%]	Vickers hardness [HV]
Ti-20Cr-0.2Si	Casting	874	669	6	318
Ti-25Pd-5Cr	Casting	880	659	5	261
Ti-13Cu-4.5Ni	Casting	703	/	2,1	/
Ti-6Al-4V	Casting	976	847	5,1	/
Ti-6Al-4V	SPD ^a	954	729	10	346
Ti-6Al-7Nb	Casting	933	817	7,1	/
Ti-Ni	Casting	470	/	8	190

SPD^a (Severe Plastic Deformation)

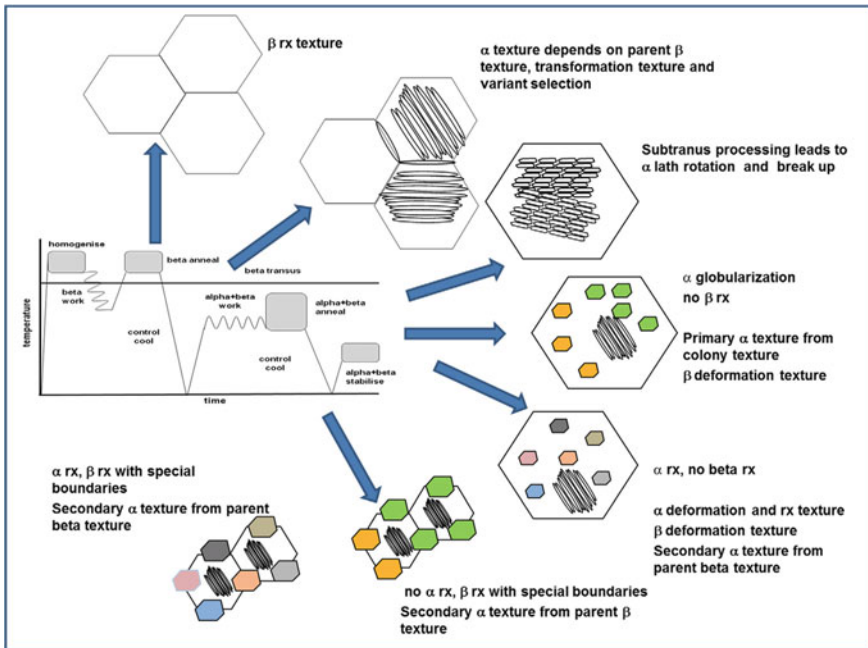


Fig. 2.8 A diagram illustrating the processing course and texture formation in titanium alloys [10]

2.3 Implant Osseointegration

Dental implants are utilised commonly in modern dentistry to replace lost teeth. As important factors influencing implant osseointegration, the form, chemical content, and macro and microtopography [28] of the implant surface have all been researched widely. Osseointegration [29] is a biological process that involves direct structural

and functional contact between vital bone and a non-vital implant without the insertion of connective tissue. Titanium and titanium alloys have been used widely as biomedical materials in orthopaedic and dental surgery for over 20 years, due to their high mechanical properties, corrosion resistance, lack of cell toxicity, and very low inflammatory response in peri-implant tissues, demonstrating high biocompatibility. A thin native oxide film that forms spontaneously on the titanium surface contributes to their good biological performance. The titanium surface can be changed chemically or physically, or both, to promote biomaterial-tissue interaction.

Osseointegration is the direct, structural, and functional connection that occurs between a crucial bone and the implant surface without the presence of soft tissue. Albrektsson and colleagues [30] identified the qualities required for rigid osseointegration as biocompatibility, shape, implant surface, implant site, surgical method and loading conditions.

However, seeing osseointegration as a prerogative of any implant device is wrong, because it does not generate the same effects, such as in bone of poor quantity and quality.

Titanium (Ti) possesses two extremely valuable metal properties: corrosion resistance and the best strength-to-weight ratio of any metal. It is also unalloyed, stronger than certain equivalent materials such as contemporary steel, and 40% lighter. Ti can be alloyed with a variety of elements to boost its strength and formability (Al, V, Nb, Zr). It also possesses high temperature performance, creep resistance, weldability, heat treatment reaction to ageing and formability. Because of the creation of an insoluble and continuous titanium oxide layer on the surface with one of the highest temperatures of reaction: $H = -912 \text{ kJ/mol}$, Ti and its alloys are corrosion resistant. The oxide (often TiO_2) develops in air in nanoseconds (10^{-9} s) and grows to a thickness of 20–100 Å in 1 s. This oxide binds strongly to the parent Ti, protects it from other contaminants, and is oxygen impenetrable. In addition, the oxide on the Ti-surface contributes to Titanium's high biocompatibility. Commercially pure (Cp) Ti is available in four grades (1–4), with different levels of oxygen (0.18 to 0.40 wt.%) and iron (0.20 to 0.50 wt.%). These slight concentration changes have a major impact on the physical characteristics of the metal. Oxygen, in particular, has a significant influence on Ti's ductility and strength [1–7]

A foreign body response occurs when a dental or orthopaedic implant is inserted into bone tissue. This response is divided into five stages: (i) Blood-material interactions, (ii) Blood clot formation, (iii) Inflammatory responses, (iv) Callus formation, and (v) Bone remodelling. Platelets, neutrophils, monocytes, macrophages, lymphocytes, stem cells, endothelial cells, osteoclasts and other cells all engage in this process and impact each other at various stages [14]. Specifically, shortly after implantation, a protein coating forms on the surface of implants. Platelets will be activated and adhered to the surface of the blood, triggering blood coagulation and complement system activation. Neutrophils are recruited to start the acute inflammatory response. The monocytes attracted to the biomaterial-tissue interface will differentiate into macrophages in an effort to phagocytose the implant, potentially resulting in chronic inflammation. The number of macrophages usually peaks at around one week and then declines. The adaptive immune system, which is controlled primarily

by infiltrating lymphocytes, dominates the subsequent immune reaction. Following that, stem cells and endothelial cells are recruited to aid in the remodelling stage, which is influenced primarily by osteoclasts and osteoblasts. These events involve a number of distinct molecular and cellular actors, who work together to integrate the dental implant successfully into the bone tissue. Modifying the physicochemical surface properties of implants can influence these biological processes [14, 30, 31].

The majority of these features were utilised in the development of a new mathematical model based on a mechanobiological approach [31]. The initial biological cascade of events that occurs after the placement of a dental implant is illustrated schematically on Fig. 2.9.

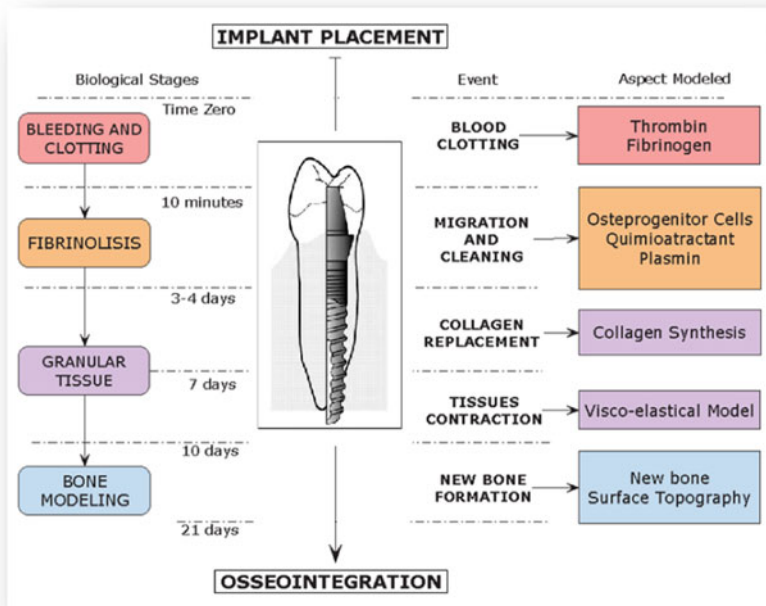


Fig. 2.9 A schematic of a mechanobiological approach of dental implant osseointegration. The sequence of biological phases is depicted on the left, and the events and aspects modeled at each stage are depicted on the right. The boxes summarize the most significant elements used at each step, as well as the simplifications made to the complicated chain of biological and mechanical phenomena that leads to dental implant osseointegration

2.4 Surface Modification of Dental Implants

A dental implant’s shape has been explored thoroughly, providing medical professionals and scientists with implants of acceptable macrodesign and varied dimensions that allow for successful osseointegration. Screw-shaped endosseous implants with parallel or tapered (root-like) sides are the most often utilised implants. The advancement of biomaterials in modern Implantology is linked to the improvement of implant micro design, which leads to the creation of various implant surface modification ideas [32–36].

Surface roughness is well known to play an essential role in implant fixation. Implants with rough surfaces outperformed previously used implants with machined polished surfaces in terms of bone apposition and regrowth on the bone-to-implant contact. Figure 2.10 depicts the distribution of surface roughness of effectively implanted and clinically biofunctional materials. Surface roughness manipulated to a range of 1–50 μm is associated with a good implant survival rate. As a result, some authors proposed that there is a desirable roughness range. A moderate surface roughness of 1.5–5 μm is expected to benefit the healing process and implant primary stability [34].

Mechanical, chemical and physical techniques, as well as their combinations, are used to modify implant surfaces. Mechanical techniques, such as machining, grinding, polishing and blasting, involve the physical shaping or removal of a material’s surface. Mechanical surface modification goals include obtaining specific surface topographies and roughness, removing surface contamination, and/or

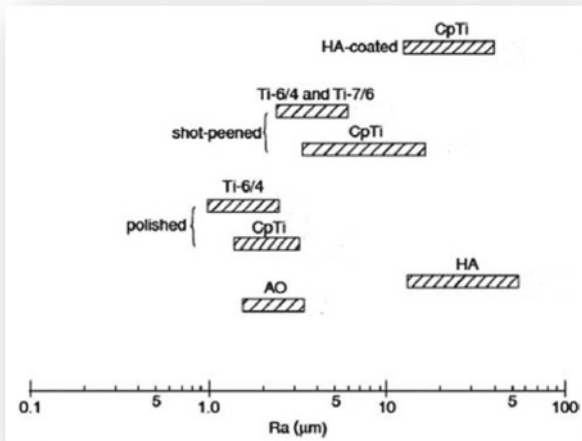


Fig. 2.10 Distribution of diverse Ti implant surface roughness. AO–anodic oxidation, HA–hydroxyapatite

improving adhesion in the following bonding stages. Chemical therapy, electrochemical treatment (anodic oxidation), sol–gel, chemical vapour deposition (CVD), and biochemical modification, are all examples of chemical methods. Electrochemical or biochemical reactions occur at the interface between the titanium and a solution during the aforementioned therapies. Thermal spraying and physical vapour deposition are examples of physical techniques that do not involve chemical reactions. Thermal, kinetic and electrical energy are primarily responsible for the creation of surface modified layers, films, or coatings on titanium and its alloys.

Different treatments are used in practice to alter the titanium surface [32]. Hydrox-apatite coatings are used to produce a rough, potentially bioactive surface, whether or not they are preceded by acid etching. Oxide blasting procedures, with or without chemical etching, are used to produce rough surfaces, and thick oxide layers obtained by anodic or thermal oxidation are now employed to expedite the osseointegration process. Other parameters that may influence bone bonding include oxide thickness, crystallinity, and ions in the exterior layer.

As a consequence, because it is challenging to link surface properties to clinical outcomes, the ideal microtopography of the surface remains unknown. Although more precise information is needed, various surfaces have undergone controlled clinical trials and are commercially available.

In the last 50 years, titanium implants have gone through many surface-modification revolutions [14], (see Fig. 2.11).

On the other hand, titanium surface treatment trends are shown in Fig. 2.12. The use of plasma spraying and acid etching techniques has sparked the most enthusiasm. The plasma spray method is clearly preferred, due to its advantages in producing porous implant surfaces for increased bone contact. The coating surface's characteristics are influenced heavily by the coating materials used. Aside from that, research

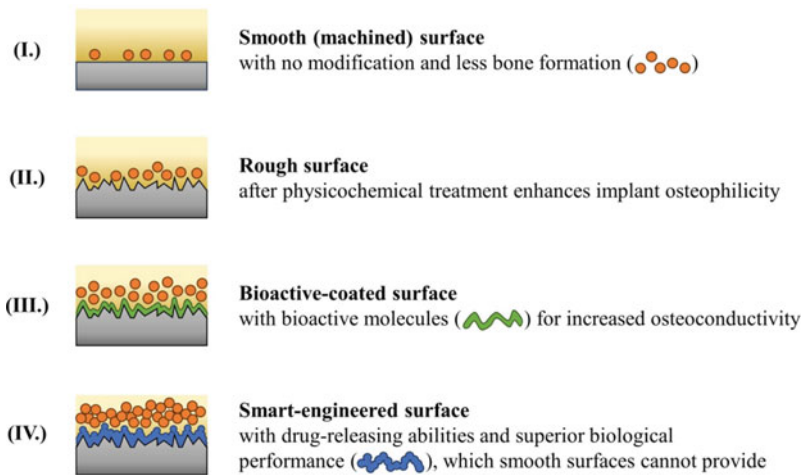


Fig. 2.11 The revolution in implant surface engineering for osseointegration

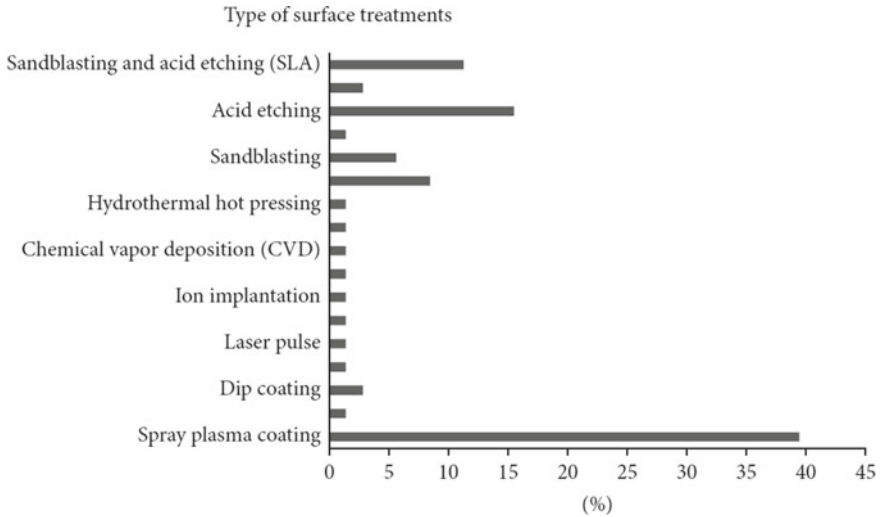


Fig. 2.12 Frequently used surface treatments on Ti implants [36]

on plasma spray revealed excellent growth cells on the implant surface and good bone contact, which accelerated bone formation [36].

2.4.1 Micro Level Surfaces

The following options are available [37]:

Mechanical methods: (a) Machining, (b) Grinding, (c) Polishing, and (d) Blasting, involve physical treatment, shaping, or removal of the material's surface.

The typical objectives are to: (I) Obtain specific surface topographies and roughness, (II) Remove surface contamination, and/or (III) Improve adhesion in subsequent bonding steps.

Chemical methods: (a) Chemical treatment, (b) Electrochemical treatment (anodic oxidation), (c) Sol-gel, (d) Chemical vapour deposition (CVD), and (e) Biochemical modification.

During the chemical treatment, electrochemical treatment and biochemical modification, chemical, electrochemical or biochemical reactions occur, respectively, at the Ti interface.

Physical methods: (a) Thermal spraying, and (b) Physical vapour deposition (PVD), Chemical reactions do not occur. The formation of a surface modified layer, films or coatings on titanium and its alloys are attributed mainly to the thermal, kinetic and electrical energy.

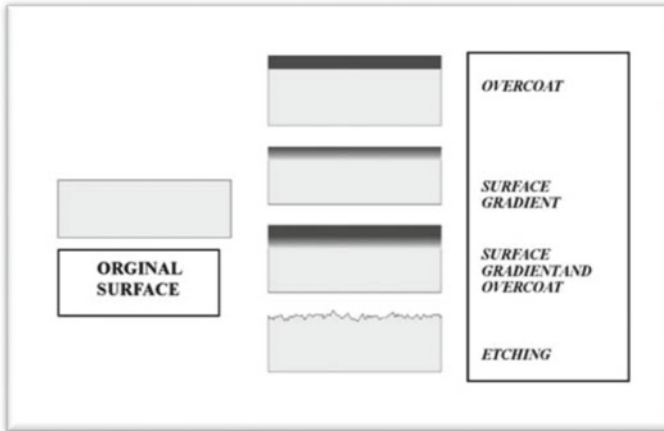


Fig. 2.13 Different plasma approaches for modifying biomaterial surfaces are represented schematically, adapted from [38]

Plasma-surface modification (PSM) is an efficient and cost-effective surface treatment technology that has the unique feature of enhancing surface properties and biocompatibility while leaving the bulk properties of the materials unchanged [38], Fig. 2.13.

Laser-surface modification, often known as laser surface texturing [39], is a relatively new and popular surface modification technique. Its benefits are related with accurate, targeted and directed surface roughening, as well as control over the roughening dimension. Controlled surface roughening can produce an acceptable micron-scale topography in relation to the shape, structure and orientation of bone cells.

2.4.2 Surfaces with Nanostructures

There has been a rise of interest in the possible impact of nanostructured implant surfaces on bone healing and apposition in recent years. The shape and chemistry of the Ti implant surface can both be altered at the nanoscale.

The following are examples of nanoscale surface changes (Fig. 2.14) [40]:

- (A) Self-assembled monolayers that can modify the surface chemistry and topography, resulting in novel physical and/or biological surface properties.
- (B) Nanoscale ($x \leq 100$ nm) deposition and chemical modification techniques that can achieve a micron-scale distribution ($y \geq 100$ nm)
- (C) Nanoscale ($x \leq 100$ nm) compaction approaches that can realise a distribution on the nanoscale
- (D) Nanoscale ($x \leq 100$ nm) isotropic surfaces obtained by subtractive and additive methods. The distribution can take place at either the nano or micron sizes.

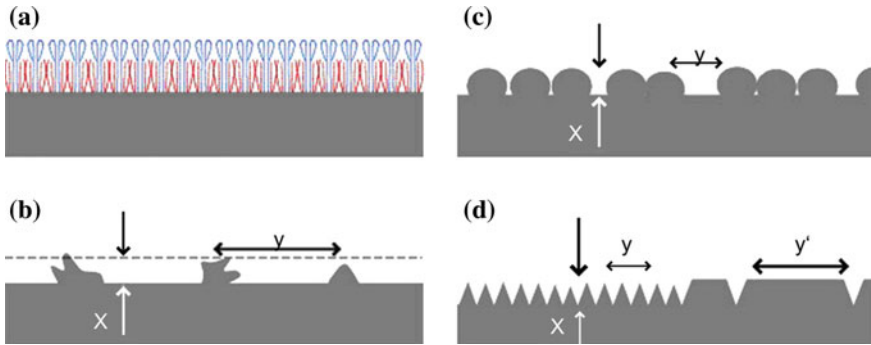


Fig. 2.14 Surface change at the nanoscale [40]

Surface modification methods that have been created on an atomic (nano) scale include:

- Monolayer self-assembly.
- Physical method (particle compaction, ion beam deposition).
- Chemical method (acid etching, peroxidation, NaOH oxidation or anodisation).
- Deposition of nanoparticles (sol–gel, crystalline deposition).
- Photolithography.

When cells come into contact with nano-modified surfaces, several cell reactions such as protein adsorption, cell adhesion, cell proliferation, or cell differentiation and spreading can be expected.

To date, three types of nano-structured surface modification have been developed in contrast to typical micron-structured surface modification:

1. Nano-structured diamond covering on the surface (diamond like carbon, DLC). Mechanical qualities such as hardness, wear resistance, corrosion resistance, and longevity have been improved, as has biocompatibility. CVD is used to apply the layers to the device surface.
2. Surface coating with hydroxyapatite (HA) or crystalline Calcium phosphate (CaP) nanoparticles, which improves both bone and metal interaction. When compared to microparticle coatings of the same materials, abrasion and particle loosening are reduced, reducing the negative characteristics of these materials. It has been demonstrated that HA nanoparticles enhance osteoblast adhesion, proliferation and mineralisation.
3. Surface coating of ceramic-fused-to-metal compounds improves chemical bonding, resulting in increased hardness and wear resilience.

Nanotopography alters cellular responses. Surface nanotopography appears to influence cell interactions at surfaces, and affect cell activity when compared to standard sized topography (Fig. 2.15). There are distinct physical relationships between cells and surface characteristics at the nano-, cell-, and micron scales [41]. Nanotopography has been found to influence cellular behaviour in a range of cell

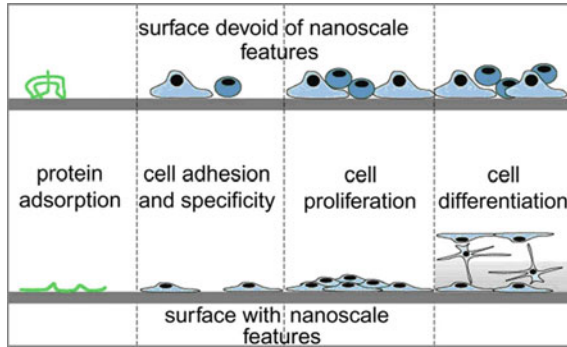


Fig. 2.15 Illustrates a broad spectrum of nanoscale topographical effects discovered in cellular protein adsorption that are affected by nanoscale bulk material alteration. Cell specificity and cell adhesion extent are both altered. Cell spreading can be boosted or diminished, depending on the nano-architecture. Cell proliferation appears to be aided by nanoscale topography via currently unknown processes. Several studies have indicated that nanoscale topography improves osteoblast differentiation [40].

types, including epithelial cells, fibroblasts, myocytes and osteoblasts. Nanostructured surfaces have distinct properties that influence cell adhesion via both direct (cell-surface interactions) and indirect (protein-surface interactions).

2.4.3 Example of Etching

Etching is used to modify the surface of titanium in order to improve implant function in bone [42, 43].

Fluoride-modification of dental titanium (Ti) implants is employed in this study [42] to increase peri-implant bone development, bone-to-implant contact, and adhesion strength. The surface topography, chemistry, and biocompatibility of polished Ti surfaces treated with hydrofluoric acid solution (HF) were investigated in this study. The 60 polished and cleaned titanium disks were subjected to fluoride alteration by HF treatment, whereas 15 disks were left unmodified as a control group. The 60 disks were divided into four groups of 15 and immersed in a 50 ml disposable high density polyethylene (HDPE) beaker filled with 0.2 vol.% HF at pH 2.1 for 40, 90, 120, or 150 s (groups 1, 2, 3, and 4). Figure 2.16 shows blue light interferometer, SEM and AFM images of the modified titanium disks in 0.2 vol.% HF.

We can conclude as follows: Both the exposure time and the initial surface topography influence the change of the titanium surface when exposed to 0.2% HF. This surface modification process is most reproducible when these two factors are well controlled. It is probable that the combination of reduced hydrocarbon content, fluoride, hydride, and oxide presence, and the micro and nano-level topography

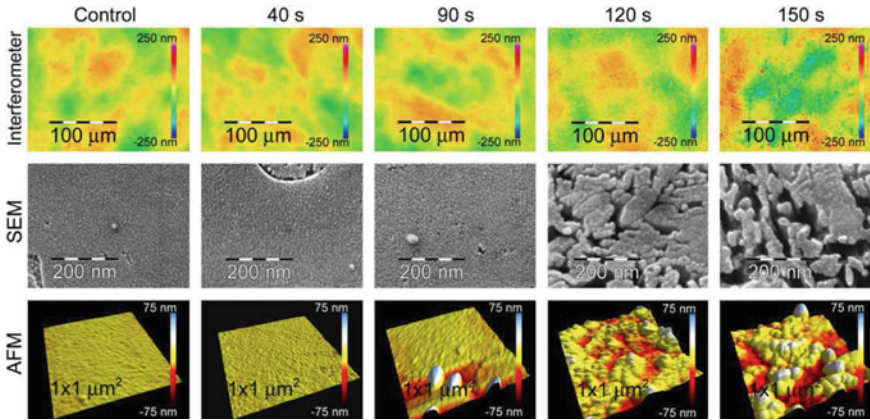


Fig. 2.16 Images from the blue light interferometer, SEM, and AFM of the modified titanium disks in 0.2 vol.% HF. Topographical alterations at the micro and nano-levels were found as a function of HF immersion time, particularly after 120 and 150 s [42]

formed by HF treatment creates a favorable environment for cell growth with better biocompatibility.

2.4.4 Example of Surface Sol-Gel Processing (SSP)

Surface sol-gel processing (SSP), a variation on the bulk sol-gel technique, is a relatively novel method for producing bioreactive nanostructured titanium oxide for thin film coatings. Atomic force microscopy (AFM) and X-ray photoelectron spectroscopy (XPS) were used to analyse the surface topography, roughness and composition of sol-gel produced Ti6Al4V titanium alloy coatings [44].

Surface sol-gel processing, a variation of the bulk sol-gel dip-coating procedure, can be utilised to create ultrathin metallic oxides with nanoscale precision. The layer-by-layer procedure begins with the chemisorption of a hydroxyl functionalised surface in a metal alkoxide solution, followed by rinsing, hydrolysis and drying of the film, as shown in Fig. 2.17. This sol-gel reaction occurs on the substrate's surface each time the hydroxyl groups TiOOH are regenerated, to form a monolayer of TiO₂, and repeating the process results in multilayers of the thin oxide film. If a denser or more crystalline oxide is needed, a calcination or sintering procedure may be used, although this is frequently unnecessary. The technique, which employs a metal alkoxide reactive to OH groups, is applied easily to any hydroxylated surface, and the sol-gel approach is independent of each cycle, allowing individual layers to be nanostructured [44].

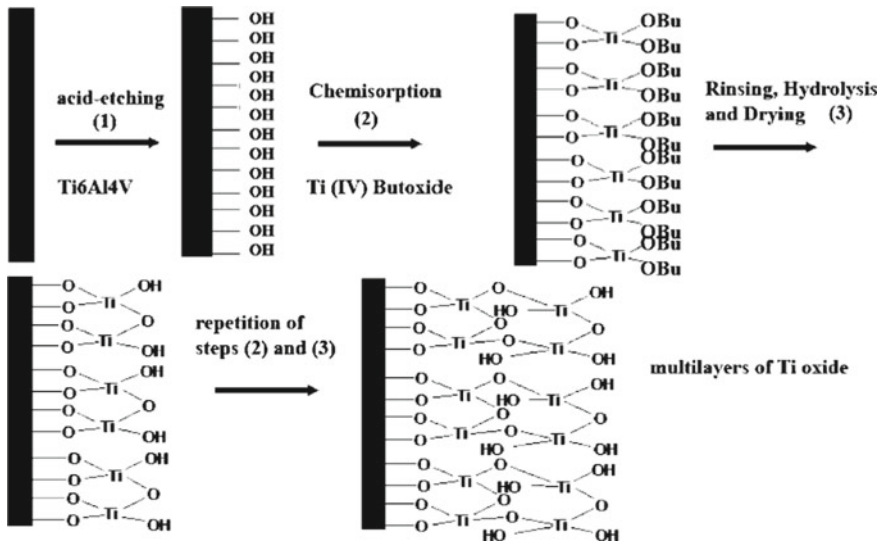


Fig. 2.17 The layer-by-layer SSP deposition operations are illustrated schematically. Surface sol-gel technique on Ti6Al4V substrates, including the following steps of (1) hydroxylation of the substrate using Piranha acid, (2) immersion of the substrate in a titanium solution (Ti) butoxide in 1:1 toluene: ethanol, and (3) washing, immersing, and drying the substrate. The oxide forms multilayers as the process of chemisorption, rinsing, hydrolysis, and drying is repeated [44]

2.4.5 Example Using a Variety of Methods and Materials

Surface modification at the nanoscale can be accomplished using a variety of methods and materials. One option is to use a dental alloy with a high gold content due to gold's exceptional biological compatibility, as well as its high electrochemical resistance, functionality and longevity. Gold is resistant to oxidation and plaque formation and is compatible with gingival tissues [45].

The potential effects of gold nanoparticles (GNPs) on the promotion of osteoblast development make them interesting materials for use as osteogenic agents. This study used an osseo-integrated titanium (Ti) implant surface coated with GNPs to encourage bone repair. Three-Mercaptopropyl trimethoxysilane (3-MPTMS) was used to treat the silanised Ti surface chemically, and Au-S bonding was used to fix the GNP layer (Ti-GNP) on the surfaces. The GNP layer's homogeneous immobilisation on the surface and its appropriate coverage of the titanium oxide surface were both confirmed by Atomic Force Microscopy (AFM) and Scanning Electron Microscopy (SEM).

Osteointegration is one of the most crucial elements in determining whether bone-anchored metallic implants in dentistry are successful or unsuccessful. Successfully anchored metallic implants fuse with alveolar bone by interacting favourably with the osteoblasts, which deposit new bone on their surfaces quickly. GNPs are particularly attractive materials for application as osteogenic agents according to earlier studies,

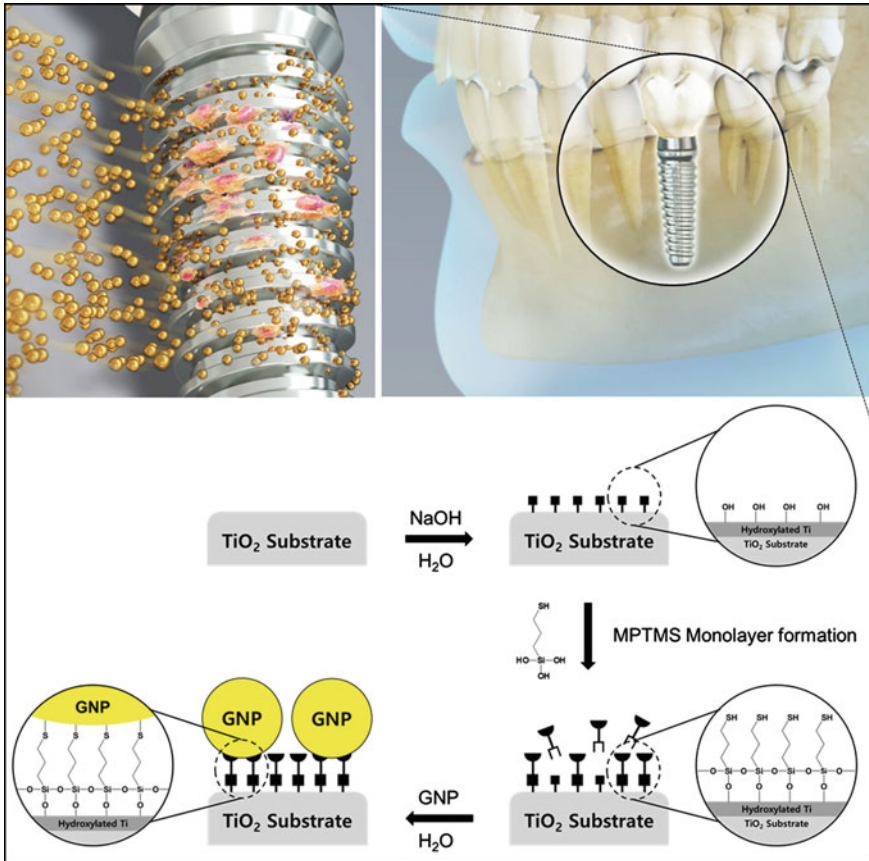


Fig. 2.18 Schematic diagram of a Ti substrate surface immobilised with GNPs by self-assembled monolayers of MPTMS and GNPs [45]

because of their potential impacts on osteoclast suppression and osteoblast differentiation. According to Fig. 2.18, Au–S bonds on the surface of the MPTMS-treated Ti stabilised the GNPs. The GNPs used had a citrate-stabilised average diameter of 28 nm. The Ti surface was treated chemically with NaOH to create a rough layer of amorphous titanium oxide, which was then used to conjugate the produced GNPs onto the Ti surface. Following that, self-assembled monolayers of MPTMS and GNPs were created on the NaOH-treated Ti surfaces via spontaneous chemisorption.

2.4.5.1 Our Experiences [46, 47]

SEM examination was performed on several samples of endosseous implants used routinely in modern dentistry treatment. The implant macrodesign depicts two

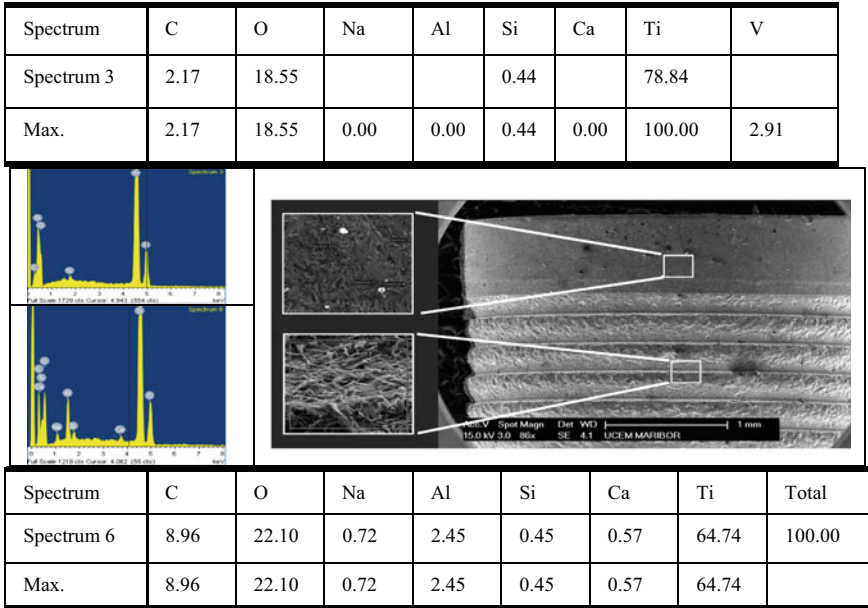


Fig. 2.19 SEM image of a micron-scale implant surface

implant components: a collar and an implant body with threads. SEM microscopy and chemical composition analyses were used to examine both pieces.

Figure 2.19 depicts the SEM microstructure of an implant surface. Because the chemical analysis revealed that the implant body included more Na, Al, C, O, and Ca than the implant neck, it may be assumed that a surface was modified using blasting procedures using Al_2O_3 and SiC.

The magnified portion of the implant body is shown at the bottom of Fig. 2.19. The surface morphology is plainly visible to be on the micrometre scale. At the micro to 10 μm scale, an attractive surface morphology with dispersed gaps and surface shells provides a sufficient platform for osteoblast cell attachment and spreading.

The main authors hypothesised that adding nanoparticles to the described micron-scale surface morphology would result in benefits such as quicker cell attachment, spreading and differentiation.

On the nanoscale we were able to create perfect GNPs and nanofibres, as illustrated in Fig. 2.20. The formation of GNPs and nanofibres are explained in detail in the refs. [46, 47].

The nanoparticles would be applied to an implant surface using either spray deposition or plasma deposition procedures. Particle nanoconfiguration could promote cell activity on the implant surface, whereas nanofibres can operate as an extra matrix for bone cells, boosting osseointegration and bone-to-implant contact.

An example of the adhesion of the GNPs to the microsurface of the Ti implant is shown in Fig. 2.21.

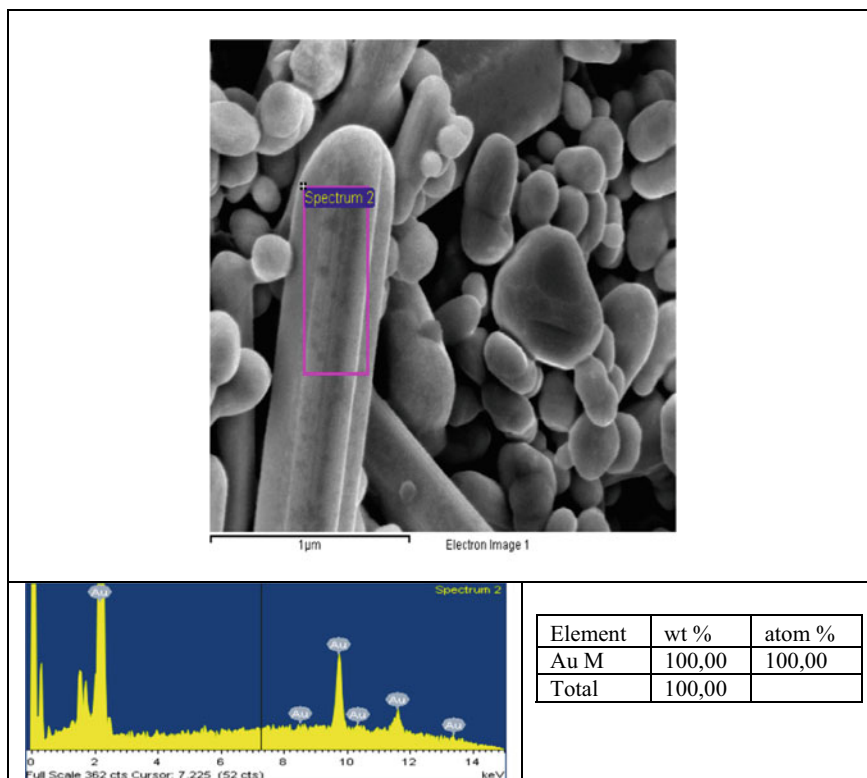


Fig. 2.20 Structural analysis. (up)–SEM micrography of Au fibres, (down)–spectrum of EDS analysis marked as “spectrum 2” at Fig. 2.20 (up). (Quantificational spectrum for the rectangular area)

2.5 Examples of Expertise

2.5.1 Plasma Spraying Hydroxide Apatite Coatings on Cp-Titanium Grade 2 Surfaces

Thin hydroxide apatite coatings were applied to Cp-Titanium Grade 2 samples using innovative high voltage pulse power equipment PJ-100 (Plasma Jet, Serbia), resulting in a more stable implant structure that might be used in future clinical applications. The different surface preparations of the Cp-Titanium Grade 2 samples before coating with hydroxide apatite were used in the comparative analysis [48].

Microstructural examination of the changed hydroxide apatite/implant surface was done by SEM imaging, as well as Auger Electron Spectroscopy, with the purpose of detecting morphology and the elements present in the new surface of

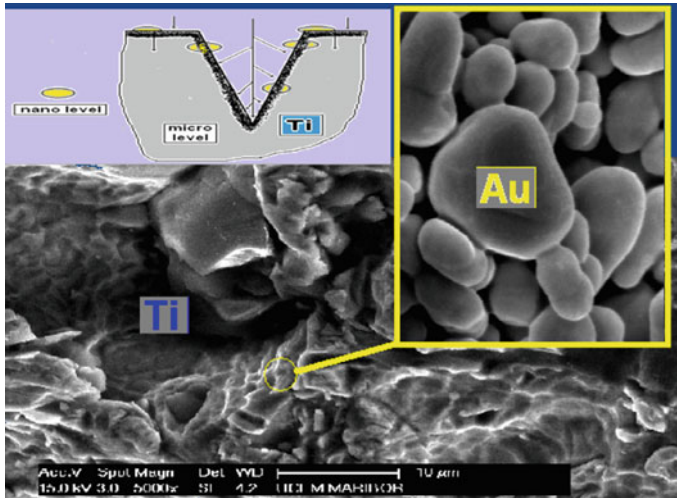


Fig. 2.21 Micron-scale implant surface on SEM

the samples. The findings revealed that the modified surface of Cp-Titanium Grade 2 with hydroxide apatite is remarkably close to the structure of bone.

Preparation of the samples. As is well known, the surface roughness of the metal implant has a considerable influence on the adhesion between the ceramic coating and the metal implant. As a result, numerous parameters, including water pressure, air flow, corundum granulation and roughening nozzle diameter, are used to optimise the roughening process. The roughening chamber was handcrafted from hardened steel. A sample capture tool (also homemade) was employed as a separate set of tools that rotated at more than 1000 rpm. The samples were roughened under the following conditions: fluid pressure of 8 bar, nozzle diameter of 10 mm, and corundum granulation of 1–2 mm. The surface roughness (Ra) obtained ranged from 4.72 to 5.28 μm . (Perthen Perthometer). To eliminate traces of oil from the compressor, the samples were cleaned with toluene and acetone after roughening.

After that, the specimens were submerged in 5.0 ml of 5 M NaOH aqueous solution for 24 h. They were then removed from the solution and rinsed gently with distilled water before drying at 40 °C for 24 h in an air environment. The treated metal was then heated at a rate of 5 °C/min for 5 h in an Ni–Cr electrical furnace in an air atmosphere to 300 °C (sample F1), 500 °C (sample F2), 700 °C (sample F3), and 800 °C (sample F4). All of the samples were cooled to room temperature in the furnace after thermal treatment. An untreated sample (F0) was also used.

Finally, the samples for XPS examinations were mounted onto a button heater (Heatwave) using tungsten wires to keep the sample corners tight, following ultrasonic cleaning with toluene and then acetone. The thermocouple was spot welded to the front edge of the sample. The plasma spray technique was carried out using the plasma installation PJ-100 (Plasma Jet, Serbia). Power 52.0 1.5 kW, voltage 120

2 V, current 430 5A, argon flow 38.5 1.2 L/min, powder carrier gas, air 8 L/min, and powder mass input 2.0 0.1 g/s were the basic parameters of the coating deposition installation. The deposition was carried out using commercially available HA powder (Metco, USA) with an average granulation of 90 m (the granulation values of the HA powder were derived from the manufacturer's specifications).

The coatings were placed manually on the top part (10 mm × 2 mm) of the cylinder (25.0 mm × 70 mm) composed of SS AISI 316 LVM material for mechanical testing. Disk-shaped specimens (diameter 10 mm, height 2 mm) were used for all subsequent research. For HA deposition, the samples were placed on a drum (200 mm) of plasma installation (rotation velocity 3.7 rev/s). The entire coating procedure was completed in 2–3 brief intervals of 7 to 10 s each, with a break rate of a few minutes between deposition cycles. The Ti disks were heated at 200 °C prior to plasma treatment, which was shown to be ideal for achieving maximum partition of the HA crystalline phase in the procedure.

Results. The quantitative study of the XRD patterns for coatings formed on the surface of various chemically and thermally treated Ti substrates is presented in Table 2.5 (SOD is 80 μm). The calculated crystallinity index (Ic) and crystalline HA and ACP phase concentrations are shown. It was discovered that the HA phase was dominating in all situations, however, the amount of produced ACP phase was greatly reduced due to the slower rate of coating cooling if the substrate was previously heated at 200 °C. The collision of partially melted commercial HA powder inside high temperature plasma with Ti substrate causes a longer period for HA re-crystallisation. The extended re-crystallisation period resulted in larger HA crystallite sizes and a decreased ACP concentration in the HA coating (in agreement with evidence obtained in our previous investigations).

The cross-sections of hydroxyapatite coatings produced by plasma jet deposition for samples F0-F4 reveal their depths clearly, as shown in Table 2.6.

The data in Table 2.6 show that there are no significant differences in the depth of these coatings. The depth range for the entire segment for the same sample (the same plasma treatment conditions) was in the range of 20 nm. These values show that the coating depth was highly uniform for each sample, with the maximum depth deviation (from its average value) being between 9.7 and 19.8 nm.

Sample F0's HA coating (Fig. 2.22a) has a typical highly rough surface with a very intriguing shape. The smallest mosaic details were just a few m in size, while very huge and mutually interconnected portions predominated. The resulting morphology

Table 2.5 Semi-quantitative analysis of the XRD patterns

Sample	HA phase	Amorphous phase
F0	72 ± 5	28 ± 5
F1	77 ± 5	23 ± 5
F2	74 ± 5	26 ± 5
F3	75 ± 5	25 ± 5
F4	76 ± 5	24 ± 5

Table 2.6 HA coatings' depth

Sample labels	Average depth, nm	Maximal depth, nm	Minimal depth, nm	Maximal deviation from the average value, nm
(a) F ₀	206	221.7	192.9	15.7
(b) F ₁	205.8	216.2	191.4	14.4
(c) F ₂	152.4	172.2	138.5	19.8
(c) F ₃	156.2	167.4	140.7	15.4
(d) F ₄	156.1	164.3	146.5	9.7

is typical of rapidly cooled systems that were subjected to melting on the edges of different particles. The particular type of surface topology appears to be particularly promising for cell adhesion. The construction was stratified, with exposed hills and valleys. Deep voids can be seen in some places. The mosaic details in the uneven shape of very big agglomerates have dimensions of around 50 nm.

Sample F1's HA coating (Fig. 2.22b) has a rather homogeneous surface with approximately parallel patterns that resemble textile threads. The motifs are more subtle. The intertwined elements are quite orderly, with areas that are slightly raised and lowered. The details were roughly 1 μm or less in size.

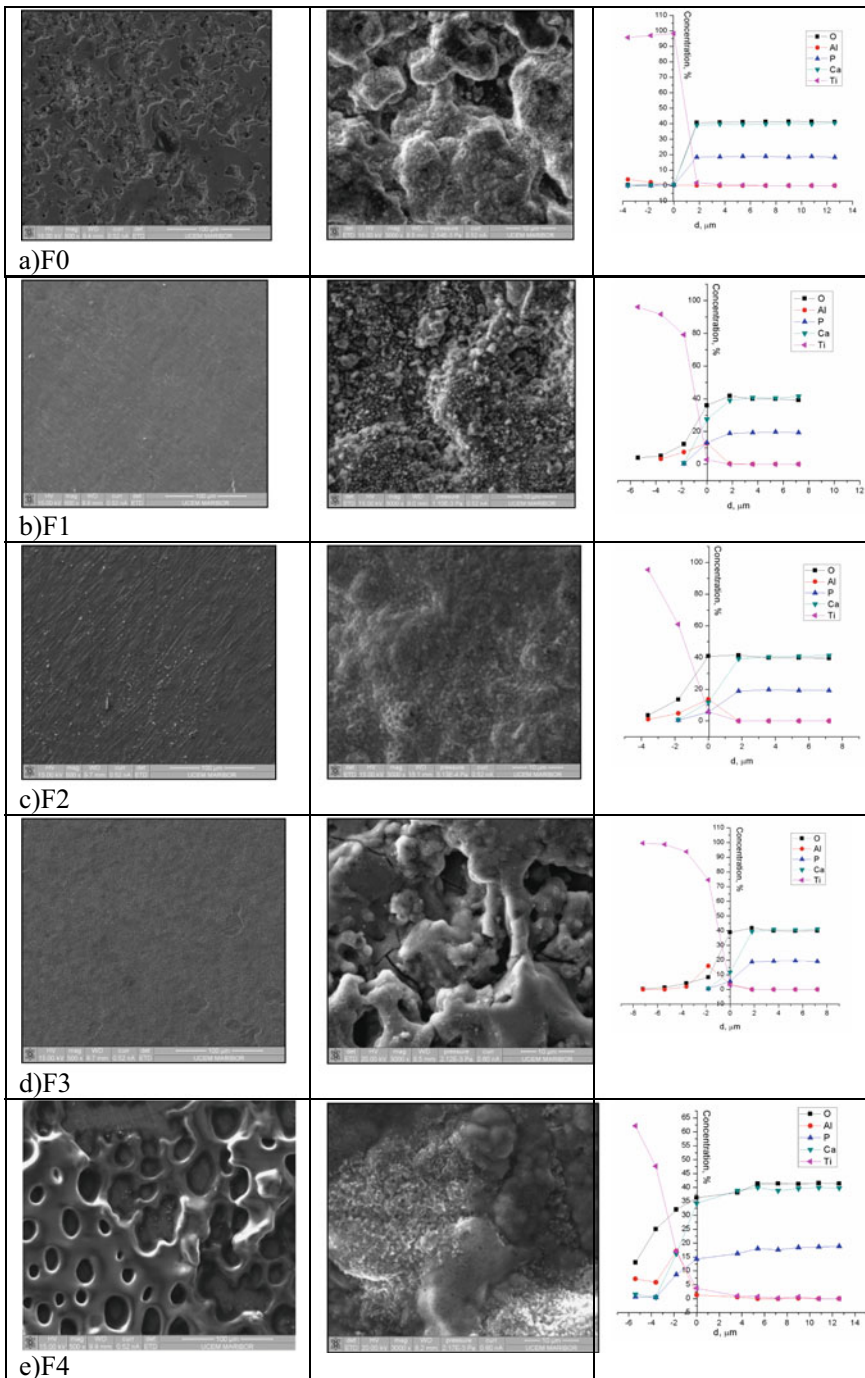
Sample F2's HA coating (Fig. 2.22c) has a highly rough surface with practically parallel patterns, and is speckled with white and black motifs in the form of furrows with typical morphology. Individual particle sizes ranged from 0.7 to 2.9 nm in very fine detail.

Sample F3's HA coating (Fig. 2.22d) has a distinct surface morphology with a worm-like structure and finer expressed granules than the prior cases. Individual particles may be seen clearly. Their readings ranged from 0.3 to 0.6 nm. The mosaic is pretty consistent. The granules were elongated and prismatic in shape. There are no obvious voids, and it appears that the HA layers were sorted properly, with no build-up that would result in the formation of valleys and hills, as shown in examples F0-F2.

Sample F4's HA coating (Fig. 2.22e) has a very particular arrangement of cavities and elevations. It appears to be a very fine knit network, with numerous visible layers and holes ranging in size from 7 to 36 nm. The depths of the network's continuous interconnected portions were of very similar dimensions. These morphologies depict the first layer beneath the perforated layers (ropes in the network) as having a very smooth surface and modest parallel patterns. Individual particle sizes ranged from 0.25 to 1.45 nm.

The EDS examination of the HA coating (shown in Fig. 2.23) revealed the presence of all the components contained inside the coating, from the titanium substrate to the coating's top. The same image also shows the altered region of the substrate during plasma jet deposition.

The concentrations of the various elements shown in the graphs above are quite comparable. The Ti substrate and HA coatings' boundaries are plainly evident. Small



◀**Fig. 2.22** Left: SE micrographs of Cp-Ti2 surfaces: **a** F0, **b** F1, **c** F2, **d** F3 and **e** F4. Middle: SE micrographs of HA coating on different substrates: **a** F0, **b** F1, **c** F2, **d** F3 and **e** F4. Right: EDS of cross-section of various samples of HA coatings: **a** F₀, **b** F₁, **c** F₂, **d** F₃ and **e** F₄ depending on the distance from one side of the boundary (left) or the other (right)

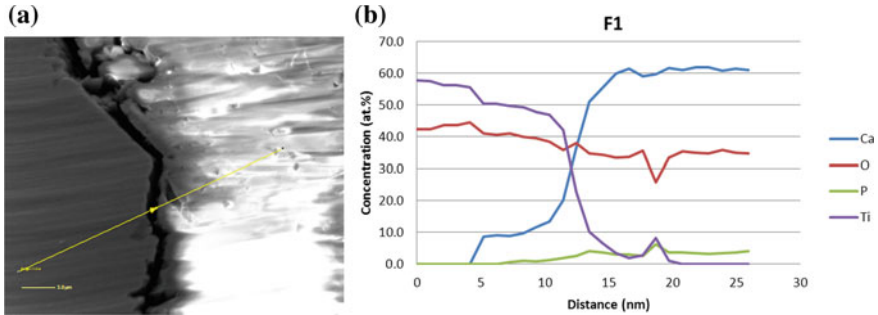


Fig. 2.23 **a** SEI of the AES line scan interface between the substrate and the HA layer for sample F1, **b** AES line scan of the interface HA and substrate, revealing the distribution of the elements Ca, O, Ti, and P

amounts of oxygen and aluminium were detected in all cases, whereas the concentration of Ti fell sharply to zero. Small amounts of calcium and phosphorus were detected on the boundary's left side. Also, at a distance of 3.6 nm, the maximum amount of Al was observed for sample F0 (3.95 wt. %), but the highest level of Al was observed at the boundary for F1, F2, F3, and F4: 12.8 wt. % for F1, 13.7 wt. % for F2, 16wt. % for F3, and 17 wt. % for F4.

Untreated sample F0 had a very low oxygen level at the left side of the boundary, whereas sample F1 had 3.9 wt. % at 3.6 m left from the boundary and 35 wt. % at the boundary, sample F2 had 1.1 wt. % at 3.6 m left from the boundary and 13.7 wt. % at the boundary, sample F3 had 1.9 wt. % and 16 wt. % at the boundary at 1.8 μm left from the boundary, and sample F4 had 20.45 nm.

The border was narrower or wider, and ion mixing from the right and left sides of the barrier was clearly apparent at 1.8 μm left of the boundary (for samples F2, F3 and F0). The boundary was thinner in samples F1 and F4, and the fall in Ti was quite severe. In all cases, the maximum depth of penetration of Ca and P ions was roughly 3.8 nm inside the substrate depth. These figures demonstrate good agreement across all the samples. There was no more interference (mixing) of ions from the Ti substrate with the ions trapped inside the HA coatings at a distance of 1.8 nm on the right inside the HA coatings.

The concentration of Ca, P, and O ions approached saturation in deeper layers of the HA coatings, becoming homogeneous with the increasing distance.

Figure 2.23. shows a typical Secondary Electron Image (SEI) of the interface of the Auger Electron Spectroscopy (AES) line scans between the substrate and HA coatings for sample F1, together with the spectrogram of the Ca, O, Ti, and P distribution.

This graph illustrates the decrease in Ti content clearly (present until the coating depth reached a value of 20 nm) and increase in Ca content in the coating between 4 and 17.5 nm. Both of these curves are standard S curves, oriented inversely to one another. The oxygen level reduced marginally, with the greatest value seen inside the chemically and thermally treated titanium (between 0 and 4 nm). Between 4 and 10 nm, the amount of HA coating decreased somewhat (the part in which Ca atoms are propagated due to the high velocity of calcium hydroxide particles melted on the surfaces by the plasma jet). Following that, the oxygen content changed statistically within specific limitations.

Similar results are shown in Fig. 2.24, where the kinetic energy of the back scattering electrons was used to explain the concentrations of various elements present over counts per second (CPS). The existence of Ca, Ti, and O is demonstrated by the specific values of these energies, which vary between the sites P1-P4 (sites at various distances from the boundary with the hydroxyapatite). Furthermore, for each of the observed sites, these values are shown in Table 2.7.

The calcium phosphate deposition follows the nucleation process, as reported by Kobubo [49] and Kim [50]. Furthermore, the electric charge interaction will encourage this process strongly. The increased surface energy favours calcium phosphate nucleation, and the basic TiOH with the negative could first adsorb the positive charge calcium ion (Ca^{2+}) to balance the surface charge until too much charge

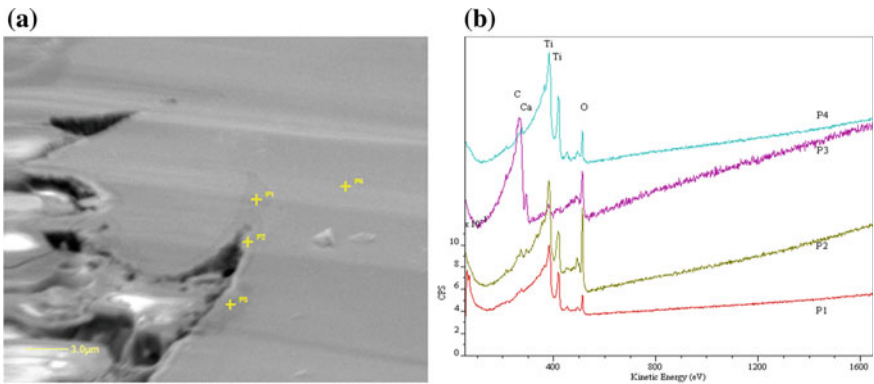


Fig. 2.24 a SEI marked places of AES, b AE spectra from the Figure (a)

Table 2.7 shows the atomic percentages of the elements detected by AES

Spot	Concentration, (at. %)			
	C	Ca	O	Ti
P1	11.2	0.0	35.2	53.6
P2	12.2	6.5	60.4	20.9
P3	46.3	25.6	24.3	3.9
P4	17.6	3.6	31.0	47.9

accumulation to generate a positive layer, calcium titanate. The positive layer then combines with the negatively charged phosphate ion (PO_4^{3-}) to create amorphous calcium phosphate, which crystallises to the OCP phase despite the percentage of amorphous calcium phosphate residue.

Finally, this study presents a novel plasma jet method for depositing hydroxyapatite on titanium surfaces that have first undergone NaOH etching and subsequent heat treatment. Additionally, the HA phase, with crystallite sizes ranging from 15.5 to 31 nm, made up the majority of the coatings as they were being deposited.

Furthermore, Auger Electron Spectroscopy demonstrated processing advantages that resulted in higher adhesion strength, by implanting Ca ions in the depth of the oxide area of the substrate. As a result, this improved plasma jet approach with unusually high plasma kinetic energy appears promising for the fabrication of nanostructured HA coatings with distinctive microstructural features, which are desirable for improving the biological aspects of HA coatings.

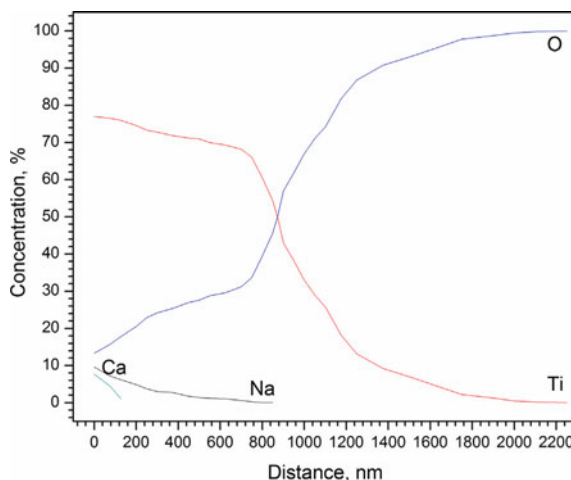
According to research, there is a strong potential for deposition of HA on titanium substrates using a novel plasma installation for any medicinal application.

2.5.2 Corrosion on the Surface of a Titanium Substrate Generated by a Combination of Alkaline and Heat Treatment

The structure changes throughout the depth of the gradient layers of the titanium substrate were examined using XRD, FTIR, and AES, after etching with NaOH and subsequent thermal treatment at various temperatures ranging from 300 to 800 °C. Specifically, the changes in the Ti substrate were investigated during NaOH etching and subsequent thermal treatment at 700 °C and ionic exchange of Na^+ with Ca^{2+} ions. This method allowed for insight into the chemical alterations and changes in the Ti oxidation states, as well as subsequent phase analyses, along the depth of the titanium oxide coatings. Furthermore, Secondary Electron Imaging (SEI) revealed very intriguing nanotopology in all samples. A particularly intriguing topology was seen for the sample in which the Na^+ ions were replaced with Ca^{2+} ions, consisting of very thin nano-designed walls between mutually interconnected pores. This structure may be suited for hydroxyapatite deposition via biomimetic or plasma techniques, as well as a scaffold for cell adhesion and proliferation [51].

Such an interesting result can be observed in Fig. 2.25, where, in samples that were etched by NaOH, then treated with $\text{Ca}(\text{NO}_3)_2$, and heated thermally at 700 °C, the Na^+ ions were replaced partially with Ca^{2+} ions (at a depth of about 300 nm, whereas Na^+ ions were present in virtually double the depth). Only the top layers were predicted to contain Ca^{2+} ions, due to the fact that the diffusion of Ca^{2+} ions into deeper layers was constrained by the gradient's decline in Ca^{2+} ion concentration as a result of the preceding replacement of Na^+ with Ca^{2+} ions. Regardless of the overall amount of Ca^{2+} that replaced Na^+ and the depth of its propagation, the presence of Ca^{2+} ions embedded in the surface promotes the crystallisation (by creating a

Fig. 2.25 Auger depth profile of the sample after treatment with NaOH, ionic exchange of Na^+ with Ca^{2+} ions, and thermal treatment at 700°C . [51]



high density of nucleuses) of calcium rich phases such as hydroxyapatites and their effective adherence.

2.6 Dental Implant Antimicrobial Surface Engineering

Dental implants that have developed severe biofilms [52] may result in peri-implant infections that affect the soft tissues and result in bleeding, suppuration and even bone loss [53].

To keep a healthy peri-implant environment, engineering techniques have been used to create antimicrobial surfaces with topographical/chemical and medication loading features that inhibit the adherence and proliferation of pathogenic bacteria [54, 55].

The surface elements that lead to biofilm accumulation along with solutions how to counteract them are in detail, illustrated schematically in [14]. Thus, the design's left side shows material properties that encourage bacterial interactions with surfaces and microbial colonisation, which have a detrimental effect on the environment's delicate balance around implants, i.e.:

- (1) Roughness tends to increase the surface-to-bacteria contact area, which promotes bacterial adhesion and offers shear force protection;
- (2) Topographical patterns with spaces larger than the bacterial dimension may encourage bacterial colonisation;
- (3) Electrostatic interactions affect bacterial attraction to surfaces with opposite charges;
- (4) Surface energy directs the interaction between the surface, fluid and bacteria, which can promote bacterial adhesion.

The right panel provides an overview of engineering antibacterial and antifouling solutions for avoiding or managing microbial adherence and biofilm formation on dental implants, i.e.:

- (A) Antimicrobial-loaded surfaces can exhibit antibacterial activity through contact killing or antimicrobial release from bioactive coatings and films;
- (B) Smart surfaces can exhibit antimicrobial activity in response to internal or external stimuli (such as pH, temperature and light), which can result in the production of ROS and local hyperthermia that can harm bacteria;
- (C) Membrane damage and repelling/repellent properties of physicochemical surface modifications, such as micro/nano-patterned texturing, electrically charged and hydrophobic surfaces, offer bacteriostatic or bactericidal effects. Reactive oxygen species, near-infrared and LCST all stand for low critical solution temperature [14].

References

1. H.J. Rack, J.I. Qazi, Titanium alloys for biomedical applications. *Mater. Sci. Eng. C* **26**(8), 1269–1277 (2006)
2. M. Geetha, A.K. Singh, R. Asokamani, A.K. Gogia, Ti based biomaterials, the ultimate choice for orthopaedic implants—a review. *Prog. Mater. Sci.* **54**(3), 397–425 (2009)
3. H.L. Freese, M.G. Volas, J.R. Wood, 3 Metallurgy and technological properties of titanium and titanium alloys. *Titan. Med.* **25** (2001)
4. Y. Li, C. Yang, H. Zhao, S. Qu, X. Li, Y. Li, New developments of Ti-based alloys for biomedical applications. *Materials* **7**(3), 1709–1800 (2014)
5. V.S. de Viteri, E. Fuentes, Titanium and titanium alloys as biomaterials. *Tribol. Fundam. Adv.* **1**(5), 154–181 (2013)
6. ASTM International, ASTM F67–06-Standard Specification for Unalloyed Titanium, for Surgical Implant Applications (UNS R50250, UNS R50400, UNS R50550, UNS R50700) (2006)
7. ASTM, F., Standard specification for wrought titanium-6aluminum-4vanadium ELI (extra low interstitial) alloy for surgical implant applications (UNS R56401), in *ASTM F136–13* (2013)
8. G.H. Hille, Titanium for surgical implants. *J. Mater.* **1**, 373–383 (1966)
9. M. Niinomi, Mechanical properties of biomedical titanium alloys. *Mater. Sci. Eng. A* **243**(1–2), 231–236 (1998)
10. D. Banerjee, J.C. Williams, Perspectives on titanium science and technology. *Acta Mater.* **61**(3), 844–879 (2013)
11. D.M. Brunette, P. Tengvall, M. Textor, P. Thomsen, *Titanium in Medicine: Material Science, Surface Science, Engineering, Biological Responses and Medical Applications* (Springer, Berlin, 2001), p.232
12. J. Jakubowicz, Ti-based biomaterials: synthesis, properties and applications. *Materials* **13**(7), 1696 (2020)
13. F. Rupp, L. Liang, J. Geis-Gerstorfer, L. Scheideler, F. Hüttig, Surface characteristics of dental implants: a review. *Dent. Mater.* **34**(1), 40–57 (2018)
14. B.A. van Oirschot, Y. Zhang, H.S. Alghamdi, J.M. Cordeiro, B.E. Nagay, V.A. Barao, E.D. de Avila, J.J. van den Beucken, Surface engineering for dental implantology: favoring tissue responses along the implant. *Tissue Eng. Part A* **28**(11–12), 555–572 (2022)
15. R. Smeets, B. Stadlinger, F. Schwarz, B. Beck-Broichsitter, O. Jung, C. Precht, F. Kloss, A. Gröbe, M. Heiland, T. Ebker, Impact of dental implant surface modifications on osseointegration, in *BioMed Research International*, 2016 (2016)

16. M.A.H. Gepreel, M. Niinomi, Biocompatibility of Ti-alloys for long-term implantation. *J. Mech. Behav. Biomed. Mater.* **20**, 407–415 (2013)
17. M. Geetha, A.K. Singh, K. Muraleedharan, A.K. Gogia, R. Asokamani, Effect of thermomechanical processing on microstructure of a Ti–13Nb–13Zr alloy. *J. Alloy. Compd.* **329**(1–2), 264–271 (2001)
18. M. Semlitsch, F. Staub, H. Weber, Titanium-aluminium-niobium alloy, development for biocompatible, high strength surgical implants-Titan-Aluminium-NIOB-Legierung, entwickelt für körperverträgliche, hochfeste implantate in der chirurgie (1985)
19. K.Y. Xie, Y. Wang, Y. Zhao, L. Chang, G. Wang, Z. Chen, Y. Cao, X. Liao, E.J. Lavernia, R.Z. Valiev, B. Sarrafpour, H. Zoellner, S.P. Ringer, Nanocrystalline β -Ti alloy with high hardness, low Young's modulus and excellent in vitro biocompatibility for biomedical applications. *Mater. Sci. Eng. C* **33**(6), 3530–3536 (2013)
20. K. Wang, The characterization of Ti-12Mo-6Zr-2Fe a new biocompatible titanium alloy developed for surgical implant, in *Beta Titanium Alloys in the 1990's*, (1993), pp. 49–60
21. A.K. Shukla, R. Balasubramaniam, S. Bhargava, Properties of passive film formed on CP titanium, Ti–6Al–4V and Ti–13.4 Al–29Nb alloys in simulated human body conditions. *Intermetallics* **13**(6), 631–637 (2005)
22. D.M. Brunette, P. Tengvall, M. Textor, P. Thomsen, M. Textor, C. Sittig, V. Frauchiger, S. Tosatti, D.M. Brunette, Properties and biological significance of natural oxide films on titanium and its alloys, in *Titanium in Medicine: Material Science, Surface Science, Engineering, Biological Responses and Medical Applications* (2001), pp. 171–230
23. T. Hanawa, K. Asami, K. Asaoka, Repassivation of titanium and surface oxide film regenerated in simulated biofluid. *J. Biomed. Mater. Res. Off. J. Soc. Biomater. Jpn. Soc. Biomater. Aust. Soc. Biomater.* **40**(4), 530–538 (1998)
24. G.D. Parfitt, The surface of titanium dioxide. *Prog. Surf. Membr. Sci.* **11**, 181–226 (1976)
25. M. Esposito, J. Lausmaa, J.M. Hirsch, P. Thomsen, Surface analysis of failed oral titanium implants. *J. Biomed. Mater. Res.* **48**(4), 559–568 (1999)
26. R.M. Pilliar, Porous-surfaced metallic implants for orthopedic applications. *J. Biomed. Mater. Res.* **21**(A1 Suppl), 1–33 (1987)
27. D.M. Brunette, P. Tengvall, M. Textor, P. Thomsen, D.M. Brunette, Principles of cell behavior on titanium surfaces and their application to implanted devices, in *Titanium in Medicine: Material Science, Surface Science, Engineering, Biological Responses and Medical Applications* (2001), pp. 485–512
28. D. Banerjee, A.L. Pilchak, J.C. Williams, Processing, structure, texture and microtexture in titanium alloys, in *Materials Science Forum*, vol. 710. (Trans Tech Publications Ltd., 2012), pp. 66–84
29. P.I. Branemark, Osseointegration and its experimental background. *J. Prosthet. Dent.* **50**(3), 399–410 (1983)
30. T. Albrektsson, A. Wennerberg, On osseointegration in relation to implant surfaces. *Clin. Implant Dent. Relat. Res.* **21**, 4–7 (2019)
31. J.C. Vanegas-Acosta, D.A. Garzón-Alvarado, A finite element method approach for the mechanobiological modeling of the osseointegration of a dental implant. *Comput. Methods Programs Biomed.* **101**(3), 297–314 (2011)
32. X. Liu, P.K. Chu, C. Ding, Surface modification of titanium, titanium alloys, and related materials for biomedical applications. *Mater. Sci. Eng. R. Rep.* **47**(3–4), 49–121 (2004)
33. A. Wennerberg, C. Hallgren, C. Johansson, S. Danelli, A histomorphometric evaluation of screw-shaped implants each prepared with two surface roughnesses. *Clin. Oral Implant Res.* **9**(1), 11–19 (1998)
34. P. Gehrke, J. Neugebauer, Implant surface design: using biotechnology to enhance osseointegration. *Interview. Dent. Implantol. Update* **14**(8), 57–64 (2003)
35. D. Buser, R.K. Schenk, S. Steinemann, J.P. Fiorellini, C.H. Fox, H. Stich, Influence of surface characteristics on bone integration of titanium implants. A histomorphometric study in miniature pigs. *J. Biomed. Mater. Res.* **25**(7), 889–902 (1991)

36. A. Jemat, M.J. Ghazali, M. Razali, Y. Otsuka, Surface modifications and their effects on titanium dental implants, in *BioMed Research International*, 2015. (2015)
37. A. Wennerberg, T. Albrektsson, On implant surfaces: a review of current knowledge and opinions. *Int. J. Oral Maxillofac. Implant.* **25**(1) (2010)
38. P.K. Chu, J.Y. Chen, L.P. Wang, N. Huang, Plasma-surface modification of biomaterials. *Mater. Sci. Eng. R. Rep.* **36**(5–6), 143–206 (2002)
39. A.Y. Fasasi, S. Mwenifumbo, N. Rahbar, J. Chen, M. Li, A.C. Beye, C.B. Arnold, W.O. Soboyejo, Nano-second UV laser processed micro-grooves on Ti6Al4V for biomedical applications. *Mater. Sci. Eng. C* **29**(1), 5–13 (2009)
40. G. Mendonça, D.B. Mendonça, F.J. Aragao, L.F. Cooper, Advancing dental implant surface technology—from micron-to nanotopography. *Biomaterials* **29**(28), 3822–3835 (2008)
41. K.J. Klabunde, J. Stark, O. Koper, C. Mohs, D.G. Park, S. Decker, Y. Jiang, I. Lagadic, D. Zhang, Nanocrystals as stoichiometric reagents with unique surface chemistry. *J. Phys. Chem.* **100**(30), 12142–12153 (1996)
42. S.F. Lamolle, M. Monjo, M. Rubert, H.J. Haugen, S.P. Lyngstadaas, J.E. Ellingsen, The effect of hydrofluoric acid treatment of titanium surface on nanostructural and chemical changes and the growth of MC3T3-E1 cells. *Biomaterials* **30**(5), 736–742 (2009)
43. G. Cervino, A. Meto, L. Fiorillo, A. Odorici, A. Meto, C. D’Amico, G. Oteri, M. Cicciù, Surface treatment of the dental implant with hyaluronic acid: an overview of recent data. *Int. J. Environ. Res. Public Health* **18**(9), 4670 (2021)
44. M.C. Advincola, F.G. Rahemtulla, R.C. Advincola, E.T. Ada, J.E. Lemons, S.L. Bellis, Osteoblast adhesion and matrix mineralization on sol–gel-derived titanium oxide. *Biomaterials* **27**(10), 2201–2212 (2006)
45. D.N. Heo, W.K. Ko, H.R. Lee, S.J. Lee, D. Lee, S.H. Um, J.H. Lee, Y.H. Woo, L.G. Zhang, D.W. Lee, I.K. Kwon, Titanium dental implants surface-immobilized with gold nanoparticles as osteoinductive agents for rapid osseointegration. *J. Colloid Interface Sci.* **469**, 129–137 (2016)
46. I. Milinković, R. Rudolf, K.T. Raić, Z. Aleksić, V. Lazić, A. Todorović, D. Stamenković, Aspects of titanium-implant surface modification at the micro and nano levels. *Materiali in tehnologije* **46**(3), 251–256 (2012)
47. R. Rudolf, V. Lazić, P. Majerič, A. Ivanič, G. Kravanja, K.T. Raić, *Dental Gold Alloys and Gold Nanoparticles for Biomedical Applications*. (Springer International Publishing AG, 2022)
48. R. Rudolf, D. Stamenković, Z. Aleksić, M. Jenko, I. Đorđević, A. Todorović, V. Jokanović, K.T. Raić, Hydroxyapatite coatings on cp-titanium grade-2 surfaces prepared with plasma spraying. *Materiali in tehnologije* **49**(1), 81–86 (2015)
49. T. Kokubo, H.M. Kim, M. Kawashita, Novel bioactive materials with different mechanical properties. *Biomaterials* **24**(13), 2161–2175 (2003)
50. H.M. Kim, T. Himeno, M. Kawashita, J.H. Lee, T. Kokubo, T. Nakamura, Surface potential change in bioactive titanium metal during the process of apatite formation in simulated body fluid. *J. Biomed. Mater. Res. Part A Off. J. Soc. Biomater. Jpn. Soc. Biomater. Aust. Soc. Biomater. Korean Soc. Biomater.* **67**(4), 1305–1309 (2003)
51. V. Jokanović, M. Vilotijević, B. Jokanović, M. Jenko, I. Anžel, D. Stamenković, V. Lazić, R. Rudolf, Investigations of corrosion on the surface of titanium substrate caused by combined alkaline and heat treatment. *Corros. Sci.* **82**, 180–190 (2014)
52. S.W. Lee, K.S. Phillips, H. Gu, M. Kazemzadeh-Narbat, D. Ren, How microbes read the map: effects of implant topography on bacterial adhesion and biofilm formation. *Biomaterials* **268**, 120595 (2021)
53. H. Chouirfa, H. Bouloussa, V. Migonney, C. Falentin-Daudré, Review of titanium surface modification techniques and coatings for antibacterial applications. *Acta Biomater.* **83**, 37–54 (2019)
54. S. Renvert, G.R. Persson, F.Q. Pirihi, P.M. Camargo, Peri-implant health, peri-implant mucositis, and peri-implantitis: Case definitions and diagnostic considerations. *J. Clin. Periodontol.* **45**, S278–S285 (2018)
55. G. Battiston, R. Gerbasi, K. T. Raić, Kinetics of TiO₂ film growth in low pressure system using titaniumtetrakisopropoxide (TTIP). *Metal. J. Metall. MJoM*, (Special Issue: Modern Mater. Technol.) **8**(3), 183–190 (2002)

Chapter 3

Processing of Cobalt-Chrome Dental Alloys



Abstract Cobalt–Chromium (Co–Cr) alloys are used in dental prosthetics for removable partial denture restorations, complete cast metal-ceramic restorations, dental bridges, crowns, and implants. Their mechanical properties, high strength and hardness, combined with good corrosion and tarnish resistance provide them with the necessary biocompatibility and performance for extensive use. The chapter presents a brief overview of the physico-chemical properties and the processing options of Co–Cr alloys. Using modern dental laboratory processing techniques allows for the fabrication of dental prostheses by conventional casting, milling and additive manufacturing. The main principles and workflow of these processes are given, highlighting key aspects for producing dental prosthetic restorations using Co–Cr alloys.

3.1 Introduction to Cobalt-Chrome Dental Alloys

Historically, noble metals were generally used for dental applications, due to their excellent biocompatible, anti-corrosive properties and good mechanical characteristics. Since the 1980s the increasing costs of noble metals has driven the development of base metal alloys for use in dental prosthetics [1]. Nickel and Cobalt were used predominantly as the base metal, due to their alloys having good mechanical properties and high corrosion resistance. Cobalt–Chromium (CoCr) alloys are now used widely for dental prosthetics, as they are well known for their biocompatibility, high strength and hardness, high melting points, with excellent corrosion and tarnish resistance [1–3]. These alloys contain around 60 wt.% cobalt and up to about 30 wt.% chromium [4], with other metals, such as molybdenum (Mo), gallium (Ga), iron (Fe), nickel (Ni), ruthenium (Ru) and tungsten (W) added for strengthening purposes [1, 5]. These materials are also used widely for other medical treatments, such as stents, intervertebral disc replacements, and in knee or hip arthroplasty [5]. In dentistry they have been used successfully for clinical applications as full cast, metal-ceramic restorations, for dental bridges, crowns and implants, or removable partial denture restorations [6].

3.2 Development of Co–Cr Alloys

Elwood Haynes first discovered Co–Cr alloys in the early 1900s by combining cobalt and chromium for producing some components for an internal combustion engine and for tougher tools used for machining [7]. Some of the developed alloys also contained other elements, like tungsten and molybdenum. As the Co–Cr alloys had stainless characteristics with a star-like luster, they were named Stellites, after the Latin word “Stella” which means “star”. Stellite is a trademarked name of the Kennametal group, previously from the Deloro Stellite Company [8]. Haynes found that these alloys were capable of enduring oxidation and corrosive fumes without showing any signs of tarnish, even when exposed to boiling nitric acid. Contemporary Co–Cr alloys, refined from this early work, are now used regularly in various areas requiring great wear resistance and strength, such as in the aerospace industry, for gas turbines, engine components, bearings, blades, dental materials, orthopaedic implants and cutlery [9]. Their use in biomedical applications has become especially extensive, as their excellent properties in this field are favoured in artificial joints and surgical prostheses, hips and knees, prosthetic heart valves, pacemakers, as well as dental fixed and removable prosthetics and implants [7].

Co–Cr alloys were first used for dental prosthetics in the 1930s for removable partial denture frameworks. As they were lighter than noble metal alloys, while still having corrosion resistance and excellent mechanical properties, they began to be used more frequently for removable partial dentures. In the 1950s, they began to be used for fixed dental prostheses in metal ceramic applications. However, the use of noble metal alloys for fixed tooth restorations was still predominant until the 1970s, when noble metal prices started rising and alternatives were being sought after. In modern dentistry, Co–Cr alloys are being used predominantly in removable partial dentures. For fixed prosthetics, they are also gaining a higher use percentage due to economic reasons as compared to noble metals, while also replacing Ni-based dental alloys because of increasing Ni allergies in the general population and the resulting stricter regulations for alloys containing Ni [1].

3.3 Production of Co–Cr Alloys

Co–Cr alloys are generally produced from pure metals of Co and Cr, obtained from cobalt oxide and chromium oxide ores with reduction processes. The pure metals are then combined under vacuum by electric arc or induction melting [10]. These metals are highly reactive with oxygen to form oxides, so the process needs to be carried out under vacuum or an inert atmosphere. Processing the alloy by various techniques or methods, such as wrought or hot forging, hardfaced deposit and casting, yields the desired shape of the alloy intended for the application. Co–Cr alloys are quite difficult to machine, requiring specialised, high performance machining tools. As they have a considerable toughness, these alloys are also often machined by grinding

rather than by cutting. A powder form is produced by spraying molten alloy metal through small nozzles in an inert argon atmosphere. The molten metal droplets are cooled rapidly, in order to produce fine solid particles of the alloy [9].

3.4 Physico-Chemical Properties

Cobalt (Co) is a hard and brittle transition metal with an atomic mass of 58.933 amu in the fourth period of the Periodic Table between iron and nickel. It has the appearance of a silvery-grey metal with a faint blue shine. At room temperature it has a hexagonal close-packed (HCP) crystal structure, while above 421 °C, it appears in a face-centred cubic (FCC) crystal lattice structure. This ferromagnetic metal has a density of 8.9 g/cm³, with a melting point of 1495 °C, a curie temperature of 1121 °C, low magnetic permeability of about 2/3 of iron and a high damping characteristic due to its ductility. Cobalt forms a passive oxide film, which protects the underlying metal from further oxidation. It is used typically in wear and corrosion-resistant, high-strength alloys, as well as alloys subjected to vibration, high temperatures or aggressive chemicals [7].

Chromium (Cr) is an extremely hard transition metal with an atomic mass of 51.996 amu in the fourth period of the Periodic Table between vanadium and manganese. It has a shiny steely-grey appearance that can be polished highly, with a high reflectance of light and a high resistance for tarnishing. It has a body-centred cubic (BCC) crystal lattice structure, a density of 7.15 g/cm³, a melting point of 1907 °C, is antiferromagnetic at room temperature and paramagnetic at temperatures above 38 °C. Chromium also forms a passive oxide film in air, which prevents further oxidation of the metal. This film is very dense with a spinel structure only a few atoms thick. Chromium is used most commonly in metal alloys, while smaller quantities of this metal are used in compounds for chemical processes, or as coatings for decorative purposes [11] (Fig. 3.1).

Increasing the percentage of Cr in Co–Cr alloys increases the alloys' wear and corrosion resistance and provides good magnetic properties. With the presence of carbon, Cr forms carbides, which strengthens the alloy further. This may be undesirable, as very hard and brittle materials may break or chip off by impact or higher strains in the mouth, making them unsuitable for use in dentistry. Contemporary dental Co–Cr alloys have diverse contents of Co, Cr, Mo, W, Ti, Ga, Mn, Si, Fe, Nb, Ce, C, N, etc. Important, and mostly used alloying elements in Co–Cr dental alloys are tungsten (W) and molybdenum (Mo). These elements enhance the strength of the alloy matrix, provide some hardness with low ductility, a higher density (better for casting) and hot hardness. They also increase hardness further by forming hard and stable carbides [7, 12]. The other mentioned elements are also used in relatively small amounts, to improve the casting, flowability, melting point, thermal expansion, grain size, toughness or oxidation characteristics for porcelain bonding.

The superior properties of Co–Cr alloys are the result of the crystallographic properties of cobalt, along with the strengthening effects of Cr, Mo and W, and the

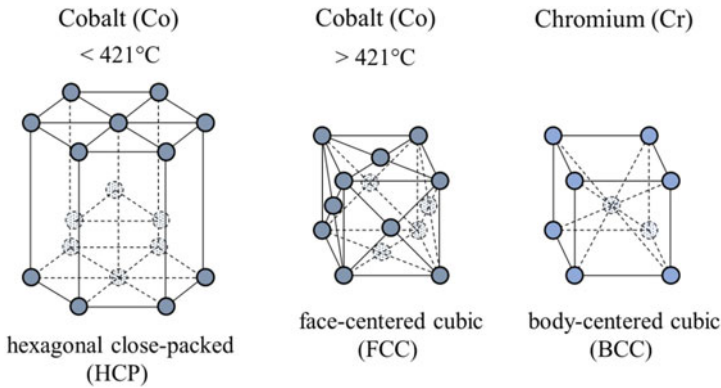


Fig. 3.1 Crystal lattice structures of Co and Cr

formation of carbides with these elements [7]. Co–Cr alloys have a Face Centred Cubic (FCC) lattice—a γ phase at high temperatures, which affects the ductility, and the Hexagonal Close Packed (HCP) lattice an ϵ phase at room temperature, which affects corrosion and wear resistance [13]. The chromium content of 22–28 wt.% in the Co–Cr alloy forms the passive oxide layer on the surface, and, M23C6 type carbides are formed due to its presence, which increase the hardness and wear resistance. More stable M6C carbides are formed instead of M23C6 in Co–Cr alloys with tungsten and molybdenum concentrations over 4 wt.%. The carbon content in Co–Cr alloys can reach up to 0.35 wt.%, forming carbide precipitates with sizes ranging from 50 to 300 nm, found in the interdendritic areas of the Co–Cr alloy microstructure. Cobalt-based alloys go through a slow FCC to HCP martensitic transformation, keeping the FCC in a metastable state under normal cooling rates. The properties of Co–Cr alloys are, thus, dependent on the γ and ϵ phase ratio, which depends on the alloy processing and the presence and distribution of carbides in the microstructure [12–15]. A Cr weight content of 30% is the solubility limit for Co–Cr alloys, where the additional Cr is found in the very brittle σ phase, imprinting this feature on the entire alloy [16].

3.5 Corrosion-Resistant Properties

The biocompatibility of Co–Cr alloys comes from the formation of a hard, passive, Cr-based oxide layer on the surface of these alloys [17], made mainly of Cr_2O_3 , but also containing minor amounts of cobalt, which prevents further corrosion of the alloy (Fig. 3.2). In dentistry this passivation layer also reduces the release of metal ions from the alloy into the mouth, which may potentially cause local and systemic toxicity, allergies, or carcinogenicity [15, 18]. The passivation layer and how this

oxidised surface interacts with the physiological environment have an important role in biocompatibility, mainly in the form of ion release from the alloy into the body.

The release of ions is measured with static immersion tests. In these tests dental alloy samples are immersed in a corrosive solution, typically, an artificial saliva or a buffered electrolyte solution that simulates the oral environment. The samples are kept stationary in the solution for a specified period, often several days or weeks, to allow for corrosion to occur. The Standard for dental metallic materials for fixed and removable restorations, ISO 22674, requires immersion over 7 days. During the immersion, corrosion products may form on the samples' surfaces. After the test duration, the samples are removed, cleaned and inspected visually or analysed further to assess the corrosion behaviour, such as the presence of pitting, discolouration, or changes in surface roughness. The solution simulating the oral environment is also analysed for metallic ions, indicating the quantity of ion release from the metal in the oral environment. According to ISO 22674, the total ion release of all the alloy constituent metals together should be below 200 $\mu\text{g}/\text{cm}^2$ for the duration of the testing week.

An especially detrimental type of corrosion for dental alloys is pitting corrosion, which is a very concentrated, localised breakdown that leaves holes (crevices) on

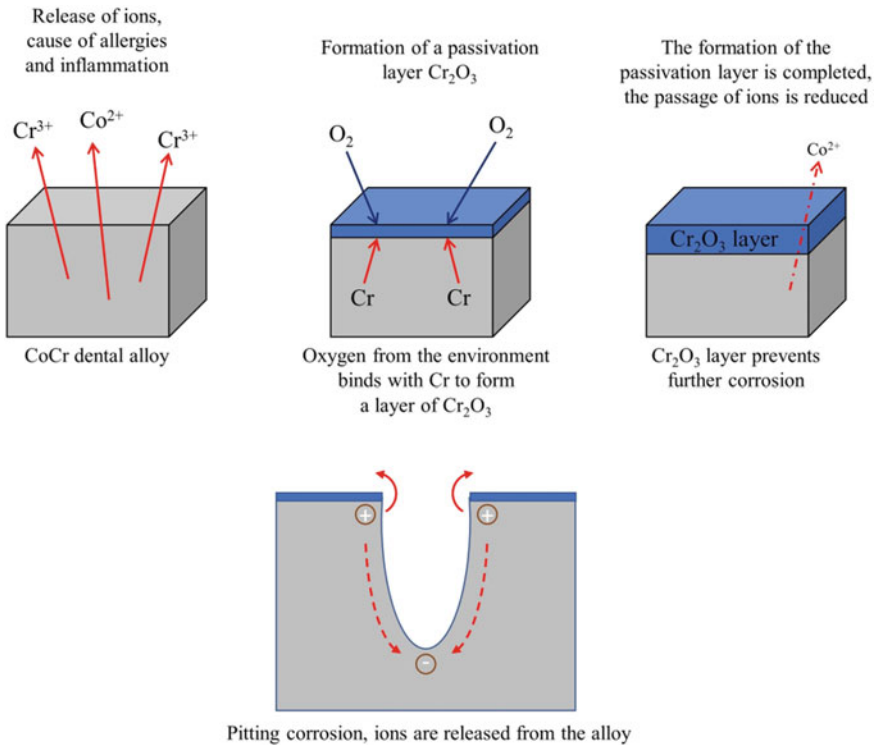


Fig. 3.2 Formation of a passivation layer on a Co–Cr alloy, with a representation of pitting corrosion

the material's surface (Fig. 3.2). This form of corrosion results from the localised disruption of the passive layer's barrier of protection for the alloy. Pitting corrosion in Co–Cr dental alloys is generally less common compared to other materials, but may occur due to the composition of the alloy, the presence of impurities, the environment, fabrication techniques, and the specific oral conditions to which the alloy is exposed. Certain oral environments, such as those with high acidity or a high chloride ion concentration, can increase the likelihood of localised pitting corrosion. It was shown that additions of precious metals in the alloy increase the resistance to pitting corrosion, however, not enough to provide a valuable improvement from a patient's point of view [19]. Ensuring proper conventional Co–Cr alloy compositions and fabrication techniques is, thus, a more practicable approach to reduce the occurrence of this type of corrosion.

3.6 Possible Indications

Co–Cr dental alloys are suitable for long-spanning metal-ceramic restorations or removable partial dentures, due to their high elastic modulus and toughness, as well as their low cost. In comparison with gold alloys, they have an elastic modulus almost twice as high, which gives the advantage of fabricating thinner profiles for the dental restorations while maintaining rigidity. This characteristic allows for improved aesthetics with less tooth structure reduction. On the other hand, they also have a lower density than gold alloys, which makes it possible to fabricate long, extensive, or bulky prostheses when needed, while keeping the weight low [20]. Due to their exceptional physical and chemical properties, Co–Cr alloys are suitable for basically every category of metal dental restorations [21]:

- Crowns (unveneered or veneered with ceramic or composite).
- Bridges (unveneered or veneered with ceramic or composite).
- Denture frameworks (so-called metal denture base alloys).
- Implant prosthetics (e.g. abutments, bars).
- Orthodontics: retainers, orthodontic appliances, wires.
- Solders.
- Laser welding rods (fillers).

3.7 Fabrication Techniques of Dental Prostheses

Dental prostheses of all types are used for the replacement of single or several teeth, for restoring masticatory function, dentition (the development and arrangement of teeth) and prevention of further tooth deterioration. The preparation of the intended dentures for a specific patient takes place in a commercial dental laboratory or dental office on prescription of the dentist treating the patient. Medical practice usually

gives indications for dental prostheses to adults with a fully developed tooth arrangement. The tooth restorations can be produced using a conventional lost wax precision casting, with digital computer-aided design and computer-aided manufacturing (CAD/CAM) techniques, or with a combination of these methods. Since aesthetics are an important factor in today's society, the produced metallic frameworks are then veneered with ceramics or composites. Acrylics were used previously, but are now no longer in use, or are being phased out of use slowly in some countries, due to their low aesthetics and wear resistance. Full ceramic restorations with no metals are considered as the highest level of aesthetics, while they are not best suited for long-spanning dental bridges or removable partial dentures, due to their low strength and ductility. The metallic-ceramic restorations are, thus, considered as the best option for these indications.

The digital CAD/CAM techniques may be divided into subtractive manufacturing or additive manufacturing. Subtractive manufacturing uses milling from a block of the dental alloy material, or milling of a plastic or wax blank disc, with a subsequent conventional metal cast for fabrication of the dental restoration (a combination of digital and analogue techniques). Additive manufacturing, commonly referred to as 3D printing, is usually done with the most widely used methods for dental restorations, Selective Laser Melting (SLM) or Electron Beam Melting (EBM). Figure 3.3 shows the workflow of some techniques for fabricating tooth restorations from metal dental alloys. Co–Cr dental alloys are used widely in all of these methods, as they are available in the form of small cylinders for casting, as solid disc blocks for milling, or as a powder for 3D printing. Due to their availability in dental fabrication techniques, clinical performance, cost, biocompatibility and mechanical properties, Co–Cr alloys are currently considered the material of choice for base-metal dental framework fabrication [22].

The conventional lost wax casting technique for making a prosthesis involves obtaining an impression of the patient's oral cavity, pouring a plaster mould of the oral cavity, creating a wax model of the tooth restoration, and then investing the tooth restoration, casting the selected metal and polishing the final prosthesis. This technique presents an affordable option for clinicians, but it is complex and time-consuming [22]. Depending on the characteristics of the material used and the worker's skill, the risk of inaccuracy may rise during this process. An automated CAD/CAM technology was thus introduced in the dental industry to improve on this fabrication, with possibilities for greater production, ease of use, time savings, as well as for reducing the influence of human error and laboratory variables [22–24].

Additive manufacturing techniques have been gaining popularity in dental prosthetics, due to their quick and precise manufacturing properties, with low material waste as compared to milling. With the progressing development of these technologies they are becoming more affordable and less demanding for use, resulting in an increasing adoption rate of these techniques in dental laboratories. As a disruptive technology, the nature of additive manufacturing for producing custom shapes of metal structures is especially suitable for dental prostheses, where each metal framework may be considered as an original product, or a custom medical device, suitable only for the particular patient that it was designed for.

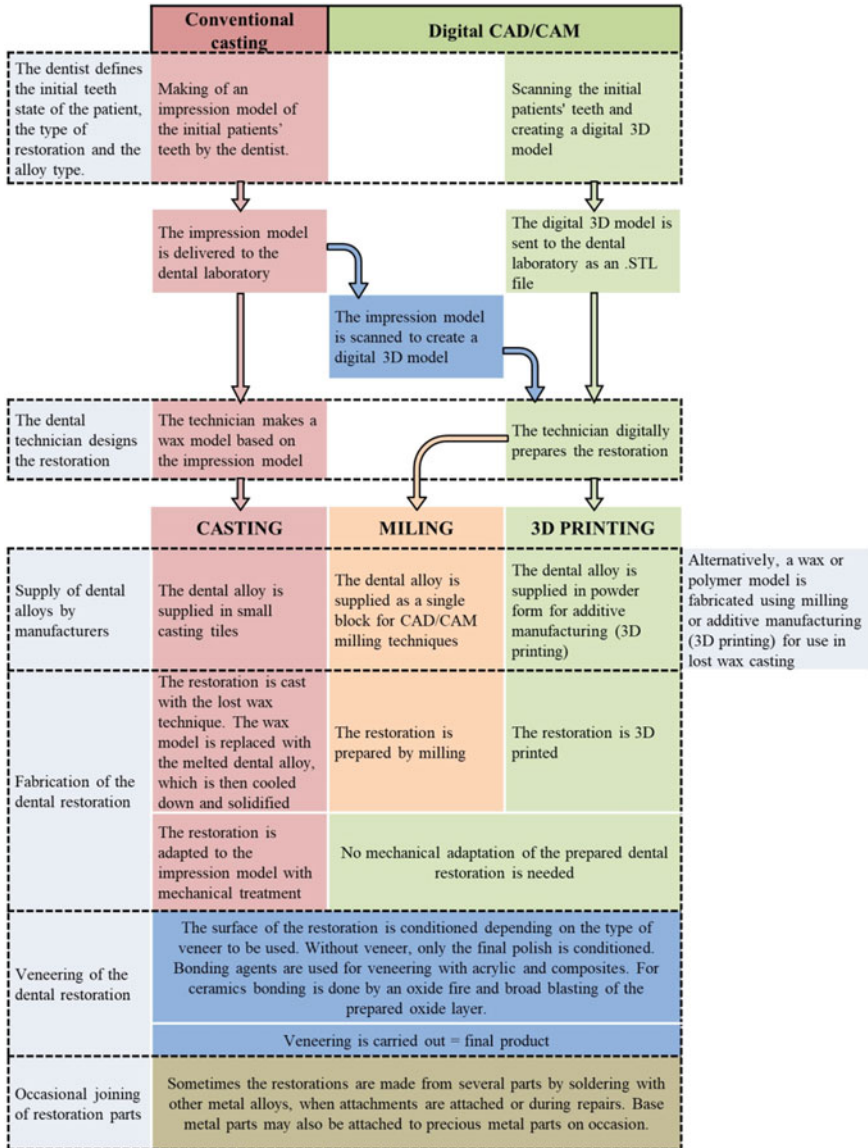


Fig. 3.3 Workflow of the different fabrication techniques of dental prostheses

3.7.1 Precision Casting of Co–Cr Dental Alloys

Precision lost wax casting is the conventional technique for fabricating dental restorations; it is affordable, accurate and is an established technique, used for several decades. The precise steps and materials used may vary, depending on the specific

dental laboratory or clinician’s preferences, while the procedure typically involves the following steps (Fig. 3.4):

1. **Tooth preparation:** The tooth receiving the restoration is prepared by removing any decayed or damaged portions and shaping it to accommodate the restoration.
2. **Impression taking:** An impression of the prepared tooth and the surrounding area is taken using dental impression materials. This captures the exact shape and size of the tooth to be restored.
3. **Wax pattern creation:** A wax pattern of the restoration is fabricated based on the impression. This is done by sculpting the tooth replacements in wax at the precise shape and size, considering all the aspects demanded by the particular clinical situation. The wax pattern replicates the shape and contours of the final dental restoration.
4. **Investing:** Sprues are attached to the wax pattern, creating a wax sprue system. The sprue system allows for the flow of molten metal during the casting process. The wax pattern and sprue system are then invested (encased) in a refractory material, such as investment plaster or investment powder. The investment material hardens around the wax pattern, creating a mould.
5. **Wax elimination:** The invested mould is heated to remove the wax pattern, leaving behind a cavity in the shape of the desired restoration.
6. **Casting:** Once the wax has been eliminated, the mold is preheated to remove any remaining moisture and ensure a proper casting temperature. Molten metal is then

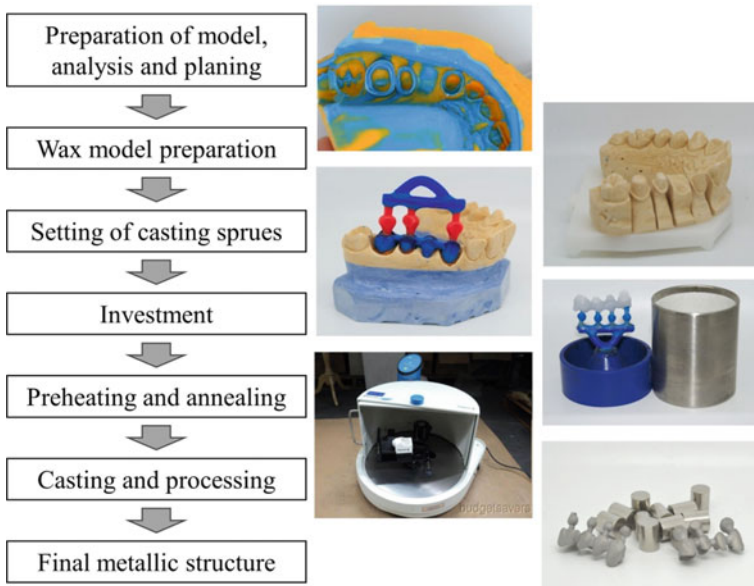


Fig. 3.4 Procedural steps for lost wax casting of dental restorations

cast into the mould using a centrifugal or vacuum-pressure casting machine. The molten metal fills the cavity left by the wax pattern.

7. **Finishing:** After the casting has solidified, the investment material is broken away and the casting is retrieved. The casting is then finished carefully and polished to remove any excess metal, to achieve a proper fit, and enhance the aesthetics.
8. **Veneering:** Additionally, the metal framework is veneered with ceramics or composites, to provide for a more aesthetically suitable restoration.
9. **Cementation (for a fixed prosthesis):** Finally, the dental restoration is cemented or bonded to the prepared tooth of the patient using dental cement, ensuring a secure and durable placement.

The procedure is time consuming and complex, with several variables and risks for inaccuracies, depending on the dental doctors' and dental technicians' proficiency, laboratory conditions, or other factors during the various steps that need to be performed for a fabrication of a tooth replacement.

Typically, Co–Cr dental alloys have casting temperatures around 1300–1500 °C, comparable to Ni-based alloys, higher than noble dental alloys (1000 °C for non-ceramic alloys, 1300–1400 °C for Au–Pt ceramic alloys) and lower than Ti dental alloys (around 1700 °C) [25]. The casting and pouring temperature have an effect on castability, along with fluidity and solidification shrinkage. Castability, which is an alloy's ability to replicate the mould details, is crucial for a successful casting process, since the objective is to make a copy of the wax pattern geometry that is as accurate as possible. Castability is one of several qualities that are essential for dental alloys to operate well in clinical settings, because accurate replication of details is essential to a restoration's long-term success [25]. The casting method was shown to have little effect on the castability of alloys, whether they are cast using torch/centrifugal casting or induction/vacuum-pressure casting [26].

The porosity was also shown to be greater in casting Co–Cr alloys than in Ni-based alloys, while Ti has higher porosity values than Co–Cr. Porosity is an important factor in casting quality, as even little pores put clasp arms and occlusal rests at risk of breaking. The main cause of porosity in castings is trapping inert gas within the molten metal. There are two sorts of porosities that affect strength: surface notches and internal porosity. If the size and number of internal porosities are negligible, their impact on the strength of the framework is minimal. However, narrow and lengthy surface notches are vulnerable to corrosion and metallic fatigue, and may have a negative impact on the longevity of the structure [25].

The casting temperature is an important factor in castability and the formation of porosity. For Co–Cr dental alloys these characteristics are intermediate when compared to Ni, Ti, or noble metal alloys, with other alloys having higher castability, less porosity (Ni, noble metals), or lower castability and more porosity (Ti). This slight disadvantage is offset by the previously mentioned beneficial properties of Co–Cr for dental purposes, as well as by the low cost, making corrections and repeat fabrications of dental restorations more accessible.

The surface roughness of dental cast prosthetics can also change according to the casting conditions. The adhesion of bacterial plaque and incidence of tooth cavities,

gingivitis, and periodontal disease are all influenced considerably by the surface roughness. Increased roughness had been observed by using traditional casting techniques. In previous research a roughness “limit value” of $Ra\ 0.09 \pm 0.01\ \mu\text{m}$ was used to determine the acceptable polished condition. According to reports, rougher surfaces require more finishing and polishing steps. Polishing Co–Cr alloys is constrained by technical issues and increased difficulty of grinding and polishing procedures when using traditional chair side and laboratory instruments. Studies have shown that there is significant metal structure loss from the metal framework during finishing and polishing, particularly for partial removable dentures, which causes a poor fit and improper contact at the tooth interface and affects the stability and retention of the framework. Due to the hardness of these alloys, cleaning and polishing the restoration after casting requires specialised equipment, which restricts these procedures severely in dental offices. The composition, casting technique, and interaction of molten metal with the components of investment material all have an impact on the hardness of the cast alloy [20].

The microstructure of cast Co–Cr alloys is characteristically dendritic, with precipitates in the eutectic interdendritic areas [12, 24], as seen in Fig. 3.5. During solidification, constituents such as W and Mo in the alloy diffuse to the interdendritic areas, or precipitate on the grain boundaries. Reducing the alloying element contents such as Mo in the initial solution increases the concentration of this alloying element in the interdendritic precipitates [12, 15]. Impurities and other inclusions in the microstructure affect the functional clinical properties of alloys adversely, as was shown in some Co–Cr alloy dental bridges, which were breaking in patients’ mouths. These dental bridges were fabricated with inclusions of contaminations during casting in the dental laboratory, as some residues and oxides from previous castings were incorporated in dental restorations [15]. In order to be appropriate for clinical use, the cast Co–Cr alloy should have a homogeneous and dendritic microstructure without inclusions, which is achievable by having a well-controlled casting procedure [15, 16].

3.7.2 Milling of Co–Cr Dental Alloys

Fabricating Co–Cr dental frameworks with conventional casting methods is challenging, due to the alloy’s high melting temperatures, reduced ductility and high hardness. This is combined with the relatively unexpected behaviour of the lost-wax technique with regards to structural homogeneity, where structural defects could occur due to incorrect alloy penetration during casting. The use of computer-aided manufacturing (CAM) methods has made it possible to provide high quality macro- and microstructures in Co–Cr dental frameworks, with high control of the block or powder characteristics throughout production. Milling, for example, is a subtractive CAM technique that involves cutting a premade Co–Cr block to the required shape. However, in addition to the considerable waste associated with milling processes, the high hardness of Co–Cr causes significant wear of machining equipment when

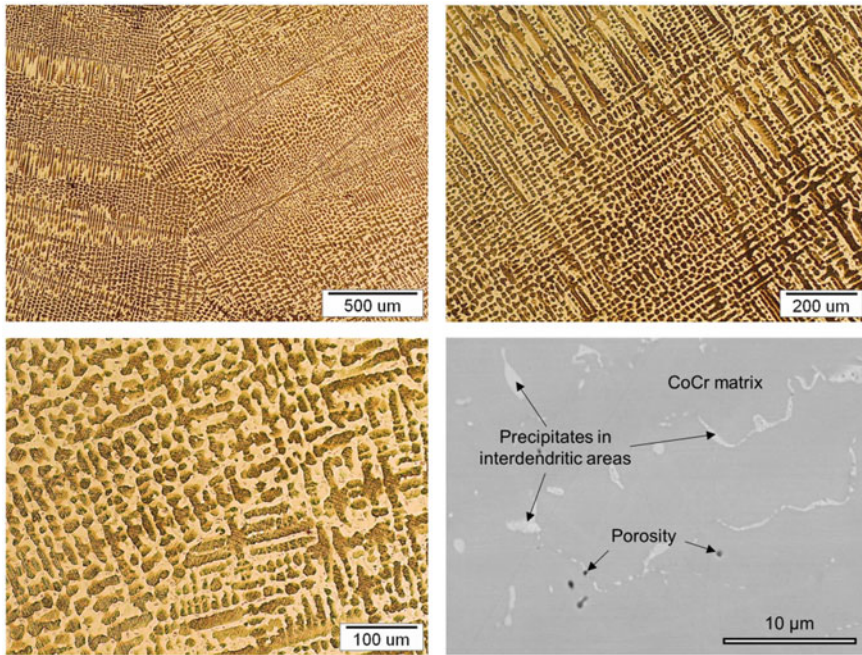


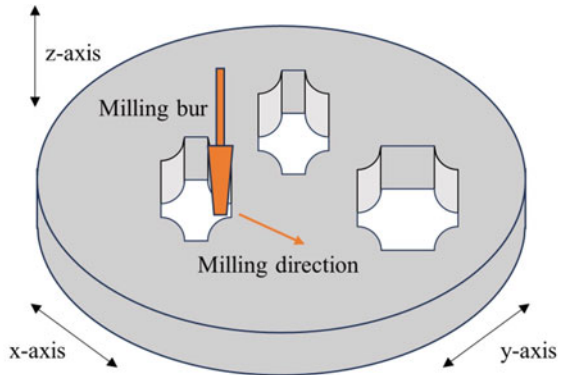
Fig. 3.5 Typical microstructure of a Co–Cr dental alloy, images from optical and electron microscopes

milling a fully sintered Co–Cr block [27]. Due to the complexity of dental restoration surfaces, milling machines use burs with different sizes for producing a single restoration, with an accuracy of tool positioning within $10\ \mu\text{m}$ [28] (Fig. 3.6).

In the past CAM methods were imprecise, and were linked to the prosthesis's poor quality and accuracy. However, continuous systems development and refinement, also in scanning technology, modelling software and production systems, greater ability for quality control, framework precision, parallel material development, the possibility of virtual evaluation and simpler fabrication, has increased the adoption of CAM techniques greatly in prosthodontics. The digital techniques exclude steps from conventional casting that may be sources of error, such as impression, waxing and casting. Additionally, fabrication time and costs are also reduced. One of the main benefits of milling is ensuring the durability of the dental framework, as it is milled from an industrial-grade blank, which has a higher quality control of the material manufacturer rather than the commercial laboratory. This can decrease fabrication errors in dental prostheses, as there are less inconsistencies and porosity in the material [28]. A disadvantage of this method is the large material waste produced, as milling may remove up to 80% of the initial block material for producing dental restorations.

In order to reduce the load on the milling machines, due to the high mechanical properties of Co–Cr alloys, soft milling was developed as a method, where milling

Fig. 3.6 Simplified drawing of the milling process in a 3-axis milling system, with a representation of dental restorations prepared by milling (machined using WorkNC Dental, the CAD/CAM software from Sescoi, presently owned by Hexagon AB)



is performed on softer milling blocks, made from wax-bound Co–Cr powder. The powder binder presents about 1–2% of the block’s composition, and is burnt away during sintering of the milled product. Densification then raises the alloy material to its optimal strength [27].

3.7.3 Additive Manufacturing of Co–Cr Dental Alloys

The development of additive technologies as an alternative to subtractive ones began in the late 1980s. They are distinguished by the construction of a single layer at a time from a liquid or powder that is joined by melting, fusing, or polymerisation, producing objects from polymers, composites, metals and alloys. Recently, additive manufacturing processes, referred to as 3D printing, have been used widely for rapid prototyping. This breakthrough in production technology enabled the production of new shapes and geometric properties by enabling the production of complex parts without additional processing. Improvements in time to market, ecological

impact and design compared to traditional industrial processes are expected with the development of these technologies.

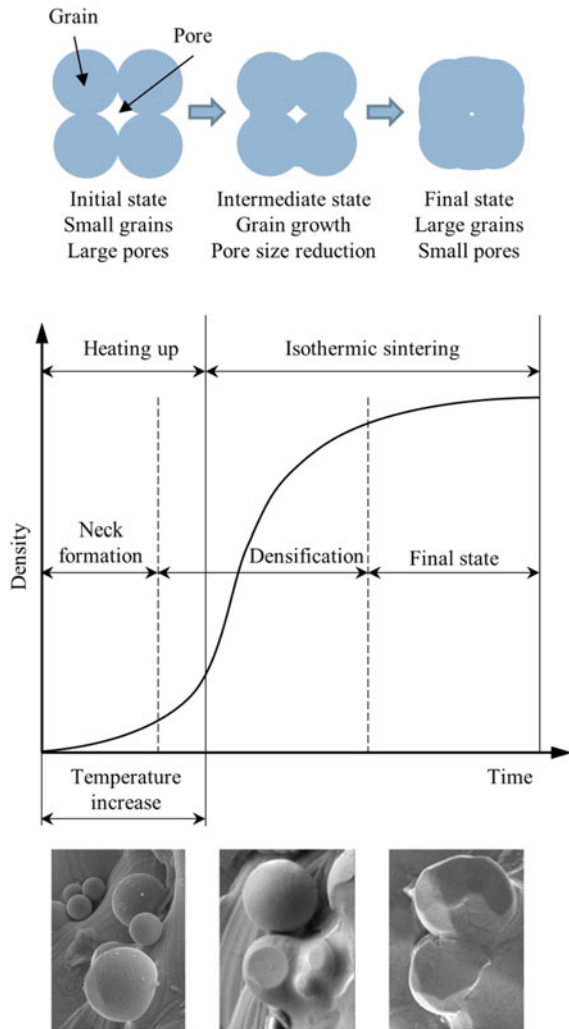
Two main approaches are used for fabricating dental restorations from Co–Cr alloys with additive manufacturing. One possibility is creating wax or polymeric cast patterns by 3D printing and casting a dental alloy framework from the printed object. The second possibility is producing a dental restoration directly from Co–Cr powder using Selective Laser Melting (SLM), Electron Beam Melting (EBM), or Selective Laser Sintering (SLS). These technologies use a focused high-powered laser or electron beam to fuse small particles of material into an object with the desired three-dimensional shape. Additive manufacturing reduces the required production and processing steps of conventional methods, while also reducing the material waste and time of fabrication greatly, and enabling greater freedom in object design.

Additive manufacturing of material powder in fabricating dental restorations may be divided into two types of particle fusion. In SLS, the discrete powder particles are joined layer by layer by sintering, or partly melting the individual particles. SLS is usually used for processing of polymers and ceramics [29], while also being possible for metals. The produced polymer object may then be used for casting of the alloy and fabrication of the dental restoration. In SLM or EBM the discrete particles are joined by complete melting, forming a localised melted region of material, which solidifies rapidly during fabrication, retaining the desired shape. These technologies are being used predominantly for metals.

Solid state sintering occurs at temperatures below the melting point, where diffusion of atoms and vacancies between material particles begins to occur. As particles grow together, their free energy is being lowered and a neck is formed, which continues to grow as long as the temperature is high enough to provide the necessary kinetic energy for the transport of vacancies and atoms (Fig. 3.7). A wide variety of materials can be processed this way; however, it is a slow process. For metallic materials, the heat supplied to a powder particle can also melt only a shell at the grain border of the powder particle, while the particle core stays unaffected. The molten shell then acts as a binder between the non-molten particle cores [30].

SLM is used for producing fully dense metal objects with optimal mechanical properties comparable to bulk materials. With SLM, the metal particles' melting and binding depends on the material properties, surface tension, viscosity of the liquid metal, laser absorption, beam diameter, laser power, scanning speed, laser energy density and powder layer thickness [30]. A melt pool is formed at the point of contact with the beam. As the beam moves forward the thermal energy is dissipated quickly to the substrate or previous solidified layer, due to the higher thermal conductivity of the solid compared to the surrounding powder [31], solidifying the metal, leaving residual stresses in the metal, especially for larger structures. Traces of the melting may also be visible in the microstructure (Fig. 3.8). The parameters for new materials need to be determined experimentally, in order to produce dense products with low porosity, with good accuracy, surface roughness, hardness and strength [29]. As the process produces a characteristic homogeneous microstructure, the mechanical properties are usually also higher than in the typical dendritic microstructure, as stated by the manufacturers (Table 3.1) and reported in several investigations [22,

Fig. 3.7 Formation of a neck between discrete powder particles and densification by sintering during the SLS process



24, 27]. According to the fabrication conditions, the circumstances for fully melted and partially melted particles may not be very straightforward when producing fully dense objects [30].

SLS and SLM produce residual stresses in the fabricated metal framework, due to the thermal gradients during processing. Thus, the framework may not fit as a dental restoration due to resulting deformations. Accordingly, the Co–Cr framework should be annealed at 750–800 °C in a protective atmosphere (argon) to remove these stresses, with a procedure known as thermal stress relieving. This procedure is mandatory for dental frameworks with 4 or more units (Fig. 3.9).

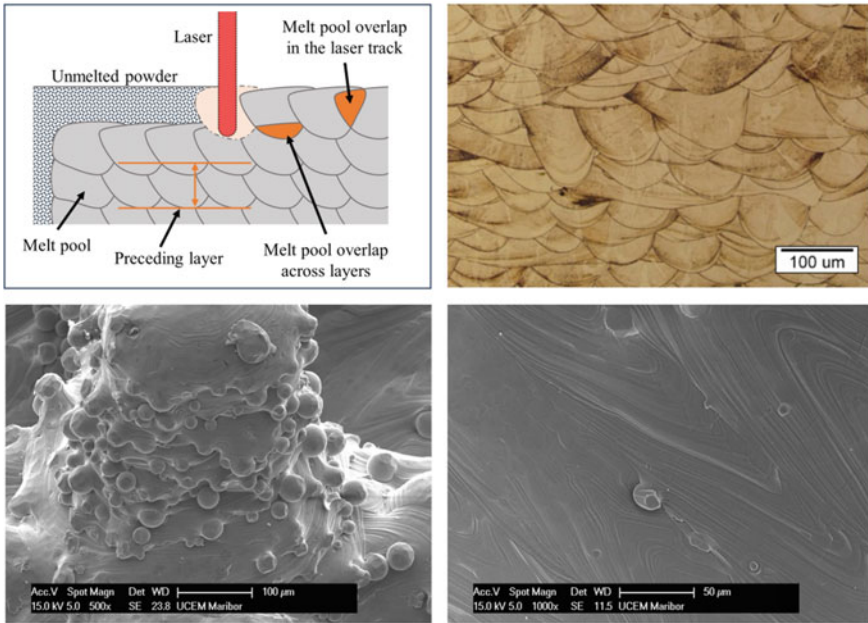


Fig. 3.8 Top: Schematic of melt pool overlapping during the SLM process, and a microstructure of a Co–Cr alloy with visible melt pools. Bottom: Electron microscope images of a side-view with visible SLM layers, and of an alloy surface with visible laser tracks

3.7.4 Veneering of Co–Cr Dental Alloys

Co–Cr dental alloys may be veneered with porcelain or resin composites to provide an aesthetic function for the prosthetic. Prostheses with porcelain fused to a metal framework are considered as high-quality dental restorations. The metal framework is covered with multiple layers of ceramics for the crowns, combining the high hardness and aesthetics of ceramics with the high toughness and resistance to fatigue of the underlying metal. The resin composite veneers are softer, with a wear resistance similar to dental enamel, and are employed in indications where a softer coating is required [32].

Co–Cr alloys have a relatively low coefficient of thermal expansion (Table 3.1), which means they expand and contract at a similar rate to the veneering materials. This property reduces the risk of material fracture or delamination between the alloy and the veneer due to thermal cycling. The high melting point also presents good characteristics for ceramic firing, without concern for introducing deformations during ceramic firing for low fusing or high fusing ceramic powders, at temperatures from 800 °C to 1100 °C. These alloys have a surface roughness that allows for effective bonding with ceramic or composite veneering materials. The roughened surface enhances the mechanical interlocking and adhesion between the alloy and the veneer, improving the overall bond strength. An oxidative heat treatment at temperatures

Table 3.1 Co–Cr alloy compositions and thermo-mechanical properties from various manufacturers (taken from technical data declared by the manufacturers in 2023)

Composition (wt.%)	Wirobond 280 Bego	Wirobond C + Bego	Remanium star dentaurum	Biodur soft DFS diamon	Starbond easy Scheftner dental	Keralloy KB siladent
	Casting	SLM powder	Casting milling SLM powder	Casting	Milling SLM powder	Casting
Co	60.2	63.9	60.5	61.0	61.0	64.0
Cr	25.0	24.7	28.0	24.0	27.5	21.0
W	6.2	5.4	9.0	8.0	8.5	6.0
Mo	4.8	5.0		2.5		6.0
Ga	2.9					
Si	<1.0	1,0	1.5	1.0	1.6	1.0
Mn	<1.0		<1.0	1.0	<1.0	1.0
C					<1.0	
Fe				1.0	<1.0	1.0
Nb			<1.0	1.0		
N			<1.0			
ISO 22674 type	IV	V	V	IV	IV	V
Density [g/cm ³]	8.6	8.6	8.6	8.6	8.7	8.8
Young's modulus [GPa]	221	215	190 ^{Cast} 202 ^{Mill} 230 ^{SLM}	200	190	194
Proof strength (R _{p0.2}) [MPa]	475	1090	620 ^{Cast} 320 ^{Mill} 800 ^{SLM}	482	610	570
Tensile strength [MPa]	680	1315	845 ^{Cast} 506 ^{Mill} 1170 ^{SLM}	609	830	734
Elongation at fracture [%]	9	4	10,2 ^{Cast} 5,9 ^{Mill} 11 ^{SLM}	5	10	10
Vickers hardness [HV10]	280	470	280 ^{Cast} 281 ^{Mill} 395 ^{SLM}	314	285	286
Solidus temperature [°C]	1355	1380	1320	1300	1310	1309

(continued)

Table 3.1 (continued)

Composition (wt.%)	Wirobond 280 Bego	Wirobond C + Bego	Remanium star dentaurum	Biodur soft DFS diamon	Starbond easy Scheftner dental	Keralloy KB siladent
	Casting	SLM powder	Casting milling SLM powder	Casting	Milling SLM powder	Casting
Liquidus temperature [°C]	1430	1420	1420	1395	1410	1417
Casting temperature [°C]	1500	N/A	1520	1500	1480–1530	1460
CTE 25–500°C [10 ⁻⁶ K ⁻¹]	14.3	14.3	14.1 ^{Cast} 14.1 ^{Mill} 14.4 ^{SLM}	14.4	14.4	14.1

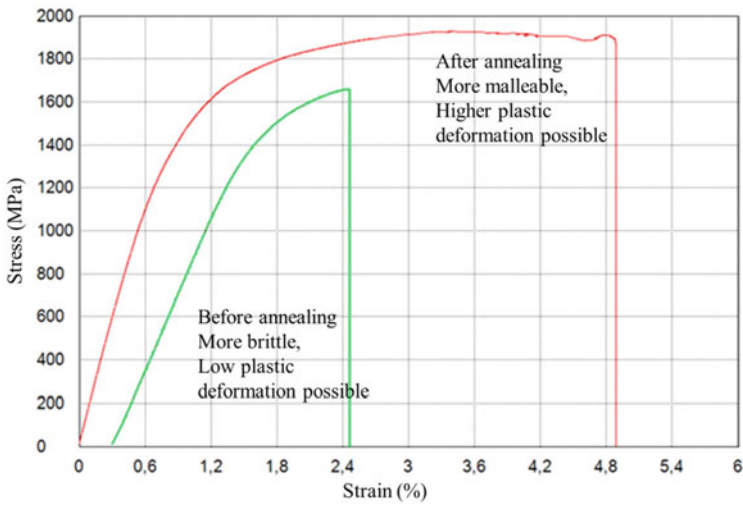


Fig. 3.9 Example of a stress–strain curve before and after annealing for relieving residual stresses

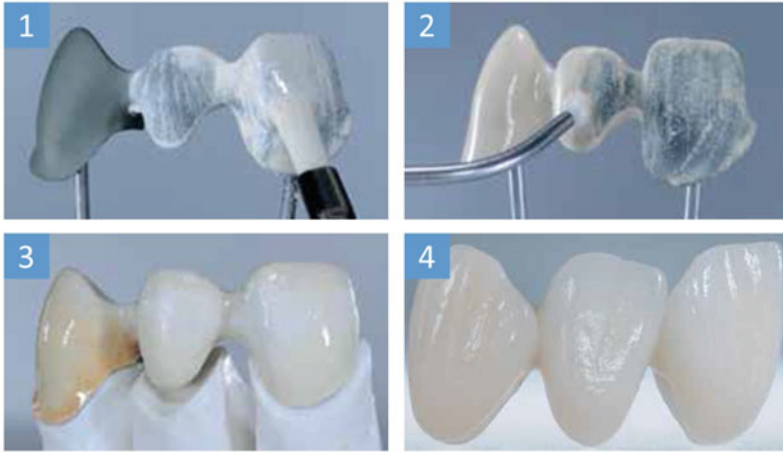


Fig. 3.10 Representation of a first and second opaquer burning, with a ceramic firing and the final metal-ceramic dental bridge

around 900–980 °C creates an oxide layer on the surface of the alloy, improving the bonds between the Co–Cr alloys and ceramics further, making them more adherent and resistant. Other important characteristics of an oxide layer are its colour and thickness. Additional finishing treatments also affect the ceramic bonding, such as sandblasting, acid etching and hardening agents [16]. Overall, Co–Cr dental alloys present no major difficulties in following conventional veneering procedures, from surface preparation with sandblasting, decontamination, to the multistep opaque and ceramic firings (Fig. 3.10).

Several studies were performed for determination of veneer bonding strength, durability, clinical longevity and long-term complications, showing the high quality of these dental restorations with few complications. Veneer characteristics were also studied in relation to conventional casting, milling and additive manufacturing, with results showing no detrimental effect on the veneer bond or other functions between using the different production processes for fabricating the metal framework [24, 32, 33].

References

1. Y.S. Al Jabbari, Physico-mechanical properties and prosthodontic applications of Co–Cr dental alloys: a review of the literature. *J. Adv. Prosthodont* **6**, 138 (2014). <https://doi.org/10.4047/jap.2014.6.2.138>
2. A. Carek, J.Z. Babic, Z. Schauerl, T. Badel, Mechanical properties of Co–Cr alloys for metal base framework. *Int. J. Prosthodont Restor. Dent.* **1**, 13–19 (2011). <https://doi.org/10.5005/jp-journals-10019-1003>

3. X. Han, T. Sawada, C. Schille et al., Comparative analysis of mechanical properties and metal-ceramic bond strength of Co–Cr dental alloy fabricated by different manufacturing processes. *Materials* (Basel) **11**, 1801 (2018). <https://doi.org/10.3390/ma11101801>
4. R. Messer, J. Wataha, Dental materials: biocompatibility, in *Encyclopedia of Materials: Science and Technology*. ed. by K.H.J. Buschow, R.W. Cahn, M.C. Flemings et al. (Elsevier, Oxford, 2002), pp.1–10
5. A. Vaicelyte, C. Janssen, M. Le Borgne, B. Grosogeat (2020) Cobalt–Chromium dental alloys: metal exposures, toxicological risks, CMR classification, and EU regulatory framework. In: *Cryst 2020*, vol. 10, p. 1151. <https://doi.org/10.3390/CRYST10121151>
6. W. Braemer, Biocompatibility of dental alloys. *Adv. Eng. Mater.* **3**, 753 (2001). [https://doi.org/10.1002/1527-2648\(200110\)3:10%3c753::AID-ADEM753%3e3.0.CO;2-G](https://doi.org/10.1002/1527-2648(200110)3:10%3c753::AID-ADEM753%3e3.0.CO;2-G)
7. M.S. Hasan, A.M. Mazid, R. Clegg, The basics of stellites in machining perspective. *Int. J. Eng. Mater. Manuf.* **1**, 35–50 (2016). <https://doi.org/10.26776/IJEMM.01.02.2016.01>
8. Kennametal Inc., Stellite (2023). <https://www.stellite.com/>. Accessed 29 May 2023
9. B.D. Ratner, A.S. Hoffman, F.J. Schoen, J.E. Lemons, *Biomaterials Science: An Introduction to Materials*, 3rd edn. (Elsevier, 2013)
10. D.J.S. Hyslop, A.M. Abdelkader, A. Cox, D.J. Fray, Electrochemical synthesis of a biomedically important Co–Cr alloy. *Acta Mater.* **58**, 3124–3130 (2010). <https://doi.org/10.1016/j.actamat.2010.01.053>
11. J. Barnhart, Occurrences, uses, and properties of Chromium. *Regul. Toxicol. Pharmacol.* **26**, S3–S7 (1997). <https://doi.org/10.1006/rtph.1997.1132>
12. M. Podrez-Radziszewska, K. Haimann, W. Dudziński, M. Morawska-Sołtysik, Characteristic of intermetallic phases in cast dental CoCrMo alloy. *Arch. Foundry Eng.* **10**, i:51–56 (2010)
13. T. Dikova, D. Dzhendov, M. Simov, Microstructure and hardness of fixed dental prostheses manufactured by additive technologies. *J. Achiev. Mater. Manuf. Eng.* 60–69 (2015)
14. G. Barucca, E. Santecchia, G. Majni et al., Structural characterization of biomedical Co–{Cr}–{Mo components produced by direct metal laser sintering. *Mater. Sci. Eng. C* **48**, 263–269 (2015). <https://doi.org/10.1016/j.msec.2014.12.009>
15. D. Majerič, V. Lazič, P. Majerič et al., Investigation of CoCr dental alloy: example from a casting workflow standpoint. *Crystals* **11**, 849 (2021). <https://doi.org/10.3390/CRYST11080849/S1>
16. W.A. Uriciuc, A.B. Boşca, A.M. Băbțan et al., Study on the surface of Cobalt–Chromium dental alloys and their behavior in oral cavity as cast materials. *Mater* (Basel, Switzerland) **15** (2022). <https://doi.org/10.3390/MA15093052>
17. W. Elshahawy, I. Watanabe, Biocompatibility of dental alloys used in dental fixed prosthodontics. *Tanta Dent. J.* **11**, 150–159 (2014). <https://doi.org/10.1016/j.tdj.2014.07.005>
18. J.C. Wataha, Biocompatibility of dental casting alloys: a review. *J. Prosthet. Dent.* **83**, 223–234 (2000). [https://doi.org/10.1016/S0022-3913\(00\)80016-5](https://doi.org/10.1016/S0022-3913(00)80016-5)
19. L. Reclaru, H. Lüthy, P.-Y. Eschler et al., Corrosion behaviour of cobalt–chromium dental alloys doped with precious metals. *Biomaterials* **26**, 4358–4365 (2005). <https://doi.org/10.1016/j.biomaterials.2004.11.018>
20. T.S. Kueh, F. Reza, Evaluation of physical properties and casting accuracy of chrome-cobalt alloys with different casting systems and investments. *J. Phys. Sci.* **23**, 91–102 (2012)
21. VDDI, Cobalt in dental alloys. VDDI – Assoc. Ger. Dent. Manuf. (2021)
22. A.G.C. Presotto, J.M. Cordeiro, J.G.C. Presotto et al., Feasibility of 3D printed Co–Cr alloy for dental prostheses applications. *J. Alloys Compd.* **862**, 158171 (2021). <https://doi.org/10.1016/j.jallcom.2020.158171>
23. J.-Y. Park, H.-Y. Kim, J.-H. Kim et al., Comparison of prosthetic models produced by traditional and additive manufacturing methods. *J. Adv. Prosthodont* **7**, 294 (2015). <https://doi.org/10.4047/jap.2015.7.4.294>
24. D. Stamenković, M. Popović, R. Rudolf et al., Comparative study of the microstructure and properties of cast-fabricated and 3D-printed laser-sintered Co–Cr alloys for removable partial denture frameworks. *Mater* **16**, 3267 (2023). <https://doi.org/10.3390/MA16083267>
25. L. Rejab, I. Hasan, S. Al-Hamdani Evaluation the castability of titanium casting alloy. *Al-Rafidain Dent. J.* **13**, 396–402 (2020). <https://doi.org/10.33899/rden.2020.165360>

26. E. Ansarifard, M. Farzin, A. Zohour Parlack et al., Comparing castability of Nickel-Chromium, Cobalt-Chromium, and non-precious gold color alloys, using two different casting techniques. *J. Dent. (Shiraz, Iran)* **23**, :7–12 (2022). <https://doi.org/10.30476/DENTJODS.2021.87573.1275>
27. A. Barazanchi, K. Li, B. Al-Amleh et al., Mechanical properties of laser-sintered 3D-printed Cobalt Chromium and soft-milled Cobalt Chromium. *Prosthesis* **2**, 313–320 (2020). <https://doi.org/10.3390/prosthesis2040028>
28. J. Abduo, K. Lyons, M. Bennamoun, Trends in computer-aided manufacturing in prosthodontics: a review of the available streams. *Int. J. Dent.* **2014**, 1–15 (2014). <https://doi.org/10.1155/2014/783948>
29. D. Dzhendov, T. Dikova, Application of selective laser melting in manufacturing of fixed dental prostheses. *J. IMAB – Ann. Proc. (Sci. Pap)* **22**, 1414–1417 (2016). <https://doi.org/10.5272/jimab.2016224.1414>
30. J.P. Kruth, P. Mercelis, J. Van Vaerenbergh et al., Binding mechanisms in selective laser sintering and selective laser melting. *Rapid Prototyp. J.* **11**, 26–36 (2005). <https://doi.org/10.1108/13552540510573365/FULL/PDF>
31. S.L. Sing, W.Y. Yeong, F.E. Wiria, Selective laser melting of titanium alloy with 50 wt% tantalum: Microstructure and mechanical properties. *J. Alloys Compd.* **660**, 461–470 (2016). <https://doi.org/10.1016/j.jallcom.2015.11.141>
32. Ó. Barro, F. Arias-González, F. Lusquiños et al., Characterization of Co–Cr–W dental alloys with veneering materials manufactured via subtractive milling and additive manufacturing LDED methods. *Materials (Basel)* **15**, 4624 (2022). <https://doi.org/10.3390/ma15134624>
33. M. Revilla-León, M. Gómez-Polo, S.H. Park et al., Adhesion of veneering porcelain to Cobalt–Chromium dental alloys processed with casting, milling, and additive manufacturing methods: A systematic review and meta-analysis. *J. Prosthet. Dent.* **128**, 575–588 (2022). <https://doi.org/10.1016/j.prosdent.2021.01.001>

Chapter 4

Prosperous Shape Memory Alloys (SMAs)



Abstract Beginning with the Shape Memory Mechanism, two types of Shape Memory Alloys (SMA) are considered: (i) Nickel-Titanium Alloys and (ii) Copper-based Alloys. SMA orthodontic appliance NiTi Orthodontic Wire is thoroughly discussed. In the section Expertise Examples, we highlight: (1) Comparison of commercially available NiTi orthodontic wires, (2) Experimentation with continuous casting of nitinol, and (3) Microstructure, mechanical characteristics, and corrosion behavior of NiTi and CuAlNi alloys made by continuous casting. Ni-Ti wire corrosion and biocompatibility are specifically addressed. We highlight (I) the surface characterisation of NiTi orthodontic archwires following mechanical loading simulation in CaCO_2 -2 cell culture and (II) the deposition of an atomic layer of a TiO_2 on Ni-Ti SMAs for corrosion prevention in a simulated body fluid.

Abbreviations

CuAlNi	Copper/Aluminium/Nickel SMA
EDX	Energy Dispersive X-ray analysis
FIB	Focused Ion Beam
HV	Hardness according to Vickers
ICP-MS	Inductively Coupled Plasma-Mass Spectrometry
Intermediate R	phase characterised by their rhombohedral structure
NiTi	Nickel/Titanium SMA
MTT	Colorimetric assay for measuring cell metabolic activity
SEM	Scanning Electron Microscope
SMA	Shape Memory Alloy
SME	Shape Memory Effect
SE	Super-Elasticity
A_s	(Austenite–start) temperature
A_f	(Austenite–finish) temperature
E_1	elastic modulus of austenite
E_2	elastic modulus of austenite to martensite

E_3	elastic modulus of martensite
M_s	(Martensite–start) temperature
M_f	(Martensite–finish) temperature
σ_{SM}	the initial stress value of the transformation region or plateau
σ_{FM}	the final stress value of the transformation plateau
σ_f	the stress value at failure

4.1 Introduction

Arne Lander, a Swedish chemist, found the Shape-Memory Effect in a gold-cadmium alloy in 1932 [1]. Buehler and Wang invented the Nickel-Titanium Shape-Memory Alloy (NiTi-SMA/Nitinol) in 1959 [2]. The use of NiTi-SMA in Orthodontics started in 1970, when Andreasen [3] advocated for its use. The Unitek Corporation created the first orthodontic wire on the market (now 3 M Unitek, Monrovia, CA, USA). NiTi dental wires are now used widely in Orthodontics.

The Shape-Memory Effect (SME) and Super-Elasticity (SE) are two special properties obtained from a martensitic/austenitic phase transformation that contribute to this material's broad applicability. The crystal structure of the austenite phase (stable at high temperatures and low stress) differs from that of the martensitic phase (stable at low temperature and high stress). The austenitic phase has a body-centred cubic crystal structure, whereas the martensitic phase has a monoclinic structure. This material's phase change is caused by shear distortion of its lattice structure rather than atomic diffusion [4].

Alloys that recall their shape emerged from a phenomenon known as the Shape Memory Effect (shape memory), which refers to the ability of some plastically deformed metals and alloys to return to their original shape when heated, due to the complete or nearly complete disappearance of the deformation. Under certain conditions, these materials take place in the so-called thermoelastic martensitic transformation that produces unusual macroscopic effects, whereby the phenomenon of shape memory can be manifested in: (a) Unidirectional SME, (b) Two-way SME, and (c) Pseudoelasticity [5].

Because they respond to temperature changes by deforming visibly, SMAs are SMART materials [6].

SMAs are classified into a variety of groups [1, 7, 8]:

- (a) NiTi-based alloys (NiTi, NiTiCu, NiTiNb),
- (b) Cu-based alloys (CuZnAl, CuAlNi, CuAlMn, CuAlBe),
- (c) TiNb-based alloys (TiNb, TiNbZr, TiNbZrTa), and
- (d) Fe-based alloys (FePt, FePd, FeNiCo, FeMnSi, FeMnAl).

Different methods are used to create these materials: (i) Induction melting, (ii) Arc melting, (iii) Powder metallurgy, (iv) Rapid solidification, (v) Mechanical alloying and (vi) Additive Manufacturing [9].

The most significant alloys that exhibit this effect are nickel- and titanium-based alloys, as well as copper-based alloys. Alloys based on Ni–Ti (so-called nitinol) are known for their strong shape memory ability. Due to their high price and complex production, they have been replaced by cheaper and more accessible copper-based alloys [10].

The copper-based alloys that exhibit the shape memory effect are: Cu–Al–Ni, Cu–Au–Zn, Cu–Sn, Cu–Zn, Cu–Zn–Si, Cu–Zn–Sn, Cu–Zn–Al, Cu–Zn–Ga, etc. These alloys, compared to Ni–Ti alloys, have slightly weaker mechanical properties, due to larger grains and greater elastic anisotropy. However, they can be improved, without worsening the effect of shape memory significantly, by crushing the grains, using rapid solidification methods, powder metallurgy or by adding elements such as: Zr, V, B, Ti, Cr, etc. [1, 8].

In addition, copper-based alloys can be produced in a simpler and more economical way, so they are cheaper compared to Ni–Ti alloys, whose production and processing technology is expensive and complicated. Also, their application in various fields is great [11, 12].

4.2 Shape Memory Mechanism

The martensite crystal structure is the basis for achieving the shape memory effect. It can be reached in two basic ways:

- (I) By subjecting the alloy to a pressure whose strength is proportional to the temperature, or
- (II) Sudden quenching of the alloy from some critical temperature.

Using the second method, which is much more widespread, the martensite structure is formed spontaneously, by shearing of alloy atoms, or by processes of nucleation and crystal growth.

SMA's are unique materials that can regain their form when the temperature is raised. These materials exhibit two distinct properties: SME and SE (Fig. 4.1). Both effects are characterised by martensitic phase transformation, which is induced by temperature changes (shape memory) or stress application (superelastic effect), resulting in changes in either phase or microstructure. The austenite phase is stable at high temperatures and low strains, whereas the martensitic phase is stable at lower temperatures and low stresses. The crystal structures of these phases vary. The martensitic phase has a monoclinic crystal structure, whereas the austenitic phase has a body-centred cubic crystal structure. Atomic diffusion does not occur during the transition from one structure to the other. Shear lattice distortion causes the change. So, the diffusion-less transformation is, in fact, the martensitic transformation. When the alloy is deformed above A_f , SME enables it to return to its original shape. The SMA returns to its initial shape by undergoing austenite transformation. The stress-strain-temperature diagram in Fig. 4.1 depicts a typical NiTi specimen evaluated under uniaxial loading in completely martensitic and fully austenitic phases. The

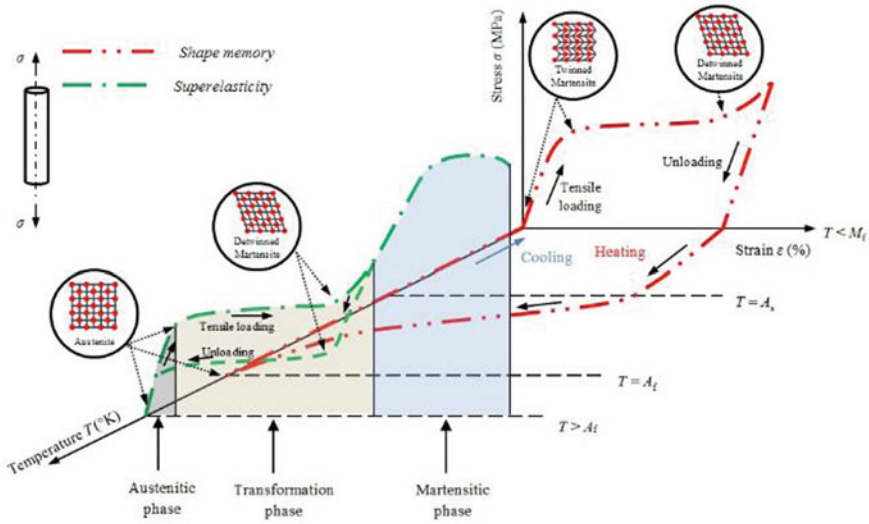


Fig. 4.1 The Shape Memory and Superelastic impact of NiTi alloy is demonstrated by a stress-strain-temperature diagram. Temperature and stress changes cause crystal transition

SMA’s superelastic effect (SE) is represented above A_f . SE has been linked to stress-induced change. The superelastic impact is depicted in Fig. 4.2. When stressed, the SMA’s microstructure transforms from austenite to detwinned martensite. When unloaded, the SMA returns to its natural shape. The induced tension during unloading is lower than the induced stress during loading. Hysteresis is the difference en route between loading and unloading [5, 13, 14].

SMA NiTi wires’ excellent biocompatibility and functional characteristics allow for widespread use in Orthodontics. In general, NiTi SMA wires have good corrosion resistance. Nickel ions are released, despite the fact that protective layers of TiO_2 are formed on the surface of the filaments. Regardless of this, biocompatibility tests indicate that SMA NiTi alloys are low in cytotoxicity and genotoxicity [2, 3].

4.3 Nickel–Titanium Alloys

The Ni–Ti alloy exhibits a thermoelastic martensitic transformation, that is responsible for either *shape memory* or *superelasticity*. These alloys (so-called *nitinol*) have an exceptional property that is reflected in the phenomenon that, after heating, the deformed alloy returns to its original shape. The atomic ratio of Ni to Ti in these alloys is approximately 1: 1, Fig. 4.3.

The chemical composition of Ni–Ti alloys is very important, because it has a decisive influence on the phase transition’s temperature. For example, the equiatomic composition (50 at.% Ni and 50 at.% Ti) exhibits the maximum A_f temperature

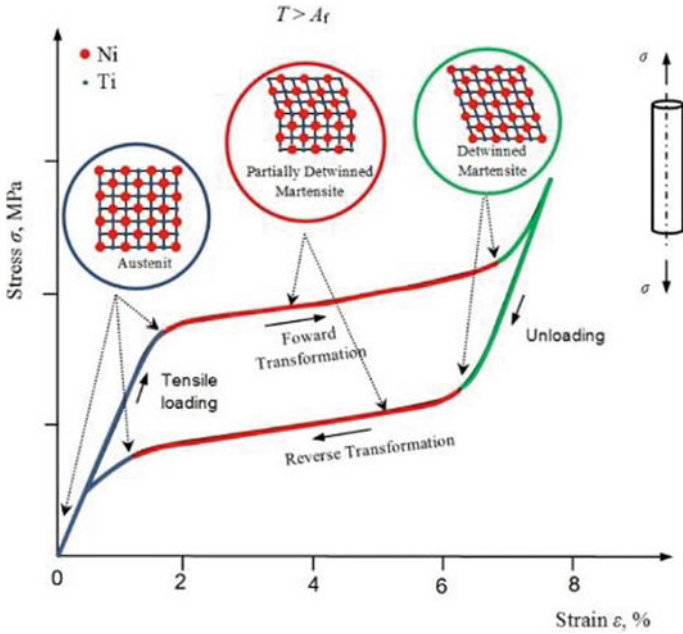


Fig. 4.2 The superelastic impact is depicted schematically (stress-strain curve for SMA under uniaxial loading)

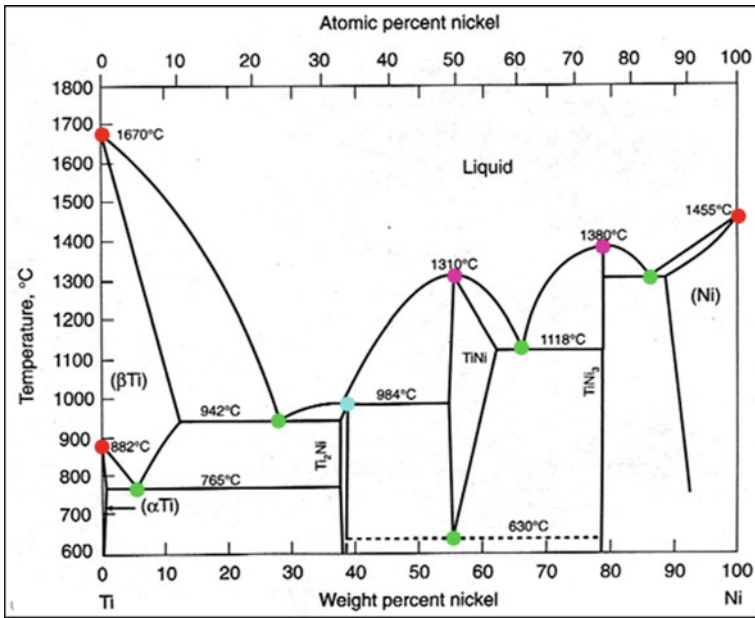


Fig. 4.3 Ni–Ti equilibrium diagram

120 °C. By increasing the value of the Ni atomic percentage, the transformation temperature decreases. For 51 at.% nickel it is $A_f -40$ °C [6, 7].

4.3.1 *Manufacture of Ni–Ti Alloys [15, 16]*

Manufacturing technologies/methods are usually classified as summarised in Table 4.1.

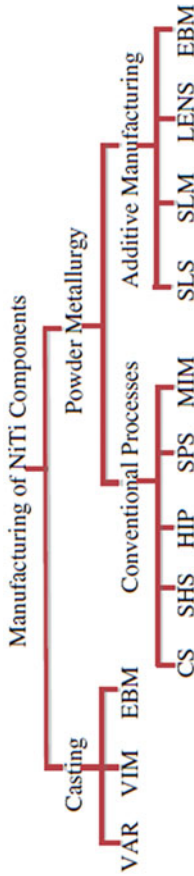
Vacuum Induction Melting (VIM) and Vacuum Arc Remelting (VAR) are the two most common melting techniques. They both provide suitable material for SMA NiTi orthodontic wire according to the requirements (ASTM F2063).

Production of NiTi orthodontic wire is a complex process. Figure 4.4 shows a schematic view of the processes that occur after the following:

1. *Vacuum melting/casting*: The manufacture of NiTi alloys is often done by Vacuum Induction Melting (VIM) in a graphite crucible. The VIM is used because the molten state of NiTi is very reactive if the Ti is close to fifty percent. The graphite, or calcia (CaO), crucible is preferred for VIM because the others contaminate the molten NiTi with oxygen. Vacuum Arc Remelting (VAR) is used to make the raw materials (Ni and Ti) before the NiTi alloy is melted. This VAR method is used to achieve the best possible alloy homogeneity and purity. The double vacuum melting process (VAR → VIM) guarantees quality, and the mechanical properties of the NiTi alloy are maintained.
2. The ingots are hot worked with *press forging*.
3. *Rotary swaging* follows to different shapes. Around 800 °C looks to be the optimum temperature for hot working. At this temperature, the alloy is readily workable and the surface is not overly oxidised.
4. This is followed by cold working on sizes (rolling) according to the product (rod, wire). Cold working NiTi is difficult, because the metal work hardens rapidly.

The procedure (Fig. 4.4) of hot and cold treatments, followed by the rolling procedure, obtained a tapered shape, followed by the procedure of annealing the wire or rod into a coiled state. Because of the work-hardness, numerous reductions and frequent inter-pass annealing are required at 600–800 °C. This is followed by the procedure of descaling, and then comes the process of fine drawing of wire and annealing again. After these phases follows the actual production profile (round, square, rectangular). The rectangular wires can be manufactured by drawing round wires. The next step is then cleaning of the wire, followed by training of the wire. Training is thermo-mechanical treatment to achieve the optimised properties. Superelastic NiTi materials are heat treated in the vicinity of 500 °C. For Shape Memory Alloys a suitable temperature is in the range between 350 and 450 °C [15, 16].

Table 4.1 Review of the NiTi manufacturing methods



Method	Description
VAR	Vacuum arc remelting
VIM	Vacuum induction melting
EBM	Electron beam melting
CS	Conventional sintering
SLS	Selective laser sintering
SLM	Selective laser melting
SHS	Self-propagating high temperature synthesis (combustion) synthesis
HIP	Hot isostatic pressing
SPS	Spark plasma sintering
MIM	Metal injection moulding
LENS	Laser engineered net shaping

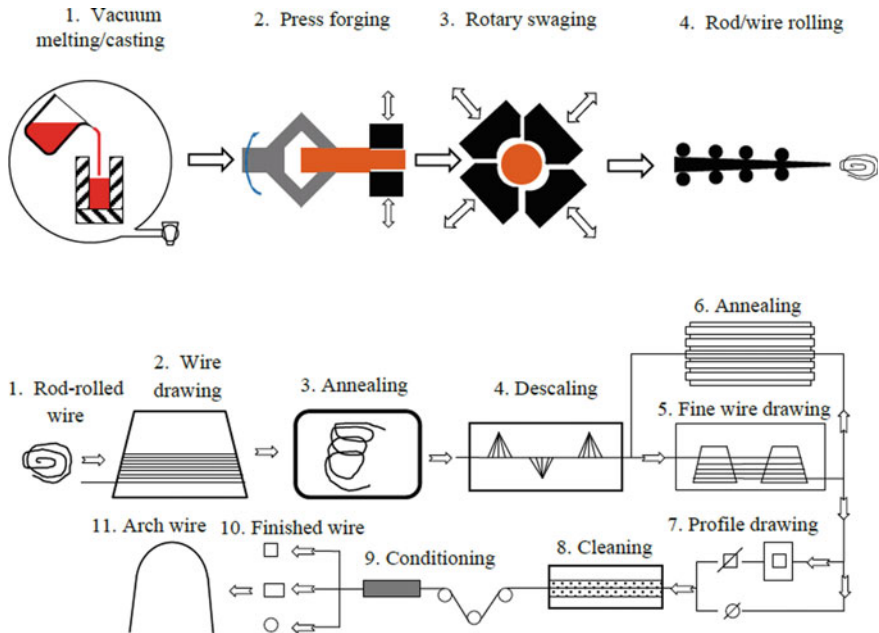


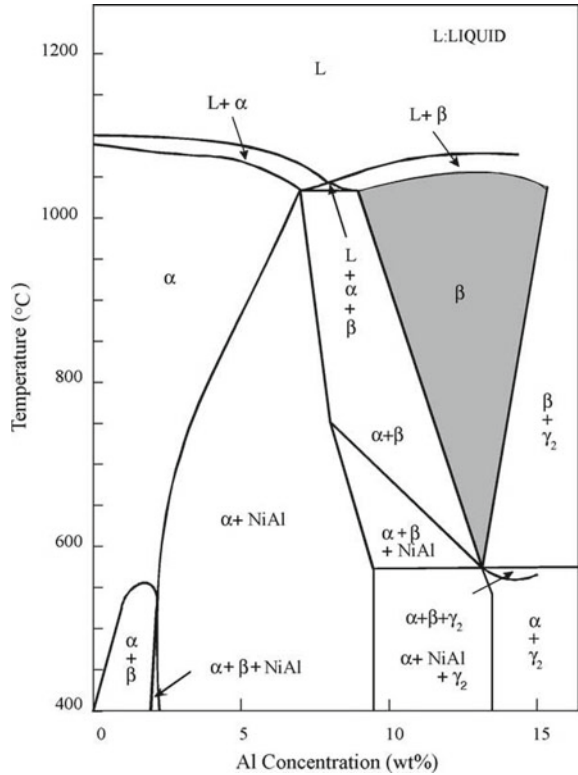
Fig. 4.4 Schematic representation of the manufacturing process of NiTi alloy (top) with the production of finished NiTi wire (bottom)

4.4 Copper-Based Alloys

Shape-memory copper-based alloys of today are derived from three binary alloy systems: (I) Cu–Zn, (II) Cu–Al, and (III) Cu–Sn. At the same time, the effect of shape memory has been studied extensively in Cu–Zn alloys with additions of Al, Si, Sn, Ga and Mn, and Cu–Al alloys with additions of Ni, Be, Zn and Mn. The addition of alloying elements to Cu–Zn and Cu–Al alloys was carried out in order to regulate the temperature of the martensitic transformation and optimise the thermal stability and mechanical properties [12, 17, 18, 26].

Cu-based SMAs have been a promising material due to their lower cost and simpler manufacturing procedure when compared to Ti-based SMAs. CuAlNi alloys, shown in Fig. 4.5 [26], have been identified as promising materials for high temperature uses (HT-SMAs). This is because they have a high thermal stability at temperatures above 100 °C. These alloys, however, have limitations, such as high brittleness due to the emergence of a γ_2 -phase at grain boundaries and grain size increase during heat treatment. As a result, their disadvantages have limited their use in commercial applications, particularly in SE applications. Surely, the solution is to refine the grain of the CuAlNi SMAs by introducing alloying elements such as Be, or by varying the Ni and Al compositions. As a result, the mechanical properties of Cu-based SMAs can be improved greatly [17, 18].

Fig. 4.5 Cu–Al–Ni ternary phase diagram, vertical cross-section at 3 wt.% Ni [26]



4.5 Orthodontic Appliance by SMA NiTi Orthodontic Wire

In the process of the orthodontic treatment of protruding teeth the technique of a gentle and continuous force is used on the teeth. The force exerted on the tooth to create stresses acts first on the tooth and then it is transferred to the periodontal ligament. These stresses subsequently cause a change in the blood supply to the periodontal ligament, leading to the transformation of the jaw. At the same time, it is used to move teeth into their correct position in the oral cavity. Fixed orthodontic braces are used for efficient operation of forces on several teeth at the same time (Fig. 4.6). These orthodontic braces consist of brackets which are attached to the crown of the tooth, so that they are glued or fastened to the teeth with special bands. When the Orthodontist has placed the bracket on each tooth on the upper or lower jaw, the orthodontic wire is then introduced. The arch-wire, which is inserted into the slots in the brackets, causes force on the tooth, and, consequently, the movement during the course of treatment [10, 19, 20]. At the same time, multi-axial deformation of the orthodontic wire is present.

The desirable properties of orthodontic wires are, mainly, the following: good biocompatibility, good spring-back, good range, and tough and low fraction. It's also

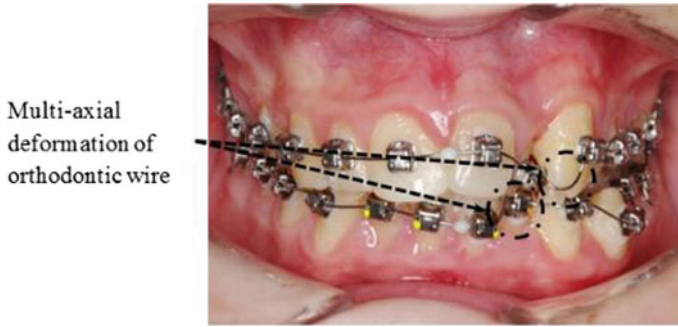


Fig. 4.6 Fixed orthodontic appliance by SMA NiTi orthodontic wire

important that the formability is resilient, so that the Orthodontist may deform it into loops or a band fused onto a clasp, and must have the ability to return to its original shape. The wire must also be the most aesthetic, so that it does not disturb the looks of the human mouth. An ideal arch-wire with ideal properties does not exist [21, 22].

The reason why the SMA NiTi was introduced into orthodontic practice is that it has good biocompatibility and has a specific mechanical property (super elasticity), which SMAs possess. An important feature of the functional SMA used for the orthodontic wire is the low modulus of elasticity, which creates a small force on the teeth and large recoverable strain (range), which, in turn, creates a continuous duration of force during orthodontic treatment. These properties are important in the process of orthodontic treatment, and this improves the superelasticity of SMA NiTi successfully [10].

4.6 Examples of Expertise

4.6.1 Comparison of Commercially Available NiTi Orthodontic Wires

New NiTi wires (diameter of 0.014"– 0.3556 mm), from different producers, taken from original packages were used in the studies [23], Table 4.2.

Semi-quantitative EDX analysis with SEM observations were used to determine the microchemical composition and microstructure characteristic, DSC analysis was used to determine the phase temperatures, and a tensile test was used to determine the mechanical properties of the wires.

EDX—semi quantitative chemical analysis. The chemical composition of all six archwires was determined using longitudinal cross-sections and wire surfaces. Semi-quantitative chemical microanalysis was performed using an electron microscope Sirion NC 400 equipped with an energy dispersive X-ray (EDX) detector. Figure 4.7

Table 4.2 Orthodontic archwires from various manufacturers [23]

No	Type of the wire	Short name
1 (a)	Damon CuNiTi	D
2 (b)	Thermo-Active	DT
3 (c)	NiTi	G
4 (d)	NiTi	O
5 (e)	Thermo	OT
6 (f)	Rematitan	RD

depicts the Ni content on the surface and longitudinal section of the individual wires. Except for wire D, which has a lower Ni concentration due to the presence of Cu, all the wires contained more than 50 at.% of Ni. Figure 4.7 also demonstrates that the percentage of Ni on the surface and in the bulk is similar (a noticeable difference is only visible in wire D).

Phase transformation temperature. M_s (martensite-start) and M_f (martensite-finish) temperatures, as well as A_s (austenite-start) and A_f (austenite-finish) temperatures, are important for phase transformation in NiTi wires. Some SMA materials may have an intermediary R-phase with a rhombohedrum crystal structure. The beginning of phase formatting is known as R_s , and the conclusion is known as R_f . Differential Scanning Calorimetry (DSC) is used frequently to measure these temperatures under stress-free conditions. The specimens for DSC analysis in our investigation were cut from orthodontic wires. Each specimen for DSC analysis was made up of a 3–4 mm length piece of wire. The DSC studies were carried out on a NETZSCH STA 449 machine with a liquid nitrogen cooling accessory. To obtain the cooling DSC curves, the specimen was heated to 100 °C and then cooled to –100 °C. The specimen was

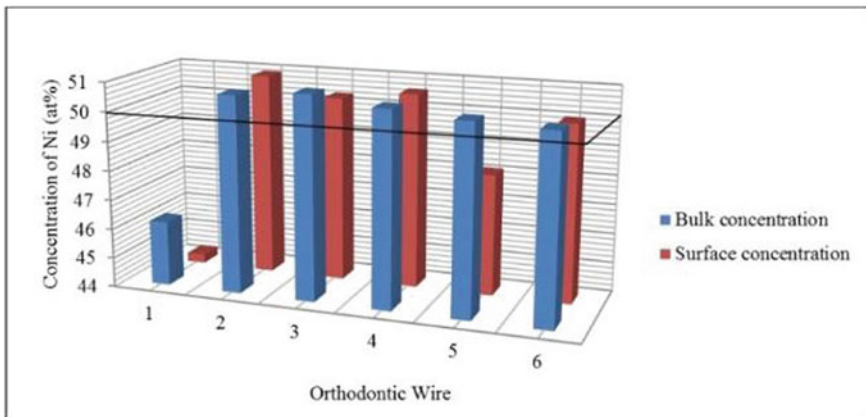


Fig. 4.7 Diagram of Ni in at.% concentration in separate orthodontic wire [23]

then heated from $-100\text{ }^{\circ}\text{C}$ to $100\text{ }^{\circ}\text{C}$ to produce the heating DSC curve. The cooling rate was $10\text{ }^{\circ}\text{C}/\text{min}$, as is typical for SMA NiTi.

Figure 4.8 shows the DSC plots for both the heating and cooling trends for individual orthodontic wires. All the heating curves presented with temperatures A_f less than $37\text{ }^{\circ}\text{C}$ (body temperature), showing a superelastic effect during orthodontic treatment.

Table 4.3 shows the temperatures of the phase transition. The temperatures required for full austenite stability varied from 14.3 to $26.8\text{ }^{\circ}\text{C}$. The R-phase was first seen in the dental wire RD. The temperatures required for full martensite stability varied from $-14.58\text{ }^{\circ}\text{C}$ to $-71.3\text{ }^{\circ}\text{C}$. Above $0\text{ }^{\circ}\text{C}$, the orthodontic wires D, O, and RD began their transition into the R phase or, respectively, martensite, while the temperature of food consumed had the final impact on the phase changes. This caused the SMA properties to alter. In particular, in the martensitic phase, these alloys have a reduced modulus of elasticity, expressing higher forces on the teeth. Consumption of food warmer than body temperature, on the other hand, causes the phase to change back to austenite as a result of stress increasing the passage into the transformation region. (in accordance with the increasing temperature).

Stress–Strain Curve. The mechanical characteristics of NiTi alloys are unique. A static tensile test's stress–strain graph is affected by the microstructure (austenite or martensite). Tensile experiments were carried out on a Zwick/Roell ZO 10 under the following conditions:

- room temperature of $22\text{ }^{\circ}\text{C}$,
- strain rates $0,025\text{ s}^{-1}$ (velocity of deformation $v = 1, 5\text{ mm}/\text{min}$),
- pre-load of 5 N .

The findings are expressed as a stress strain (σ - ϵ) curve. The following parameters are thought to be important in describing the material behaviour of the curve: E_1 is the slope of the loading curve's initial portion (elastic modulus of austenite). E_2 is the transformation period or region's slope (austenite to martensite). E_3 is the slope of the curve's concluding section (elastic modulus of austenite). The initial stress number of the transformation region or plateau is denoted by σ_{SM} . The σ_{FM} is the transformation plateau's final stress value. The stress number at failure is denoted by σ_f . The initial strain number of the transformation region or plateau is denoted by ϵ_{SM} . The ϵ_{FM} is the transformation plateau's ultimate stress strain. The ϵ_f represents the strain number at failure. The tension strain curve for each orthodontic wire is depicted in Fig. 4.9.

Good spring-back is one of the most valued properties of an ideal orthodontic archwire. The spring-back is the amount of time it takes for an activated wire to recoup after being deactivated. In other words, wire can be deformed into loops or bends in complex shapes to optimise its stored elastic energy, and then revert to its original shape after deactivation. Although SMAs can recover to their original austenitic phase, transformation and martensitic regions (up to the yield point of the material where plastic deformation begins to fracture), orthodontic wires are almost never stressed in the martensitic region, as shown in Fig. 4.9.

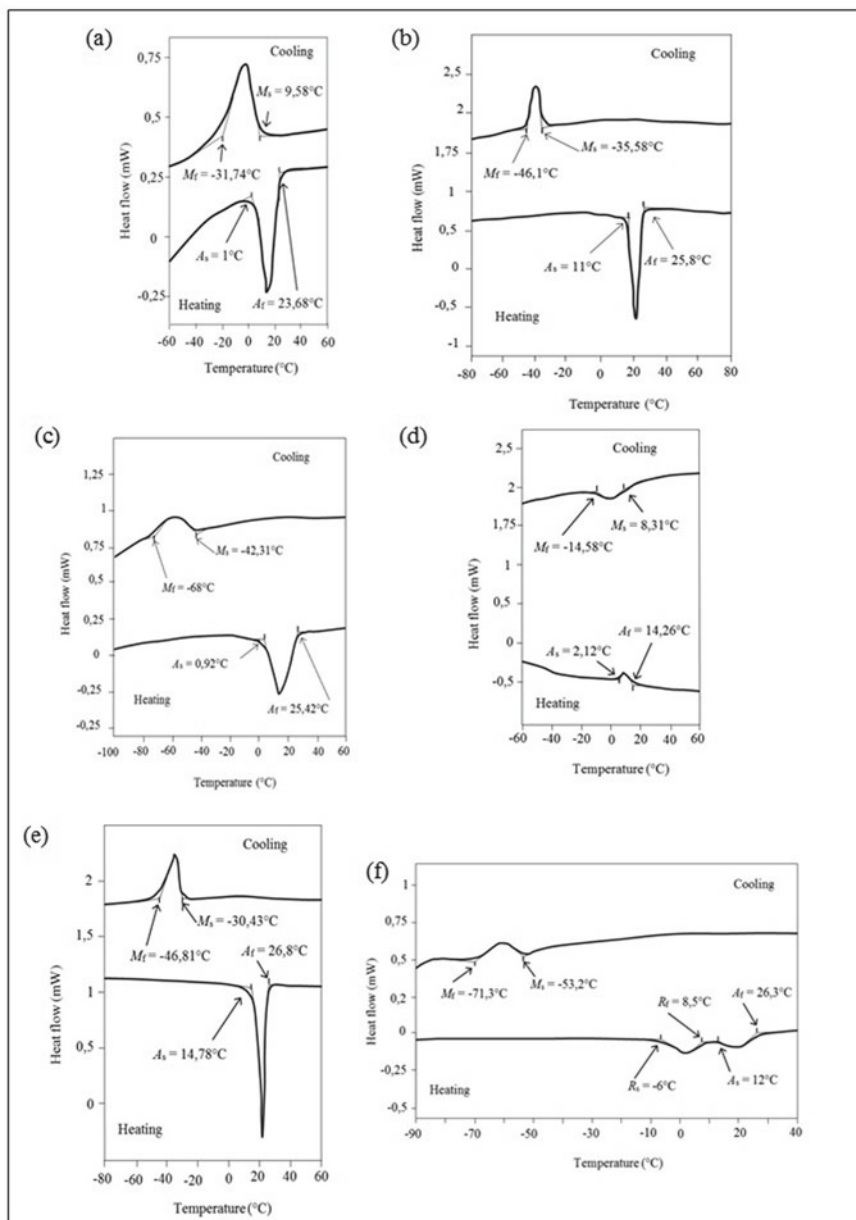


Fig. 4.8 DSC curves and phase transition temperature for the orthodontic wire: **a** 1-D, **b** 2-DT, **c** 3-G, **d** 4-O, **e** 5-OT, **f** 6-RD [23]

Table 4.3 Temperatures of phase transformation [23]

Number of wire	Short name	M_f (°C)	M_s (°C)	R_s (°C)	R_f (°C)	A_s (°C)	A_f (°C)
1	D	-31.74	9.58	-	-	1.00	23.68
2	DT	-46.10	-35.58	-	-	11.00	25.80
3	G	-68.00	-42.31	-	-	0.92	25.42
4	O	-14.58	8.31	-	-	2.12	14.26
5	OT	-46.81	-30.43	-	-	14.78	26.80
6	RD	-71.30	-53.20	-6.00	8.50	12.00	26.30

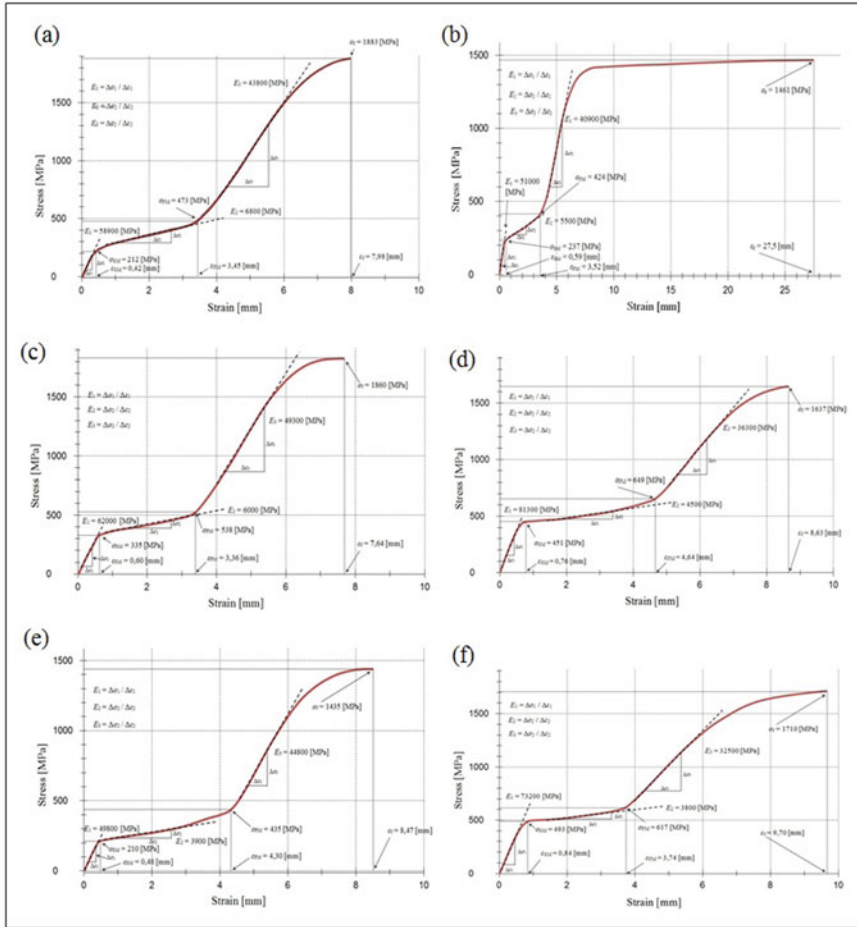


Fig. 4.9 Material response for a monotonic test up to failure for the wire: **a** 1-D, **b** 2-DT, **c** 3-G, **d** 4-O, **e** 5-OT, **f** 6-RD [23]

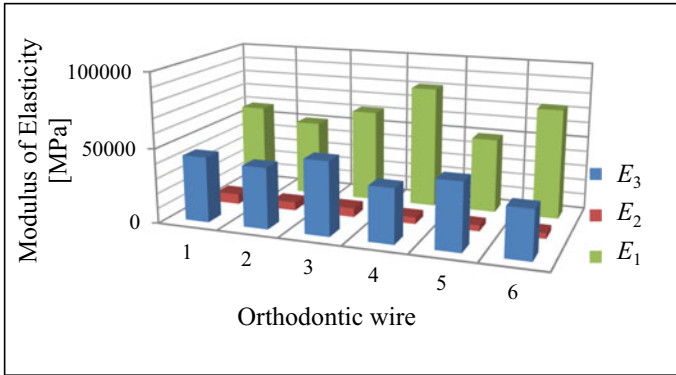


Fig. 4.10 Modulus of elasticity for the austenite E_1 transformation E_2 and martensitic E_3 phases [23]

The modulus of elasticity for the austenite, transition and martensite phases is shown in Fig. 4.10. In the austenitic phase, the orthodontic wire O had the highest stiffness of elasticity. All orthodontic wires have the same modulus of elasticity in the transformation period, ranging from 3800 to 6800 MPa. In orthodontic treatment, the ideal mechanical properties of the wires vary, depending on the treatment level. Low stiffness is essential at the start of therapy. When the levelling stage of orthodontic treatment is completed and significant tooth movement is required, the stiffness of the wire must be increased. As a result, it is obvious that the optimum mechanical properties of orthodontic wires change during the course of orthodontic treatment.

In the early stages of treatment, when minimal forces are required, it is critical for orthodontic wires to have a low modulus of elasticity. SMA NiTi wires are used in the early stages of orthodontic therapy for this reason.

Another critical aspect of orthodontic therapy is the application of continuous forces. In the transformations plateau, the SMA NiTi provides nearly continuous power. Figure 4.11 depicts the initial strain value for the transformation SM and the end strain value FM of the transformation. Wires O and OT exhibited a broad range of transformation plateau and an excellent spring-back.

Figure 4.12 compares the initial stress value of the transformation region SM with the end stress value of the transformation plateau σ_{FM} . The orthodontic wire RD exhibited the most tension. The dental wire D had the lowest σ_{SM} .

4.6.2 Experimental Continuous Casting of Nitinol

Commercially available nitinol is presently produced using traditional casting techniques, which result in blocks that are difficult and time-consuming to process. Continuous casting, in which molten metal solidifies straight into a semi-finished product, eliminates the need for ingot casting and processing, saving time and money.

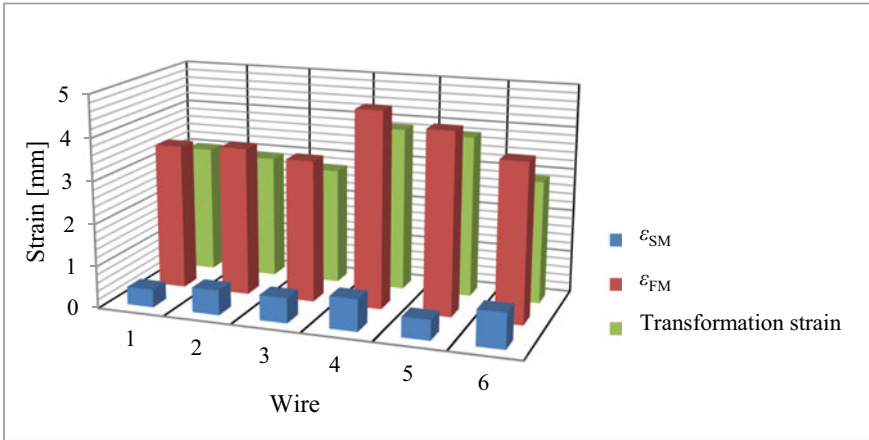


Fig. 4.11 Strain ϵ_{SM} , ϵ_{FM} and total transformation strain [23]

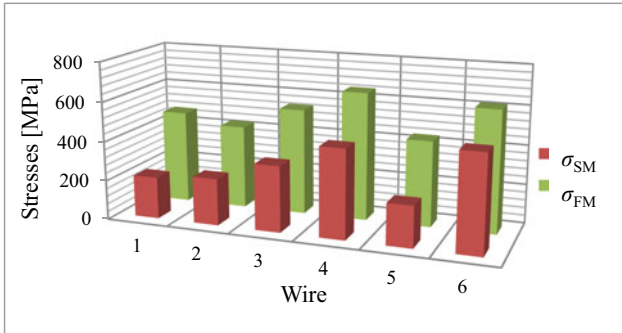


Fig. 4.12 Experimental results for stress σ_{SM} and σ_{FM} [23]

However, there were no comprehensive reports on continuous casting of nitinol in the literature. Therefore, the continuously cast $\phi = 12$ mm nitinol strands will be displayed here [24]. Smelting pure Ni and Ti in a medium frequency induction furnace with a graphite crucible is difficult, because it is technologically demanding to prevent a stormy reaction between Ni and Ti and to achieve a homogeneous melt without a prolonged long holding period. The stormy reaction is reproduced readily in a clay-graphite crucible. Strands of nearly equiatomic chemical compositions were produced with acceptable surface quality. The microstructure of strands with more than 50 at.% Ni was Ti_2Ni and cubic NiTi, whereas the microstructure of strands with less than 50 at.% Ni was $TiNi_3$ and cubic NiTi. This is consistent with the findings of other researchers, and suggests that the eutectoid decomposition $NiTiTi_2Ni + TiNi_3$ does not occur.

A review of the materials and casting parameters is displayed in Table 4.4. Macro photographs of the four strands are shown in Fig. 4.13.

Table 4.4 Materials and casting parameters [24]

		Trial (Stand) 1	Trial (Stand) 2	Trial (Stand) 3	Trial (Stand) 4
Base metals purity/wt. %	Ni	99.8	99.8	99.99	99.99
	Ti	Scrap, 99.8	Scrap, 99.8	99.99	99.99
Target composition/wt. %	Ni	55.08	55.08	55.08	55.08
	Ti	44.92	44.92	44.92	44.92
Stands-analysed/wt. %	Ni	63.2	56.5	54.6	54.6
	Ti	34.4	43.3	45.4	45.4
	Fe	1.53	0.2	–	–
Crucible	Electrographite		Clay-graphite	Clay-graphite	Clay-graphite
Nozzle	ZrO ₂		ZrO ₂	ZrO ₂	Si ₃ N ₄
Nozzle diameter/mm	11.1				
Mould	Copper, water-cooled				
Mould diameter/mm	12.0 mm				
Starter bar tip	Steel	Steel	Ti, grade 2	Ti, grade 2	
Melt temperature/°C	1420		1420	1420	1420
Casting sequence	Pull-pause				
Stroke/mm	8				
Pause/s	0.3	0.3	0.5	0.5	
Productivity/mm · min ⁻¹	630	630	422	422	

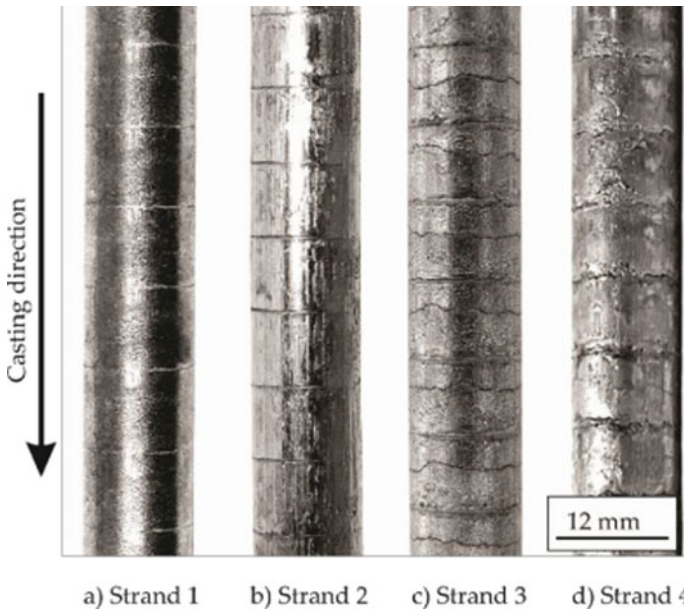
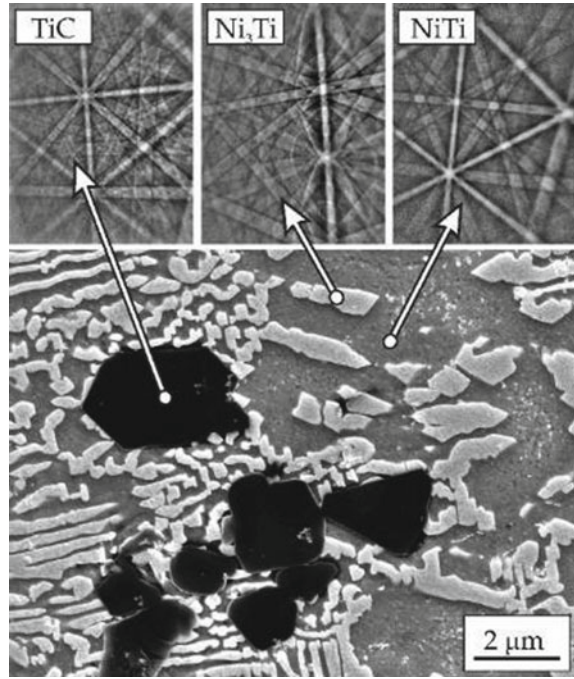


Fig. 4.13 Macro photographs of the strands [24]

Fig. 4.14 SEM image of strand 2's microstructure. Three distinct phases were noted. Cubic NiTi (light grey) predominates, followed by hexagonal Ni₃Ti (almost white) and a few tiny groups of TiC-particles (dark, almost black). The EBSD system generated Kikuchi patterns for these three stages, which are displayed on top [24]

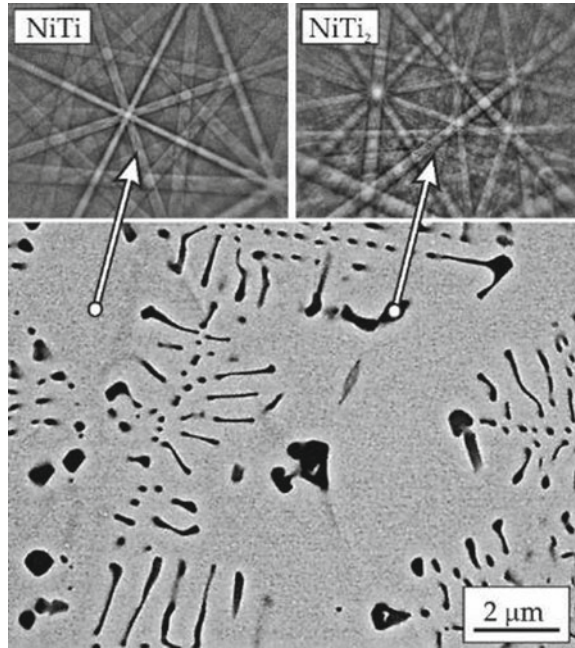


Electron microscopy observations and phase studies were performed on strands 2 (Fig. 4.14) and 3 (Fig. 4.15). Strand 1 was ineffective, due to its insufficient chemical composition (Table 4.4). The alloy produced in experiment 3 was reused in trial 4. Apart from the worse surface, no significant differences were anticipated when compared to strand 3.

The following are the study's key findings:

- (1) It is difficult to smelt pure Ni and pure Ti in a medium frequency VIM furnace with a graphite crucible. Because the crucible heats up much faster than the metallic batch, it is difficult to avoid a stormy exothermic reaction and excessive sputtering between the Ni and Ti.
- (2) Stirring the melt in a graphite crucible is inefficient in a middle frequency VIM furnace. As a result, the nitinol produced by smelting pure metals is inhomogeneous.
- (3) The use of a clay-graphite crucible overcomes the problem of controlling energy input during the exothermic reaction efficiently, and allows for efficient melt stirring. However, in terms of melt purity, the acceptability of clay-graphite requires confirmation using chemical analysis techniques with lower detectability limits for carbon and oxygen than those used in this study.
- (4) Directly from the melting crucible, continuous casting was achieved of nitinol strands with a reasonably small diameter of 12 mm and good surface quality.

Fig. 4.15 Strand microstructure 3. Image from a SEM. There were two distinct phases noted. Cubic NiTi (grey) dominates, followed by cubic NiTi₂ (dark, almost black). The top shows Kikuchi patterns of NiTi and NiTi₂ acquired by the EBSD system [24]



Finding the ideal combination of casting parameters and materials for the crucible, nozzle, and mould, on the other hand, takes more time.

- (5) The microstructures of continuously cast nitinol strands 2 and 3 consisting of Ti₂Ni and cubic NiTi support the hypothesis that the eutectoid decomposition NiTiTi₂Ni + TiNi₃ does not exist at 630 °C.

4.6.3 Microstructure, Mechanical Properties and Corrosion Behaviour of NiTi and CuAlNi Alloys Prepared by Continuous Casting

This part will present the results of research [24–26] based on well-known foundations [27–32].

4.6.3.1 Thermo-Mechanical Processing

The materials used in this research were NiTi, with high purity nickel (Ni > 99.98 wt.%) and titanium (Ti > 99.995 wt.%), as well as CuAlNi. Grinding removed the oxide coating of titanium prior to melting. The alloys were melted four times to ensure homogeneity. The material was used within three groups of samples:

- (1) The first group of ingots, the control group, represented by alloy samples NiTi 1, were prepared by classic casting methods.
- (2) The second group of ingots, denoted by the number 2, also NiTi alloys, were prepared by continuous casting.
- (3) The third group, test samples, denoted by the number 3, represent CuAlNi alloy samples, also obtained by the method of continuous casting.

A vacuum induction melting (VIM) furnace and a vertical continuous caster comprised the test sample experimental apparatus. A suitable quantity of solid alloy (about 20 kg) was placed in a pot and remelted in an induction furnace under vacuum conditions (10^{-2} mbar). After heating at the temperature of casting (around 50 °C above the temperature of melting, for NiTi = 1350 °C and for CuAlNi = 1100 °C), the melt flowed continuously under an Ar atmosphere (to avoid any chance of oxidation) into the mould, where it solidified. The alloy solidifies in a crystalliser cooled by water (quenching was carried out in order to ensure a low-temperature β -phase, which is the carrier of martensitic transformation), and bars with 10 mm in diameter came out of the modified moulds.

The samples were cut by electro-erosion to dimensions suitable for further processing.

4.6.3.2 Microstructure of the Samples

The samples' microstructure was investigated using a Nikon EPIPHOT 300 light microscope. Optical microstructures of the samples, including 200 and 1000 \times magnification, are collected in Table 4.5. It is shown in microphotographs of the sample NiTi2, when compared to NiTi1, that the rapidity of cooling was inversely proportional to the size of grain, and directly proportional to the concentration of structure defects (free sites, dislocations...). This is related to better mechanical properties. The defects lower the temperatures of phase transformations.

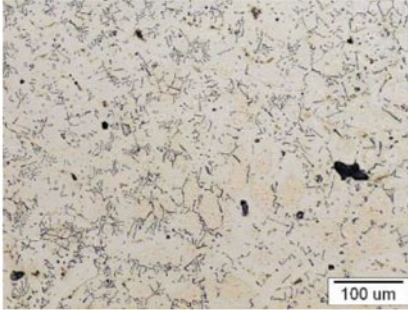
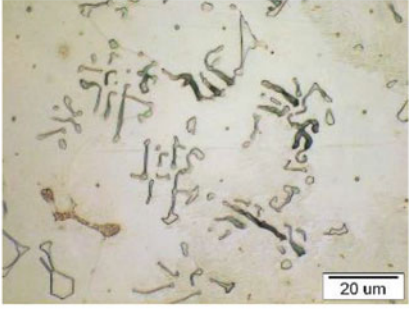
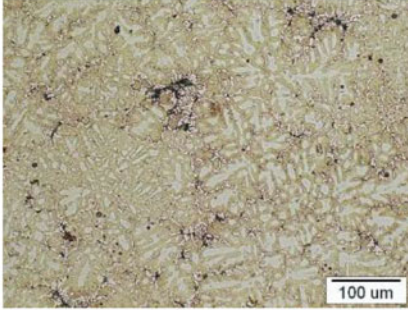
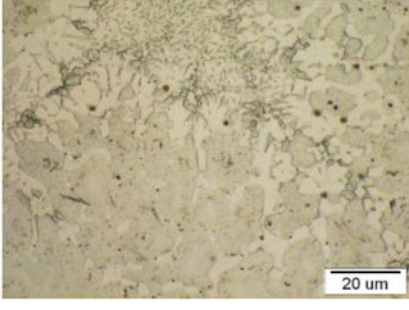
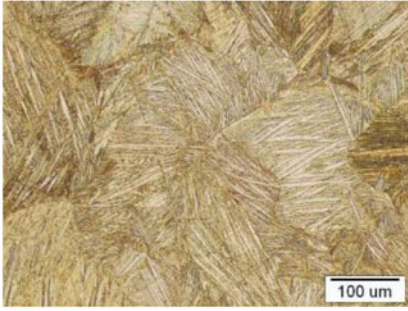
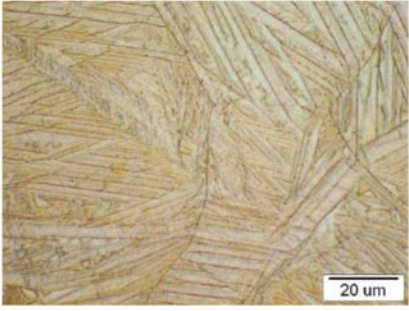
The resulting figures of CuAlNi displayed a microstructure which was made up of large β -phase grains and needle-like plates of martensite. The optical microphotographs show a typical martensitic microstructure. The martensite needles have a different orientation. The boundaries of grains are visible and the obtained microstructure consists of large grains.

4.6.3.3 Chemical Composition of the Samples

The chemical composition and texture were identified by X-ray diffraction (XRF), and the microchemical composition of the individual phases was supported through energy-dispersive X-ray spectroscopy (EDX) analysis.

EDX analysis was performed of samples NiTi 1 (NiTi as cast), NiTi 2 (NiTi CC) and CuAlNi (CuAlNi CC). Several measuring areas in the central and peripheral parts of the sample are specified for each of these samples, as are several measuring

Table 4.5 Microstructure of the samples

<p>NiTi 1- 200 ×</p> 	<p>NiTi 1- 1000 ×</p> 
<p>NiTi 2- 200 ×</p> 	<p>NiTi 2- 1000 ×</p> 
<p>CuAlNi – 200 ×</p> 	<p>CuAlNi – 1000 ×</p> 

points within each measuring area. The specimens were not etched for the EDX analysis, but only polished, to eliminate the possibility of etching influencing the findings.

NiTi 1—Fig. 4.16 presents two measuring areas in the central part of the sample. In one measuring area, 5 measuring points were selected, and in the other 4 measuring points. If we compare the measurement results in the central and marginal parts of

the sample, it can be seen that the smallest Standard Deviation of the measurement is at the marginal part of the sample. In other words, the content of Ni and Ti is distributed more evenly in this part of the sample in relation to the central part.

NiTi 2—It can be seen that, in the central and marginal areas of the sample, the content of Ni and Ti is in a wide range. There are areas where the Ni content is 1.98 wt.% (marginal part of the sample) and 68.78 wt.% (central part of the sample). Also, the presence of O₂ and Fe in different amounts was detected in all measuring areas, Fig. 4.16.

CuAlNi—If we look at the results of EDX analysis of the central part of the sample and the marginal parts, it was noticed that, in all cases, the Standard Deviations are low, and that the average values of the elements are approximate, which indicates that the sample structure is homogeneous, Fig. 4.17.

4.6.3.4 Mechanical Property—Microhardness

The samples' microhardness was assessed using the static Vickers method to identify their mechanical properties.

The specimens were repolished prior to the trial. Vickers micro-indentation hardness was determined in accordance with the ISO 6507-1:2018 Standard. The hardness HV5 was recorded on each specimen from each experimental group on the ZWICK 3212 using a Nominal value of 49.03 N test force load for 15 s, and the HV50 on the WPN HPO 250 using a 490.3 N load for 15 s.

Tables 4.6 and 4.7 show the results of the measured hardness on the test samples. The results of HV5 measurements showed that the Standard Deviation of this measurement was the smallest in the NiTi 1 sample (6.24), and the largest in the CuAlNi 3 sample (19.50). Based on this, it can be concluded that the microstructure of these samples is inhomogeneous, especially in CuAlNi 3 and NiTi 2 (Standard Deviation 15.72).

As for measuring the microhardness of HV50, the situation was quite different. As for the Standard Deviation of the measurement, in this case the CuAlNi 3 sample had the smallest measurement deviation (12.43), while the NiTi 1 sample had the largest standard measurement deviation (22.89). In this case, the structure was shown to be inhomogeneous in NiTi 1 and NiTi 2 (Standard Deviation 20.32).

4.6.3.5 Corrosion

The testing of alloy corrosion potential was carried out in accordance with the protocol for testing the materials with application in Dentistry—ISO 1027: 2009. The testing includes three tests: (1) Immersion, (2) Electrochemical, and (3) Sulfide tests.

Focus Ion Beam (FIB) was performed after testing the corrosion of the samples. An EDX analysis was carried out at the section site. The thickness of the surface layer after the corrosion testing was measured in this manner. In order to obtain results as

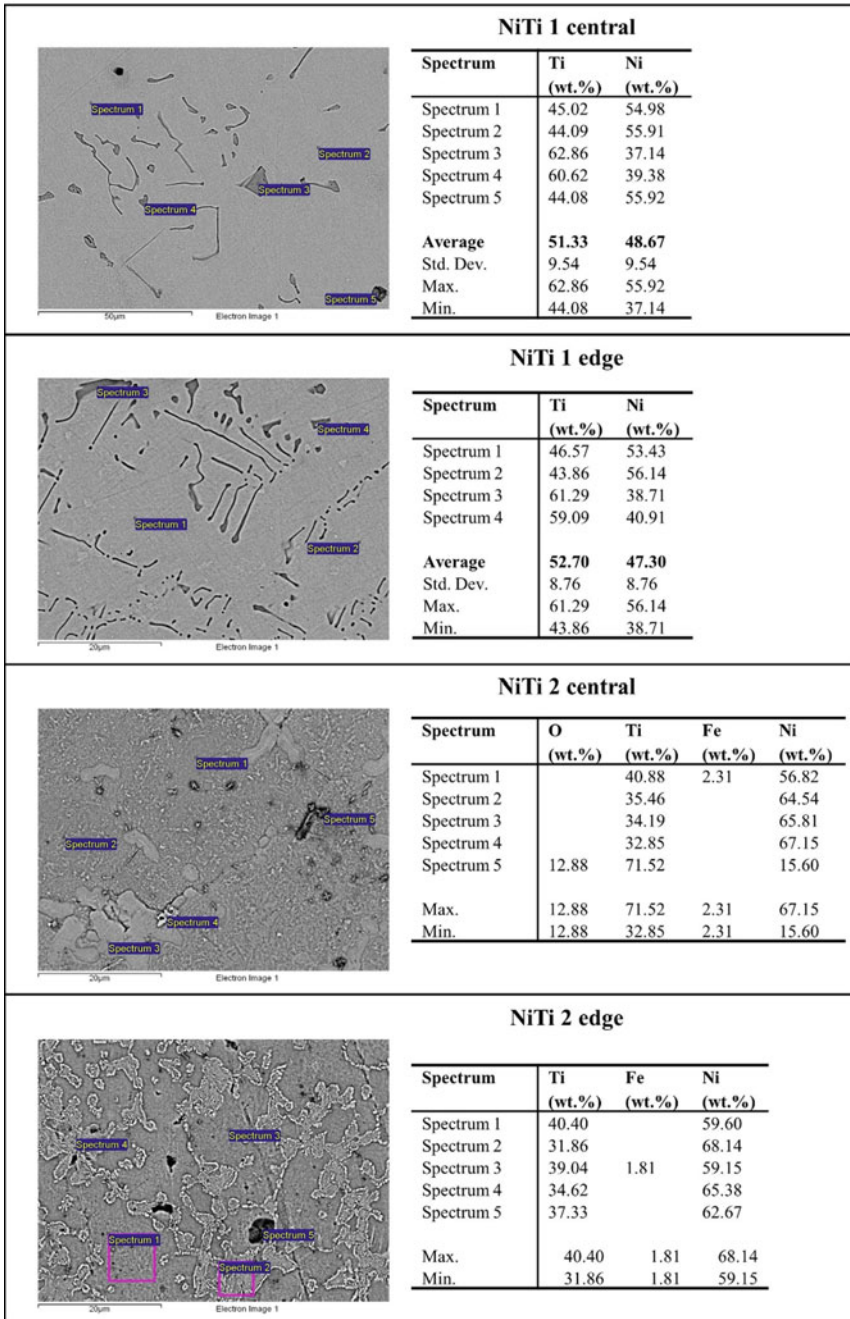


Fig. 4.16 EDX analysis of the central part and edge of NiTi 1 and NiTi 2 samples

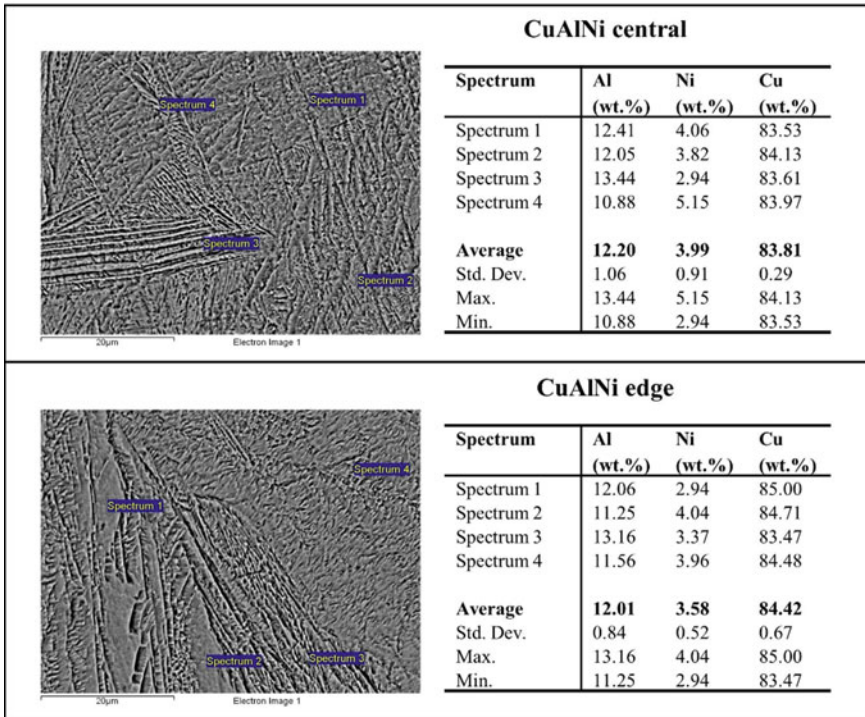


Fig. 4.17 EDX analysis of the central part and edge of a CuAlNi sample

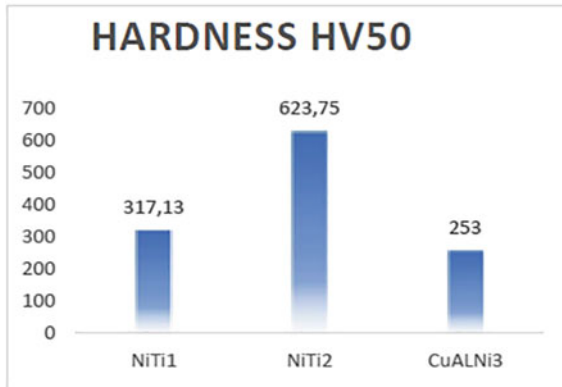
accurate as possible, an EDX analysis was carried out at the section site, so that it would be possible to establish which elements were present at which phase.

(1) Immersion Test—provides quantitative data on the release of metal ions under in vitro conditions, which are more aggressive than conditions in the oral cavity. As far as reagents are concerned, lactic acid (C₃H₆O₃) 90%; sodium chloride (NaCl); water, were used, which is in accordance with the ISO Standard 3696, 1987; ethanol or methanol (C₂H₅OH or CH₃OH); compressed air without water or oil, in accordance with the ISO Standard 7183. The apparatus where testing was carried out consisted of borosilicate glass containers (ISO 3585), and the dimensions of the containers were approximately Ø = 15 and 150 mm in height. The surface of the samples for testing must be processed with silicon carbide paper so as to be in accordance with the ISO Standard 6344-1:1998. The pH value of the obtained solution should be 2.3 ± 0.1. If the solution does not have the envisaged acidity (for an acid solution, the pH value is below 7), such a solution should be discarded and the reagents should be checked.

0.1 mm of surface layer should be removed after thermal processing. Wet silicon paper P1200 was used when it came to final processing of the surface. The samples were cleaned in an ultrasonic cleaner, for the duration of 2 min, in either ethanol or

Table 4.6 Hardness results HV50

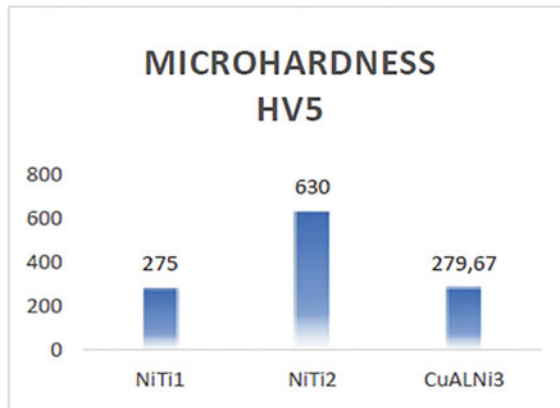
Hardness HV50			
	NiTi 1	NiTi 2	CuAlNi 3
	357	639	247
	325	644	261
	329	614	261
	301	614	249
	290	586	229
	326	644	264
	320	635	247
	289	614	266
Average	317,13	623,75	253,00
Min.	289	586	229
Max.	357	644	266
STDV	22,89	20,32	12,43



methanol. After that, they were washed with water and dried in compressed air with neither oil nor water in it—it should be placed in the container. A solution with the appropriate pH value should be added to the container. The amount of the solution should be 1 ml of solution per 1 cm² of sample surface. It is necessary for the samples to be completely covered in the solution. The volume needs to be measured precisely, with 0.1 ml accuracy.

Table 4.7 Microhardness results HV5

Microhardness HV5			
	NiTi 1	NiTi 2	CuAlNi 3
	280	613	280
	268	644	299
	277	633	260
Average	275,00	630,00	279,67
Min.	268	613	260
Max.	280	644	299
STDV	6,24	15,72	19,50



The container has to be closed so that the solution is prevented from evaporating. The temperature of the container should be maintained at $37 \pm 1 \text{ }^\circ\text{C}$, over the course of 7 days \pm 1 h. After the samples are removed from the container, the pH value of the remaining solution should be measured.

A reference solution should be kept in an additional container, so it would be possible to compare it with the solution that the samples themselves were in. Reference solutions will be used to detect the impurity of each sample. The samples for the immersion test were shaped into plates with the following dimensions: 7.5 × 40 mm, width 0.6 mm.

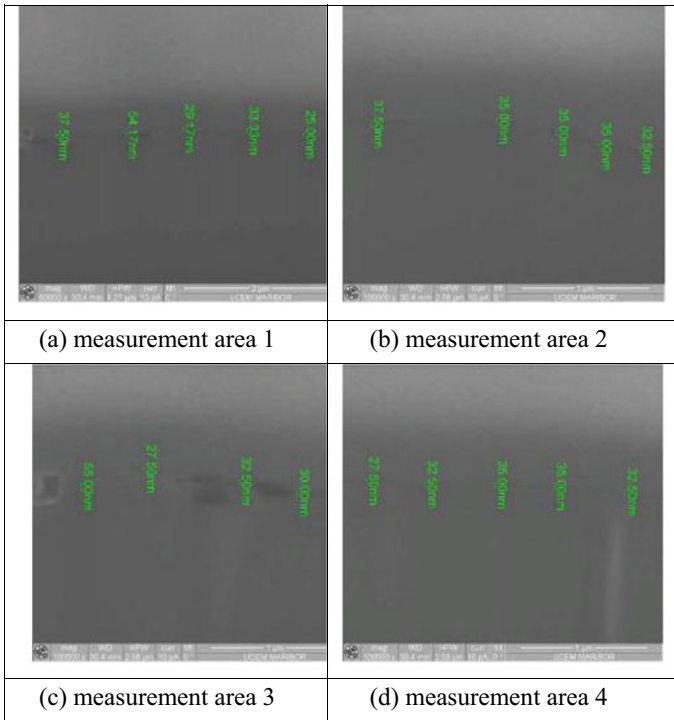


Fig. 4.18 The thickness of the layer on NiTi 1 sample

Examples after immersion testing

NiTi 1—In Fig. 4.18, a surface layer with varied thickness was perceived on the sample itself. The thickness of this layer was measured in four measurement areas, with five measurement points selected within each area.

An EDX analysis was carried out at the section site of the as-cast NiTi 1 sample. The measurement was performed at 3 measurement sites, and there were 5 to 7 measurement points chosen at each of the measurement sites, Fig. 4.19. Table 4.8 provides the results of the measurements, and the images of the measurement sites are shown within every Figure that presents a measurement area (see Fig. 4.19).

CuAlNi—Four measuring areas, and, within each area, 5 measuring points were selected, where the thickness of the surface layer was measured. Based on the obtained results, the average surface layer thicknesses were calculated for each area. The minimum surface layer thickness was found to be $6.91 \mu\text{m}$ and the maximum thickness was $8.40 \mu\text{m}$. In the other two measurement areas, the thickness of the surface layers were close in value, 7.77 and $7.97 \mu\text{m}$.

An EDX analysis was carried out at the section site of the CuAlNi sample. The measurement was performed at 3 measurement sites, and there were 5 to 6 measurement points chosen at each of the measurement sites, Fig. 4.20. Table 4.9 provides

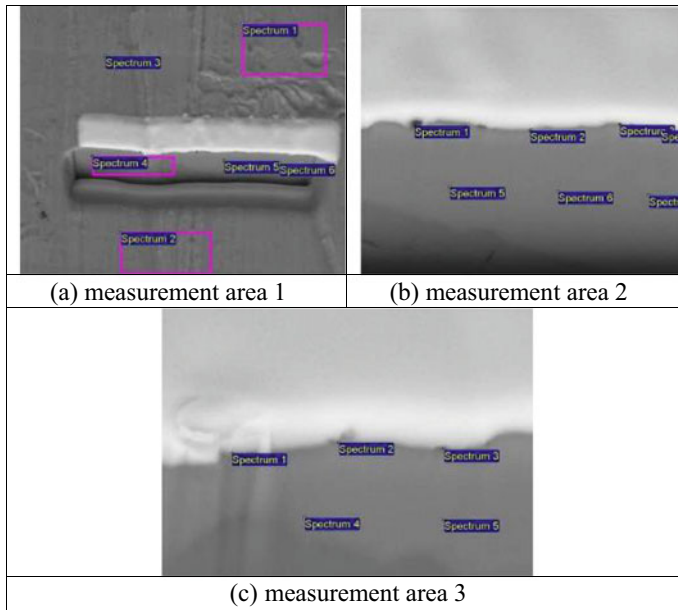


Fig. 4.19 FIB cross-section of the NiTi 1 sample after immersion testing

Table 4.8 The results of EDX analysis at the site of FIB section—NiTi 1 sample, after immersion testing (M. A.—Measurement Area in Fig. 4.18)

Spectrum	AREA 1: in wt.%		AREA 2: in wt.%			Area 3: in wt.%		
	Ti	Ni	O ₂	Ti	Ni	O ₂	Ti	Ni
Spectrum1	44.26	55.74	2.18	36.45	61.37	6.50	36.06	57.44
Spectrum2	42.48	57.52	2.77	36.64	60.59	2.48	39.97	57.55
Spectrum3	46.93	53.07	3.46	41.73	54.80	8.11	36.43	55.46
Spectrum4	43.66	56.34	2.48	38.14	59.38	5.07	43.79	51.14
Spectrum5	41.04	58.96	7.16	43.68	49.16	6.21	38.32	55.47
Spectrum6	41.63	58.37	6.53	43.67	49.80			
Max	46.93	58.96	7.16	43.68	61.37	8.11	43.79	57.55
Min	41.04	53.07	2.18	36.45	49.16	2.48	36.06	51.14

the results of the measurements, and the images of the measurement sites are shown within every Figure that presents a measurement area (see Fig. 4.19).

(2) Electrochemical Testing. Within this study a cell made of borosilicate glass was used for testing (in accordance with the ISO Standard 3585). A scanning potentiostat was used, whereas the range of potential was ± 1600 mV. The working electrode, that is, the sample holder, can be made of high-purity carbon or platinum. The reference

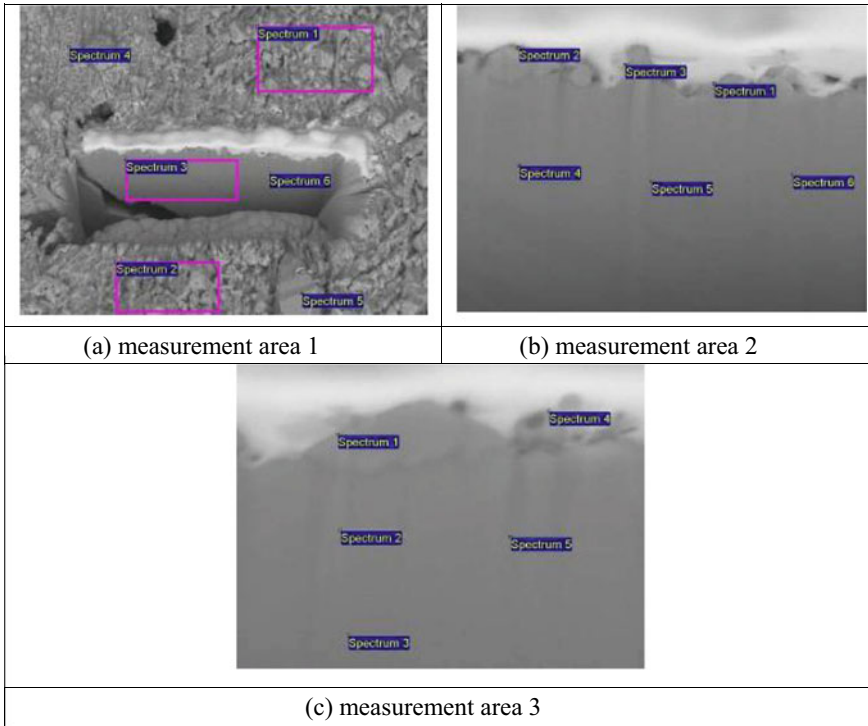


Fig. 4.20 FIB cross-section of the CuAlNi sample after immersion testing

Table 4.9 The results of EDX analysis at the site of FIB section—CuAlNi sample, after immersion testing (M. A.—Measurement Area in Fig. 4.20)

Spectrum	AREA 1: in wt.%				AREA 2: in wt.%				AREA 3: in wt.%			
	O ₂	Al	Ni	Cu	O ₂	Al	Ni	Cu	O ₂	Al	Ni	Cu
Spectrum1		7.53		92.47	7.64	11.38		80.99	4.98			95.02
Spectrum2		6.88		93.12	4.16	1.39		94.45	7.07	8.15	5.25	79.52
Spectrum3	7.85	6.49	12.63	73.03	6.34	8.40		85.25	7.11	6.41	9.25	77.22
Spectrum4				100.00	7.71	4.61	6.71	80.97	5.78	3.09	3.45	87.68
Spectrum5				100.00	5.81	6.13	11.98	76.08	6.25	9.07	7.45	77.23
Spectrum6	7.45	7.97	11.49	73.08	7.29	7.18	9.12	76.41				
Max	7.85	7.97	12.63	100.00	7.71	11.38	11.98	94.45	7.11	9.07	9.25	95.02
Min	7.45	6.49	11.49	73.03	4.16	1.39	6.71	76.08	4.98	3.09	3.45	77.22

electrode is either a saturated calomel electrode (SCE) or an Ag/AgCl electrode (saturated silver chloride electrode—SSE). Silicon carbide paper was used for the preparation of the surface (in accordance with the ISO Standard 6344-1: 1998) with a polishing paste. For the observation of the surface, a light microscope was used which had a $50 \times$ magnification. The electrolyte used for testing was made by dissolving 9 g of NaCl in 950 ml of water. The pH value of the solution was set to 7.4 ± 0.1 by using 1% $C_3H_6O_3$ or 4% NaOH. After that, the electrolyte has to be diluted with 1.000 ml of water. As far as the production of the samples themselves is concerned, they were obtained through casting. The surface of samples for testing should be prepared in the appropriate manner i.e. sandblasted with alumina particles, $125 \mu\text{m}$ in size. The surfaces of samples, which were exposed to the effects of the solution, should be 0.01 cm^2 for each sample, and it is necessary for it to be cleaned with an ultrasonic cleaner in acetone, alcohol and water, for the duration of 2 min per each of the respective agents. A sample should be kept in water before being relocated into the testing cell. When the measuring is over, what follows is the gauging of potential, that is, anode polarization. The potentiodynamic scan is initiated for the duration of 5 min after the measurement of open circuit potential has finished. A light microscope with a $50 \times$ magnification was used for observation of the surface. The samples for electrochemical corrosion testing were shaped into plates measuring $7.5 \times 7.5 \text{ mm}$, width 0.6 mm.

Figure 4.21 shows anode polarization curves for the alloys NiTi1 (as cast) and NiTi2 (CC) in a solution of 0.9% NaCl, $\text{pH} = 7.4$, with an Ar atmosphere. The current of complete passivation for NiTi2 is several milliamperes, which is visible from the potentiostat curve at 0.3 V. With increasing potential, at 0.7 V, what was noticed was current instability, which matched the metastable state of pit formation and repassivation. With a further increase in potential, what occurred was the initiation and propagation of pitting corrosion, which was registered on the polarization curve in the form of peaks that are a consequence of constant changes in the current density.

Fig. 4.21 Polarization curves of as-cast NiTi and NiTi CC

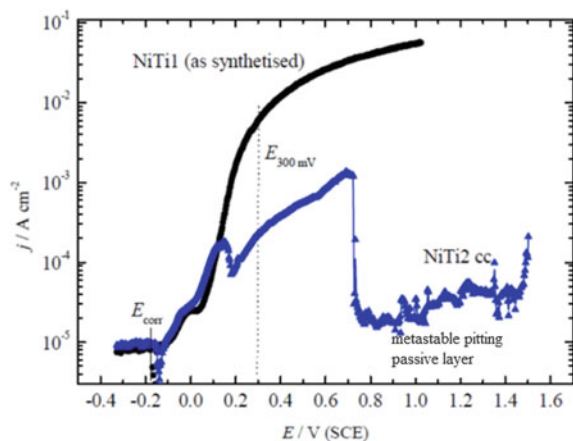
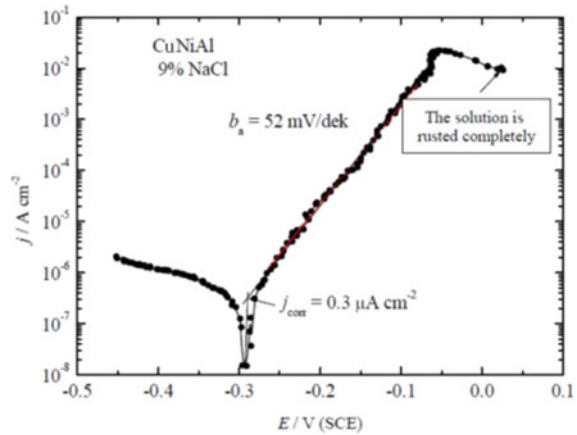


Fig. 4.22 The polarization curve of CuNiAl alloy



The polarization curve of CuNiAl alloy after corrosion testing is given in Fig. 4.22. The solution was 0.9% NaCl, pH = 7.4, the atmosphere was Ar, and $v = 1 \text{ mVs}^{-1}$. It can be perceived that what one was dealing with here was a complete, active dissolution without passivation. The anode part of the curve ($E > -0.3$) was matched by the reaction of the alloy dissolution.

(3) Sulfide Test. For the purpose of testing each of the samples, a fresh solution was prepared—22.3 g of sodium sulfide was diluted in 1.000 ml of water. Each of the samples was dipped into the testing solution for 10–15 s with a controlled temperature ($23 \pm 2 \text{ }^\circ\text{C}$). For surface processing, silicon carbide paper was used, in accordance with the ISO Standard 6344-1: 1998, and so was a polishing paste ($1 \text{ } \mu\text{m}$). The surface had to be cleaned with an ultrasonic cleaner in acetone, alcohol and water, for the duration of 2 min per each of the respective agents. Compressed air without oil or water should be used for drying the samples. When testing, one sample has to be placed into the immersion device with a fresh solution for testing. The melt for testing must be replaced every $24 \pm 1 \text{ h}$. The sample should be removed after $72 \pm 1 \text{ h}$ and washed with water. After that, the sample has to be immersed into ethanol or methanol, and then dried with compressed air without oil or water.

Example after sulfide testing

The results of the NiTi CC sample after sulfide testing, with a marked FIB cross-sectional location, are given in Fig. 4.23 and Table 4.10.

Considering the results obtained on the microstructure, mechanical properties and corrosion behaviour of NiTi and CuAlNi alloys, it can be concluded that [24–26]:

1. The amount of crystal lattice defects (free sites, dislocations, etc.) was the smallest in the NiTi samples obtained by continuous casting (CC).
2. Further advantages of CC are small-grain structure, better alloy homogeneity. During rapid solidification, what occurs is thermal stress as being responsible

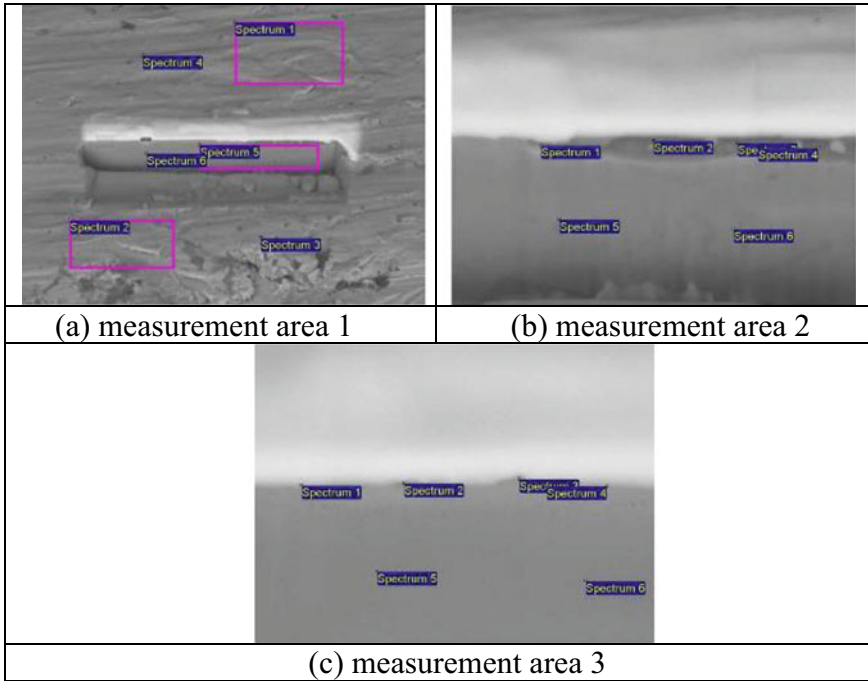


Fig. 4.23 FIB cross-section of the NiTi 2 sample after sulfide investigation

Table 4.10 Results of EDX analysis at the FIB cross-section point—NiTi₂ sample, after sulfide testing (MA—measuring area in Fig. 4.23)

Spectrum	AREA 1: in wt.%			AREA 2: in wt.%			AREA 3: in wt.%		
	O ₂	Ti	Ni	O ₂	Ti	Ni	O ₂	Ti	Ni
Spectrum1		44.53	55.47	14.04	37.57	48.39	9.68	37.36	52.97
Spectrum2		49.44	50.56	13.18	63.20	23.61	14.29	36.01	49.70
Spectrum3		35.95	64.05	18.99	55.16	25.85	8.84	45.26	45.90
Spectrum4		45.47	54.53	19.43	55.40	25.17	18.98	29.43	51.59
Spectrum5	10.61	44.06	45.33	8.55	36.53	54.92	5.24	36.86	57.90
Spectrum6	5.58	37.73	56.68	7.95	40.32	51.73	4.20	35.95	59.84
Average				13.69	48.03	38.28	10.20	36.81	52.98
SD				4.92	11.28	14.84	5.59	5.05	5.18
Max	10.61	49.44	64.05	19.43	63.20	54.92	18.98	45.26	59.84
Min	5.58	35.95	45.33	7.95	36.53	23.61	4.20	29.43	45.90

for the emergence of defects within the crystal lattice, which are responsible for lowering the temperatures of the phase transformations.

3. As for the results of EDX analysis that were used to test the presence of chemical elements, it was established that the samples NiTi CC and CuAlNi were homogeneous in terms of their composition. In other words, the elements that were part of the alloy's composition were arranged homogeneously in the central and peripheral parts of the sample.
4. With the increasing rapidity of cooling, the size of a grain will diminish and the concentration of crystal lattice defects will increase, which results in the improvement of mechanical properties and the lowering of transformation temperatures. NiTi CC samples have higher hardness compared to NiTi1 as-cast samples.
5. It is contradictory that the EDX analysis showed a homogeneous composition of NiTi1 and CuAlNi, while the solidity tests showed non-homogeneity.
6. Corrosion: A microstructural analysis was performed in order to explore the great differences in corrosion properties between the control alloy and the test samples (NiTi CC and CuAlNi CC). Taking the overall results into account, the sample that proved to be the best of all samples was the as-cast NiTi1, in terms of surface layer thickness, and also in terms of composition homogeneity.

The total average surface thickness was the least after all tests, which means that this sample was resistant to corrosion. As for the composition at the section site, a small departure was noticed only in the measurement area and after the sulfide test. Based on all of the aforementioned, the as-cast NiTi1 sample proved to be the best.

4.6.4 Stress Dependent Electrical Resistivity of Orthodontic NiTi Wire

NiTi archwires with superelastic characteristics may endure a high degree of tooth misalignment due to their considerably extensive elastic ranges associated with the metallurgical phase change and low flexural stiffness [33, 34]. As the transformation reverses during deactivation, they tend to generate a nearly constant force [14]. Superelastic NiTi arch wires with a diameter of 0.014" are advised for the initial stage of orthodontic therapy to maximise biomechanical efficiency [23]. Even in patients with severe malocclusions, these wires can be engaged fully in each tooth's bracket slot while exerting relatively minimal stresses and not exceeding their elastic limits [33]. NiTi wires may be bent up to 70° to reach the superelastic plateau, where plastic deformation is impossible. That much crowding is most likely to be seen in the anterior region of the lower dental arch, as well as any region of the dental arch where extreme rotations and crowding of teeth are present [34].

In orthodontic treatment, the complex orthodontic wire is deformed as shown in Fig. 4.6. In this case, the orthodontic wire was subjected to two-dimensional, or mostly three-dimensional, pressures. Because the majority of mechanical tests on SMA NiTi orthodontic wires are conducted in one dimension, the data given for

transformation stresses are in uniaxial tension or compression loading. In reality we know that there is very little pure load, because the majority of loading is a combination of bending stresses (tension + compressive) and torsion + bending stresses (Fig. 4.24).

It is feasible to demonstrate the existence of the different phases in SMA using the approach of electrical resistance measurement [35–38]. It is useful to know what degree of transformation is caused by separate deformation of the orthodontic wire in orthodontic practice.

We present methods for simulating the one-axis and multi-axis stress states of orthodontic wire in this paper. The electrical resistance measurement was used

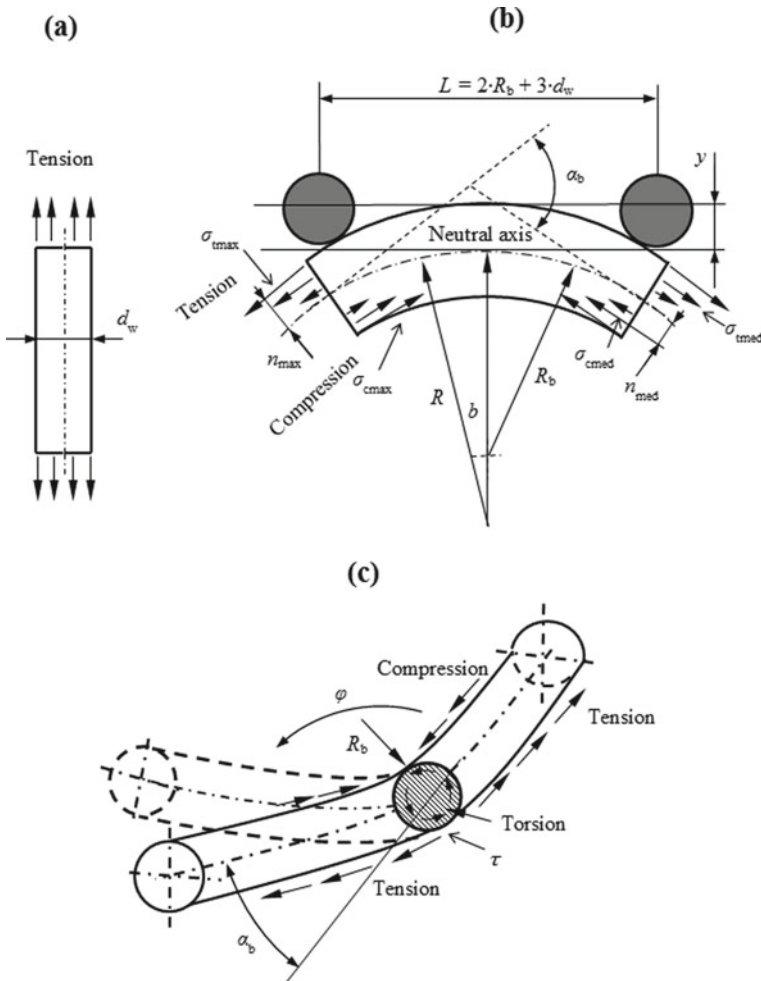


Fig. 4.24 a Tension stresses at uni-axle loading; b Bending stresses; and c Complex deformed wire (bending and torsion) [40]

to determine the deformation that triggers the phase transformation in the SMA NiTi. We investigated the electrical resistance of a uniaxial load in the first stage, and then repeated the experiment with multi-axial deformation in the second. The measurement findings were transformed into electrical resistivity, and compared to the analytically calculated stresses at various deformations in the wire.

Materials. We used a widely available orthodontic wire from SMA NiTi with a diameter of 0.014" for the investigation. (0.356 mm). $M_f = -14.58$ °C (martensite start), $M_s = 8.31$ °C (martensite end), $A_s = 2.12$ °C (austenite start), and $A_f = 14.26$ °C were the phase transformation temperatures (austenite finish). The tensile deformation stress deformation (–) shapes were as follow: Austenite's elastic modulus was $E_{1t} = 81,300$ MPa, and the slope of the transition phase or region (austenite to martensite) was $E_{2t} = 2800$ MPa. $E_{3t} = 36,300$ MPa was the elastic elasticity of the martensite. For the commencement of the transformation, the initial stress value was $\sigma_{SMt} = \sigma_{crit} = 451$ MPa. $\sigma_{FMt} = 649$ MPa was the final stress value at the conclusion of the transformation. $\varepsilon_{SMt} = 1.38\%$ was the initial deformation value at the commencement of the transformation plateau. The ultimate tension strain of the transformation plateau was $\varepsilon_{FMt} = 8.4\%$. At stress, the transformation strain was $\varepsilon_{rt} = 7\%$ [23].

Many studies have been conducted on the comparison of tensile—compressive and shear stress based on the available literature data. For example, we highlighted the most frequently used Von Mises yield criterion, adapted and modified by Orgéas and Favier and/or Stutz [39].

4.6.4.1 Experimental Analysis [40, 41]

We simulated various stress levels in the orthodontic system following application in experimental measurements using two electrical resistance measuring devices:

- (1) The Simulation of Uni-Axial Stress (SUAS) deformation device consisted of two basic components: a tensile module with an overall dimension of approximately $66 \times 37 \times 25$ mm and a load cell.
- (2) The Simulation of Multi-Axial Stress (SMAS) deformation device was made up of rigid and moving components, and had an overall size of about $110 \times 41 \times 25$ mm.

A Micro-ohmmeter AOiP OM 21 was used to detect the voltage between the two inner probes, while a constant current source was used to pass constant current through the two outer probes. The electrical resistivity measurement had an accuracy of ± 0.1 cm. The evaluation system is depicted schematically in Fig. 4.25.

For a wire of length l and cross-sectional area A , the electrical resistivity ρ was:

$$\rho = \frac{V \cdot A}{I \cdot l} = R \cdot \frac{A}{l},$$

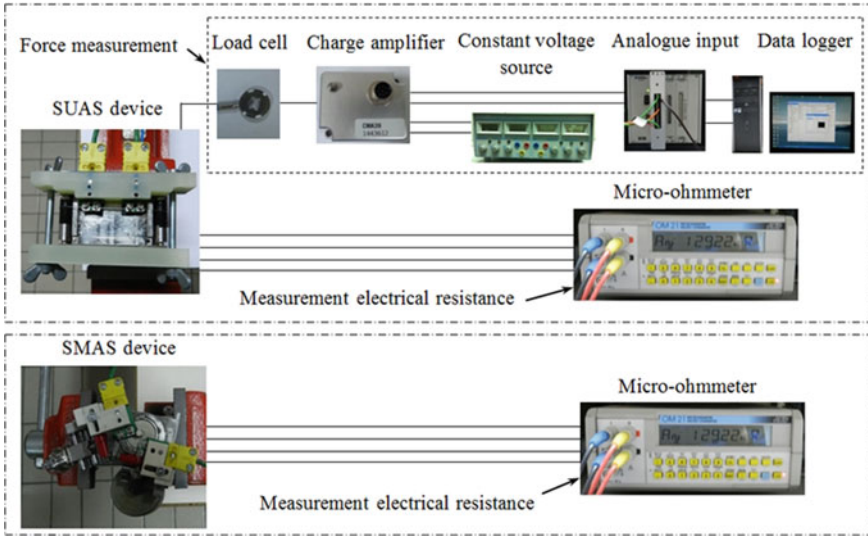


Fig. 4.25 Schematic view for the SUAS and SMAS systems [40]

R denotes the wire's electrical impedance. The voltage difference was recorded between the two inner probes. The distance l at the SUAS device was fixed (20 mm), whereas the distance l at the SMAS device varied with the bending angle b . The wire's cross-sectional size was the intersection with a diameter of 0.014" (0,305 mm). At 22 °C, the electrical resistance of the NiTi orthodontic wire was measured during various deformations, with the initial microstructure being austenite throughout the entire volume.

Examples of results:

Torsion Deformation. Figure 4.26 depicts the findings of electrical resistivity measurements in the torsion deformation. This study was carried out on the SMAS device, with torsion angles ranging from 0 to 540°. As a result, we have succeeded in all three categories (austenite, transformation plateau and martensite). It has been demonstrated that the transformation plateau begins with a parabolic curve, whereas the transformation plateau ends with a linear curve of the curve for the tensile and bending force. As with the transition plateau, the martensite curve had a linear slope.

Combination of torsion and bending deformation. Figure 4.27 depicts the findings of electrical resistivity measurements at complex stress states (bending and torsion). At bending radius $R_b = 2$ mm, Fig. 4.27a depicts the connection between bending angle, electrical resistivity and tensile or compressive equivalent stress. We used the 180° torsional force. Because of the stress, the material had an austenitic microstructure, as shown in Fig. 4.26. As a result, a change in the slope of the electrical resistivity

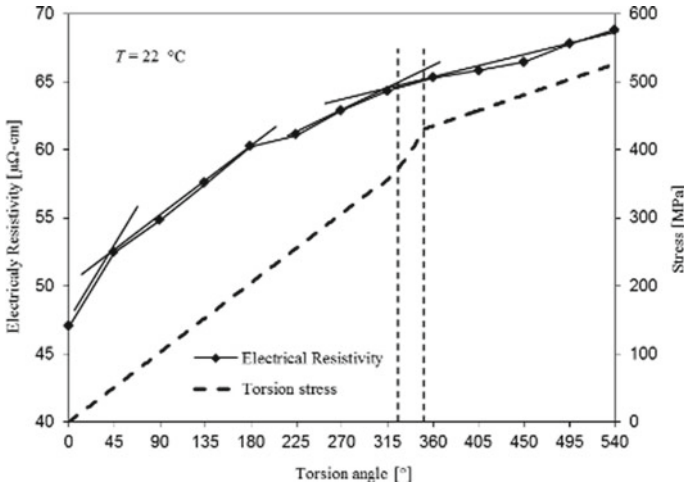


Fig. 4.26 The electrical resistivity of NiTi orthodontic wire varied with torsion force and torsion angle [40]

line was noticed prior to the bending angle of 30°, as shown in Fig. 4.27a. It indicated that a transformation occurred at 500 MPa equivalent on the tension side and 560 MPa equivalent on the compressive side.

Figure 4.27b depicts the loading combo in which we used 360° torsional loading. Due to the stress, the material had a martensitic microstructure, as shown in Fig. 4.26. The electrical resistivity curve was linear, with no transitions or variations in slope. The torsion stress produced complete stress-induced martensite in the material. As a result, the bending distortion had had no effect.

Finally, we can say that we created two special devices for measuring electrical resistance in various kinds of loads and combining them with orthodontic wire.

These findings were compared to the stresses determined analytically in the orthodontic wire. They were shown to induce complex, or three-axial stress state phase transformation rather than simpler loads such as uniaxial and two-axial loading. Finally, we present the phase change deformation, which is related closely to the useful superelasticity effect of the Shape Memory Alloy NiTi [40, 41].

4.6.4.2 Surface Characterisation of NiTi Orthodontic Archwires After Mechanical Loading Simulation in CACO2-2 Cell Culture

NiTi orthodontic archwires are especially important in the early stages of orthodontic therapy, when tooth movement and archwire deflection are at their highest. The primary downside of their improved mechanical qualities is nickel leakage. Several in vitro studies examined the nickel leakage from archwires that were only immersed in a medium and received little or no simulation of all the stress and deflection forces

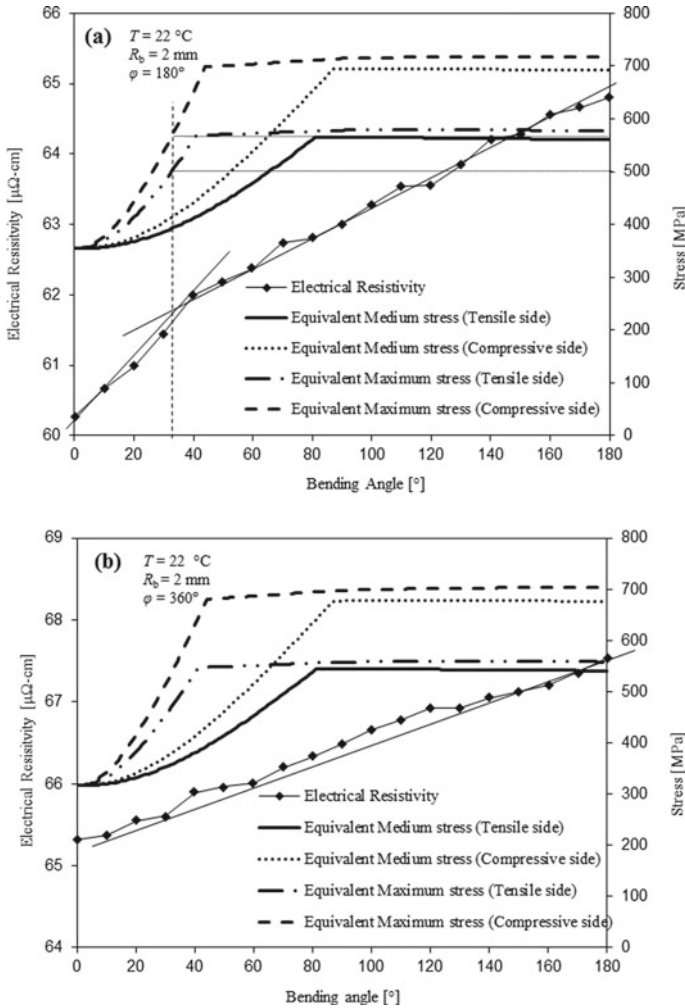


Fig. 4.27 Changes in electrical resistivity of NiTi dental wire against bending angle at equivalent (torsion-tensile and torsion-compressive) stress: **a** Bending radius $R_b = 2\text{ mm}$, rotated angle = 180° ; **b** Bending radius $R_b = 2\text{ mm}$, rotated angle = 360° [40]

that affect them. This study aimed to overcome this by replicating the deflection forces experienced by archwires inside a patient’s mouth. NiTi orthodontic archwires were immersed for 24 h in a CACO2 cell culture medium before being loaded with a multiaxial stress simulator [42]. The surface of the NiTi orthodontic archwires was polished after the testing. Significant microstructural and compositional changes were found within the first 51 nm of the archwire surface’s thickness. Inductively Coupled Plasma Mass Spectroscopy (ICPMS) was also used to assess the concentrations of liberated nickel and titanium in the CACO2 cell growth media. The amount

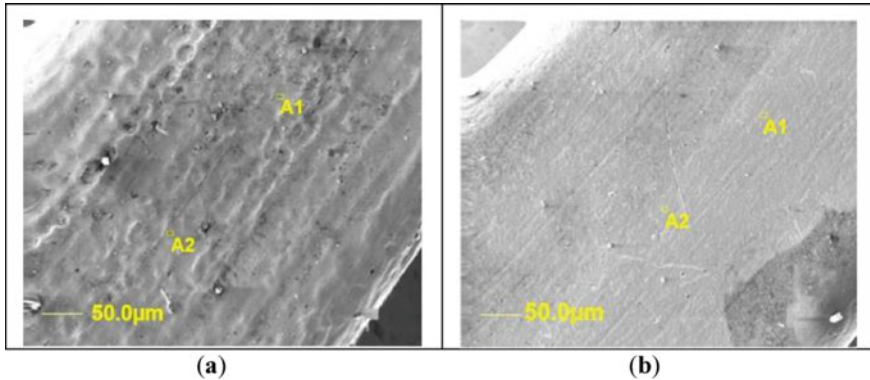


Fig. 4.28 SEM images of **a** The original archwire surface (control); and **b** The deformed archwire surface following simulation of the multi-axial stress, (SMAS) simulation test [42]

of nickel ions emitted was found to be 1.310 g/L, which was statistically significant. These findings are the first to mention the already detectable release of Ni ions in the CACO₂ cell culture medium after 24 h of mechanical loading simulation, which is critical for clinical orthodontic practice [42].

During therapy, orthodontists bend NiTi archwire and place it into each tooth's bracket slot. Bending stresses (tension and compressive), along with twisting and bending stresses, are the major stressors that deform NiTi archwires. Archwires begin unloading after being inserted inside brackets, in order to enter a more stable austenitic phase and generate forces that move teeth. The degree of periodontal loss and the distribution of stress inside a healthy, endodontically treated and repaired tooth cause teeth to move differently [43]. Fercec et al. [40] developed a multi-axial stress equipment (SMAS) simulation capable of applying uniaxial and multi-axial pressures to bend NiTi archwires. To recreate the actual situation in the oral cavity, different mechanical loadings of the archwires can be mimicked using SMAS. It should be noted that SMAS can only replicate intraoral forces induced by tooth crowding and the archwire's bending angle, and cannot imitate frictional or masticatory forces. The experiment was not meant to imitate contact of any fluid (medium) from the mouth with the archwires while loaded, according to the literature evaluation. As a result, the SMAS needed to be altered so that the NiTi archwires could make contact with the proper medium.

Our study focused on immersing NiTi orthodontic archwires in a medium and loading them immediately, while using the SMAS for 24 h at room temperature. The CACO₂ cell culture medium was chosen, since it has been utilised in cell invasion investigations and portrays heterogeneous cells. In the pharmaceutical industry, CACO₂ cell culture medium is used widely as an *in vitro* model of the human small intestine mucosa, to estimate the absorption of orally delivered medicines utilising various kits. As a result, all metals released into a patient's mouth during orthodontic therapy reach the intestines and CACO₂ cells, both of which play critical roles. Several investigations have shown that nickel and TiO₂ nanoparticles have an effect

on CACO2 cells [44–46]. Cell survival, protein synthesis, genotoxicity, oxidative stress, actin synthesis and gene expression were all affected by these metals. All of the effects of nickel on cells were observed over the course of 24 h, as in our research. The simulation test time of 24 h was chosen in accordance with the results of Staffolani et al. [47], who found that nickel release from archwires was highest on the first day. According to certain research, early Ni release increases are sustained, and do not drop over a few months [48]. The amount of nickel emitted is determined by the nickel surface concentrations reported for NiTi archwires (0.4–15 at.%) [49]. Following the testing, rigorous investigations were conducted, including the observation of surface changes on the NiTi orthodontic archwires and the measurement of ion content in the CACO2 cell culture medium as a result of archwire release. The reason for assessing nickel levels in the CACO2 cell line rather than keratocytes was that the nickel released by the orthodontic archwire only lasted a short time in the mouth. It is ingested, and, consequently, spends a significant amount of time in the colon, where it has a larger possibility of interacting with and influencing cells.

The purpose of this study was to look for changes in the surface of NiTi archwires, and, if any were discovered, to assess the surface concentration of elements and released ion content into the medium throughout a 24 h deflection period. The null hypotheses of this investigation were: (1) No changes in element concentration at 51 nm of the wire surface, (2) No substantial amount of nickel was released from the wires into the medium, and (3) The amount of nickel released was the same for the deformed and original archwires.

Materials. Commercially available NiTi archwires, Rematitan (Dentaurum, Ispringen, Germany) with the dimensions 0.40×0.56 mm ($0.016'' \times 0.022''$) were used in this research. The archwires chosen were virtually equiatomic in composition (50 at.% Ni, 50 at.% Ti). The CACO2 cell line was supplied by the American Type Culture Collection (ATCC, Manassas, VA, USA), and it represented a continuous heterogeneous human epithelial colorectal adenocarcinoma cell line.

Methods. CACO2 cell culture mechanical loading SMAS was utilised to imitate NiTi orthodontic archwires [40] with the reconstruction, which represents the addition of a chamber with a capacity of 4 mL [42]. The chamber was constructed of polymer (plexiglass) material, which is very inert, and has good mechanical and dimensional stability. It also contains no metal, which could taint the findings, and it is not electroconductive. The chamber structure was created during testing in the SMAS so that the CACO2 cell culture medium was in continual contact with the archwires. For a portion of their length the archwires inside the SMAS passed through the compartment. The compartment was sealed with a cover made of the same material as the chamber, to prevent leaking and evaporation of the liquid. The cover, which was wrapped by silicone to enclose the chamber completely, prevented evaporation, allowing that amount of medium to be placed inside during the experiment. For this study, the archwires were immersed in the CACO2 cell culture medium inside the chamber.

Results and Discussion

Surface Analysis. The surface SEM investigation indicated significant variations in microstructure between the initial and deformed archwires (see Fig. 4.28a, b). The initial archwire surface was rough, with noticeable holes and other defects, whereas the deformed archwire surface was smooth and defect-free. Mechanical loading, which caused the NiTi archwire to elongate and deform permanently [35], as well as the faster release of components from the surface into the medium, can be attributed to this.

The surface examination AES revealed element concentration in the first 51 nm of the chosen archwires. Figure 4.29a, b show the results and the different concentrations of elements found between the initial and deformed archwires.

Results of Ions' Release. Table 4.11 displays the ICPMS findings for ion release in the CACO2 cell culture media. The titanium concentrations in both samples were found to be below the measurement limit (<0.05 g/L). The concentration of nickel,

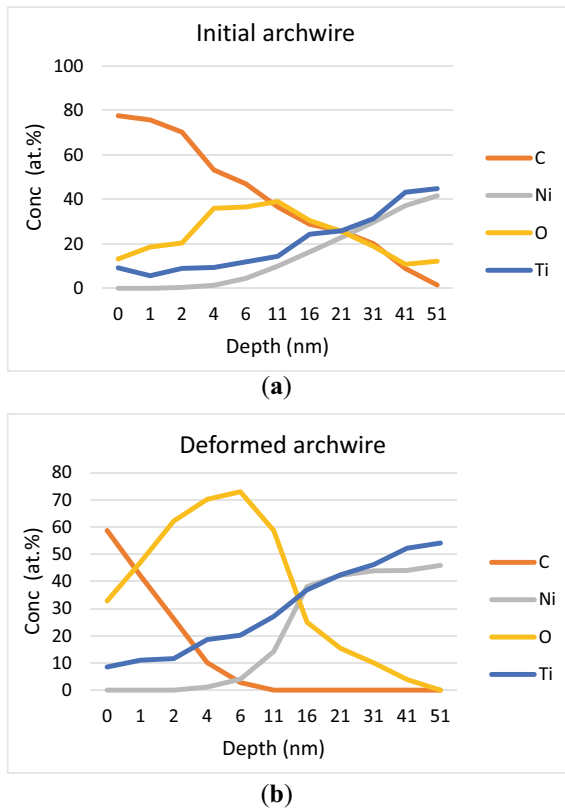


Fig. 4.29 The AES depth profiles reveal the element concentrations in the depth of each archwire from the surface to 51 nm: **a** Initial (control), **b** Deformed after the SMAS simulation test [42]

Table 4.11 Ni and Ti ion concentrations in the CACO₂ cell growth media after NiTi archwire exposure without loading (as a control sample) and after SMAS testing [42]

Sample	Conc Ni ($\mu\text{g/L}$)	Conc Ti ($\mu\text{g/L}$)
Control	1.240	<0.05
SMAS testing	1.310	<0.05

on the other hand, varied; the variation was $70 \mu\text{g/L/day}$. This indicated that there was some nickel leaking from the archwire into the media.

Based on the findings, it is possible to infer that archwire deformation is a significant factor in increasing nickel release into the CACO₂ cell culture media. After 24 h, the nickel concentration was 70 g/L higher than with an unloaded archwire. Furthermore, this reflects the average level of nickel released from a single wire with an average length of 12 cm (four pieces), whereas patients typically have two archwires in their mouth, resulting in a total value of 140 g/L additional nickel release. These findings are consistent with the literature, which mentions similar levels of Ni release from similar archwires over a comparable time span [50, 51].

It is essential to improve the surface as a research challenge and for the future safe use of NiTi archwires. The research demonstrated that the release of nickel ions from NiTi archwires is not negligible. According to the literature, one potential method could be titanium nitriding with the formation of TiN/TiN₂, as nitrogen has a greater hardening effect than oxygen [52]. Another possibility is to apply different coatings to the NiTi surface, in order to enhance its properties [53]. Other research has found that electrophoretic deposition of a bio-active glass coating has excellent results in improving the frictional, biological and aesthetic properties of stainless steel.

4.6.5 Biocompatibility of Ni–Ti Wires

Biocompatibility is defined as an interaction between the material, including its functions, and the organism [54, 55]. It means that an implanted biomaterial does not cause cytotoxicity, mutagenicity, irritation and allergic reactions. In addition, the material must be resistant to the corrosive influence of tissue fluids. The biocompatibility of materials has been evaluated by using numerous in vitro and in vivo tests, as requested by ISO Standards. These Standards describe the type of tests, depending on the type of material and the basic principles of material testings before their clinical use.

The in vitro biocompatibility tests are general, primary screening assays, which give information about the toxicity of the material, and these tests should be performed before other specific usage tests and the tests performed on animals or volunteers.

The most important biocompatibility tests are cytotoxic assays on different cells or cell lines. Most often, ISO Standards suggest, firstly, the use of continuous fibroblast

cell lines of mouse or human origin. However,, lymphocytes, macrophages, epithelial, endothelia, tumour and leukemic cell lines have been used, depending on the biomaterial's application and requirements for testing of some specific cell functions. The most applicable cytotoxicity test is based on the study of cell metabolic activity (MTT test). This relatively simple assay enables the knowledge on the degree of material cytotoxicity in the direct contact with the cells. In addition, it is very convenient for testing different solutions used for biomaterial conditioning. However, MTT is not suitable for studying the mechanisms of the adverse effects of materials, and, because of that, research should be extended to other tests, such as viability, cell cycle, necrosis or apoptosis assays. When a material is supposed to trigger an inflammatory process, it is necessary to study the production of proinflammatory mediators, especially cytokines, by the cells of innate immunity.

The influence of the chemical elements nickel and titanium. Titan is classified as highly biocompatible. On the contrary, nickel is less biocompatible and toxic. Nickel is a very strong allergen, and causes a very sensitive reaction to a greater extent than any metal or alloy. Nickel metal, nickel sulfide, nickel oxide and nickel carbonate are definitely human carcinogens [56].

Protective layer of TiO₂. The titanium and its alloys can be formed on the outer surface of the film of titanium oxide (TiO₂) with a small amount of NiO. Due to the ability to form a stable TiO₂ layer on the surface, this is one of the most biocompatible materials. In the optimum condition, which can be an excellent osteo-integration with the bone, there is also the ability to form calcium phosphate on the surface, which also prevents corrosion. Another useful property is that, in the event of damage to the protective layer, in particular titanium oxide and calcium phosphate, the layer can be regenerated [57].

4.6.5.1 Ortho Ni–Ti Wires for Biocompatibility Tests [58]

The effect of Ortho Ni–Ti archwires on cytotoxicity in vitro was chosen because thymocytes (immature thymic T cells) are sensitive to apoptotic signals in vitro and Ni ions have a recognised pro-apoptotic effect. We employed the lowest (0.5 cm²/ml) and highest (6.0 cm²/ml) surface-to-volume ratio wires in cell culture media in an assessment of direct contact between the cells and the Ortho NiTi archwires. We employed negative control samples of laboratory glass rods with the same surface-to-volume ratio, whereas positive control samples were treated with a dexamethasone solution, which is recognised for its pharmacological modulation of apoptosis. Figure 4.30 illustrates the appearance of the thymocyte cultures with archwires, or control cultures, whereas Fig. 4.31 displays the morphological analysis findings.

The thymocytes were stained with a Turk solution and examined under a microscope after 24 h of growth with Ortho Ni–Ti or control rods. Apoptotic cells were identified using homogeneously stained heterochromatin, and the percentage of apoptotic cells was determined after examining at least 500 cells. The results are presented as means Standard Deviations (n = 5) from one sample experiment. *p < 0.05, ***p < 0.005 versus matching control samples (control glass rods).

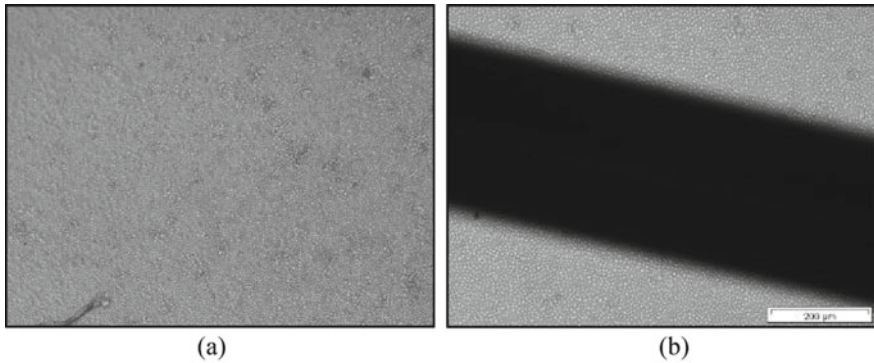


Fig. 4.30 **a** The appearance of control thymocytes grown in a full culture medium for 24 h; **b** The appearance of thymocytes grown in a complete culture medium in the presence of Ortho Ni-Ti [58]

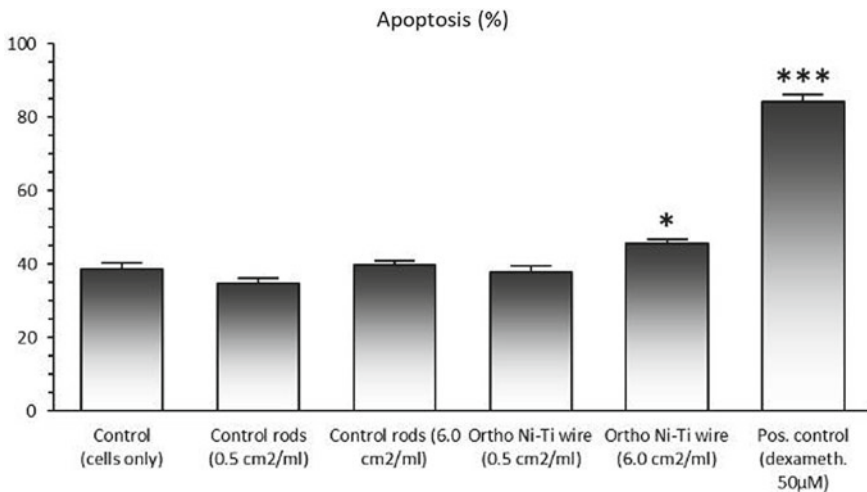


Fig. 4.31 Morphological study of thymocytes' apoptosis in culture with Ortho Ni-Ti culture [58]

The culture had a reasonably high apoptosis rate, which was unaffected by the negative control samples or the effect of Ortho Ni-Ti samples with a reduced surface area (0.5 cm²/ml). The bigger surface area of Ortho Ni-Ti put in the same volume of liquid (6.0 cm²/ml) promoted apoptosis significantly. When compared to the positive control, the percentage of apoptotic thymocytes was reduced significantly, and this effect can be categorised as weak on a scale of weak-moderate-strong. In another assay of thymocyte apoptosis, a comparable pro-apoptotic impact of Ortho Ni-Ti was confirmed by staining the nuclei with Propidium Iodide. Figure 4.32 shows a typical experiment, while Fig. 4.33 shows the average of three experiments. The somewhat smaller frequency of cells with hypodiploid nuclei is compatible with the previously established cell culture method of dynamic apoptosis development.

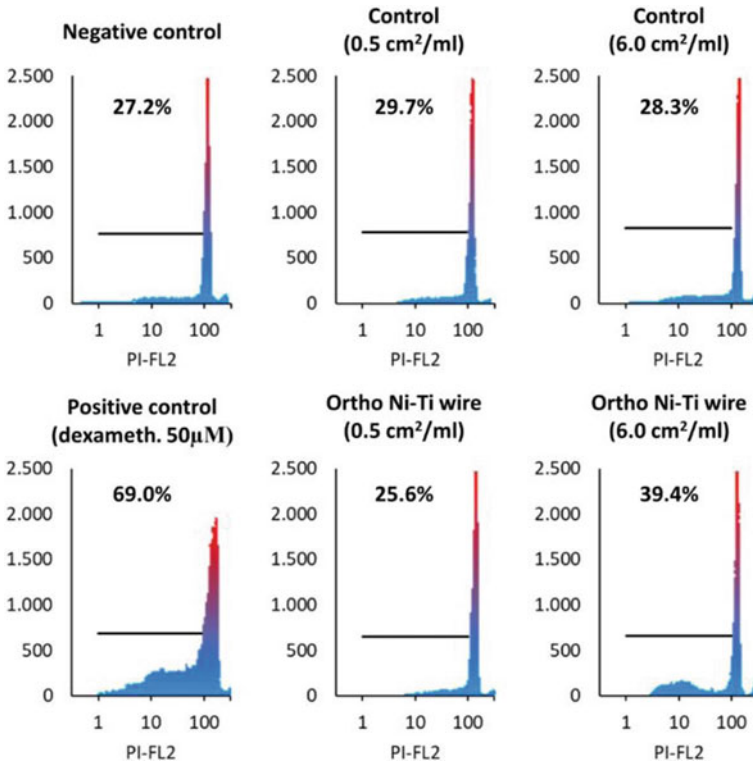


Fig. 4.32 Flow cytometry analysis of thymocyte apoptosis in culture with Ortho Ni–Ti or reference rods. The thymocytes were stained with Propidium Iodide and analysed. The apoptotic cells were identified as hypodiploid cells, because they contained less genetic material and, thus, had a reduced fluorescence intensity. Typical histograms from one typical experiment are shown [58]

In another experiment, we looked at the impact of Ortho Ni–Ti archwires on rat thymocyte apoptosis in culture. Figure 4.34 depicts the findings. Within the surface-to-volume ratio of biomaterial in a medium specified by ISO guidelines ($0.5\text{--}6\text{ cm}^2/\text{ml}$), only the greatest concentration of Ni–Ti archwires caused thymocyte death, which was significantly higher than the spontaneous apoptosis in the culture. The apoptosis was increased by using more Ni–Ti archwires than was suggested (8.0 and $12.0\text{ cm}^2/\text{ml}$), but there was no significant dose-dependent effect.

The second phase of the research aimed to investigate the cytotoxicity of Ortho Ni–Ti and TT Ortho NiTi in 24 h and 48 h cultures of rat thymocytes. These studies were chosen because thymocytes (immature thymic T cells) are sensitive to apoptotic signals *in vitro*, and there are literature data on the pro-apoptotic influence of Ni ions. In a direct contact experiment we employed a surface-to-volume of cell growth medium ratio of $2\text{ cm}^2/\text{ml}$ and alloy surface-to-volume ratios of $6.0\text{ cm}^2/\text{ml}$. We used examples of laboratory glass rods with the same surface-to-volume ratio as a negative control. The findings are depicted in Figs. 4.35 and 4.36.

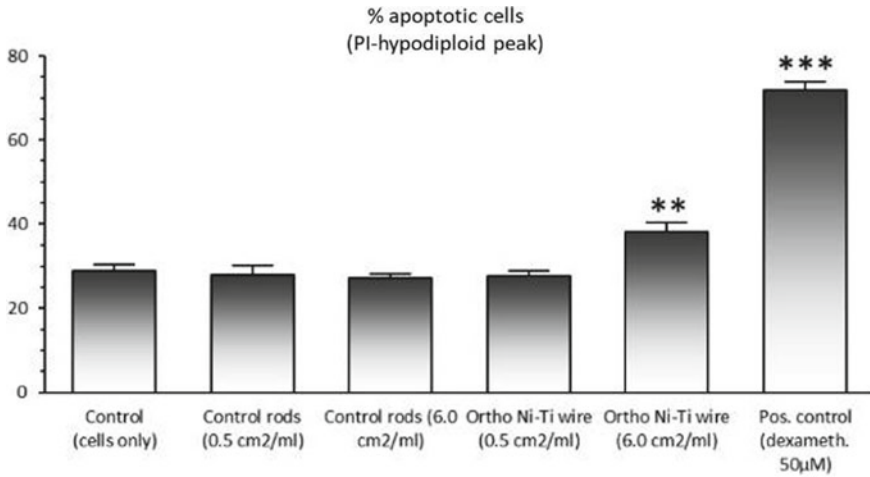


Fig. 4.33 Flow cytometry analysis of thymocyte apoptosis in culture with Ortho Ni–Ti or reference rods. The thymocytes were stained with Propidium Iodide and analysed. The apoptotic cells were identified as hypodiploid cells, because they contained less genetic material, and, thus, had a reduced fluorescence intensity. The findings are presented as the mean Standard Deviation of three experiments **p < 0.01, ***p < 0.005, when compared to the corresponding control samples. (control glass rods) [58]

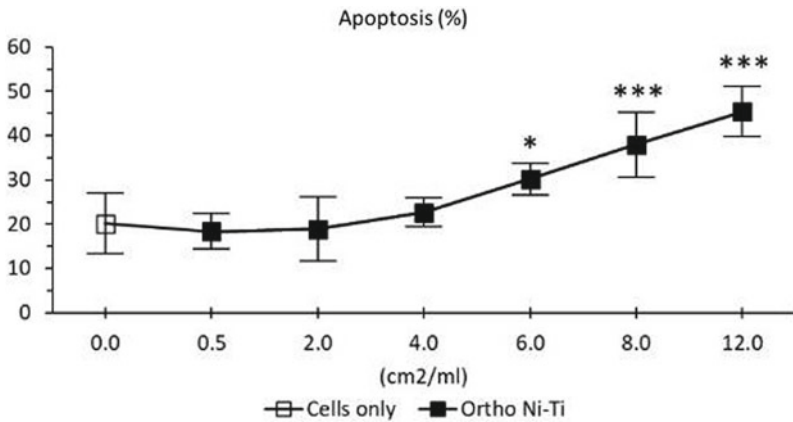


Fig. 4.34 The impact of ortho Ni–Ti surface-to-volume medium ratio in culture was dose-dependent. The thymocytes were stained with a Turk solution and examined under a microscope after 24 h of growth with Ni–Ti wires or control rods. The apoptotic cells were identified using homogeneously stained heterochromatin, and the percentage of apoptotic cells was determined after examining at least 500 cells. The findings are presented as the mean ± SD (n = 5) of one representative experiment. *p < 0.05, ***p < 0.005 versus matching control samples (control glass rods) [58].

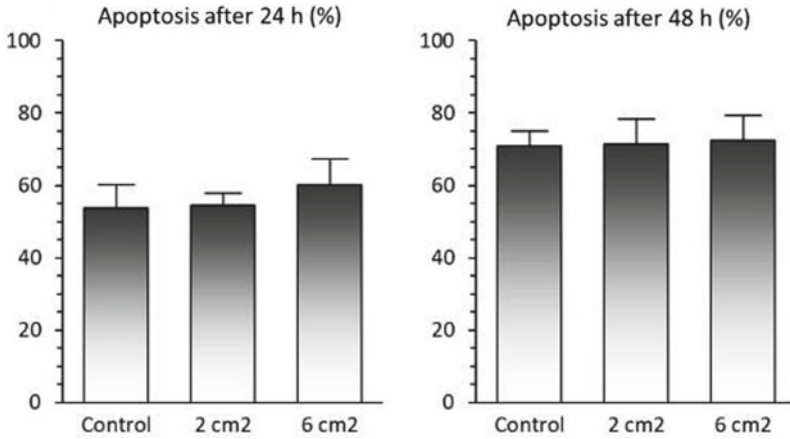


Fig. 4.35 The impact of Ortho Ni-Ti archwires on thymocyte apoptosis in culture cultures was studied using light microscopy and thymocytes stained with a Turk solution. After evaluating at least 500 cells, apoptotic cells were detected using homogeneously stained heterochromatin, and the proportion of apoptotic cells was measured. The results are reported as the mean Standard Deviation of five replicates [58]

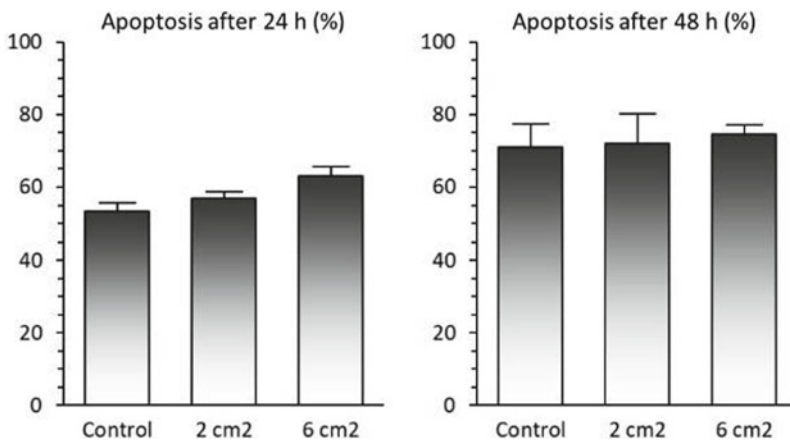


Fig. 4.36 The effect of TT Ortho Ni-Ti archwires on thymocyte apoptosis after 24 and 48 h in culture. The thymocytes were coloured with a Turk solution and viewed under a microscope after the culturing. After evaluating at least 500 cells, apoptotic cells were detected using homogeneously stained heterochromatin, and the proportion of apoptotic cells was measured. The results are reported as the mean Standard Deviation of five replicates [58]

Based on these findings, it is possible to infer that neither of the studied archwires causes thymocyte apoptosis, regardless of the surface-over-volume of medium ratio used, whether standard (2 cm²/ml) or applied maximally within ISO Standards (6 cm²/ml), and the cultivation timing (24 or 48 h).

4.6.6 *Biocompatibility of Rapidly Solidified Cu–Al–Ni SMA Thin Ribbon*

Cu–Al–Ni SMAs possess slightly weaker mechanical properties compared to the Ni–Ti SMAs. In spite of that, their application in dentistry is less frequent than Ni–Ti SMAs [1, 7, 12, 59]. Therefore, in order to understand their biocompatibility better, the microstructure, corrosion and cytotoxicity in vitro were considered on rapidly solidified Cu–Al–Ni SMAs thin ribbons, manufactured via melt spinning. The control alloy had the same composition as the test alloy, but no shape memory impact [60].

As evaluated by the lower Cu and Ni release into the conditioning medium, the results show that rapidly solidified (RS) ribbons are much more corrosion resistant than the control alloy. These findings support the conclusion that RS ribbons were not harmful to L929 murine fibroblasts or rat thymocytes. Furthermore, the RS ribbon conditioning medium suppressed cellular proliferation and IL-2 production in activated rat splenocytes to a significantly smaller extent. Conditioning the RS ribbons in culture medium for four weeks abolished the inhibitory effects almost completely [60].

The microstructure of RS strips shows that they are martensitic with minimal boron phases. In contrast, the control Cu–Al–Ni alloy displayed a complex multiphase microstructure. Energy Dispersive X-ray and Auger Electron Spectroscopy (AES) indicated the production of Cu and Al oxide layers after conditioning, demonstrating that the metals in RS ribbons are less susceptible to oxidation and corrosion than the control alloy. Finally, these results show that fast solidification increases the corrosion stability and biocompatibility of Cu–Al–Ni SMA ribbons in vitro [60].

The AES technique was employed to gain a better understanding of the oxidation processes that occurred on the alloy surfaces during conditioning. The technique enabled AES depth profiling and a closer examination of the sample surface's compositional depth profiles (to within 5 nm in our case). According to the AES measurements, the surface of the control alloy is enriched in O, Al, and Cu (Fig. 4.37). Furthermore, the energy location and form of the Auger peaks in the AES spectrum of these elements (counts per second vs electron kinetic energy) indicate clearly that the surface layer contains O atoms linked to Al and Cu atoms, as shown in Fig. 4.37a and b. The RS ribbons' Auger spectra revealed that the generated layer was primarily Al, Cu, and O (as in the control samples). Figure 4.37c and d show that, in contrast to the reference alloy samples, Ni was discovered on the contact surface [60].

4.6.7 *Deposition of an Atomic Layer of a TiO₂ on Ni–Ti SMAs/Corrosion Protection in a Simulated Body Fluid*

In this investigation [61], atomic layer deposition (ALD) tests were performed on a continuous vertical cast (CVC) NiTi rod (produced in house) and commercial Nitinol

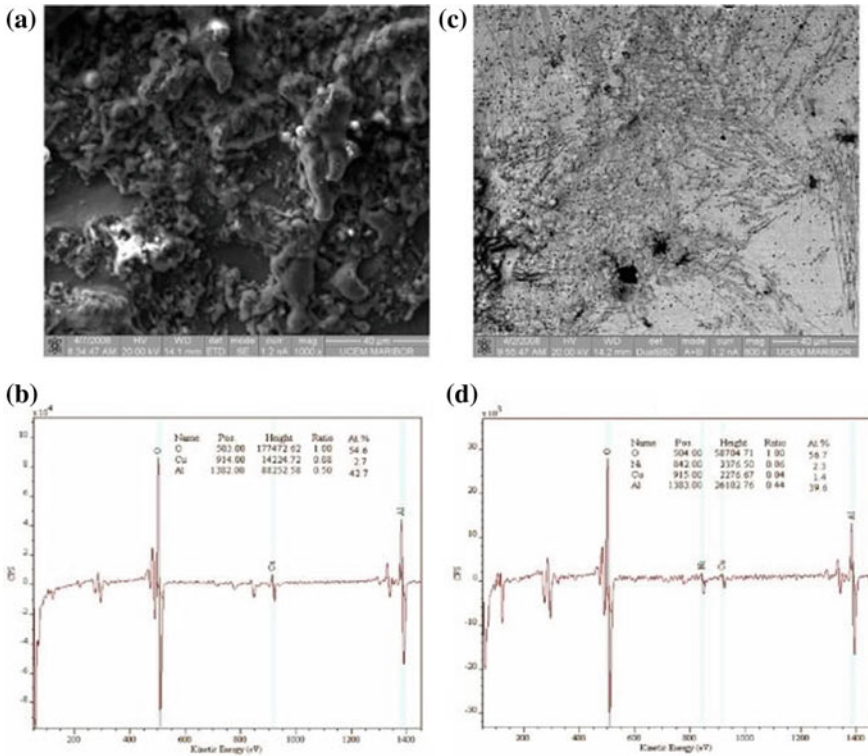


Fig. 4.37 **a** SEM image of the control alloy sample surface after conditioning for 4 weeks; **b** Auger spectra from the surface in **(a)**: 54.5 at.% O, 2.7 at.% Cu, 42.7 at.% Al; **c** SEM image of the RS ribbon surface after conditioning for 4 weeks; and **d** Auger spectra from the surface in **(c)**: 56.7 at.% O, 2.3 at.% Ni, 1.4 at.% Cu, 39 [60]

(com NiTi) as the control material, both of which were already rolled. At 250 °C, the TiO₂ layer was deposited using ALD in a Beneq TFS 200 system. The TiCl₄ and H₂O pulse lengths were 250 and 180 ms, respectively, followed by nitrogen purge cycles (3 s after the TiCl₄ pulses and 2 s after the H₂O pulses).

After 1,100 repeated cycles of ALD depositing, the average thickness of the TiO₂ layer for the CVC NiTi rod was 52.2 and 51.7 nm for the commercial Nitinol, as confirmed by X-Ray Photoelectron Spectroscopy (XPS) and a Scanning Electron Microscope (SEM) using Energy-dispersive X-ray (EDX) spectroscopy.

In a simulated body fluid at body temperature (37 °C), the corrosion resistance of CVC NiTi and commercial Nitinol was investigated, with and without the TiO₂ coating. The commercial NiTi with TiO₂ had the lowest corrosion current density (0.16 A/cm²) and the biggest passive area, according to the potentiodynamic polarisation studies. Because of the thin and compact coating, the electrochemical impedance spectroscopy studies revealed that the CVC NiTi rod and commercial Nitinol have only a resistance through the oxide layer for the first 48 h of immersion. The TiO₂/

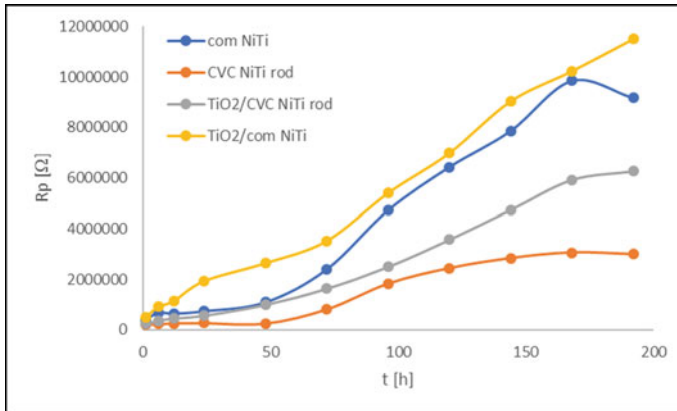


Fig. 4.38 Total corrosion resistance versus duration of exposure for all specimens tested [61]

CVC NiTi rod and TiO₂/commercial Nitinol had resistances through the oxide and porous layers throughout the submergence because the TiO₂ layer was formatted on the surfaces.

The total corrosion resistance diagram (Fig. 4.38) shows clearly that the corrosion resistance of all four specimens improved with time. This was caused by the formation of a protective oxide layer. It is also worth mentioning that, when the TiO₂ layer was placed on the specimen, the corrosion resistance improved instantly, whereas, in the case of the CVC NiTi rod and commercial Nitinol, there was no noticeable change in resistance in the first 48 h as a result of the thin oxide layer. The corrosion resistance of the TiO₂/commercial Nitinol rod was the best, followed by commercial Nitinol and the TiO₂/CVC NiTi rod, with the CVC NiTi rod having the worst corrosion resistance. The poorer corrosion properties of the CVC NiTi rod were caused by chemical inhomogeneity and a greater nickel concentration than in commercial NiTi.

Finally, it was demonstrated that adding a TiO₂ layer to the Nitinol surface improved corrosion resistance, but the chemical composition and microstructure of the substrate on which the ALD coating is applied still play a major part [61].

References

1. K. Otsuka, C.M. Wayman (eds.), *Shape Memory Materials* (Cambridge University Press, 1999)
2. G.B. Kauffman, I. Mayo, The story of nitinol: the serendipitous discovery of the memory metal and its applications. *Chem. Educ.* **2**, 1–21 (1997)
3. W.A. Brantley, T. Eliades, Orthodontic materials: scientific and clinical aspects. *Am. J. Orthod. Dentofac. Orthop.* **119**(6), 672–673 (2001)
4. R.S. Elliott, J.A. Shaw, N. Triantafyllidis, Stability of crystalline solids—II: application to temperature-induced martensitic phase transformations in a bi-atomic crystal. *J. Mech. Phys. Solids* **54**(1), 193–232 (2006)

5. A. Ziolkowski, *Pseudoelasticity of Shape Memory Alloys: Theory and Experimental Studies* (Butterworth-Heinemann, 2015)
6. N.B. Morgan, M. Broadley, Taking the art out of smart!-forming processes and durability issues for the application of NiTi shape memory alloys in medical devices, in *Proceedings for the Materials and Processes for Medical Devices Conference* (Anaheim, CA, 2004), pp. 247–252
7. S.A. Thompson, An overview of nickel–titanium alloys used in dentistry. *Int. Endod. J.* **33**(4), 297–310 (2000)
8. P.K. Kumar, D.C. Lagoudas, Introduction to shape memory alloys, in *Shape Memory Alloys: Modeling and Engineering Applications*. (Springer, US, Boston, MA, 2008), pp.1–51
9. E. Patorr, M. Berveiller, *Technologie des Alliages a' Me'moire de Forme*. Herme's (1994)
10. A. Wadood, Brief overview on nitinol as biomaterial. *Adv. Mater. Sci. Eng.* (2016)
11. A. Agrawal, R.K. Dube, Methods of fabricating Cu–Al–Ni shape memory alloys. *J. Alloy. Compd.* **750**, 235–247 (2018)
12. L. Peltier, O. Perroud, P. Moll, J. Slowensky, P. Charbonnier, A. Eberhardt, A. Hautcoeur, Production and mechanical properties of Cu–Al–Ni–Be shape memory alloy thin ribbons using a cold co-rolled process. *Shape Mem. Superelasticity* **7**(2), 344–352 (2021)
13. D.C. Lagoudas (ed.), *Shape Memory Alloys: Modeling and Engineering Applications* (Springer Science & Business Media, 2008)
14. D.J. Fernandes, R.V. Peres, A. Mendes, C.N. Elias, Understanding the shape-memory alloys used in orthodontics. *Int. Sch. Res. Not.* (2011)
15. G. Laplanche, A. Kazuch, G. Eggeler, Processing of NiTi shape memory sheets–Microstructural heterogeneity and evolution of texture. *J. Alloy. Compd.* **651**, 333–339 (2015)
16. K. Mehta, K. Gupta, *Fabrication and Processing of Shape Memory Alloys* (Springer International Publishing, Cham, 2019), pp.6–7
17. S.K. Vajpai, R.K. Dube, P. Chatterjee, S. Sangal, A novel powder metallurgy processing approach to prepare fine-grained Cu–Al–Ni shape-memory alloy strips from elemental powders. *Metall. and Mater. Trans. A* **43**(7), 2484–2499 (2012)
18. H.P. Xu, G.F. Song, X.M. Mao, Influence of Be and Ni to Cu–Al alloy shape memory performance, in *Advanced Materials Research*, vol. 197 (Trans Tech Publications Ltd., 2011), pp. 1258–1262
19. G.F. Andreasen, T.B. Hilleman, An evaluation of 55 cobalt substituted Nitinol wire for use in orthodontics. *J. Am. Dent. Assoc.* **82**(6), 1373–1375 (1971)
20. H. Walia, W.A. Brantley, H. Gerstein, An initial investigation of the bending and torsional properties of Nitinol root canal files. *J. Endod.* **14**(7), 346–351 (1988)
21. K.C. Shah, D. Chao, B.M. Wu, O.T. Jensen, Shape-memory retained complete arch guided implant treatment using nitinol (Smileloc) abutments. *Oral Maxillofac. Surg. Clin.* **31**(3), 427–435 (2019)
22. O.T. Jensen, C.E. Jansen, Y. Seo, G. Yellich, Guided nitinol-retained (Smileloc) single-tooth dental restorations. *Oral Maxillofac. Surg. Clin.* **31**(3), 437–446 (2019)
23. J. Fercec, M. Kos, M. Bruncko, I. Anžel, B. Glišić, E. Marković, R. Rudolf, Comparison of niti orthodontic archwires and a determination of the characteristic properties. *Mater. Teh.* **48**(1), 99–104 (2014)
24. G. Lojen, A. Stambolić, B. Šetina Batič, R. Rudolf, Experimental continuous casting of nitinol. *Metals* **10**(4), 505 (2020)
25. M. Lazić, M.M. Lazić, M.J. Karišik, M. Lazarević, A. Jug, I. Anžel, J. Milašin, Biocompatibility study of a Cu–Al–Ni rod obtained by continuous casting. *Processes* **10**(8), 1507 (2022)
26. G. Lojen, I. Anžel, A. Kneißl, A. Križman, E. Unterweger, B. Kosec, M. Bizjak, Microstructure of rapidly solidified Cu–Al–Ni shape memory alloy ribbons. *J. Mater. Process. Technol.* **162**, 220–229 (2005)
27. R. Dasgupta, A look into Cu-based shape memory alloys: present scenario and future prospects. *J. Mater. Res.* **29**(16), 1681–1698 (2014)
28. D. Abolhasani, S.W. Han, C.J. VanTyne, N. Kang, Y.H. Moon, Enhancing the shape memory effect of Cu–Al–Ni alloys via partial reinforcement by alumina through selective laser melting. *J. Market. Res.* **15**, 4032–4047 (2021)

29. E.M. Mazzer, M.R. da Silva, P. Gargarella, Revisiting Cu-based shape memory alloys: recent developments and new perspectives. *J. Mater. Res.* **37**(1), 162–182 (2022)
30. K. Mukunthan, L.C. Brown, Preparation and properties of fine grain β -CuAlNi strain-memory alloys. *Metall. Trans. A* **19**, 2921–2929 (1988)
31. K. Adachi, K. Shoji, Y. Hamada, Formation of X phases and origin of grain refinement effect in Cu–Al–Ni shape memory alloys added with titanium. *ISIJ Int.* **29**(5), 378–387 (1989)
32. J.W. Kim, D.W. Roh, E.S. Lee, Y.G. Kim, Effects on microstructure and tensile properties of a zirconium addition to a Cu–Al–Ni shape memory alloy. *Metall. Trans. A* **21**, 741–744 (1990)
33. W.R., Proffit, H.W. Fields Jr., D.M. Sarver, *Contemporary Orthodontics* (Elsevier Health Sciences, 2006)
34. I. Mihálcz, Fundamental characteristics and design method for nickel-titanium shape memory alloy. *Period. Polytech. Mech. Eng.* **45**(1), 75–86 (2001)
35. J. Uchil, K.K. Mahesh, K.G. Kumara, Electrical resistivity and strain recovery studies on the effect of thermal cycling under constant stress on R-phase in NiTi shape memory alloy. *Phys. B* **324**(1–4), 419–428 (2002)
36. G. Airoldi, D.A. Lodi, M. Pozzi, The electric resistance of shape memory alloys in the pseudoelastic regime. *Le J. Phys. IV* **7**(C5), C5-507 (1997)
37. V. Novák, P. Šittner, G.N. Dayananda, F.M. Braz-Fernandes, K.K. Mahesh, Electric resistance variation of NiTi shape memory alloy wires in thermomechanical tests: experiments and simulation. *Mater. Sci. Eng. A* **481**, 127–133 (2008)
38. X.D. Wu, Y.Z. Fan, J.S. Wu, A study on the variations of the electrical resistance for NiTi shape memory alloy wires during the thermo-mechanical loading. *Mater. Des.* **21**(6), 511–515 (2000)
39. L. Orgéas, D. Favier, Stress-induced martensitic transformation of a NiTi alloy in isothermal shear, tension and compression. *Acta Mater.* **46**(15), 5579–5591 (1998)
40. J. Ferčec, I. Anžel, R. Rudolf, Stress dependent electrical resistivity of orthodontic wire from the shape memory alloy NiTi. *Mater. Des.* **55**, 699–706 (2014)
41. J. Ferčec, B. Glišić, I. Ščepan, E. Marković, D. Stamenković, I. Anžel, R. Rudolf, Determination of stresses and forces on the orthodontic system by using numerical simulation of the finite elements method. *Acta Phys. Pol., A* **122**(4), 659–665 (2012)
42. N. Lepojević, I. Ščepan, B. Glišić, M. Jenko, M. Godec, S. Hočevar, R. Rudolf, Characterisation of NiTi orthodontic archwires surface after the simulation of mechanical loading in CACO2-2 cell culture. *Coatings* **9**(7), 440 (2019)
43. M. Chieruzzi, S. Pagano, S. Cianetti, G. Lombardo, J.M. Kenny, L. Torre, Effect of fibre posts, bone losses and fibre content on the biomechanical behaviour of endodontically treated teeth: 3D-finite element analysis. *Mater. Sci. Eng. C* **74**, 334–346 (2017)
44. A.R. Calabro, D.I. Gazarian, F.A. Barile, Effect of metals on β -actin and total protein synthesis in cultured human intestinal epithelial cells. *J. Pharmacol. Toxicol. Methods* **63**(1), 47–58 (2011)
45. J.W. Richter, G.M. Shull, J.H. Fountain, Z. Guo, L.P. Musselman, A.C. Fiumera, G.J. Mahler, Titanium dioxide nanoparticle exposure alters metabolic homeostasis in a cell culture model of the intestinal epithelium and *Drosophila melanogaster*. *Nanotoxicology* **12**(5), 390–406 (2018)
46. A. García-Rodríguez, L. Vila, C. Cortés, A. Hernández, R. Marcos, Effects of differently shaped TiO₂NPs (nanospheres, nanorods and nanowires) on the in vitro model (Caco-2/HT29) of the intestinal barrier. *Part. Fibre Toxicol.* **15**(1), 1–16 (2018)
47. N. Staffolani, F. Damiani, C. Lilli, M. Guerra, N.J. Staffolani, S. Belcastro, P. Locci, Ion release from orthodontic appliances. *J. Dent.* **27**(6), 449–454 (1999)
48. B. Clarke, W. Carroll, Y. Rochev, M. Hynes, D. Bradley, D. Plumley, Influence of nitinol wire surface treatment on oxide thickness and composition and its subsequent effect on corrosion resistance and nickel ion release. *J. Biomed. Mater. Res. Part A: Off. J. Soc. Biomater., Jpn. Soc. Biomater., Aust. Soc. Biomater. Korean Soc. Biomater.* **79**(1), 61–70 (2006)
49. S.A. Shabalovskaya, J. Anderegg, F. Laab, P.A. Thiel, G. Rondelli, Surface conditions of Nitinol wires, tubing, and as-cast alloys: the effect of chemical etching, aging in boiling water, and heat treatment. *J. Biomed. Mater. Res. Part B: Applied Biomater.: Off. J. Soc. Biomater., Jpn. Soc. Biomater., Aust. Soc. Biomater. Korean Soc. Biomater.* **65**(1), 193–203

50. B.A. Ramazanzadeh, F. Ahrari, B. Sabzevari, S. Habibi, Nickel ion release from three types of nickel-titanium-based orthodontic archwires in the as-received state and after oral simulation. *J. Dent. Res., Dent. Clin., Dent. Prospect.* **8**(2), 71 (2014)
51. M. Colic, S. Tomic, R. Rudolf, E. Markovic, I. Scepan, Differences in cytocompatibility, dynamics of the oxide layers' formation, and nickel release between superelastic and thermo-activated nickel-titanium archwires. *J. Mater. Sci. - Mater. Med.* **8**, 1 (2016)
52. A.M. Kamat, S.M. Copley, A.E. Segall, J.A. Todd, Laser-sustained plasma (LSP) nitriding of titanium: a review. *Coatings* **9**(5), 283 (2019)
53. S. Arango, A. Peláez-Vargas, C. García, Coating and surface treatments on orthodontic metallic materials. *Coatings* **3**(1), 1–15 (2012)
54. P. Parida, A. Behera, S.C., Mishra, Classification of biomaterials used in medicine (2012)
55. J. Black, G. Hastings (eds.), *Handbook of Biomaterial Properties* (Springer Science & Business Media, 2013)
56. H.H. Huang, Y.H. Chiu, T.H. Lee, S.C. Wu, H.W. Yang, K.H. Su, C.C. Hsu, Ion release from NiTi orthodontic wires in artificial saliva with various acidities. *Biomaterials* **24**(20), 3585–3592 (2003)
57. N. Schiff, B. Grosogeat, M. Lissac, F. Dalard, Influence of fluoridated mouthwashes on corrosion resistance of orthodontics wires. *Biomaterials* **25**(19), 4535–4542 (2004)
58. R. Rudolf, J. Ferčec, V. Lazić, V. Veselinović, C. Tomić, Characterisation of NiTi orthodontic archwires characteristic functional properties, in *CMBEBIH 2017: Proceedings of the International Conference on Medical and Biological Engineering 2017* (Springer Singapore, 2017), pp. 323–332
59. F. Suska, M. Källtorp, M. Esposito, C. Gretzer, P. Tengvall, P. Thomsen, In vivo/ex vivo cellular interactions with titanium and copper. *J. Mater. Sci. - Mater. Med.* **12**, 939–944 (2001)
60. M. Čolić, R. Rudolf, D. Stamenković, I. Anžel, D. Vučević, M. Jenko, G. Lojen, Relationship between microstructure, cytotoxicity and corrosion properties of a Cu–Al–Ni shape memory alloy. *Acta Biomater.* **6**(1), 308–317 (2010)
61. R. Rudolf, A. Stambolić, A. Kocijan, Atomic layer deposition of aTiO₂ layer on nitinol and its corrosion resistance in a simulated body fluid. *Metals* **11**(4), 659 (2021)

Chapter 5

Emerging Gold Dental Alloys



Abstract Well-known for their established reputation in restorative dentistry, gold alloys offer an excellent combination of strength, biocompatibility, and aesthetic appeal. Combined with other noble and base metals like palladium, silver, platinum, copper and zinc, these dental alloys exhibit enhanced mechanical properties while maintaining their inherent corrosion resistance and superior biocompatibility. Dental practitioners and patients benefit from these high quality materials, as they provide reliable tooth preparations and provide for durable long-lasting restorations. As research and development introduces cheaper contemporary materials, they are being compared to gold dental alloys, which have been highly suited for clinical use for decades. Gold dental alloys are preserving their high standard status in the dental community, especially for long-span bridges and for patients with bruxism. Their development has diminished in recent times due to their high prices, while conventional and redesigned gold dental alloys described in the chapter still represent a leading choice for patients susceptible to allergies, and for patients requiring or requesting the best for a lasting dental restoration with high aesthetics.

5.1 Introduction

Gold alloy objects have always been an integral part of everyday life, initially as a means of payment (tiles and ducats), jewellery, decorative objects and decoration. Over time, due to their favourable properties, gold alloys have found wide application in Dentistry, as well as for implant materials in the human body and in medicine. The flourishing of Nanotechnology created the conditions for the mass production of gold nanoparticles powders of various qualities with application in medicine and cosmetics.

Elemental gold, Au (lat. Aurum) has a characteristic yellow (“golden”) colour, relatively high melting and boiling temperatures, significantly high density and low hardness. Gold has: atomic number 79, density 19.3 g/cm³, melting point 1064 °C, Brinell hardness 190 MPa and yield strength 205 MPa. The crystal structure of gold is a surface-centred cubic. Of all the elements, besides silver and copper, gold has

the highest conductivity of heat and electricity, as well as ionisation energy among all precious metals.

Gold has great plasticity, i.e. it is suitable for forging and extraction (one gram of gold can be extracted for 3 m, and by forging or rolling you can get sheets (“gold foil”) up to 10 μm thick).

Pure gold is stable and resistant to the effects of air, water, alkaline solutions, bases, most acids and molten salts. It is possible to dissolve it only in a suitable mixture of acids, so-called *aqua regia*.

Gold is absorbed poorly in the human body, while poisoning with gold and its compounds is very rare and does not have a fatal outcome. Gold and its soluble salts have low toxicity.

It is most often alloyed with silver (Ag) and copper (Cu), so the study of the three-component alloy Au–Ag–Cu is of the greatest importance. In addition to these elements, gold is additionally alloyed, especially with zinc (Zn) and palladium (Pd).

Gold and its alloys have a long tradition in Dentistry. Today, they are most often used for making all kinds of fixed compensations. In Dentistry these alloys are used due to their exceptional durability, stability and resistance to corrosion.

In its pure state this precious metal has poor mechanical properties: extremely low hardness and high ductility. Thus, pure gold is a metal which is very soft (25 HV), has a very low yield strength at a load of 0.2% (30 MPa) and a high elongation (45%). Therefore, it has no application as such, but must be alloyed with some of the alloying elements: silver, platinum, palladium, copper, zinc, etc. Depending on the alloying element, to achieve the required chemical composition and their appropriate percentage share, the parameters of the technological procedure also change. This affects the change in the mechanical and functional properties of gold alloys further, i.e. the field of application is expanding. Tensile strength and hardness, as well as increased wear resistance, are of crucial importance, to which special attention must be paid during the technological process. By changing the composition and casting temperature, there are changes in the structure or microstructure, and, finally, in the colour of the alloy. Since the basic metal phase in the alloy affects the mechanical properties of the material, and therefore its application, by controlling the conditions of the production process it is possible to improve the microstructure greatly, and, thus, the mechanical and functional properties. During the technological process of production there is the formation of unstable phases, which tend to transform into a stable state - so that we can describe such a situation as a metastable state. In addition to unstable phases with non-stoichiometric composition, other defects are present in the microstructure, such as: the appearance of different porosities, inhomogeneity, the appearance of crystallographic defects (dislocations, grain boundaries). Thermo-mechanical treatment must be performed in the direction of removing these structural imperfections, towards achieving the most stable state of the system. The metastable state of the noble alloy increases the probability of corrosion, which is undesirable, because it reduces the quality of the products themselves.

Minor changes in the chemical composition affect the temperature of the technological process, leading to changes in the structure/microstructure or in the phase composition, which can improve the mechanical properties of gold alloys. To achieve

the functional properties of gold alloys, various surface treatment techniques are used, in order to obtain the desired shine, i.e. corrosion stability with the appropriate external coating, i.e. isthmus.

5.1.1 Historical Background of Gold Alloys in Dentistry

Dentistry is a medical science that deals with the prevention of diseases and the maintenance of the health of the oral cavity and accompanying structures, as well as the treatment of diseases or conditions in that area that deviate from normal anatomical-physiological relationships [1]. Gold has been known since ancient times. Even the oldest civilizations knew about it 5,000 years ago, and it was mostly used to make jewellery. Gold has always been considered a precious metal because of its brilliant shine, great durability and relatively small and rare deposits in nature. Dentistry was still an equal branch of medicine among the ancient nations (Egyptians, Chinese, etc.), and then it dealt with materials and their application. The first gold dental prosthesis found, over 3000 BC old, dates back to the time of the Phoenicians and Etruscans [2, 3], and it was used for the first time in modern Dentistry in the eighteenth century, in Paris, when the dentist Mouton made the first gold crown. The surgeon-dentist Bourdet, also in France, was the first to publish the scientific results of research on the gold prosthetic base. In 1869 Black proposed filling the root canals with gold leaf, in order to secure the gold stake that carries the artificial tooth. In 1907, Taggarat replaced the modelled wax inlay in a closed mould with a gold alloy. It was also used, in the composition of gold-platinum alloys, for casting models of individually made extensions. It is included in dental amalgams in a very small percentage, and it was also used to make the first fixed orthodontic appliances in the USA, when gold wires were used, because, at that time, gold was the only known metal that does not corrode in the very aggressive conditions that prevail in the oral cavity.

5.2 Dental Gold Alloys

Highly noble and noble alloys For fixed dental restorations it is necessary to improve the chemical composition of gold with different chemical elements, in order to obtain alloys with appropriate properties [4]. Platinum began to be used in the 1990s instead of expensive palladium. Platinum increases the hardness and elasticity of gold, and increases the melting temperature of the Au alloy. Copper in sufficient quantity in relation to the gold content makes the Au alloy heat treatable. Silver forms solid solutions with gold and palladium, and is a common constituent of this group of alloys. In gold-copper (Au–Cu) alloys silver is effective in neutralising the reddish colour of copper, and in the case of palladium-based alloys, silver is needed to develop the white colour of the alloys. Palladium has a good range of solubility in several

metals, such as gold, silver and copper, and the ability to achieve good mechanical properties. It has excellent corrosion resistance and is relatively biocompatible, and is added to gold in small amounts (about 1.5%) to improve tarnishing and corrosion resistance without significant loss of gold's bright yellow colour. Zinc (Zn) acts as a deoxidiser during the melting and casting of noble and highly noble alloys, and enables casting in thin profiles that are in dental structures. Indium (In) can be used instead of zinc, and if it is added in larger amounts (18–30% by mass), a color similar to gold can be achieved in Pd–Ag-based alloys. Iridium (Ir) or ruthenium (Ru) are added in small amounts, to reduce the grain and achieve better mechanical properties [5, 6].

Gold-based alloys These alloys have mostly yellow colour. The ADA divided gold alloys into four types, based on their mechanical properties [7]:

- Type I—soft (60 to 90 HV).
- Type II—medium hard (90 to 120 HV).
- Type III—hard (120 to 150 HV).
- Type IV—extra hard (hardened at least 150 HV; hardened at least 220 HV).

Type I gold alloys are soft and designed for dentures, and are not exposed to significant chewing forces. Type II alloys are used widely for inlays and onlays because of their good mechanical properties, but they have less plasticity than type I alloys. Type III alloys are used for ceramic fused to metal crowns and high stress areas. Increasing the Pt or Pd content raises the melting temperature, which is useful when components are joined by soldering. Type IV gold alloys are used in high stress areas such as fixed dental bridges and parts of removable partial dentures. The cast alloy must be stiff to resist bending, possess high strength to prevent permanent distortion, and be ductile enough to adjust if the frame clip is distorted or needs adjustment [8, 9]. Changes in the colour of the alloy caused by a decrease in the gold content are replaced by an increase in copper, silver and palladium. A higher content of silver and copper reduces the corrosion resistance of these alloys. These reduced gold alloys have moderate elastic moduli, but higher hardness and yield strength [10, 11].

Dental gold alloys for inlays and crowns are usually composed of alloys containing the precious metals gold, silver, platinum and palladium. **Yellow dental gold** usually has the following composition (in wt.%): 50% to 90% Au, 1% to 30% Ag, up to 20% Pd, up to 12% Pt and the rest (other metals found). **White dental gold** can consist of alloys of different value and quality: (i) High-quality Au and Pt alloys, (ii) Slightly less valuable Ag and Pd alloys, and (iii) So-called “**white dental gold**”, actually titanium alloys or Mo/Cr/Co steel alloys, which bear such a name because of their colour.

Classic three-component gold alloy A gold alloy consisting of gold, silver and copper is the first gold alloy that has been used successfully in Dentistry. It has been used since ancient times and is still used today. This gold alloy is also a noble alloy with the smallest number of components in Dentistry. It only has three components (Au–Ag–Cu), while all the other noble alloys used in Dentistry today have more components than it. Until recently, there was no noble alloy for Dentistry that, in

addition to other metals, did not contain gold-silver-copper. That is why the Au–Ag–Cu alloy can be called a classic dental noble alloy. It is the basic alloy from which all other noble dental alloys have been developed. If silver and copper are added to gold, its hardness, strength, elasticity and toughness increase. The improvement of the mechanical properties of the gold alloy is more influenced by copper than by silver. For the production of dental prosthetic restorations, the gold alloy contains a large amount of gold. There is significantly less silver and copper in the alloy.

Silver is alloyed very easily with gold, building an uninterrupted chain of homogeneous mixed crystals. Copper is difficult to dissolve in gold, and if the alloying process does not last long enough, in addition to mixed crystals, undissolved copper crystals can be found in the alloy. Therefore, the alloying of Au–Ag–Cu requires a certain technological procedure that takes a long time. The technological process of alloying gold, silver and copper is performed by alloying a certain amount of silver and copper and subsequently adding this alloy to the molten gold, after which all three alloyed materials are cooled together. If no gold was added to the copper-silver alloy during cooling, pure crystals of copper and silver would separate out.

Only when at least 25 wt.% of gold is added to the aforementioned alloy of silver and copper, is a solid solution consisting only of mixed crystals of copper, silver and gold obtained. Thus, the unlimited dissolution of silver and copper in the solid state is achieved by adding a sufficient amount of gold. The Au–Ag–Cu alloy can be used for making dental restorations only if it has at least 18 carats, i.e. if it contains at least 75 wt.% gold. Therefore, in the Au–Ag–Cu ternary alloy, the maximum percentage of silver and copper allowed is 25 wt.%. There are a large number of alloys of gold, silver and copper that are used in Dentistry, whereby the percentage composition of gold always increases, and that of silver and copper decreases. Within these changes, depending on the purpose of the alloy, the mutual ratio of silver and copper also changes.

From the point of view of the electrochemical stability of the alloy in the mouth, alloys with a higher percentage of silver and a lower percentage of copper are more suitable [12]. However, in the case of alloys containing a very high percentage of gold, in order to improve the mechanical properties, alloys with a higher copper value and a lower percentage of silver are more suitable. With those alloys, due to the increased percentage of copper, the electrochemical stability in the mouth will not be compromised, because they contain a higher percentage of gold.

Gold and palladium alloys These alloys contain about 50 wt.% gold and about 10 wt.% palladium, while the rest is made up of silver, copper and other metals. Despite the fact that they contain relatively little gold, these alloys are very resistant to corrosion and discoloration in the mouth due to the higher amounts of palladium. The aforementioned stability of the alloy is more affected by palladium than the same weight of gold. Namely, for the stability of the alloy, it is of crucial importance that the atoms of base metals are surrounded by atoms of noble metals. As in the same weight amount of palladium, for example, in one gram, there are twice as many atoms as in the same amount of gold, palladium as a precious metal has an extremely positive effect on the resistance of alloys. (There are twice as many atoms in 1 g of palladium than in 1 g of gold, because palladium has an atomic weight of 107

and gold 197). These alloys are light yellow, almost white in colour, which comes from the palladium. Alloys of gold and palladium are very economical (spar alloys), because they contain significantly less expensive gold than all other gold alloys. Gold has been replaced by a relatively large amount of much cheaper palladium. In addition, the alloys have a significantly lower specific gravity than all other gold alloys (Fewer grams of the cheaper alloy are needed to make the replacement).

5.2.1 Biocompatibility of Dental Alloys

Biocompatibility is an important feature of any material, especially those in close contact with the body. Biocompatibility refers to the biological acceptability and tolerability of materials used in medicine. In Medicine and Dentistry biocompatibility refers to the biological acceptability and tolerability of the materials that are applied in contact with living tissue, without damaging it. Biocompatibility is the ability or property of a material to cause an appropriate biological response in the body in accordance with the application for which it is intended. Each material is characterised by a set of properties that describe it and make it suitable for a specific field of application. When any of the materials is placed in the oral cavity, there is an interaction between the biological tissue and the material itself. This relationship is dynamic, and depends on the quality of the connection of the “two materials in contact”. Dental materials can have a harmful effect on surrounding tissues: pulp, mucous membrane or tongue [13, 14].

Negative phenomena during the interaction of the material with the surrounding tissue are cytotoxicity, i.e. a phenomenon in which a destructive action is visible at the cell level, then genotoxicity, a phenomenon in which a harmful effect on the genetic material is visible, and hypersensitivity reactions, in which an excessive response of the immune system occurs to a foreign body. It is important to note that only materials that have been tested thoroughly and that do not harm human health should be available on the market. Detailed testing and research into the impact of materials is carried out under strict control and collaboration between scientists and clinicians. Materials are required to be non-harmful to the body during the entire period of use.

Materials of origin can be natural or artificial and diverse (metals and alloys, polymers, ceramics, composites, semiconductors, biomaterials). If the material is accepted and approved for use for medical purposes (e.g. a CE mark on the packaging, according to European Standards), it is considered biocompatible, but, due to the complexity of the biological medium, it is the responsibility of every doctor of dental medicine to familiarise himself in detail with all the properties and side effects of the application. of certain materials that he uses for therapeutic purposes, to study in detail the history of his patient, and recognise the potential problems that a certain material can cause in a certain patient [13, 14].

Certain precious metals and their alloys used in dental medicine gain biocompatibility by creating a protective layer on the surface called a passive film, which is an oxide of one or more components of the alloy. These films are the products of

a corrosion reaction that reduces the corrosion rate by several orders of magnitude, and essentially prevents further corrosion once the passive layer is formed. Contact between two dissimilar metals in the mouth or changes in temperature or pH in the mouth can cause the protection to fail, and,, in the case of dissimilar metals, can lead to galvanic corrosion.

The biocompatibility of alloys, as well as their inertness towards oral tissues and fluids, are one of the factors that influence the corrosion of dental alloys in a biological medium. During corrosive changes, metal ions and various compounds are released that can lead to a local or systemic reaction. Locally they can cause irritation and systemic allergic sensitisation, and cause a toxic or carcinogenic effect. The critical energy at which metal ions are released into the electrolyte depends on the type of anion and its concentration in the electrolyte. The critical energy is also affected by the number of electrons in the common cloud of the alloy's surface. In order to achieve the reaction of the release of metal ions into the electrolyte, it is necessary to overcome the local thermodynamic equilibrium between electrons and ions that make up the composition of alloys of the building and auxiliary materials in dental prosthetics. As a protection against already formed corrosion and its further development, it is possible to create a surface oxide layer on the surface of the dental alloy-electrolyte system.

On the surface of the Au dental alloy in the biological medium in the oral cavity there is the formation of two different protective layers, an oxide layer and a sulphide layer [15]. Food and drink are a source of sulphur, that reacts with the alloy and creates a sulphide film. The formation of a sulphide film leads to discolouration of the alloy and slowing down of further corrosive activity (e.g. silver-palladium alloys). Although the mentioned protective layers cause passivation of the alloy surface, and, consequently, a reduced degree of corrosion, further continuation of corrosion in the oral cavity is possible.

5.2.2 Corrosion Resistance

Corrosion resistance is the property of a material's resistance to environmental media. A material that, under the same external conditions, causes less intense destruction on the surface or undesired changes in the microstructure, is a corrosion-resistant material. This property of the material is measured and evaluated through: loss of mass (thickness) and volume, changes in mechanical and other properties during corrosion and observation of surface damage. In practice, there are different methods of corrosion protection that can be combined, namely, the application of a corrosion-resistant material, surface protection of a less-resistant material with different metallic or non-metallic coatings, then cathodic protection and structural measures, and, finally, the addition of corrosion inhibitors to the surrounding medium, etc. [16].

Corrosion is material damage that can occur in different media, for example, in water or gases, and, depending on the medium in which it occurs, it is divided into chemical and electrochemical corrosion. Chemical corrosion takes place in an

active dry medium, for example in air, where a spontaneous reaction of metals occurs with gases. Oxides, sulphides and chlorides are formed on the surface of the metal, depending on which gas the metal reacts with. The reaction of metals with gases can also occur during heat treatment, welding, casting and other procedures. Copper and chromium form oxides on the surface at room temperature. Oxidation of metal does not only have to take place on the surface, it can also penetrate into the interior of the metal object. The oxide on the surface of the metal can serve as protection of the metal from further chemical action. The surface protective layer is formed with Co, Cr and Ni because they have the same volume as the metal oxides. Electrochemical corrosion occurs in a moist medium such as the oral cavity. Electrochemical corrosion occurs in the oral cavity due to the difference in electrical potential of the material, and the electrolyte is saliva. Saliva is a medium that has a strong corrosive effect on materials in the oral cavity. Its corrosiveness increases with increasing chloride concentration and decreasing pH in the oral cavity. Likewise, soft and bony tissue acts as an electrolyte. Electrolysis takes place between two metals that have different electrical potential, and ions travel from a place of higher potential to a place of lower potential.

A review of the comparable literature shows that there are many studies that use electrochemical techniques to evaluate the corrosion resistance of precious dental alloys [17–22], but no reliable method for classifying dental alloys based on their corrosion behaviour has been proposed among the qualitative descriptions of the corrosion behaviour. The only existing Standard for the corrosion investigations of dental metallic materials is ISO 10271 [23], which consists of three parts: (1) A static immersion test, in a solution containing 10 g dm^{-3} lactic acid, 5.85 g dm^{-3} sodium chloride at $\text{pH} = 2.3$, (2) An electrochemical test in 0.9 g dm^{-3} sodium chloride at $\text{pH} = 7.2$ in an inert atmosphere, and (3) A tarnish test in 3.1 g dm^{-3} $\text{Na}_2\text{S} \times 9\text{H}_2\text{O}$. Unfortunately [24], there is no quantitative and qualitative description on how to interpret the results obtained by the electrochemical test defined by ISO 10271 [23]. In addition, because oxygen is removed from the electrolyte by an inert gas (which could simulate the anaerobic conditions that could exist deep inside periodontal pockets and beneath dental plaque), the real corrosion potentials could not be established, due to the absence of the oxidising species (oxygen) in the electrolyte [16].

In a study [16], pure platinum and nine commercial dental alloys (producer: Zlatarna Celje d.o.o. Slovenia—see Table 5.1) with the contents of noble metals ranging from 27 wt.% to 97.6 wt.% were investigated by the procedure described in the *Standard ISO 10271:2009, Dental metallic materials—Corrosion test methods, test part 4.2*. Electrochemical testing for corrosion resistance was performed in an argon purged solution of 0.9% NaCl at $\text{pH} = 7.2$ [23]. The open circuit potentials, E_{ocp} , and polarisation resistance, R_p , were determined over two hours of immersion. From the polarisation curve the following characteristic parameters were found out: Zero current potential, $E_{z,n}$, active peak potentials, $E_{c,n}$, with corresponding current density $j_{c,n}$, breakdown potential, E_p , with corresponding current density j_p , and current density, $I_{0,3}$, at the potential $E_{0,3} = E_{z,1} + 0.3 \text{ V}$. In the first stability group, the so-called most stable dental alloys can be classified the high-noble dental alloys, with the chemical composition of at least 60 wt.% of noble metals, and with gold

Table 5.1 Composition and density of the tested dental alloys

Trade mark®	Chemical composition, wt. %	Noble metals, wt. %	Density, gcm ⁻³
Bioker	Au 85.9; Pt 11.7; Zn 1.5; Ir, In < 1	97.6	18.9
Aurodent 20	Au 83.3; Ag 10.0; Cu 5.9, Zn < 1	83.3	16.8
Aurodent BIO	Au 83.3; Ag 10.0; Cu 6.7	83.3	16.8
Dentor BIO	Au 78.3; Pt 5.0; Ag 10.0; Cu 6.7	83.3	16.2
Dentor S	Au 75.5; Pd 1.2; Pt 4.4; Ag 11.0; Cu 6.7; Zn 1.2	81.1	16.4
Midor S	Au 46.0; Pd 6.0; Ag 39.5; Cu 7.5; Zn, Ir < 1	52.6	12.9
Midor SE	Au 40.0; Pd 4.0; Ag 47.0; Cu 7.5; Zn, Ir, < 1	44	12.4
Auropal S	Au 10.5; Pd 21.0; Ag 58.2; Cu 9.3; Zn < 1	31.5	11.2
Auropal SE	Au 2.0; Pd 25.0; Ag 64.0; Cu 8.0. Zn < 1	27	10.7

content at least 40 wt.%; the second stability group, the so-called stable alloys, can be classified as the noble dental alloys, with the chemical composition with at least 25 wt.% to 60 wt.% of noble metals; in a third group, the so-called unstable alloys, can be classified predominantly as base dental alloys, with the chemical composition less than 25 wt.% noble metals.

5.2.3 Resistance to Wear and Damage

Wear, like friction, is not a property of the material, but represents the response of the given tribosystem. It represents surface damage or removal of material from one or both sides of two solid surfaces that are in contact with each other during motion. The consequences of material wear can be the complete removal of material from the surface, or only the movement of material on the contact surfaces. In the case of only transfer of material from one surface of the materials in contact to another, the final volume or mass loss at the interface is zero, i.e. there is no material separation as wear particles. The material loss increases as the wear damage progresses. Basic wear mechanisms:

- Abrasion and abrasive wear
- Adhesion
- Material fatigue
- Tribo-corrosion.

Abrasion: Is defined as wear by extrusion of material caused by hard particles or hard protrusions. Abrasion is considered one of the most prevalent mechanisms of wear, as much as 50% of the wear process is due to abrasion. It is described using

two phases of the unit event. In the first phase, the abrasive penetrates the surface of the material under the influence of the normal component of force, and, in the second phase, the material is squeezed out of the worn surface under the influence of the tangential component of force.

Abrasive wear: Describes the abrasion resistance through two phases. In the first stage, there are several influencing factors, the most important of which is the ratio between the microhardness of the abrasive and the surface material. In the second phase, the most influential factor in crack progression is ductile, brittle or surface fatigue.

Adhesion: When studying the way materials are bonded to the base surface (e.g. adhesive on tooth enamel), important properties are surface energy (the energy required to create a certain uniform unit of the material surface) and surface tension (the force required to extend the surface of the material by a certain amount). The ability of a liquid material to bind to a solid is described by the Contact Angle between the liquid and the solid substrate (wettability), and the speed of liquid penetration into the pores of the solid substrate also depends on the viscosity of the liquid. Adhesion is defined as the transition of material from one sliding surface to another during relative movement, due to the process of welding solid phases.

It is described in three phases. In the first phase, an adhesive bond of varying strength is formed at the point of contact of the protrusions, and in the second phase the adhesive bond is broken, while, in the third phase, particles break off, the shape of which is mainly leaf-like. Adhesion resistance is determined by tribological compatibility. Tribological compatibility of materials is the ability of materials that are in contact with each other not to be prone to welding. Materials with the crystal structure HCP/HCP have the best tribological compatibility, while materials with the crystal structure FCC/FCC have the worst tribological compatibility.

Material fatigue: Is defined as the separation of particles from the surface due to cyclic stress changes. Such a process is described by unit events in 3 phases. In the first phase, microcracks are created, and, in addition, it is also called the incubation phase, because there is no separation of particles in it. The second phase is characterised by the progression of these microcracks, and, in the third phase, the particles fall out in the form of tiles or chips. This causes damage to the surface in the form of holes, so this form of wear is called pitting. The fatigue resistance of the surface is called the dynamic durability of the surface.

Tribocorrosion: Is wear in which chemical or electrochemical reactions of the material with the environment prevail. Such wear can be described through two phases of unit events. In the first phase, a layer of corrosion products is formed, after which, in the second phase, the layer of corrosion products is partially destroyed. Resistance to tribocorrosion is defined as the chemical passivity of the material in a certain medium [25].

Tribocorrosion resistance on the example of dental alloys. Prosthetic fixed dentures are exposed to strong chewing forces and corrode faster than others where frictional forces are not so pronounced. This happens if the passivated oxide layer is removed from the surface of the alloy when chewing food or brushing the teeth. When the new layer is removed, the surface of the replacement is worn more and more, and

thus corrosion can affect the alloys in deeper layers as well. The chemical inertness of materials in certain media is one of the fundamental criteria for the resistance of such materials to tribocorrosion. Passivation in this case implies that the barriers that prevent oxidation must not be thicker than a micrometre. Passivation conditions are not always the same, and are specific to certain materials. The passivation of different materials is affected by different conditions; high pH helps prevent passivation of aluminium, chlorine ions and low pH help prevent the passivation of stainless steel, and high temperature prevents the passivation of titanium. Corrosion of precious alloys can also occur due to inhomogeneity, porosity of the material, or if the surface is polished. In sufficiently although corrosion as a phenomenon is negative, once formed the oxide layer can serve as a barrier between two different metals that are in contact. In order for the tribosystem to be complete, it must be resistant to breakage and elastic and plastic deformation. The requirements are even greater, namely, for the material to be durable, it must be resistant to wear and corrosion.

5.2.4 Substance Release and Allergies

Extensive investigations are performed for the substance release of dental alloys in the mouth area and saliva, for determining the suitability of these alloys for prosthetic restorations [26–30]. Substance release tests on base metal dental alloys are usually compared to gold alloys. From the common elements present in dental alloys, *in vitro* cell viability tests showed that, gold (Au), palladium (Pd), platinum (Pt) and indium (In) ions have no cytotoxic effect, while Chromium (Cr), copper (Cu) and silver (Ag) ions were toxic, and nickel (Ni), zinc (Zn) and cobalt (Co) ions were highly toxic [29]. In a study for type IV gold alloy crowns, Zn release was the highest among all constituting elements of the alloys, in spite of the low concentration of Zn in the alloys [30, 31]. Similarly, a cytotoxicity study of seven commercially available high gold dental alloys showed only Zn release [31]. From a biocompatibility viewpoint, no signs of gingival inflammation were detected by the naked eye around the tested crowns [30]. Attention was paid to the ion release rates of noble dental alloys, cautioning clinicians not to assume that all noble alloys are completely inert and biocompatible with oral tissues [26, 29]. However, there are other reports, stating that the allergies that do appear in gold alloys are actually because of traces of other elements in the alloy, not gold [32]. Some reports indicated the issue of allergic responses as a result of polymetalism [33], where the different metals in the oral environment create an electrogalvanic potential, resulting in an occasional stinging sensation or a metallic taste in the mouth. In extremely rare cases, allergies to gold are present, where the use of gold for dental restorations should be considered, following a positive contact allergy patch test [34].

For gold–palladium alloys it is important to investigate the influence of palladium on the dental alloy's functionality. Palladium is used frequently as a replacement element for Platinum, due to its similar properties, and because its purchasing costs were historically lower than those of the Platinum. Au–Pt alloys were more

expensive, weaker, more flexible, more technically sensitive to fabricate, and more corrosion-prone than their Au–Pd counterparts [35]. Palladium mixes easily in alloys with Gold, and it prevents the corrosion of silver in the oral cavity [36]. In the 1990s there were some controversies in Germany over possible adverse biological effects of using palladium in dental alloys [37]. In an ionic form and at sufficiently high concentrations, palladium has toxic and allergic effects on biological systems. Palladium allergy almost always occurs in individuals who are sensitive to nickel. The incidence appears to range from 93 to 100%. Yet, the incidence of a Pd allergy by itself is relatively rare [35]. However, there are no well documented cases of adverse biological reactions to palladium in the metallic state. Furthermore, in spite of the potential adverse biological effects of palladium ions, the risk of using palladium in dental casting alloys appears to be extremely low, because of the low dissolution rate of palladium ions from these alloys [37]. In general, in dental patients who are sensitive to Pd, tooth restorations using Pd-containing materials should not be used, although Pd has been used without allergic effects in some of these individuals. The usage of these alloys has decreased as of late, because of the fluctuating price of Palladium.

5.2.5 Recasting Gold Dental Alloys

Due to the high costs of gold and other noble dental alloys, recasting sprues and metal remaining in the crucible from the casting of dental restorations is common in dental laboratories. Such reuse is a controversial topic in dental laboratory practice. Several studies are aimed at investigating the usability of recast noble dental alloys and recast alloys' abilities to resist corrosion. The results from analyses show that the only compositional changes resulting from recasting were small decreases in the zinc and copper contents, and an increase in minor elements, probably impurities [38–40]. The results indicate that the noble alloys tested produced acceptable castings that are corrosion resistant when recast, only after they were subjected to a small number of recasting cycles [40, 41]. As an example, a severe degradation of properties was observed after the fifth cast of an Ag–Pd–Cu–Au alloy [42]. A systematic review of this topic was performed, reviewing 34 studies published between 1983 and 2014 [43]. The number of recastings ranged from 1 to 10. The percentage of new alloy ranged from 0 to 100 wt.%, although the mean value was 50 wt.%. This study revealed that recasting up to 4 times seems acceptable only if at least 50% of new alloy is added during each recasting procedure [43]. For metallic-ceramic systems, the alloys can be recycled 2 times without significant changes on the properties of the metal-ceramic interface [44].

5.2.6 *Life Expectancy*

Studies investigating the lifespan of gold dental alloy restorations, show quite high survival rates after several years of fixing them in the mouths of patients. The 7-year survival rate before a metal-ceramic complication of any kind was 92.4% in one of the studies [45]. This supports claims that metal-ceramic restorations perform very well clinically, including in practices outside academic environments.

In a study researching the lifespan of gold dental alloys, 95 participants were provided with 190 noble metal ceramic single crowns, and 138 participants with 276 fixed dental prosthesis retainer crowns on vital posterior teeth. The survival rate for “loss of crown or tooth” was 94.3% at 8 years for single crowns and 94.4% at 11 years for fixed dental prosthesis retainer crowns. The survival rate for “metal ceramic defect” was 88.8% at 11 years for single crowns and 81.7% at 11 years for fixed dental prosthesis retainer crowns. The results show good longevity for metal ceramic crowns provided in private practice settings. Bruxism was indicated as a risk for metal ceramic defects [46].

The 20-year survival rates for “loss of crown or tooth” are 78.8% for single crowns and 67.8% for retainer crowns [47]. Veneering ceramic defects occurred rather frequently, resulting in respective 20-year technical success rates of 74.2% for single crowns and 62.9% for retainer crowns. However, veneering ceramic defects causing crown losses were very rare events, indicating that posterior metal ceramic crowns are a highly reliable option in private practice settings [47].

A study was aimed to present the up to 25-year clinical performance and survival of 2,340 high gold-based metal-ceramic single crowns placed in a specialist prosthodontic practice. One commercial laboratory fabricated all crowns using only high-gold alloys with a minimum gold content of 75% and complying with ISO specifications 22,674 and 9693. All the patients were recalled between January 2008 and December 2009 and examined by the author. The clinical performance of the 2,211 favourably rated high gold-based metal ceramic single crowns was excellent, with an estimated cumulative survival of 97.1 and 85.4% at 10 and 25 years, respectively. Biologic factors in 2,340 crowns accounted for the majority (75.9%) of the 133 failures (5.7% of the crowns). Material stability was excellent, with no metal fractures and only four instances of porcelain fracture requiring composite repair or crown replacement. Patient complaints regarding unacceptable aesthetics resulted in 22 crowns (0.1%) being replaced after a mean clinical service time of 14 years [48].

Another study showed the survival of different dental restorations over a time span of 50 years. A total of 223 restorations were placed in 47 patients between 1966 and 1996 and reviewed annually until 2016. These restorations included 154 metal-ceramic crowns (101 posterior and 53 anterior), 25 posterior gold crowns, 22 anterior ceramic veneers, and 22 anterior ceramic crowns. Restorations were in occlusion. The mean survival for metal-ceramic crowns was estimated as 47.53 years (95% confidence interval [CI]: 45.59–49.47 years) and survival of anterior ceramic veneers, crowns, and gold crowns (100% survival) was high, over 50 years in clinical practice with annual follow-up and good oral hygiene [49].

Although high noble metal alloys are being competed by newer fully ceramic restorations, study results show that high noble restorations still represent an excellent therapeutic option, due to their long-term performance, even in modern Dentistry [50].

5.2.7 Comparison of Gold Dental Alloys to Ceramic Alternatives

Modern Restorative Dentistry is using fully ceramic restorations increasingly, which is an acknowledged alternative to the conventional metallic restorations veneered with ceramics. With fully ceramic, feldspar or glass–ceramic restorations, the substructure and veneer is made from these materials, such as zirconia veneered with porcelain. Several controlled trials were made for analysis of these tooth restorations, as there is still uncertainty regarding metal-free long-term performance compared to metal-based crowns and bridges. A review focusing on 9 trials involving 448 patients with dental bridges, crowns and bridges on implants, with durations up to 10 years showed little significant differences (regarding fractures, allergies, aesthetics, plaque build-up or wear), recommending clinicians to base decisions on which material to use for fixed prosthodontic treatment on their own clinical experience, whilst taking into consideration the individual circumstances and preferences of their patients [51].

High survival rates are reported for both types of restorations, with 93.3% for zirconia-based crowns, 96.0% for gold metal-based crowns after 2.5 years [52], or 97.7% for zirconia-based crowns and 97.4% for gold metal-based crowns after 5 years [53], with no significant differences in the aesthetic, functional and biological outcomes. Chipping of the veneering porcelain was the most frequently seen event that led to short-term (less than 3 years) failure and complications, which limits the range of indication, and there is still a need for improvement in non-metallic restorations [52–55]. Dental ceramics are the most suitable tooth coloured restorative material, impervious to oral fluids and biologically compatible. They are chemically indestructible in the oral environment [56].

According to the results of these clinical studies, ceramics-based rehabilitations represent a valid alternative to metal-based for tooth restorations [53, 54]. Ceramics-based restorations cover the entire range of indications, while metal-reinforced restorations still retain their place in dental practice, especially for long-span bridges [57] and treating patients with bruxism [58]. Metal-ceramic restorations still represent the “gold standard” against which the durability of all-ceramic restorations is measured, due to their long-term performance [58, 59].

A more recent study shows 5- and 10-year survival rates of completely veneered high noble metal alloy, base metal alloy (cobalt-chromium) and zirconia ceramic fixed partial dentures, with data from 400 study participants. The 5- and 10-year survival rates were 94.7 and 77.8% for high noble, 93.7 and 81.2% for Co–Cr, and 92.9 and 53.3% for zirconia ceramic fixed partial dentures, showing a diminished

success rate for zirconia ceramic dentures as compared to the metallic framework dentures [60].

5.2.8 Outlook for Gold Dental Alloys

As new materials emerge for prosthetic dentistry, they are evaluated for suitability, usually by comparing them to gold alloys, which are recognised as the “gold standard” in producing tooth restorations. They present a high biological safety, with negligible toxicity, allergy, and carcinogenicity as a result of elemental release into the mouth due to corrosion. The use of high-noble or noble alloys with single-phase microstructures for dental prosthetics is recommended for achieving the highest safety for patients, with very few exceptions [61].

Gold dental alloys have been highly suited for clinical use for decades, with several alloys present on the market, which differ in composition for catering to individual patients’ allergies, dietary habits, or other circumstances in the oral cavity and tissues. Gold alloy metal-ceramic restorations have a high aesthetic function, while, currently, fully ceramic restorations (feldspar, glass matrix and oxide ceramics) are often used for crowns and bridges, also due to their high aesthetics and mechanical/biocompatible properties. However, gold alloy or metallic restorations still retain their place in dental practice, especially for long-span bridges and for patients with bruxism. They are still the best in long-term performance. Replacing them due to failure in the oral cavity is also less demanding than replacing fully ceramic restorations.

Due to the high costs of gold dental alloys in comparison with cheaper contemporary materials, their usage in dental practice has decreased in the past few decades. This has also resulted in a reduced development of these alloys. However, due to their compelling combination of mechanical properties, excellent biocompatibility and high aesthetics, along with their advantages for long-span dental bridges and performance over several decades of use, they are recognised as a high standard in dental prosthetics. Presently, gold dental alloys still represent a leading choice for patients susceptible to allergies, and for patients requiring or requesting the best in long-term performance with high aesthetics.

5.3 Examples of Expertise

5.3.1 *Use of Dental Alloys with a High Proportion of Gold (High-Gold Dental Alloys)*

Gold dental alloys with high creep resistance and an adequate coefficient of thermal expansion, comparable to porcelain, are useful for dental restorations, where a bond is created between the porcelain and the surface of the dental alloy. This gives them the necessary properties to make fixed crowns and long bridges covered with porcelain. Dental alloys for the porcelain technique must have a solidus temperature of approximately 100 °C higher than the sintering temperature of dental porcelain, so that the dental structure does not deform during sintering of the porcelain—it settles. High-temperature fired porcelains require a sintering temperature between 900 °C and 980 °C, while low-temperature fired porcelains are characterised by a maximum temperature of 800 °C.

Another important property of dental alloys for the porcelain technique is the coefficient of thermal expansion (CTE), which must be compatible with porcelain in order to prevent the formation of internal stresses in the porcelain coating during cooling below the firing temperature. Porcelain can withstand higher compressive stresses than tensile stresses, so it is desirable that the thermal expansion of the dental alloy is slightly above the expansion of porcelain. In this way, the desired compressive stresses are generated in the porcelain shell during cooling, instead of tensile stresses. Unlike metal or dental alloy, the thermal expansion of porcelain is not independent of the cooling rate. Slow cooling after sintering leads to higher thermal expansion of the porcelain, so the higher CTE of the dental alloy can be compensated by slower cooling. The CTE coefficients of high gold and platinum dental alloys are largely balanced by high temperature sintered porcelains. Only high-gold, silver or dental alloys from the platinum group are available for low-temperature sintering porcelains.

Alloying elements such as copper, indium and tin are present in high-gold dental alloys in small amounts, and serve to harden the alloy and also for the ability to bond the porcelain to the metal surface (these are the so-called micro-alloying elements). During the sintering cycle, oxides of these metals are formed on the surface of the dental alloy. The standard required bond strength of 25 MPa can be achieved with a very thin layer of this oxide of less than 1 μm on the surface of the dental alloy. In dental alloys with a higher content of alloying elements, due to the lower content of gold and precious metals, the oxide layers are thicker, which leads to unsatisfactory aesthetics, and, in worse cases, to cracks and fractures in the porcelain coating (Fig. 5.1).

Gold represents one of those materials from which it is possible to make various noble dental alloys. The addition of alloying elements in gold-based dental alloys makes it possible to achieve properties that expand the use of these alloys for various dental purposes. We know dental alloys with a high gold content (above 50 m.%) and with a lower gold content (below 50 m.%). In this paper, we will present the

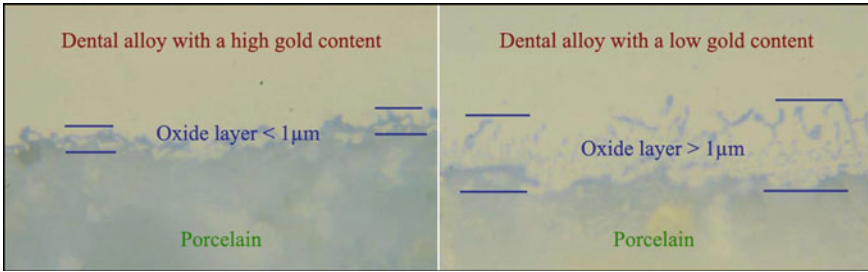


Fig. 5.1 Schematic representation of the oxide layer formation, depending on the proportion of Au (adapted from [62])

development of the high-grade dental alloy Bioker, with a high proportion of gold for the porcelain technique, which takes place in Zlatarna Celje d.o.o. The high-gold dental alloy BOKER for porcelain technology has the chemical composition (in mass %): Au 85.90%; Pt 11.70%; Zn 1.50%; other (Rh, Ir, Nb, Mn, In, Fe) <math>< 1\%</math>. The development is related to designing the chemical composition and monitoring the basic and functional properties of the dental alloy. Figure 5.2 shows the resulting layer of porcelain on the surface of the dental alloy for the Bioker porcelain technique.

In order to determine the biocompatible properties, it is necessary to obtain information about the release of ions, the cytotoxicity of these ions and the electrochemical potential of the dental alloy. To obtain these data, it is necessary to pass a series of tests designed to meet the requirements of international legislation. In the following, we present some of the tests that were carried out for this purpose for the Bioker dental alloy (Fig. 5.3):

- Cytotoxicity test in vitro, where the dental alloy is in direct contact with fibroblast cell cultures
- Primary skin irritation test on rabbits, after a single use of the dental alloy
- Sensitisation tests on guinea pigs, according to the Buehler method.

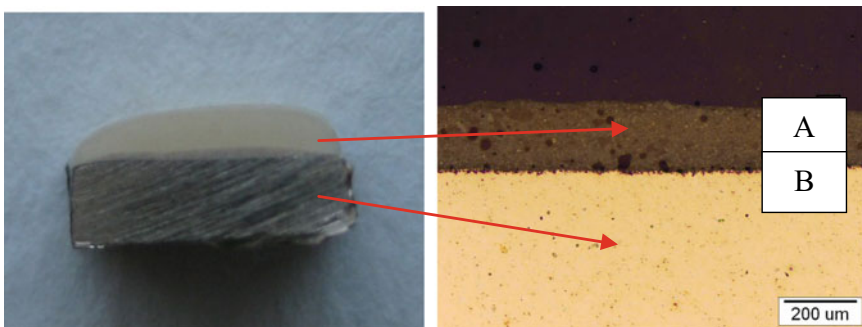


Fig. 5.2 Display of the resulting layer of porcelain on the surface of the Bioker dental alloy sample (A–porcelain, B–boundary surface between the porcelain and the dental alloy)

Fig. 5.3 Visual appearance of the BIOKER dental alloy



All the above tests were performed in the independent Medical Research Institute (VMA) Belgrade Serbia, in accordance with the Code of Ethics, and in accordance with modern requirements for animal welfare and laboratory practice.

Cytotoxicity test in vitro: We exposed a sample of the BIOKER dental alloy to L929 cells originating from mouse muscle tissue. For the negative control we used a material that does not have a cytotoxic effect—a dental vacuum cleaner, and for the positive control we used a preparation that has a cytotoxic effect—a solution with 4% phenol. The cells were grown in a petri dish at a temperature of 37 °C. The dental alloy sample, as well as the negative and positive samples, were added in direct contact with the cells and incubated for 24 h. After incubation, we evaluated the cytotoxic effect of the dental alloy samples on the cells, taking into account the percentage of abnormalities, degeneration, fragmentation and decay of the cells around the sample. In the BIOKER dental alloy, the estimated cell degradation was the same as in the control sample of L929 cells without additional material: 1.67%.

Primary skin irritation test on rabbits: Six samples of tiles measuring 5 mm × 5 mm of BIOKER dental alloy were applied directly to the shaved skin of three albino rabbits (the test took place at the Veterinary Institute in Belgrade, Serbia). One plate of dental alloy was applied to both sides of the rabbit's head (left and right). In addition, we added 2 tiles of control material that does not irritate the skin (plexiglass), also on both sides of the head. The dental alloy plate samples were covered with gauze and left in contact with the skin for 4 h. The plates of the dental alloy and the control material were removed after 4 h. We then observed the skin changes after 1, 24, 48 and 72 h after the removal of the dental alloy, by recording the number of erythemas and edemas that occurred when the dental alloy came into

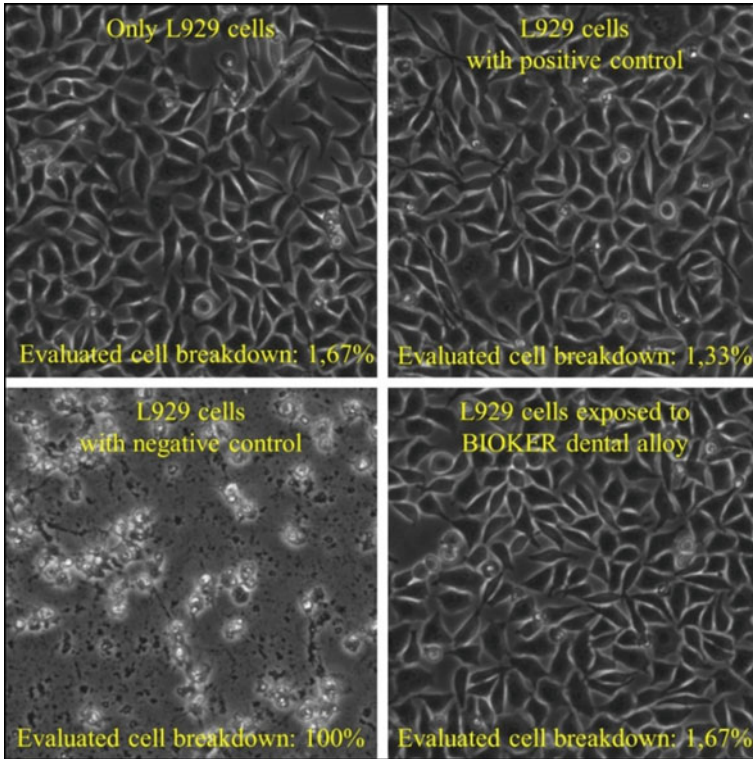


Fig. 5.4 Demonstration of changes in cell breakdown after primary skin irritation and sensitisation tests on the Boker dental alloy

contact with the skin (redness, rashes and swelling on the skin). With the BOKER dental alloy, there were noticeable changes on the skin: 0—Fig. 5.4.

Sensitisation test: Similar to the irritation test, one tablet of dental alloy was applied to the shaved skin of 10 albino guinea pigs and left in contact for 6 h. For the control we used a material that has been proven not to irritate the skin—Plexiglas. It was applied to 5 control guinea pigs. The tiles were removed after 6 h of exposure. The skin was again exposed to contact with the dental alloy 3 times a week for a period of 4 weeks. After each removal of the dental alloy, we observed and recorded the number of erythemas and edemas that occurred after the contact of the dental alloy with the skin. With the BOKER dental alloy, there were no noticeable changes on the skin.

Final conclusion of the tests: The Boker dental alloy does not show cytotoxicity, skin irritation and sensitisation.

Long-term use of high-gold dental alloys: The research carried out showed part of the tests that must be carried out to prove the biocompatibility of dental alloys. In doing so, it is also necessary to take into account the intended use of dental alloys in patients and their possible specific exposure over a longer period of time. Clinical tests

show the exceptional stability of high-gold dental alloys in the mouth, the absence of allergies, and the excellent preservation of healthy tissue without discolouration after the removal of the dental prosthesis, even after several decades of use. This is especially typical for patients who maintained adequate oral hygiene, which was reflected in the fact that the natural teeth remained suitable for the production of a new prosthetic extension without additional grinding and treatment.

The role of gold in dental prosthetics is currently not sufficiently clear, as it is being displaced by increasing competition from alternative materials. Taking into account the facts that gold dental alloys have proven durability, functionality, aesthetics and high biocompatibility, together with ease of manufacture, the comparison shows that the optimal material for prosthetic dental structures is still a dental alloy with a high gold content.

5.3.2 Development of a New Au–La Alloy

Gold alloys are used in Dentistry, not only for their preferred golden colour, but also because they maintain an extremely high chemical stability in the mouth. They also possess several desirable mechanical properties, such as high strength, ductility and elasticity [62]. When considering the formulations of gold-based high noble alloys for porcelain bonding and other applications in Dentistry, it is important to ensure all the required biomechanical properties, including not only their easy cast into thin sections, but also their good biocompatibility.

Pure gold, which has the highest biocompatibility, has relatively low yield strength and poor wear resistance, which limits its applicability in adornment and other biomedical applications. The alloying elements such as silver, palladium, zinc and platinum are usually added to improve these properties [63]. Dental alloys with high gold content were shown to have good biocompatibility, due to the high corrosion resistance of gold. However, *in vitro* studies have demonstrated the release of alloying elements in culture media, artificial saliva or distilled water. Some of them could reach the levels that cause a detectable cytotoxic effect [38, 64]. Metal corrosion depends on an alloy's composition and microstructure, biomechanical conditions, mode of casting and polishing, composition and electrolyte characteristics of solutions used for alloy conditioning, size of the alloy's surface area exposed to solutions, duration of incubation time and other factors [65].

The mechanical properties of pure gold can also be improved significantly by microalloying [66–68]. In recent years, significant effort has been made to increase the hardness of 24-carat gold alloys with a minimum of 99.5 wt.% of Au [69, 70], but such alloys exhibit only slightly higher hardness than pure gold in an annealed state. The usual alloying elements in microalloyed gold are used mainly as a grain refiner. In general, intensive work hardening can be achieved in the metals with decreasing grain size. However, in the fine-grained alloys with low stacking fault energy, deformation with twinning can prevail as the main operative deformation mode. This decreases the effect of work hardening. Therefore, in gold, which is a

metal with low stacking fault energy, no obvious strengthening can be expected by plastic deformation and grain size reduction. Therefore, it is necessary to introduce some other mechanisms of alloy strengthening, such as the introduction of alloying elements, which are very different to gold in atomic radius and have lower density, or the use of elements with very low solubility in a gold matrix.

One such approach is the microalloying of gold with rare earth elements, as suggested by theoretical analysis [71], and in our study we decided for lanthanum [72]. Microalloying with lanthanum can serve as deoxidants to facilitate bonding between the alloy and the ceramic, or to enhance the strength and colour of the alloy. Consequently, lanthanum can improve the possibility to prepare thin strips by melt spinning. Therefore, Au–La alloys, due to their specific characteristics, might be used as a potential biomaterial for various applications in Medicine and Dentistry. However, their biocompatibility and immunomodulatory properties are still unknown. Some studies suggested that lanthanum could be a toxic element [73], but little is known about its behaviour, corrosion stability and biocompatibility within a gold–lanthanum alloy. In this research, 24-carat gold was microalloyed with 0.5 wt.% La, which usually has low solubility in gold. Our aim was to characterise the Au–La alloy, and then to investigate the alloy's biocompatibility using different *in vitro* models.

For the production of the Au-La alloy a rapid solidification method was used, which was carried out using the Chill-Block Melt-Spinning technique (Fig. 5.5). An alloy of Au with La (in 0.5 wt.%) was prepared by remelting under argon overpressure. The molten alloy fell onto the wheel at a 90° angle from a 1.7 mm thick nozzle located 0.8 mm above the wheel rotating at 21 m/s. This speed was estimated to be optimal for the selected alloy cast at 1230 °C. With rapid solidification, we achieved a strong grain reduction and microsegregation, which increased the strength of the alloy further. Such mechanical properties can be exceptional for the preparation of biomedical constructs and test materials of various thicknesses. Figure 5.6 shows a typical cross-sectional microstructure of the resulting Au-La melt spun ribbon.

The characteristic texture of the Au-La microstructure indicates the direction of solidification. The wheel side of the tape, where curing begins, is at the bottom. A thin layer of fine equiaxed grains (external equiaxed zone) forms near this surface of the ribbon. These grains pass into columnar grains, and, roughly in the middle of the band, into coarse equiaxed grains. The transition from the isocentric outer zone to the columnar zone can be understood in terms of the effects of anisotropic growth. Rapid solidification had the effect of reducing the size of the resulting grains to a few microns and less. Due to the unstable conditions during solidification and cooling, in addition to grain size reduction, there was an increased concentration of thermodynamically stable and unstable microstructural defects. As a result, there was a much higher concentration of vacancies and substitution element - i.e. La. It was hypothesised that the gold solid solution could be supersaturated, and, consequently, there should be a lower proportion of intermetallic phases [74]. Under these unstable conditions, microsegregation can thus occur on the primary dendrites. In our case, coarser intermetallic particles appeared in the interdendritic space. Their share increased when transitioning from columnar to equiaxed grains [72]. Figure 5.7 presents the

Fig. 5.5 Schematic presentation of the Chill-Block Melt-Spinning technique: 1—Melt crucible, 2—Gas under pressure (Ar), 3—Molten melt, 4—Nozzle, 5—Metal stream, 6—Metal droplet, 7—Cooled rotating wheel, 8—Metal ribbon, 9—Scraper, 10—Inductor, ϑ —Pour corner

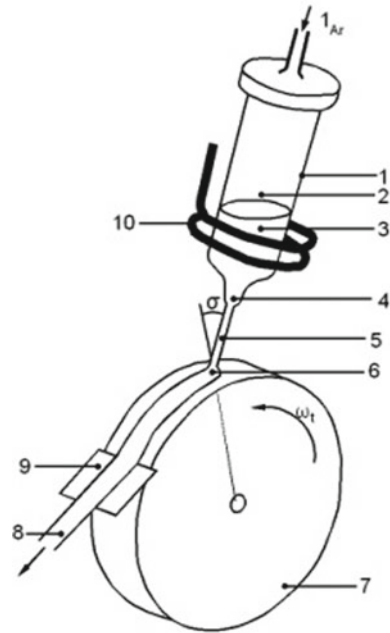


Fig. 5.6 Cross-section of a rapidly solidified Au-0.5 wt.% La ribbon

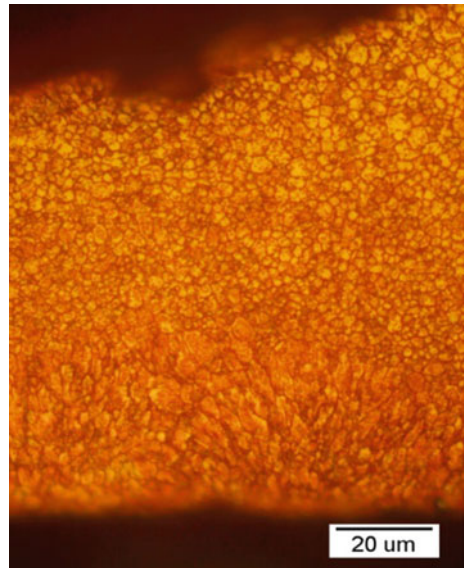
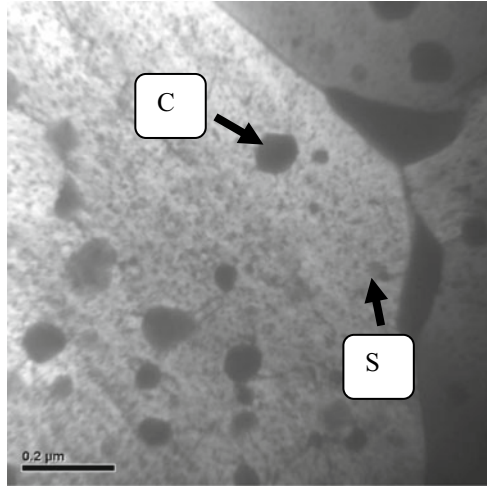


Fig. 5.7 TEM image of a rapidly solidified Au-0.5 wt.% La ribbon



microstructure of rapidly solidified ribbons (coarse equiaxed zone) obtained with Transmission Electron Microscopy (TEM). Coarser particles (C) can be observed inside the grains and on the grain boundaries. They are the result of microsegregation during rapid solidification. Small evenly dispersed particles also formed (S) inside grains, and present participations nucleated from the oversaturated solid solution during cooling.

More detailed investigations of the microhardness were carried out on the rapidly solidified samples, so that the microhardness was measured in the columnar and coarsely uniform-grained region. A much higher microhardness was achieved in the columnar zone than in the coarse zone. The microstructural gradient in the strip cross-section resulting from the solidification rate gradient leads to large differences in material hardness. In the case of the resulting Au-La strip, the difference between the hardness near the free surface and the hardness near the wheel surface was almost 25%.

The microhardnesses of pure gold, slowly solidified Au-La and rapidly solidified Au-La are presented in Fig. 5.8.

From the obtained results it was possible to determine the high strengthening effect of lanthanum and the additional strengthening by rapid hardening, as predicted in the References [75]. Pure gold has almost three times lower hardness compared to Au-0.5 wt.% La, which reached up to 86, 5 HV. This is due to the presence of a hard secondary phase containing the Au_6La intermetallic phase. Rapid solidification of this alloy increased the hardness to a maximum value of about 106.3 HV.

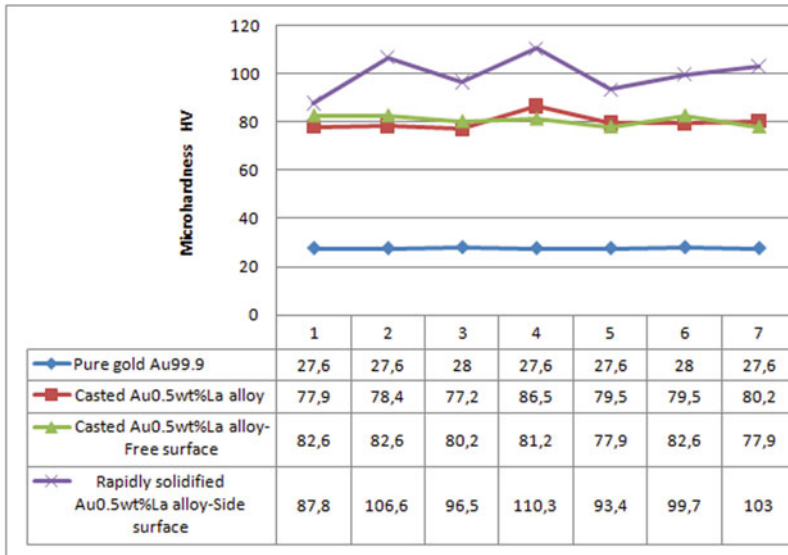


Fig. 5.8 Microhardness of pure gold, microalloyed gold and rapidly solidified Au-La ribbon

5.3.3 Development of an AuCuZnGe Alloy

Introduction

The primary use of gold alloys is in jewellery, where advancements and alloy developments may assist in improvements on gold alloys for dental uses. In the last few decades the popularity of white gold jewellery has been increasing. The white or silvery colour of these jewellery alloys is usually achieved with the addition of copper and/or silver. The addition of a smaller amount of palladium, zinc, nickel, or manganese metals to the gold base increases corrosion stability and mechanical properties [8, 9]. Nickel is well known for its effectiveness as a whitening element that allows the formation of Au alloys with good technical properties, applicable for jewellery production processes and use. The extensive use of nickel in the commercial goods and industry has increased skin contact exposure to this element, mainly through the use of jewellery, zippers, metallic buttons, dental braces, prosthetics, electronics, household utensils, and in workplaces with prolonged contact with nickel [76–79]. This exposure may induce a nickel allergy at the site of contact with the nickel-releasing item, causing allergic contact dermatitis in the form of rashes, blisters, edemas, or dry, scaly, and cracked skin [77, 78]. As nickel allergies have been well documented, the REACH Directive for registration, evaluation, authorisation, and restriction of chemicals used in European Union countries specifies the requirements of nickel release in products [78]. This restriction also transfers into dental alloys, where special declarations are to be made for nickel-containing alloys for

awareness of the presence of this element in the alloy, and its possible release into the body of a patient. Other alloy elements can also induce allergic reactions in the general population, such as palladium, which may cause allergies, usually in people who are already susceptible to nickel, while the incidence of palladium allergy by itself is relatively rare [35, 80].

To avoid allergies from metal ion release and the increase of costs from using alloy constituents such as palladium in Au alloys, other metallic elements may be studied for producing alloys with suitable properties. Several elements were considered for gold alloys, such as iron, cobalt, manganese, and gallium, but were found to be unsatisfactory during the different alloy and final product production processes. Another alternative is germanium, which allows for an accessible implementation in the established gold alloy production process [81]. Initially, the use of germanium serves a role in producing a whiter colour of the gold alloy for jewellery, but may be continued to be investigated as a constituent in gold dental alloys, due to its contributions in the alloy properties.

Germanium is a hard and brittle metalloid of a grey-white colour, with a melting point of 958 °C. It has a face-centred cubic crystal structure. Germanium decreases hardness and increases the flowability of the alloy. It is known for its use in micro-electronics, as it has electric properties between conductor and dielectric materials, classifying it as a semiconductor [82]. As an alloy component, it is also used occasionally in dental prosthetics, as an additive in palladium or Au-based alloys, and in jewellery in smaller amounts, as a deoxidiser, or for increasing flowability. Additionally, it has a relatively low density of 5.3 g/cm³. As a result it decreases shrinkage during alloy casting [81], which may be an added benefit in jewellery casting with precious gems, reducing the stress exerted on the gems, preventing their breakage, or for precision casting, where the casting dimensions are particularly important, such as in the casting of dental prosthetic crowns and bridges.

There are no known allergic reactions to germanium, and the usual percentage content of germanium in these alloys is relatively small for causing toxic reactions [80–82]. For its use in dental alloys, no negative effects are indicative for germanium. Due to its low density as compared with other noble metals, germanium has a strong alloy whitening power. Only a few percentage points of germanium of about 4–8 wt.% in the alloy whiten its colour considerably, whereas for nickel, the usual percentage for white gold alloys ranges from 10 wt.% to 15 wt.%, or even 30 wt.% for a premium white noble alloy [35]. Due to its whitening power, the germanium content is preferred to be of a lower content in the alloy, up to around 4 wt.%, as a higher content of this metal increases brittleness and reduces the hardness of the alloy.

Another aspect of the whitening element selection is the final alloy cost. In comparison with more common base metals, such as nickel, germanium is several times more expensive. As the required alloy wt.% for germanium is considerably lower, the final alloy costs are still comparable to alloys containing nickel. As such, at the time of carrying out this investigation, replacing nickel with germanium represented less than 1% of the total alloy materials' cost increase. In addition, using germanium still

represents only a fraction of the costs as compared with using noble metal whitening elements, such as palladium or platinum.

This study presents a step toward establishing germanium as a substitute for nickel in white Au alloys for general use in jewellery production and potential use in Dentistry. The use of germanium presents some favourable features and benefits, which can be considered for investigation in AuCuZnGe alloy production. The presented research shows the production of a germanium-based white Au alloy. The AuCuZnGe alloy's composition was chosen based on the following requirements:

- The white Au alloy has a 14 karat (58.5 wt.%) gold content, a widely-used white Au alloy for general jewellery production.
- The Au alloy should be made as white as possible, reducing the need for additional whitening steps for the final jewellery products with galvanic coatings.
- The germanium content should be kept as low as possible, due to its effects on the alloy's brittleness and hardness.
- The germanium alloy (as a pre-alloy) should be implemented easily in noble metal alloy production processes (casting, mechanical treatment, rolling, soldering).

The second and third requirements are in contrast to each other, as the whitening effect comes from a high content of germanium, while a lower content is needed for reducing the negative effects of this metal on the Au alloy's mechanical properties. As such, a first step, the corrosion resistance of the produced AuCuZnGe alloy, has been investigated to determine its corrosion stability properties, which are important as a major factor that may cause potential allergic reactions in the previously mentioned uses.

Thermocycling and Biocompatibility Testing of AuCuZnGe Alloy

Thermocycling of the AuCuZnGe alloy was carried out in accordance with ISO 9693–2:2016(E) and was conducted on a dental-prosthetic construction (Fig. 5.9a). The processing of the metal substructure was easy, without the need for great force or a high number of revolutions of the milling cutter. Moderate heating of the metal during processing was observed (expected—due to friction). The overall impression is that processing is faster and easier compared to other Au dental alloys, with a noticeably pleasant colour of the work and excellent optical characteristics of the ceramics on the AuCuZnGe dental alloy.

To conduct the thermocycling test two containers were needed, one with cold water (0–10 °C) and one with boiling water. The cold water was achieved using an ice pack. The boiling water was achieved with the help of an electric heater with a temperature regulator, to ensure a consistent temperature during the thermocycling process. To ensure an easy transfer of the sample between the two containers the sample was placed in a wire basket. The basket also prevented direct contact of the sample with the walls of the containers.

The test sample was placed in the wire basket, which was moved into the boiling water for 30 ± 5 s, which represents the first thermal shock. After 30 s the test sample was moved to the cold container (the second thermal shock), where the sample was left for 30 ± 5 s. The time of moving the sample from one container to another

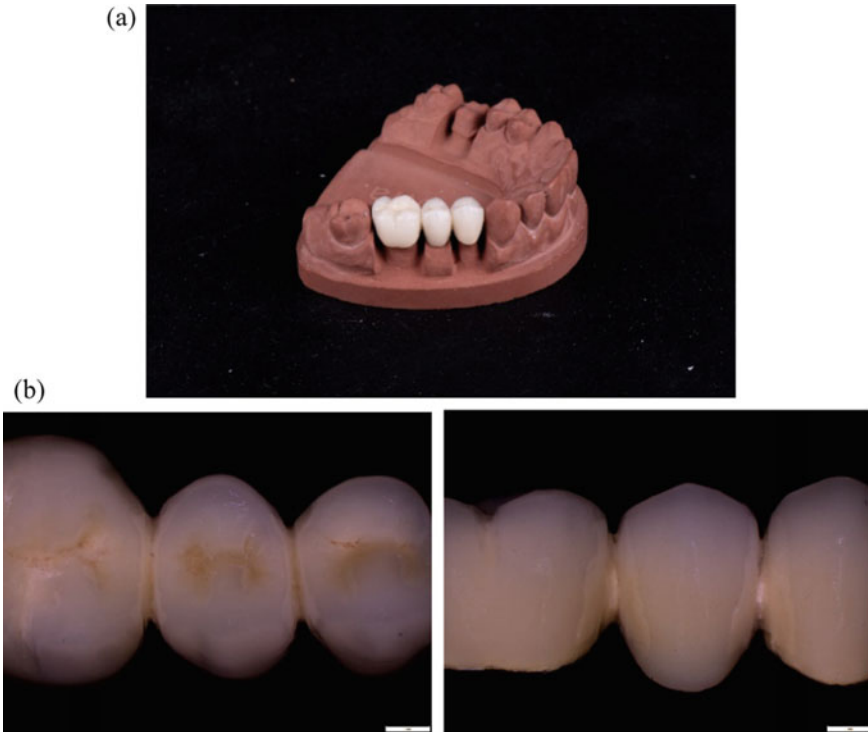


Fig. 5.9 **a** AuCuZnGe dental-prosthetic construction, **b** Steric microscope images after thermocycling of dental-prosthetic construction

takes less than 5 s. We then repeated the process until the sample was cooled 10 times. After the final cooling the sample was dried and inspected immediately, and after 48 h. The sample was inspected using steric (Fig. 5.9b) and Scanning Electron Microscopy (SEM, FEI Quanta 200 3D).

The dental-prosthetic construction was inspected using Scanning Electron Microscopy (SEM) on 16 selected areas, Fig. 5.10. In accordance with ISO 9693–2:2016(E) the sample was inspected before and 48 h after thermocycling. With the microscopic inspection no cracks were spotted on the interface between the alloy and the porcelain coating before or after the thermocycling. The SEM images of one place (area 1) that have been investigated thoroughly on the Dental-prosthetic construction shown in Fig. 5.11.

Results: After the thermocycling no cracks or imperfections were spotted on the AuCuZnGe dental-prosthetic construction. The alloy AuCuZnGe is in accordance with ISO 9693–2:2016(E) subsection 6.4.—Thermocycling.

Biocompatibility testing: Samples of the investigated alloy AuCuZnGe (as cast) and AuCuZnGe (oxidised) were placed at the bottom of a well of 12 fields. After

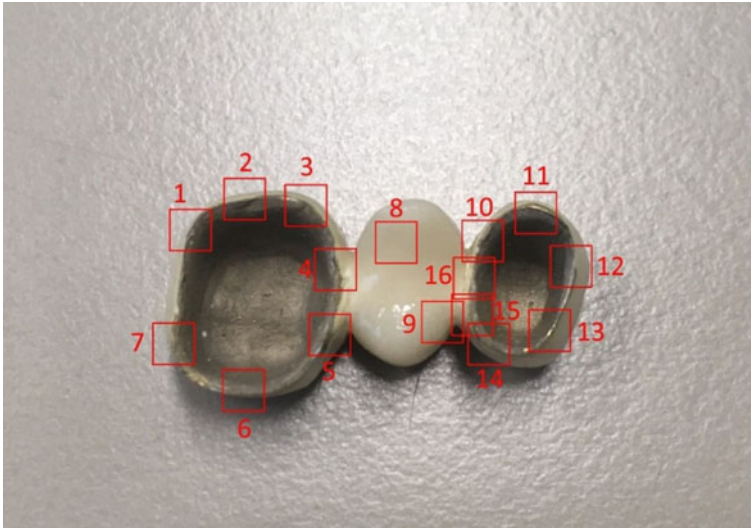


Fig. 5.10 Dental-prosthetic construction areas observed with SEM

placing the sterile materials stem cells from the dental pulp were seeded onto the surface of the material at a concentration of 5×10^4 cells per well (Fig. 5.12).

The cytotoxicity of the AuCuZnGe, after 24 h and 7 days, was measured by assessing cell viability by the direct method—MTT (3-(4,5-Dimethylthiazol-2-yl)-2,5-diphenyltetrazolium) bromide) test. A cover glass with the same dimensions as the plates of the tested alloy was used as a control. The MTT test was preceded by sterilisation of the samples in an autoclave.

After 24 h an increase in the mitochondrial activity of cells was observed in both groups of tested samples (AuCuZnGe as cast, and AuCuZnGe oxidised) compared to the control samples. No statistically significant difference was observed between the tested as cast and oxidised samples. A statistically significant difference in cell proliferation was observed only between the AuCuZnGe oxidised sample and the control (Fig. 5.13).

Note: Values of the optical density of the absorbed amount of formazin for the control sample (cover glass), oxidized and polished Au–Ge alloy sample. The absorbed amount of awarded formazan is directly proportional to the amount of viable cells.

After 7 days (Fig. 5.14.), a statistically significant increase in the mitochondrial activity of cells was observed in both groups of tested samples (AuCuZnGe as cast, and AuCuZnGe oxidized) compared to the control samples. No statistically significant difference was observed between the tested as cast and oxidized samples.

The formation of small amounts of base metal oxides during the oxidation process of the AuCuZnGe alloy had no effect on the change in biocompatibility of the alloy. After 7 days, a statistically significant increase in cell proliferation was recorded on both the oxidized and the polished surface of the AuCuZnGe alloy.

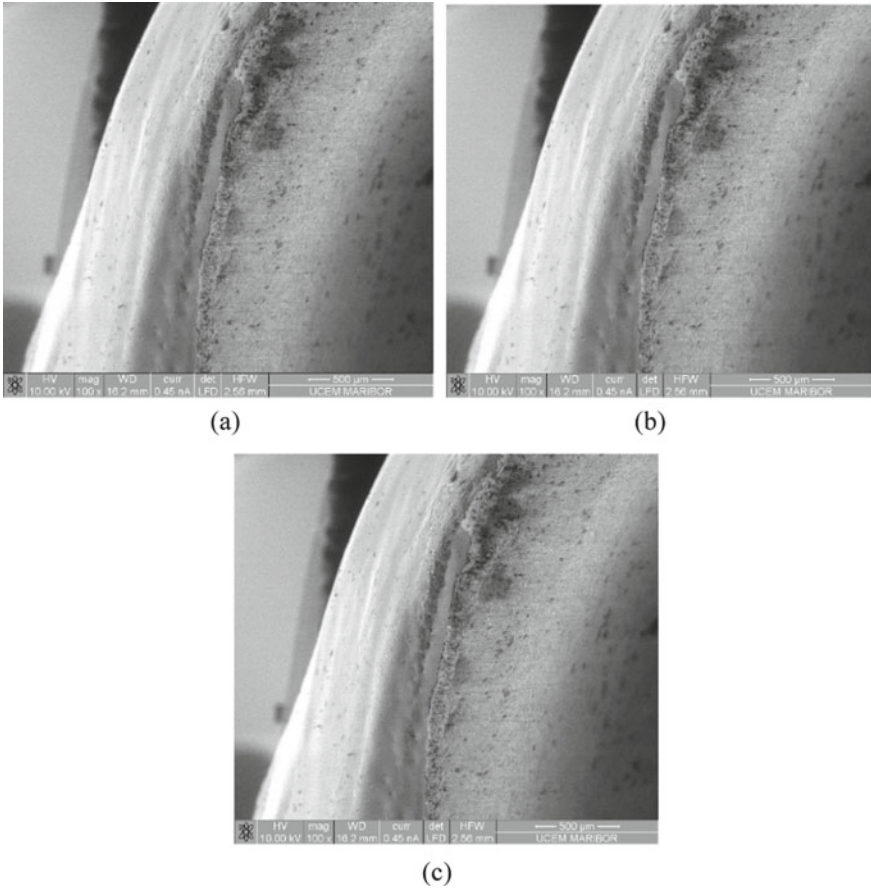


Fig. 5.11 SEM image of area 1: **a** Before thermocycling, **b** After thermocycling and, **c** 48 h after thermocycling

Concluding thoughts: Even the investigated AuCuZnGe alloy shows acceptable stability, for the commercialisation lot a of work has to be done, mainly in understanding the role of the Ge in the dental alloy. The detailed chemical composition of the AuCuZnGe alloy is the subject of a national patent.

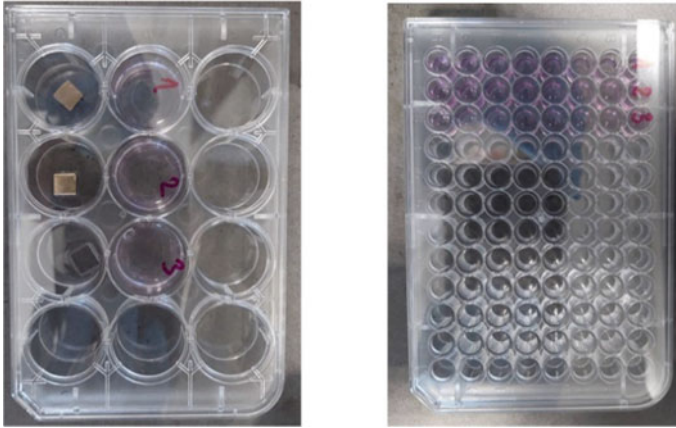


Fig. 5.12 Left: samples with a nutrient medium for cell culture in a 12-well flask, right: blue formazan

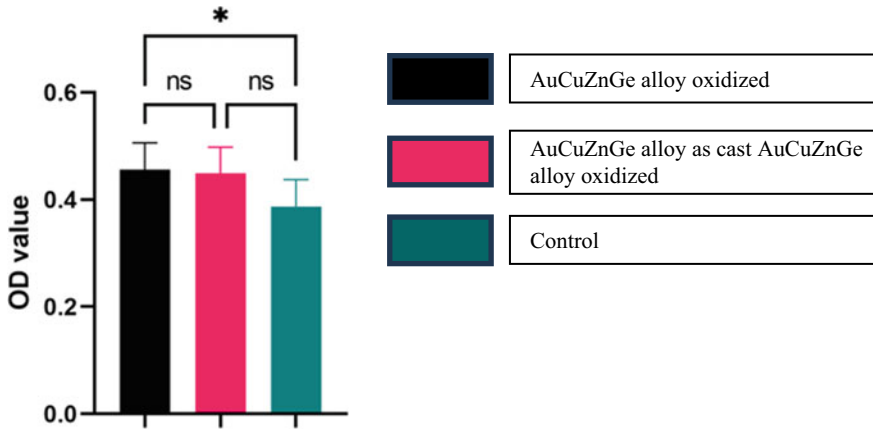
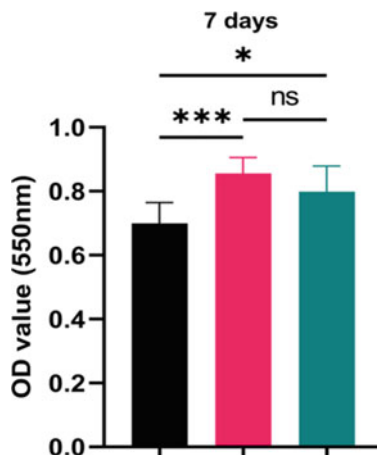


Fig. 5.13 Results of the cell viability after 24 h assessment by the MTT test

Fig. 5.14 Results of the cell viability after 7 days assessment by the MTT test



References

1. J.F. McCabe, A. Walls, *Applied Dental Materials*, 9th ed. (Wiley-Blackwell, 2008)
2. W. Hoffmann-Axthelm, *History of Dentistry* (Quintessence Pub. Co, Chicago, 1981)
3. V. Jerolimov et al., *Osnove stomatoloških materijala*. Stomatološki fakultet u Zagrebu, Zagreb (2005)
4. L. Gettleman, Noble alloys in dentistry. *Curr. Opin. Dent.* **1**, 218–221 (1991)
5. R.M. German, Precious-metal dental casting alloys. *Int. Met. Rev.* **27**, 260–288 (1982). <https://doi.org/10.1179/imr.1982.27.1.260>
6. D.A. Givan, Precious metals in dentistry. *Dent. Clin. North Am.* **51**, 591–601 (2007). <https://doi.org/10.1016/j.cden.2007.03.005>
7. O'Brien WJ (2002) *Dental Materials and Their Selection*, 3rd ed. Quintessence Pub. Co, Chicago
8. C. Cretu, E. Van Der Linghen, Coloured gold alloys. *Gold Bull.* **32**, 4 (1999)
9. G. Normandeau, White golds: a review of commercial material characteristics & alloy design alternatives. *Gold Bull.* **25**, 94–103 (1992). <https://doi.org/10.1007/BF03214721>
10. K.J. Anusavice, Noble metal alloys for metal-ceramic restorations. *Dent. Clin. North Am.* **29**, 789–803 (1985)
11. H.W. Roberts, D.W. Berzins, B.K. Moore, D.G. Charlton, Metal-Ceramic alloys in dentistry: a review. *J. Prosthodont.* **18**, 188–194 (2009). <https://doi.org/10.1111/j.1532-849X.2008.00377.x>
12. S. Canay, M. Oktmer, In vitro corrosion behavior of 13 prosthodontic alloys. *Quintessence Int. (Berl)* **23**, 279–287 (1992)
13. D.J. Sinha, A.A. Sinha, A. Vasudeva, N. Jaiswal, Biocompatibility of dental materials: a comprehensive review. *Indian J. Contemp. Dent.* **3**, 1 (2015). <https://doi.org/10.5958/2320-5962.2015.00030.3>
14. G. Schmalz, Determination of biocompatibility, in *Biocompatibility of Dental Materials* (Springer, Berlin, Heidelberg, 2009), pp.13–43
15. D.F. Williams, *Definitions in Biomaterials (Progress in Biomedical Engineering)* (Elsevier Science Ltd., Amsterdam, 1987)
16. B.N. Grgur, V. Lazić, D. Stojić, R. Rudolf, Electrochemical testing of noble metal dental alloys: the influence of their chemical composition on the corrosion resistance. *Corros. Sci.* **184**, 109412 (2021). <https://doi.org/10.1016/j.corsci.2021.109412>

17. J.-M. Meyer, L. Reclaru, Electrochemical determination of the corrosion resistance of noble dental casting alloys. *J. Mater. Sci. Mater. Med.* **6**, 534–540 (1995). <https://doi.org/10.1007/BF00151035>
18. D. Sun, W.A. Brantley, G.S. Frankel, R.H. Heshmati, W.M. Johnston, Potentiodynamic polarization study of the corrosion behavior of palladium-silver dental alloys. *J. Prosthet. Dent.* **119**, 650–656 (2018). <https://doi.org/10.1016/j.prosdent.2017.06.026>
19. R.I. Holland, Corrosion testing by potentiodynamic polarization in various electrolytes. *Dent. Mater.* **8**, 241–245 (1992). [https://doi.org/10.1016/0109-5641\(92\)90093-R](https://doi.org/10.1016/0109-5641(92)90093-R)
20. D. Sun, P. Monaghan, W.A. Brantley, W.M. Johnston, Potentiodynamic polarization study of the in vitro corrosion behavior of 3 high-palladium alloys and a gold-palladium alloy in 5 media. *J. Prosthet. Dent.* **87**, 86–93 (2002). <https://doi.org/10.1067/mp.2002.121239>
21. G. Hildebrand, A. Schreiber, M. Lohrengel, R. Strietzel, K. Liefelth, Localized electrochemical investigations of Pd73Cu13.5 ceramic firing dental alloy in DIN-saliva. *Corros. Sci.* **48**, 3629–3645 (2006). <https://doi.org/10.1016/j.corsci.2006.02.001>
22. E. Juzeliūnas, K. Leinartas, Samulevičienė M, Miečinskas P, Juškėnas R, Sudavičius A, Magnetron sputtered Au–Pd–In alloys: microgravimetric and electrochemical characterisation in simulated physiological solutions. *Corros. Sci.* **44**, 1541–1554 (2002). [https://doi.org/10.1016/S0010-938X\(01\)00169-X](https://doi.org/10.1016/S0010-938X(01)00169-X)
23. International Organization for Standardization, ISO 10271:2009, Dental metallic materials—Corrosion test methods, Geneva, Switzerland (2009)
24. C. Manaranche, H. Hornberger, A proposal for the classification of dental alloys according to their resistance to corrosion. *Dent. Mater.* **23**, 1428–1437 (2007). <https://doi.org/10.1016/j.dental.2006.11.030>
25. P. Močnik, T. Kosec, J. Kovač, M. Bizjak, The effect of pH, fluoride and tribocorrosion on the surface properties of dental archwires. *Mater. Sci. Eng. C* **78**, 682–689 (2017). <https://doi.org/10.1016/j.msec.2017.04.050>
26. G.M. Richardson, K.J. James, R.E. Peters, S.R. Clemow, S.D. Siciliano, Assessment of exposures and potential risks to the US adult population from the leaching of elements from gold and ceramic dental restorations. *J. Expo. Sci. Environ. Epidemiol.* **26**, 309–314 (2016). <https://doi.org/10.1038/jes.2015.55>
27. C. Holm, E. Morisbak, T. Kalfoss, J.E. Dahl, In vitro element release and biological aspects of base–metal alloys for metal–ceramic applications. *Acta Biomater. Odontol. Scand.* **1**, 70–75 (2015). <https://doi.org/10.3109/23337931.2015.1069714>
28. M.C. Cortizo, M.F.L. De Mele, A.M. Cortizo, Metallic dental material biocompatibility in osteoblastlike cells: correlation with metal ion release. *Biol. Trace Elem. Res.* **100**, 151–168 (2004)
29. W. Elshahawy, I. Watanabe, Biocompatibility of dental alloys used in dental fixed prosthodontics. *Tanta Dent. J.* **11**, 150–159 (2014). <https://doi.org/10.1016/j.tdj.2014.07.005>
30. W. Elshahawy, R. Ajlouni, W. James, H. Abdellatif, I. Watanabe, Elemental ion release from fixed restorative materials into patient saliva. *J. Oral Rehabil.* **40**, 381–388 (2013). <https://doi.org/10.1111/joor.12041>
31. Al-Hiyasat AS, Bashabsheh OM, Darmani H, Elements released from dental casting alloys and their cytotoxic effects. *Int. J. Prosthodont.* **15**, 473–478 (2002)
32. A. Celebić, M. Baucić, J. Stipetić, I. Baucić, S. Miko, B. Momčilović, Ion release from gold/platinum dental alloy: could release of other elements be accountable in the contact allergy attributed to the gold? *J. Mater. Sci. Mater. Med.* **17**, 301–305 (2006). <https://doi.org/10.1007/s10856-006-8225-y>
33. P. Mongkolnam, The adverse effects of dental restorative materials—a review. *Aust. Dent. J.* **37**, 360–367 (1992). <https://doi.org/10.1111/j.1834-7819.1992.tb00761.x>
34. H. Möller, Dental gold alloys and contact allergy. *Contact Dermatitis* **47**, 63–66 (2002). <https://doi.org/10.1034/j.1600-0536.2002.470201.x>
35. J.C. Wataha, K. Shor, Palladium alloys for biomedical devices. *Exp. Rev. Med. Dev.* **7**, 489–501 (2010). <https://doi.org/10.1586/erd.10.25>

36. A. Balint, M. Traistaru, G. Tanase, R. Sfeatcu, Implications of palladium with regards to high noble and noble alloys' metallurgy. *Metal. Int.* **17**, 38–42 (2012)
37. J.C. Wataha, C.T. Hanks, Biological effects of palladium and risk of using palladium in dental casting alloys. *J. Oral Rehabil.* **23**, 309–320 (1996). <https://doi.org/10.1111/j.1365-2842.1996.tb00858.x>
38. D. Stamenković, A. Čairović, M. Čolić, R. Rudolf, K. Radović, I. Đorđević, The effect of repeated casting on the biocompatibility of a dental gold alloy. *Acta Vet. Brno.* **59**, 641–652 (2009)
39. D. Stamenkovi, M. Čolić, A. Čairović, I. Anžel, L. Zorko, R. Rudolf, Study of the influence of repeated casting on the biocompatibility of a dental gold alloy, in *Zbornik referatov 50. mednarodnega livarskega posvetovanja*. Ljubljana: Društvo livarjev Slovenije, Portorož, p. 20 (2010)
40. M.F. Ayad, S.G. Vermilyea, S.F. Rosenstiel, Corrosion behavior of as-received and previously cast high noble alloy. *J. Prosthet. Dent.* **100**, 34–40 (2008). [https://doi.org/10.1016/S0022-3913\(08\)60133-X](https://doi.org/10.1016/S0022-3913(08)60133-X)
41. V.M. Maksimovic, A.D. Cairovic, J.R. Pantic, I.L. Cvijovic-Alagic, The recasting effects on the high gold dental alloy properties. *J. Min. Metall. Sect. B Metall.* **51**, 55–59 (2015). <https://doi.org/10.2298/JMMB130716023M>
42. N. Horasawa, M. Marek, The effect of recasting on corrosion of a silver-palladium alloy. *Dent. Mater. Off Publ. Acad. Dent. Mater.* **20**, 352–357 (2004). [https://doi.org/10.1016/S0109-5641\(03\)00128-3](https://doi.org/10.1016/S0109-5641(03)00128-3)
43. A.-S. Vaillant-Corroy, P. Corne, P. De March, S. Fleutot, F. Cleymand, Influence of recasting on the quality of dental alloys: a systematic review. *J. Prosthet. Dent.* **114**, 205–211.e3 (2015). <https://doi.org/10.1016/j.prosdent.2015.02.004>
44. Y. Wang, H. Huang, H. Lin, L. Jiang, Y. Pan, X. Li, H. Cheng, The influence of recycling on the properties of interface between ceramic and dental alloys. *Biomed. Res. Int.* **2020**, 1–9 (2020). <https://doi.org/10.1155/2020/3529781>
45. B. Reitemeier, K. Hänsel, C. Kastner, M.H. Walter, Metal-ceramic failure in noble metal crowns: 7-year results of a prospective clinical trial in private practices. *Int. J. Prosthodont.* **19**, 397–399 (2006)
46. B. Reitemeier, K. Hänsel, C. Kastner, A. Weber, M.H. Walter, A prospective 10-year study of metal ceramic single crowns and fixed dental prosthesis retainers in private practice settings. *J. Prosthet. Dent.* **109**, 149–155 (2013). [https://doi.org/10.1016/S0022-3913\(13\)60034-7](https://doi.org/10.1016/S0022-3913(13)60034-7)
47. B. Reitemeier, K. Hänsel, U. Range, M.H. Walter, Prospective study on metal ceramic crowns in private practice settings: 20-year results. *Clin. Oral Investig.* **23**, 1823–1828 (2019). <https://doi.org/10.1007/s00784-018-2618-4>
48. T.R. Walton, The up to 25-year survival and clinical performance of 2,340 high gold-based metal-ceramic single crowns. *Int. J. Prosthodont.* **26**, 151–160 (2013). <https://doi.org/10.11607/ijp.3136>
49. R.C. Olley, M. Andiappan, P.M. Frost, An up to 50-year follow-up of crown and veneer survival in a dental practice. *J. Prosthet. Dent.* **119**, 935–941 (2018). <https://doi.org/10.1016/j.prosdent.2017.06.009>
50. P. Rehm, H. Derks, W. Lesaar, B.C. Spies, F. Beuer, M.W.H. Böse, Restoration of 1325 teeth with partial-coverage crowns manufactured from high noble metal alloys: a retrospective case series 18.8 years after prosthetic delivery. *Clin. Oral. Invest.* **26**, 849–861 (2022). <https://doi.org/10.1007/s00784-021-04063-8>
51. C.E. Poggio, C. Ercoli, L. Rispoli, C. Maiorana, M. Esposito, Metal-free materials for fixed prosthodontic restorations. *Cochrane Database Syst. Rev.* **2017**, CD009606 (2017). <https://doi.org/10.1002/14651858.CD009606.pub2>
52. J.-Y. Shi, X. Li, J. Ni, Z.-Y. Zhu, Clinical evaluation and patient satisfaction of single zirconia-based and high-noble alloy porcelain-fused-to-metal crowns in the esthetic area: a retrospective cohort study. *J. Prosthodont.* **25**, 526–530 (2016). <https://doi.org/10.1111/jopr.12344>
53. C. Monaco, A. Llukacej, P. Baldissara, A. Arena, R. Scotti, Zirconia-based versus metal-based single crowns veneered with overpressing ceramic for restoration of posterior endodontically

- treated teeth: 5-year results of a randomized controlled clinical study. *J. Dent.* **65**, 56–63 (2017). <https://doi.org/10.1016/j.jdent.2017.07.004>
54. S. Rinke, S. Schäfer, K. Lange, N. Gersdorff, M. Roediger, Practice-based clinical evaluation of metal-ceramic and zirconia molar crowns: 3-year results. *J. Oral. Rehabil.* **40**, 228–237 (2013). <https://doi.org/10.1111/joor.12018>
 55. D. Urban, M. Jałbrzykowski, M. Gołębowska, Fatigue testing of dental bridges on selected examples. *Acta Mech. Autom.* **11**, 53–57 (2017). <https://doi.org/10.1515/ama-2017-0008>
 56. J. Krishna, V. Kumar, R. Savadi, Evolution of metal-free ceramics. *J. Indian Prosthodont. Soc.* **9**, 70–75 (2009). <https://doi.org/10.4103/0972-4052.55247>
 57. W. Höland, M. Schweiger, R. Watzke, A. Peschke, H. Kappert, Ceramics as biomaterials for dental restoration. *Exp. Rev. Med. Dev.* **5**, 729–745 (2008). <https://doi.org/10.1586/17434440.5.6.729>
 58. I. Sailer, N.A. Makarov, D.S. Thoma, M. Zwahlen, B.E. Pjetursson, All-ceramic or metal-ceramic tooth-supported fixed dental prostheses (FDPs)? A systematic review of the survival and complication rates. Part I: Single crowns (SCs). *Dent. Mater.* **31**, 603–623 (2015). <https://doi.org/10.1016/j.dental.2015.02.011>
 59. R. Hickel, Trends in materials science from the point of view of a practicing dentist. *J. Eur. Ceram. Soc.* **29**, 1283–1289 (2009). <https://doi.org/10.1016/j.jeurceramsoc.2008.08.014>
 60. F. Rathmann, M. Pohl, P. Rammelsberg, W. Bömicke, Up to 10 years clinical performance of zirconia ceramic and metal-ceramic fixed partial dentures: a retrospective study. *J. Prosthet. Dent.* (2022). <https://doi.org/10.1016/j.prosdent.2022.11.003>
 61. J.C. Wataha, Biocompatibility of dental casting alloys: a review. *J. Prosthet. Dent.* **83**, 223–234 (2000). [https://doi.org/10.1016/S0022-3913\(00\)80016-5](https://doi.org/10.1016/S0022-3913(00)80016-5)
 62. H. Knosp, R.J. Holliday, C.W. Corti, Gold in dentistry: alloys, uses and performance. *Gold Bull.* **36**, 93–102 (2003). <https://doi.org/10.1007/BF03215496>
 63. M. Colic, D. Stamenkovic, I. Anzel, G. Lojen, R. Rudolf, The influence of the microstructure of high noble gold-platinum dental alloys on their corrosion and biocompatibility in vitro. *Gold Bull.* **42**, 34–47 (2009). <https://doi.org/10.1007/BF03214904>
 64. R. Rudolf, V. Lazić, P. Majerić, A. Ivanić, G. Kravanja, K.T. Raić, *Dental Gold Alloys and Gold Nanoparticles for Biomedical Applications* (Springer International Publishing, Cham, 2022)
 65. S. Esmailzadeh, M. Aliofkhaezai, H. Sarlak, Interpretation of cyclic potentiodynamic polarization test results for study of corrosion behavior of metals: a review. *Prot. Met. Phys. Chem. Surf.* **54**, 976–989 (2018). <https://doi.org/10.1134/S207020511805026X>
 66. J. Wang, H. Qin, J. Chen, D. Yang, G. Zhang, First-Principles study on the elastic mechanical properties and anisotropies of gold-copper intermetallic compounds. *Metals (Basel)* **12**, 959 (2022). <https://doi.org/10.3390/met12060959>
 67. K.F. Leinfelder, An evaluation of casting alloys used for restorative procedures. *J. Am. Dent. Assoc.* **128**, 37–45 (1997). <https://doi.org/10.14219/jada.archive.1997.0024>
 68. A. Hensten-Pettersen, Casting alloys: side-effects. *Adv. Dent. Res.* **6**, 38–43 (1992). <https://doi.org/10.1177/08959374920060011401>
 69. G.E. Smith, Direct gold restorations, in *Sturdevant's Art and Science of Operative Dentistry*, ed. by A.V. Ritter, L.W. Boushell, R. Walter (Elsevier, St. Louis, 2019), pp.e69–e93
 70. R. Kunter, S. Mridha, Gold: alloying, properties, and applications, in *Reference Module in Materials Science and Materials Engineering* (Elsevier, 2016)
 71. T. Zupančič Hartner, R. Rudolf, A.C. Kneissl, I. Anžel, Characterisation of the metastable microstructure of Au-La alloy. In: Bührig-Polaczek A, Kneissl AC (eds) Fortschritte in der Metallographie: [Vortragstexte der 43. Metallographie-Tagung, 16–18. September 2009 in Aachen]. Werkstoff-Informationsgesellschaft MATINFO, pp. 277–282 (2009)
 72. R. Rudolf, S. Tomić, I. Anžel, T.Z. Hartner, M. Čolić, Microstructure and biocompatibility of gold-lanthanum strips. *Gold Bull.* **47**, 263–273 (2014). <https://doi.org/10.1007/s13404-014-0150-0>
 73. M.J. Barry, B.J. Meehan, The acute and chronic toxicity of lanthanum to *Daphnia carinata*. *Chemosphere* **41**, 1669–1674 (2000). [https://doi.org/10.1016/S0045-6535\(00\)00091-6](https://doi.org/10.1016/S0045-6535(00)00091-6)

74. Spaić S (1996) Fizikalna metalurgija I. Naravoslovnotehniška fakulteta, Oddelek za materiale in metalurgijo, Ljubljana
75. Y. Ning, Alloying and strengthening of gold via rare earth metal additions. *Gold Bull.* **34**, 77–87 (2001). <https://doi.org/10.1007/BF03214818>
76. M.G. Ahlström, J.P. Thyssen, M. Wennervaldt, T. Menné, J.D. Johansen, Nickel allergy and allergic contact dermatitis: a clinical review of immunology, epidemiology, exposure, and treatment. *Contact Dermatitis* **81**, 227–241 (2019). <https://doi.org/10.1111/COD.13327>
77. L.A. Garner, Contact dermatitis to metals. *Dermatol. Ther.* **17**, 321–327 (2004). <https://doi.org/10.1111/J.1396-0296.2004.04034.X>
78. J.P. Thyssen, W. Uter, J. McFadden, T. Menné, R. Spiewak, M. Vigan, A. Gimenez-Arnau, C. Lidén, The EU Nickel Directive revisited—future steps towards better protection against nickel allergy. *Contact Dermatitis* **64**, 121–125 (2011). <https://doi.org/10.1111/J.1600-0536.2010.01852.X>
79. J. Moon, M. Reeder, A.R. Atwater, Contact allergy to nickel: Still #1 after all these years. *Cutis* **107**, 12–15 (2021). <https://doi.org/10.12788/CUTIS.0156>
80. D. Peretti, M. Di Siro, S. Di Siro, Nickel-and Palladium-free master alloys for all karats of white gold—The Santa Fe Symposium. *St Fe Symp. Jewel. Manuf. Technol.* 343–362 (2017)
81. E. Rosenberg, Germanium: Environmental occurrence, importance and speciation. *Rev. Environ. Sci. Biotechnol.* **8**, 29–57 (2009). <https://doi.org/10.1007/S11157-008-9143-X/FIGURES/12>
82. J. Zheng, L. Yang, Y. Deng, C. Zhang, Y. Zhang, S. Xiong, C. Ding, J. Zhao, C. Liao, D. Gong, A review of public and environmental consequences of organic germanium. *Crit. Rev. Environ. Sci. Technol.* **50**, 1384–1409 (2020). <https://doi.org/10.1080/10643389.2019.1661175>

Chapter 6

Nanofolds in Dental Joining Practice



Abstract This chapter describes a low-temperature technique for soldering and brazing bioceramics to biometals in dentistry that uses reactive multi-layer nanofolds as a local heat source. Dental applications of Al-Au nano-multilayered foil are shown, along with examples of expertise. The authors present numerical modeling and CFD investigation of exothermic processes in Al-Au nanofolds.

6.1 Introduction

Based on the use of reactive multilayer nanofolds as a local heat source [1–3], this chapter describes a low-temperature method for soldering and brazing ceramics to metals in Dentistry. Many nanoscale layers and/or domains with selectable, quickly propagating reaction wave fronts, as well as selectable total energies, adiabatic temperatures, and ignition temperatures and powers, are present in reactive folds, with thicknesses ranging from 40 nm to less than 100 nm [4–6]. The use of reactive folds removes the need for a furnace, and reduces any heating of the bonded components significantly [7]. As a result, ceramics and metals can be fused over bigger areas without experiencing the damaging thermal stresses that are common when cooling during furnace soldering or brazing processes. This method’s origins can be traced back to US Patents [8–12].

Bonding in air with reactive multilayer folds is a quick and straightforward process (there is no need to join the bonds in a clean room or a specially-designed furnace). However, some component prepping is required. Typically, solder or braze layers are pre-applied to component bonding regions [2, 3].

Several combinations of reactive elements and alloys have been tried to date [13–19], including Al/Monel 400, Ni/Al, Zr/Al, Ni/Si, Mo/Si, Pd/Al, and Rh/Al. They all had exothermic reaction wave propagation velocities of up to 15–20 m/s, indicating the nano-folds’ strong chemical reactivity.

Reactive nano-folds can be used to create new kinds of protective coatings, join materials, and create free-standing membranes based on intermetallic or ceramic

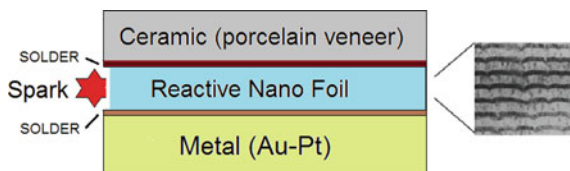


Fig. 6.1 A ceramic component (e.g. porcelain veneer) is soldered or brazed to a metallic component (e.g. Au-Pt alloy) using reactive foil (e.g. Al-Au) as a local heat source. The foil reacts chemically, and provides enough energy to melt the surrounding solder or braze layers, but not enough to heat the components seriously

compounds [3]. In this presentation, a completely novel plasma technology for the fabrication of Al-Au nano-multilayered foils is proposed for the first time [20].

Process description. In joining uses, the multilayer nano-foil is sandwiched between the two bonded components, along with two layers of solder or braze, as shown in Fig. 6.1. The foil controls the instantaneous release of heat energy for joining exactly, and, as a result, functions as a controllable local heat source. The suggested technology provides significant output improvements, exceptional energy efficiency and manufacturing productivity, exceptional bonding quality, and the ability to eliminate hazardous chemical processes [7].

6.2 Dental Applications of Al-Au Nano-Multilayered Foil

Due to the following challenges that arise in dental joining practice, Al-Au nano-multilayered foils may find entirely new applications [20]:

- (a) Porcelain Fused to Metal (PFM) Restorations - the bonding of an Alloy (Co-Cr-Mo, Au-Pt) to a porcelain veneer.

Despite the fact that dental alloys contain numerous micro-alloying elements (Ir, In, Rh, Nb, and so on) that are essential for the ability to adhere ceramics to the metal's surface, metal-ceramic bonding still has challenges. Because the extent of the oxide formation cannot be regulated easily, many alloy systems have a failure potential due to the thick and brittle oxide layer. A nano-foil inserted between the metal and ceramic layers may enhance the metal-ceramic bond, resulting in higher quality and longer life for PFM restorations.

This not only improves dental patients' overall health, but it also saves money on health-care costs in the long run.

- (b) Extensive Fixed-Removable Restorations—Attaching the abutment (Co-Cr-Mo, Au-Pt alloy) to the precision attachment (female part) and a precision attachment (male part) to the acrylic resin prosthetic base (polymethyl methacrylate).

Retainers for removable partial dentures (RPD) are typically utilised for difficult fixed-removable restorations. One of the two components of prefabricated attachments is built into the abutment, while the other is a part of the RPD. Links can exist both inside and outside the corona. Resin bonding was used to keep the extracoronal sutures in place. There is some uncertainty as to whether the obtained retention is adequate to prevent the attachments from moving. Intracoronal attachments typically consist of a male–female assembly that has been machined precisely out of Pt–Pd alloys that can withstand the high temperatures involved in casting PFM alloys.

A wax pattern is used to incorporate the female portion of the attachment. After the wax is removed, the restoration is immediately cast onto the attachment. The male half of the attachment is soldered to the frame, or it is attached to the acrylic denture foundation with auto-polymerising resin. The majority of dental techs prefer to solder the attachment's components. Attachment systems, on the other hand, can fail, particularly when used with distal extensions. To reinforce the binding, a nano-foil could be placed between the female attachment and the abutment, and between the male attachment and the denture base.

(c) Dental Implants Are the Connection Between an Alloy (CpTi, Ti-6Al-V, Ni-Ti) and Hydroxyapatite or Zirconium Oxide Coatings.

Dental implants constructed of CpTi or different Ti-alloys (Ti-6Al-4 V) have been utilised in Dentistry for many years. Because the coatings can achieve firm and direct biological fixation with the surrounding bone tissue, the clinical use of various coatings on Ti-implants (plasma-sprayed hydroxyapatite-HA coatings, diamond coatings, diamond-like carbon coatings, yttria-stabilised zirconia, ZrO_2 -3% Y_2O_3 coatings) has been adopted widely. Because of their extraordinarily high hardness, superior wear resistance, low friction and biocompatibility, they have a strong potential for usage as biomedical implants. However, the poor bonding strength between the various coatings and the Ti alloy has been a major source of concern for long-term clinical applications. HA/yttria-stabilised zirconia (YSZ)/Ti-6Al-4 V composite coatings have been developed with improved mechanical qualities to standard plasma-sprayed HA coatings. The bonding strength has increased.

The link between the HA/ ZrO_2 coating and the Ti alloy might be strengthened by sandwiching a nano-foil between an implant (Ti-6Al-4V) and the coatings. This would result in a higher-quality implant with a longer lifespan.

Finding an appropriate nanostructured metallic-ceramic coating that can offer a nanocrystalline metallic bond at the interface to the surface's firm ceramic bond is another alternative.

6.3 Example of Expertise

Plasma-assisted sputtering in a Plasmait® [21] system produced the Al-Au multi-layered foil [11]. Atoms of the Au-alloy and Al were sputtered from two separable targets/wires (diameter = 3.5 mm) of pure aluminium (99.99 wt. %) and 14-carat

gold alloy with the chemical composition (58.50 wt. % Au, 28.95 wt. % Ag, 12.45 wt. % Cu), Fig. 6.2.

With its dynamic sealing mechanism, the Plasmait® [21] machine allows for continuous processing of an endless number of materials. A Special Type Glow discharge processes wire or tape guided through the machine at pressures ranging from 1 to 10 mbar. Argon was added to the discharge for a better sputtering outcome in multilayer deposition of Au-alloy and Al, as was the case with most N₂ applications.

While processing the thin films, the wire speeds through the processing chamber was 0.5 m/s, and the processing power coupled into plasma was approximately 250 W for Au-alloy wire and 800 W for Al wire. During the processing, the corresponding parameters were optimised (pressure, power in plasma, gas composition, wire speed, and wire variety).

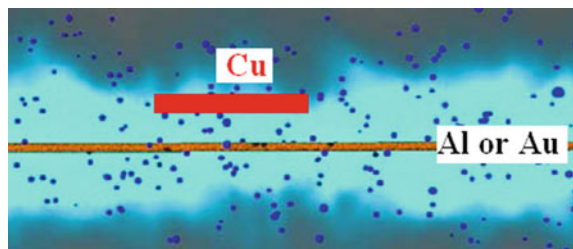
A pure copper substrate with dimensions of 10 mm × 10 mm (thickness about 0.5 mm) was put on a holder and subjected sequentially to fluxes of atoms from an Au-alloy or Al atoms. The required number of alternating layers was achieved by varying the wire speed and magnetron source power and adjusting the number of turns and thickness.

The Cu/Al-Au-Al-Au/ sample was made with Al and Au layers ranging in thickness from 100 to 400 nm. To avoid diffusion and reaction during deposition, the substrate temperature was kept below 323 K.

Scanning Electron Microscopy (SEM-Sirion 400 NC) and Energy Dispersive X-ray (EDX) analyses (Oxford INCA 350) were used to characterise the microstructures of the generated nano-foils. The polished objects were placed in the chamber of a SEM microscope with a vacuum of 10⁻⁶ mbar for electron microscopy. Microscopic inspection of the polished surface, as well as qualitative and quantitative micro-chemical analysis at characteristic points on the interface between Au-Al nanofoils and substrate Cu, is included in the analysis. We noticed surfaces with an electron beam voltage of 30 kV and at various working distances. (6.5 mm, 7.2 mm, etc.).

Finally, the nano-foils were examined using a Quanta 200 3D environmental Scanning Electron Microscope with a Focused Ion Beam (FIB), which enables sample surface cleaning and etching, transverse cutting directly from the external sample surface, cutting surface polishing, and high-resolution observations of sample microstructures.

Fig. 6.2 Ion discharge from the wire (Al or Au) toward the Cu substrate to demonstrate the plasma effect



6.3.1 Results with Discussion

Figure 6.3 depicts the substructure of the Al-Au multilayered foils. The last Au-nano-foil had a very porous surface, as seen in the top view (Fig. 6.3a). Further examination verified this hypothesis, specifically on the transverse cutting surface (Fig. 6.3b, c), where regions with small and large voids could be found across the cross-sections of all four foils. The agglomeration surrounds the voids within the lone foils. The Au-alloy atoms appear to have collected non-homogeneously on the surface of the Cu-substrate, resulting in an extremely porous microstructure. The foils exhibited a columnar microstructure, according to detailed microstructure investigations. This microstructure is found in foils placed on a cold base. Precise measurements of each foil indicated that the Al-foils were approximately 100 nm thick, whereas the Au-foils were approximately 400 nm thick. As a result, we may conclude that the thickness of Au-foil is twice that of Al-foil at similar plasma process technical parameters.

EDX line-analyses (Fig. 6.4) of cross-sections of the Al-Au-Al-Au foils showed the existence of Ag and Cu atoms in the Au foils. These elements were derived from the alloy used in the plasma device as a wire-positive anode. The distribution of elements in the Au-foils followed the chemical composition of the wire, which means that a greater weight percentage of an element causes a higher peak in the EDX spectrum. For the Al-nano foils, however, only the existence of Al could be seen.

At the Al/Au alloy surfaces, there was no transformation of pure metals to Al-Au intermetallics. There was no interdiffusion between the Cu base and the first Al layer.

We employed the cleaning and smoothing procedure in the first stage of creating Al-Au nano-foils, to ensure a high-quality surface for the Cu-substrate (macro-roughness decrease). This stage seeks to create a surface with a low degree of surface imperfections, which may result in the formation of a very homogeneous formatted nano-foil. Based on the microstructural measurements, we can conclude that this step was extremely effective, because the Cu-substrate surface in the cross-section was quite flat (on a micro-scale). We employed plasma deposition to generate nano-foils in the second stage. The produced nano-foils indicated that the mechanism of Al-deposition differed significantly from that of Au-deposition. The Al foils were thin (approximately 100 nm), compact and nearly void-free. The Au foils had a thick (about 400 nm) non-homogeneous microstructure with a noticeable number of flaws. (The foil contained pores and irregular granules). We think that the presence of alloying elements (Ag and Cu) influenced atom segregation during the plasma process, which is why the microstructure was not homogeneous.

The metals with the highest packing density that are face centered cubic (FCC) include Al and Au. To understand the change in thickness (volume) during the formation of Al and Au layers, we can compare the density and atomic packing factor (A.P.F) of pure metals (see the Table in Fig. 6.6). The atomic packing factor (A.P.F) measures how much volume the atoms fill in Au and Al, however, the density of Au is nine times more than that of Al. As a result, the Au- foils are expected to be

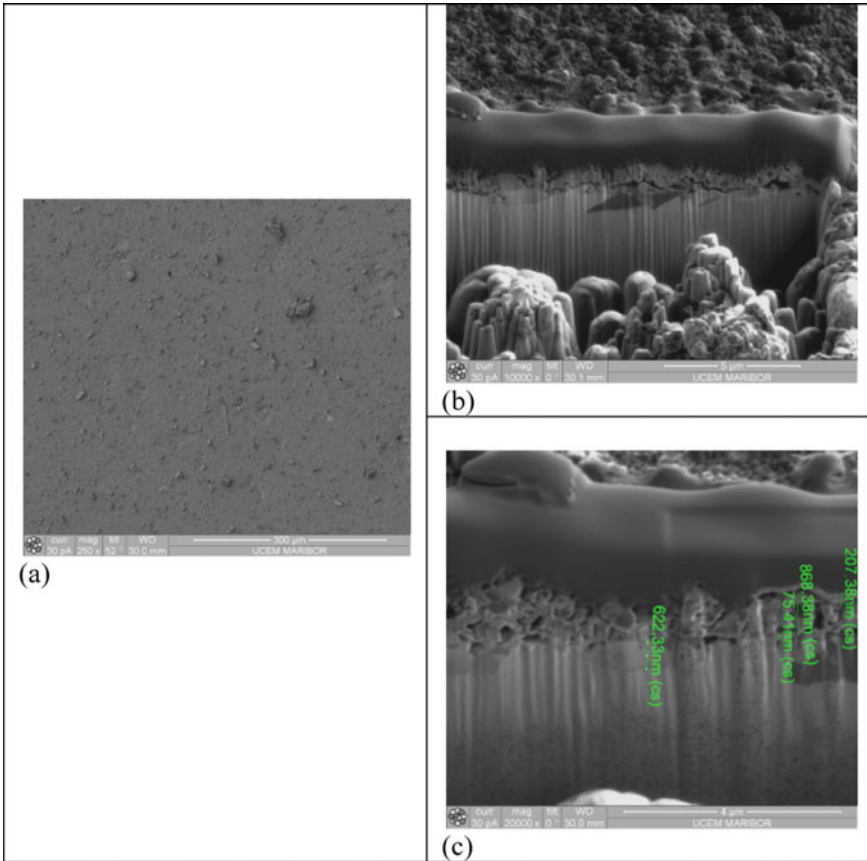


Fig. 6.3 SEM micrographs of Cu /Al-Au-Al-Au/ specimens **a** Surface, **b** Space view, and **c** Cross-section

thick for the same processing conditions (wire speed of 0.5 m/s for the Al wire and Au-alloy).

Finally, the plasma technology described here is a unique strategy in the production of nano-foils. Preliminary results of the produced nano-foils indicate that there are still issues with ensuring the constant thickness of a single foil into the sandwich nano-structure. Furthermore, the obtained nano-foil microstructure is heavily dependent on the original chemical composition of the surface wire used as a positive electrode. Another important conclusion is that the formatted nano-foils of various initial materials are dissimilar under the nearly identical technological parameters of plasma technology. Finally, the form and quality of the finished nano-foils are determined by the substrate surface preparation [20].

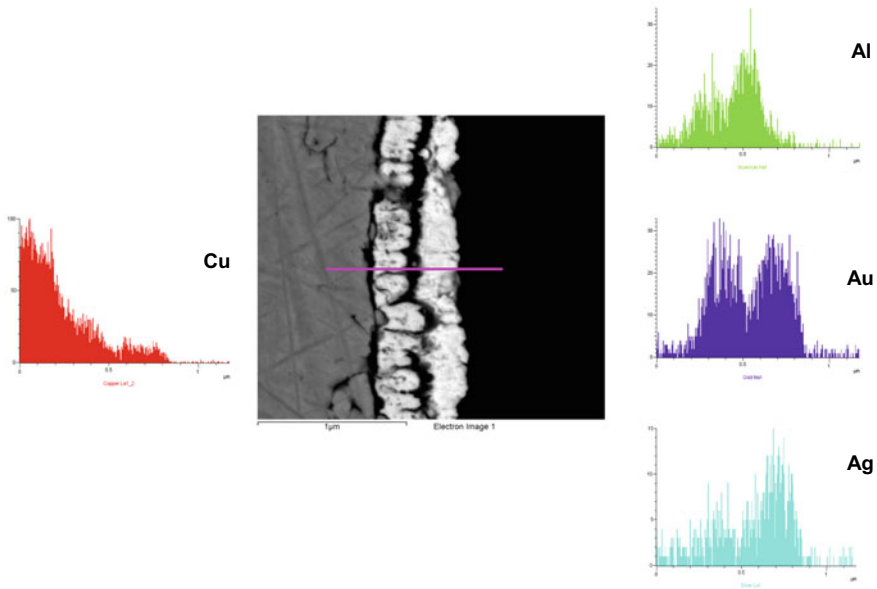


Fig. 6.4 SEM micrograph of a Cu /Al-Au-Al-Au/ specimen cross-section with EDX line analyses; the bright layers are Au and the dark layers are Al

6.4 CFD Analysis of Exothermic Reactions in Al-Au Nanofoils

The purpose of this study is to aid in the creation of a novel reactive Al-Au nano-multilayered material that allows for the rapid bonding of comparable and dissimilar materials using Computational Fluid Dynamics (CFD) analysis. The advantage of numerical modelling is that, once set up and established, a broad variety of scenarios can be investigated with little effort, and complex two-dimensional and three-dimensional problems can be solved using numerical models [22–25]. The reactive Al-Au nano-foils could be used as a controllable, localised heat source for joining uses. To optimise the performance of Al-Au foils, a thorough knowledge is required of the physical processes that govern reaction temperature, rate of heat generation, and the velocity of the reaction propagation along a foil [26].

When one end of an A-B multilayer system (here Al-Au) is ignited with a brief thermal pulse (such as a spark) at room temperature, local atoms diffuse normal to the layers, with A-A and B-B bonds being swapped for A-B bonds, as illustrated in Fig. 6.5.

Heat is released and conducted parallel to the layers during this procedure. If the atomic diffusion and energy release are rapid enough, the reactions will self-promote. These reactions can travel at speeds of up to 25 m/s and achieve temperatures of over 1500 °C.

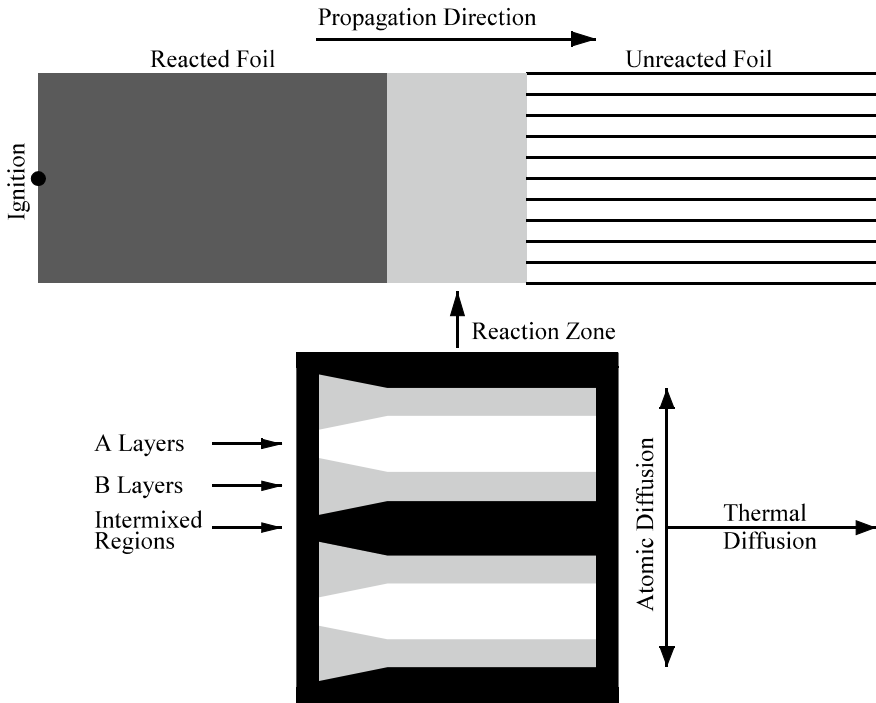
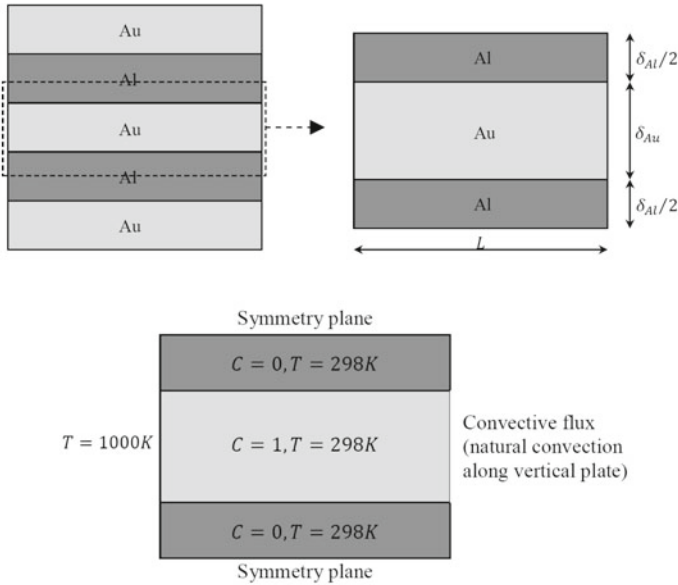


Fig. 6.5 A schematic depiction of a self-propagating reaction propagating from left to right in a multilayer foil. The unreacted foil is made up of alternating layers of elements A and B with an intermixed area in between

Numerous investigations have been conducted [1–5] of interface responses in various multilayer systems. The apparent large free energy accessible for phase formation, usually several tens of kJ/mol, is a feature shared by these multilayers. As a result, we can infer that all possible product phases should be able to form from the start of the reaction.

6.4.1 Numerical Modelling

The possibility is presented of Numerical Modelling using Computational Fluid Dynamics (CFD) in the area of nano-foils [26]. A Finite Volume Methodology (FVM) was used to answer the governing equations. The computational domain was discretised using a uniform Cartesian grid, with the corresponding number of grid points along the x and y axes. Field variables were discretised at cell centres, and the spatial and temporal derivatives were approximated with a second-order accurate numerical scheme. For the appropriate Al-Au nano-foil geometry and boundary conditions, the time-evolution of temperature and concentration fields will be given,



	Density ρ , kg/m^3	Specific heat c_p , J/kgK	Thermal conductivity λ , W/mK	Atomic Packing Factor (A.P.F)
Au	19320	130	318	0.74
Al	2700	910	237	0.74

Fig. 6.6 Schematic overview of Au-Al nano-foil, segment: $L = 2000nm$, $\delta_{Au} = \delta_{Al} = 100nm$ (up); boundary and initial conditions (middle) with physical properties for Au and Al (down)

as well as the atomic diffusion coefficient. The following assumptions underpin the formulation of the mathematical model used to explain self-propagating reactions in multi-layered Al-Au nano-foil: (1) The effects of phase changes in the foil are ignored (e.g., melting of the reactants and/or products); (2) Atomic diffusion is represented by a single binary diffusion coefficient D ; and (3) The physical properties of the foil (e.g., density, thermal conductivity and specific heat c_p) are assumed to be composition dependent. Last but not least, the breadth of the foil (z) is greater than the thickness (y) but less than the length. (x). As a consequence, thermal and atomic diffusion in a foil can be treated as a two-dimensional problem.

6.4.1.1 Governing Equations

Under the above conditions, atomic mixing is described by a time-dependent, conserved scalar field $C(x,y,t)$, where $C = 1$ for pure Au and $C = 0$ for pure Al. C 's evolution is controlled by:

$$\frac{\partial C}{\partial t} = \frac{\partial}{\partial x_j} \left(D \frac{\partial C}{\partial x_j} \right) \quad (6.1)$$

According to [22, 23], the atomic diffusivity is considered to be composition independent and to follow the Arrhenius temperature dependence:

$$D = D_0 \exp \left(-\frac{E}{RT} \right) \quad (6.2)$$

where D_0 is the Arrhenius pre exponential, E is the activation energy and R is the universal gas constant. The values $D_0 = 6.80 \times 10^{-4} \text{ m}^2/\text{s}$ and $E = 25.20 \text{ kJ/mol}$ as used in the present study are taken from the work of Fouracre [19].

The time-evolution of the concentration field is coupled with the temperature equation:

$$\frac{\partial T}{\partial t} = \frac{\partial}{\partial x_j} \left(\frac{\lambda}{\rho c_p} \frac{\partial T}{\partial x_j} \right) + \frac{\partial}{\partial t} \left[\frac{Q(C)}{\rho c_p} \right] \quad (6.3)$$

where the physical properties (thermal conductivity λ , density ρ , and specific heat c_p) of any domain control volume are provided by the fraction of the phase (Au and Al) in that volume. They can be calculated numerically as follows:

$$\lambda = \lambda_{Au} C + \lambda_{Al} (1 - C), \rho = \rho_{Au} C + \rho_{Al} (1 - C), c_p = c_{pAu} C + c_{pAl} (1 - C) \quad (6.4)$$

The rate of heat generation ($(Q(C))_t$) is supposed to be proportional to the rate of change in the composition of the foil. The linear relationship between the composition and the energy released can be presumed in the simplest case. A parabola function, on the other hand, may be more accurate:

$$Q(C) = -\rho c_p (T_{f0} - T_0) C^2 \quad (6.5)$$

and was used in the present study.

T_{f0} and T_0 are the adiabatic temperature of the reaction and the initial temperature of the foil.

6.4.1.2 Geometry, Initial and Boundary Conditions

Figure 6.6 depicts the laminar and time-dependent thermal and species transfer in a two-dimensional nano-foil.

	Density ρ , kg/m^3	Specific heat c_p , J/kgK	Thermal conductivity λ , W/mK	Atomic packing factor (A.P.F)
Au	19,320	130	318	0.74
Al	2700	910	237	0.74

6.4.2 Numerical Procedure

The governing equations were solved with the Ansys CFX numerical code, which uses standard finite volume methodology, with all variables defined at the centre of the control volumes populating the physical area under consideration. Each equation is integrated over the control volume to produce a discrete equation that links the variable at the volume's centre to its neighbours [26].

The computational space was discretised using a uniform Cartesian grid with mesh size $\Delta x = \Delta y$ along the x and y axes. $N_x = 800$ and $N_y = 80$ represent the corresponding amount of grid points. The second order accurate scheme, based on central-differences, was used for spatial discretisation of diffusive terms, while the temporal derivatives were estimated with second order accurate backward differences for a fixed time step $\Delta t = 10^{-9}$ s.

6.4.3 Results and Discussion

Figure 6.7 depicts the time development of the temperature and concentration fields. The temperature (i.e. thermal) transport is seen to be basically unidirectional (mostly in the axial direction) and happens parallel to the layering.

In contrast to previous studies [23], which modelled atomic diffusion as a one-dimensional phenomenon (occurring normal to layering), the current research demonstrates that atomic diffusion is a two-dimensional phenomenon (see Fig. 6.5). This is because the diffusion coefficient D , as described by Eq. (6.2), varies with temperature (in fact, it rises as the temperature increases) in the axial direction. Of course, if the diffusion coefficient remains constant, concentration diffusion will only occur in the streamwise path (due to the concentration gradient). Finally, the concentration diffusion process was much faster in the current research, due to the higher value of the diffusion coefficient D in comparison to the value of the thermal diffusion coefficient α .

In summary, the time-dependent temperature and concentration diffusion in the multi-layered Al-Au nano-foil was investigated numerically in this research using mathematical modelling and a finite volume-based CFD code. The atomic diffusion coefficient D was assumed to be composition independent and to follow the Arrhenius temperature dependence, whereas the physical properties (and, thus, thermal

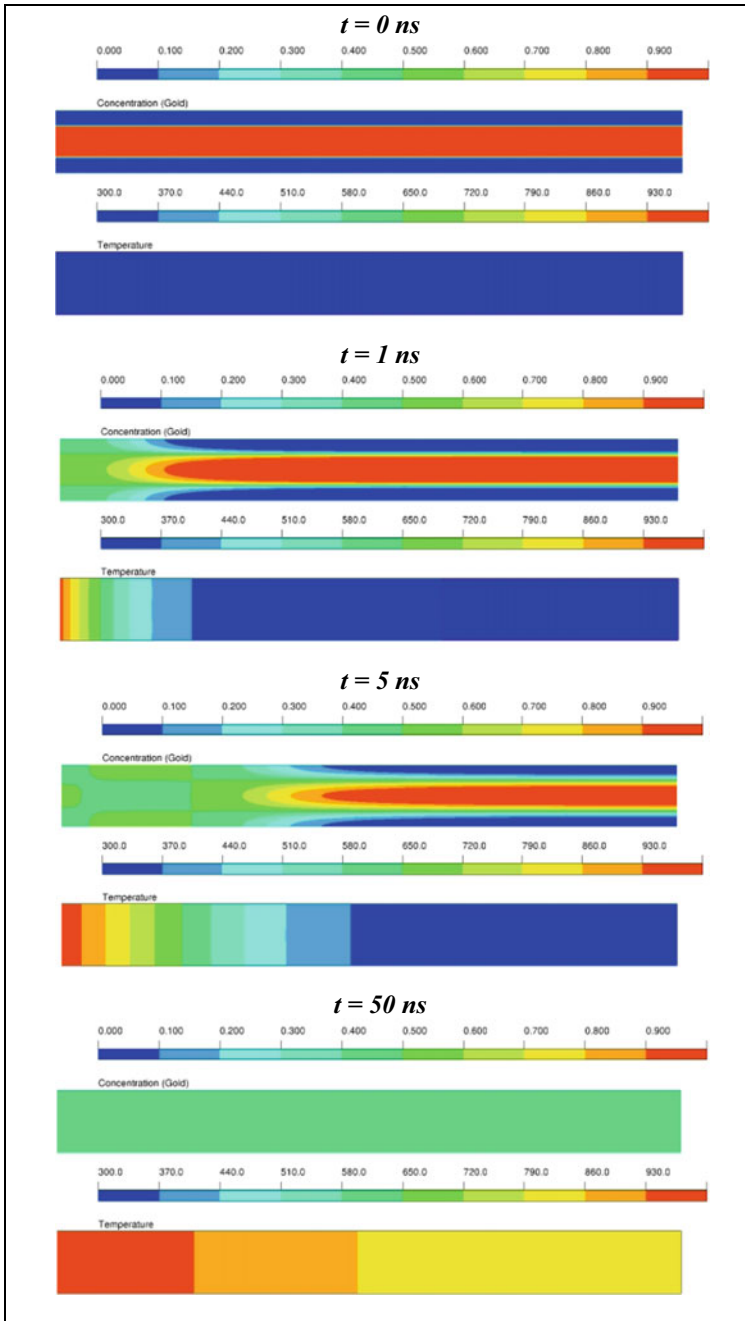


Fig. 6.7 Time evolution of the temperature and concentration field

diffusion) in any control volume of the domain were assumed to be dependent on the corresponding fraction of the phase (Au and Al) in that volume [26].

Due to the variable diffusion coefficient [19] and concentration gradient, the current numerical results indicate that temperature diffusion is essentially unidirectional (in the axial direction), whereas atomic diffusion occurs in both (i.e. the axial and streamwise) directions. The latter is an important fact (influencing the thickness of the intermixed area between the layers, as well as the heat release in the process) that has been overlooked in the majority of existing analytical and computational models.

References

1. T.P. Weihs, *Handbook of Thin Film Process Technology*, vol. 7, ed. by D.A. Glocker, S.I. Shah (Institute of Physics, Bristol, 1998)
2. A.K. Jadoon, B. Ralph, P.R. Hornsby, Metal to ceramic joining via a metallic interlayer bonding technique. *J. Mater. Process. Technol.* **152**(3), 257–265 (2004)
3. K.T. Raić, R. Rudolf, I. Anžel, A. Todorović, Multilayered nano-foils for low-temperature metal-ceramic joining. *Metalurgija* **14**(2), 143–154 (2008)
4. A.J. Swiston Jr., T.C. Hufnagel, T.P. Weihs, Joining bulk metallic glass using reactive multilayer foils. *Scripta Mater.* **48**(12), 1575–1580 (2003)
5. J. Wang, E. Besnoin, O.M. Knio, T.P. Weihs, Investigating the effect of applied pressure on reactive multilayer foil joining. *Acta Mater.* **52**(18), 5265–5274 (2004)
6. E. Besnoin, S. Cerutti, O.M. Knio, T.P. Weihs, Effect of reactant and product melting on self-propagating reactions in multilayer foils. *J. Appl. Phys.* **92**(9), 5474–5481 (2002)
7. A. Duckham, J. Levin, T.P. Weihs, Soldering and brazing metals to ceramics at room temperature using a novel nanotechnology. *Adv. Sci. Technol.* **45**, 1578–1587 (2006)
8. D.M. Makowiecki, R.M. Bionta, U.S. Pat. 5,381,944, Jan 17 (1995)
9. T.W. Barbee, T.P. Weihs, U.S. Pat. 5,538,795, July 23 (1996)
10. T.W. Barbee, Jr., T.P. Weihs, U.S. Pat. 5,547,715, August 20 (1996)
11. Fritz et al., U.S. Pat. 9,382,167 B2, Jul. 5 (2016)
12. Davis et al., U.S. Pat. 10,925,663 B2, Feb. 23 (2021)
13. S.C. Barron, S.T. Kelly, J. Kirchhoff, R. Knepper, K. Fisher, K.J.T. Livi, T.P. Weihs, Self-propagating reactions in Al/Zr multilayers: Anomalous dependence of reaction velocity on bilayer thickness. *J. Appl. Phys.* **114**(22), 223517 (2013)
14. K. Fisher, S.C. Barron, M.A. Bonds, R. Knepper, K.J.T. Livi, G.H. Campbell, T.P. Weihs, Phase transformations, heat evolution, and atomic diffusion during slow heating of Al-rich Al/Zr multilayered foils. *J. Appl. Phys.* **114**(24), 243509 (2013)
15. M.E. Reiss, C.M. Esber, D. Van Heerden, A.J. Gavens, M.E. Williams, T.P. Weihs, Self-propagating formation reactions in Nb/Si multilayers. *Mater. Sci. Eng. A* **261**(1–2), 217–222 (1999)
16. J.C. Gachon, A.S. Rogachev, H.E. Grigoryan, E.V. Illarionova, J.J. Kuntz, D.Y. Kovalev, P.A. Tsygankov, On the mechanism of heterogeneous reaction and phase formation in Ti/Al multilayer nanofilms. *Acta Mater.* **53**(4), 1225–1231 (2005)
17. A.J. Gavens, D. Van Heerden, A.B. Mann, M.E. Reiss, T.P. Weihs, Effect of intermixing on self-propagating exothermic reactions in Al/Ni nanolaminate foils. *J. Appl. Phys.* **87**(3), 1255–1263 (2000)
18. K.J. Blobaum, M.E. Reiss, J.M. Plitzko, T.P. Weihs, Deposition and characterization of a self-propagating CuO x/Al thermite reaction in a multilayer foil geometry. *J. Appl. Phys.* **94**(5), 2915–2922 (2003)

19. R.A. Fouracre, Electron microscope observations of chemical diffusion in the Al/Au system. *Thin Solid Films* **135**(2), 189–201 (1986)
20. K.T. Raić, R. Rudolf, B. Kosec, I. Anžel, V. Lazić, A. Todorović, Nanofoils for soldering and brazing in dental joining practice and jewellery manufacturing. *Materiali in tehnologije* **43**(1), 3–9 (2010)
21. www.plasmait.com
22. A.B. Mann, A.J. Gavens, M.E. Reiss, D. Van Heerden, G. Bao, T.P. Weihs, Modeling and characterizing the propagation velocity of exothermic reactions in multilayer foils. *J. Appl. Phys.* **82**(3), 1178–1188 (1997)
23. S. Jayaraman, A.B. Mann, M. Reiss, T.P. Weihs, O.M. Knio, Numerical study of the effect of heat losses on self-propagating reactions in multilayer foils. *Combust. Flame* **124**(1–2), 178–194 (2001)
24. A. Yuile, A. Schulz, E. Wiss, Müller J, Wiese S, The simulated effect of adding solder layers on reactive multilayer films used for joining processes. *Appl. Sci.* **12**(5), 2397 (2022)
25. A. Yuile, A. Schulz, E. Wiss, J. Müller, S. Wiese, The simulated effect of adding solder layers on reactive multilayer films used for joining processes. *Appl. Sci.* **12**(5), 2397 (2022)
26. K.T. Raić, R. Rudolf, P. Ternik, Z. Zunić, V. Lazić, D. Stamenković, I. Anžel, CFD analysis of exothermic reactions in Al-Au nano multi-layered foils. *Materiali in tehnologije* **45**(4), 335–338 (2011)